



**ScuDo**  
Scuola di Dottorato ~ Doctoral School  
WHAT YOU ARE, TAKES YOU FAR

Doctoral Dissertation  
Doctoral Program in Environmental Engineering (29<sup>th</sup> Cycle)

# **Deep geothermal exploration by means of electromagnetic methods: New insights from the Larderello geothermal field (Italy)**

By

**Alessandro Santilano**

\*\*\*\*\*

**Supervisors:**

Prof. A. Godio, *Politecnico di Torino*  
Prof. S. Lo Russo, *Politecnico di Torino*  
Dr. A. Manzella, *National Research Council of Italy (CNR)*

**Doctoral Examination Committee:**

Prof. D.F. Bruhn, *Delft University of Technology (Netherlands)*  
Prof. E. Cardarelli, *“Sapienza” University of Rome (Roma, Italy)*  
Prof. A. Casas, *University of Barcelona (Spain)*  
Prof. G. Crosta, *University of Milano “Bicocca” (Italy)*  
Prof. J.F. Girard, *University of Strasbourg (France)*

Politecnico di Torino  
2016

## **Declaration**

I hereby declare that, the contents and organization of this dissertation constitute my own original work and does not compromise in any way the rights of third parties, including those relating to the security of personal data.

Alessandro Santilano

2016

\* This dissertation is presented in partial fulfillment of the requirements for **Ph.D. degree** in the Graduate School of Politecnico di Torino (ScuDo).

*To my wife*

*“Everything affects everything else, and you have to understand that whole web of connections”*

*M. Mitchell Waldrop*

---

## **Acknowledgment**

I would like to thank all the people who supported me during this exciting adventure that was my PhD at the Polytechnic of Turin.

My first and most sincere acknowledgement goes to my supervisor Prof. Alberto Godio for having inspired my research. I learned from him many aspects of geophysics, including physical and mathematical issues, but Prof. Godio mostly taught me science as a way of thinking. The door of his office was always open for me, and he was always ready to listen to my technical and non-technical troubles. I thank Prof. Stefano Lo Russo for having always encouraged my studies with precious suggestions. For the CNR side of this adventure I would like to thank Dr. Adele Manzella, being the first who strongly believed in me and introduced me to the world of geophysics. Working with Adele means to work in an exciting international context and to share knowledge with the most expert scientists in the field of geothermal energy. She was the scientific coordinator of my fellowship at CNR-IGG in the frame of the IMAGE Project (EU FP7, under grant agreement No. 608553) that economically has founded part of my research. Regarding the data used in this research, the new magnetotelluric (MT) data were acquired in the Larderello geothermal field (Italy) in the frame of the IMAGE Project. I would like to thank all the people from the CNR and the Polytechnic of Turin that joined the EM surveys on the field as well as I thank Nordine Bouzid for the help in the first stages of the surveys. Other MT, geological and well data were kindly provided by ENEL GP and CNR-IGG, acquired in the frame of exploration and research projects, particularly I-GET (EU FP6) and INTAS (EU) Projects. I thank the CNR, with the help by Eugenio Trumpy and Gianluca Gola, to have provided data from the National Geothermal Database and from specific bibliographic search. During these years I met many colleagues that supported me even with few encouraging words. Among them I thank Serena Botteghi, Gerardo Romano, Alessandro Arato and Diego Franco. A special thank goes to Giovanni Gianelli for sharing its deep knowledge on geothermal systems.

Dulcis in fundo, I am indebted to my wife that supported me in these years and above all during the writing of the thesis. She has been able to tolerate me and to get herself the PhD in geochemistry at the same time, proving a strength out of the ordinary. I thank also my mother, my father and my brothers that, despite the large distance, never stopped to help and encourage me for accomplishing this adventure.



## Abstract

The main target of this research is the improvement of the knowledge on the deep structures of the Larderello-Travale geothermal field (Tuscany, Italy), with a focus on the *Lago Boracifero* sector, particularly on the heat source of the system, the tectonics and its relation with the hydrothermal circulation.

In the frame of the PhD program and of the IMAGE project (Integrated Methods for Advanced Geothermal Exploration; EU FP7), we acquired new magnetotelluric (MT) and Time Domain EM (TDEM) data in a key sector of the field (*Lago Boracifero*). These data integrate the MT datasets previously acquired in the frame of exploration and scientific projects.

This study is based also on an integrated modelling, which included and organized in Petrel (Schlumberger) environment, a large quantity of geological and geophysical data.

We also propose an integrated approach to improve the reliability of the 2D MT inversion models, by using external information from the integrated model of the field as well as an innovative probabilistic analysis of the MT data.

We present our attempt to treat the 1D magnetotelluric inverse problem with a probabilistic approach, by adopting the Particle Swarm Optimization (PSO), a heuristic method based on the concept of the adaptive behaviour to solve complex problems. The user-friendly software “GlobalEM” was implemented for the analysis and probabilistic optimization of MT data. The results from theoretical and measured MT data are promising, also for the possibility to implement different schemes of constrained optimization as well as joint optimization (e.g. MT and TDEM). The analysis of the a-posteriori distribution of the results can be of help to understand the reliability of the model.

The 2D MT inversion models and the integrated study of the Larderello-Travale geothermal field improved the knowledge about the deep structures of the system, with a relevant impact on the conceptual geothermal model.

In Micaschist and Gneiss complexes we observed a generally high electrical resistivity response locally interrupted by low resistivity anomalies that are well correlated with the most productive sectors of the field. A still partial melted igneous intrusion beneath the *Lago Boracifero* sector was detected based on the interpretation of the low resistivity anomalies located at a mid-crustal level (> 6 km).

New insights on the tectonics are proposed in this research. The fundamental role of a large tectonic structure, i.e. the Cornia Fault, located along the homonymous river, was highlighted. In our opinion, this fault played an important role in the geothermal evolution of the *Lago Boracifero* sector, favouring both the hydrothermal circulation and the emplacement of magma bodies.

In our opinion, the system can be ascribed to a “young convective and intrusive” field feed by a complex composite batholite.

# Contents

<b>Abstract</b> .....	I
<b>Contents</b> .....	III
<b>List of Figures</b> .....	X
<b>List of Tables</b> .....	XV
<b>Introduction</b> .....	1
1.1 Background .....	2
1.2 Main objectives .....	3
1.3 Thesis outline .....	3
<i>Part I</i>	
<i>Electromagnetic geophysics: theoretical background and application to the geothermal exploration</i>	
<b>The concept of geothermal play: the Convective Intrusive type in the frame of Italian and USA fields</b> .....	7
2.1 Introduction .....	7
2.1.1 Chapter overview .....	9
2.2 Structural setting .....	9
2.2.1 Larderello and Mt. Amiata geothermal fields .....	9
2.2.2 The Geysers geothermal field .....	10
2.3 Heat source and thermal regime .....	11
2.3.1 Larderello and Mt. Amiata geothermal fields .....	11
2.3.2 The Geysers geothermal field .....	12
2.4 Reservoir characteristics .....	13

2.4.1 Larderello and Mt. Amiata geothermal fields.....	13
2.4.2 The Geysers geothermal field .....	14
2.5 Discussion.....	14
2.6 Summary.....	17
<b>The role of electrical resistivity in the geothermal exploration .....</b>	<b>19</b>
3.1 Introduction .....	19
3.2 Electrical resistivity of Earth's materials.....	20
3.3 The role of mineralogy .....	23
3.4 The role of temperature .....	26
3.5 The role of multiple phase systems .....	27
3.5.1 Aqueous fluids .....	27
3.5.2 Melt.....	30
3.6 The role of pressure .....	31
3.7 Additional remarks .....	33
<b>Magnetotelluric (MT) and Time Domain EM (TDEM) methods:</b>	
<b>Theoretical Background.....</b>	<b>34</b>
4.1 Introduction on the MT method .....	34
4.2 Basic theory and assumptions behind the method.....	35
4.2.1 EM induction .....	36
4.2.2 Transfer function, apparent resistivity and phase .....	38
4.3 The concepts of MT data acquisition and processing .....	40
4.4 MT data analysis.....	42
4.4.1 Distortion .....	42
4.4.2 Dimensionality.....	43
4.5 The relation between MT data and Earth's model parameters: Forward and Inverse problems .....	43
4.5.1 MT forward problem: the 1D case.....	44
4.5.2 MT inverse problem: the deterministic and probabilistic approaches .....	45

4.6 The TDEM method.....	47
4.7 Electromagnetic methods for shallow and deep geothermal exploration in Italy: case studies .....	48
4.7.1 MT method in geothermal exploration: case studies in Italy.....	49
4.7.2 TDEM methods in geothermal exploration: case studies in Italy...51	

*Part II*

*On the probabilistic optimization of EM data*

<b>The Particle Swarm Optimization (PSO) algorithm: application to magnetotelluric data .....</b>	<b>55</b>
5.1 Introduction .....	55
5.1.1 Foreword of PSO application in geophysics.....	55
5.1.2 Introduction on GlobalEM: the software for 1D optimization of EM data .....	56
5.2 The PSO method.....	57
5.2.1 PSO theoretical background .....	58
5.2.2 Search space's constraints and boundaries .....	61
5.3 Minimization function .....	61
5.4 Flow chart of the geophysical optimization .....	63
5.5 Results .....	65
5.5.1 Test on synthetic data .....	65
5.5.2 Application to real AMT data .....	69
5.5.3 Application to real Long Period MT data.....	72
5.6 Discussion.....	76
5.7 Final remarks .....	77

*Part III*

*The Larderello-Travale geothermal field (Italy): improvement on the knowledge of the geothermal system by electromagnetic study*

<b>The 3D geological model of the Larderello-Travale geothermal system ..</b>	<b>79</b>
6.1 Introduction .....	79
6.1.1 Overview on the study areas.....	80

6.2 Historical perspective of the field.....	81
6.3 The integrated database .....	83
6.4 The conceptual model.....	85
6.4.1 Geothermal background, tectonics and heat source.....	85
6.4.2 Stratigraphy.....	88
6.5 The 3D modelling.....	94
6.5.1 Input data .....	94
6.5.2 Horizons interpolation and 3D Grid .....	99
6.6 Discussion on the 3D models .....	101
<b>The MT study of the Larderello-Travale geothermal system: the EM dataset .....</b>	<b>103</b>
7.1 Introduction .....	103
7.2 State of the art and open challenges in the EM exploration of the Larderello-Travale field .....	104
7.2.1 Previous EM studies and open challenges.....	104
7.2.2 Recent re-analysis of old dataset in southern Tuscany .....	107
7.2.3 Additional issues on the deep levels of the field.....	107
7.3 The EM data in the Larderello-Travale geothermal field.....	108
7.3.1 Overview of the old MT datasets.....	108
7.3.2 MT measurements in the Lago Boracifero sector: the new survey .....	111
7.3.3 TDEM measurements in the <i>Lago Boracifero</i> sector: the new survey .....	114
7.3.4 MT in the <i>Lago Boracifero</i> sector: Data processing.....	116
7.3.5 TDEM in the <i>Lago Boracifero</i> sector: Data processing .....	120
7.4 Data analysis.....	121
7.4.1 Dimensionality and Directionality from MT data.....	121
7.4.2 Integration of TDEM and MT data for static shift correction....	125

---

<b>Global Optimization of the EM geophysical data from the Larderello-Travale field</b> .....	129
8.1 Introduction .....	129
8.2 Test on synthetic data .....	130
8.2.1 Test on synthetic data: simulating the <i>Travale</i> sector.....	131
8.2.2 Test on synthetic data: simulating the <i>Lago Boracifero</i> sector ....	136
8.3 Optimization of observed MT data from the Larderello-Geothermal field .....	141
8.3.1 Optimization of observed MT data: insights from the “G6” and “Lard_7” soundings.....	141
8.3.2 Optimization of observed MT data: insights from the complete dataset.....	144
8.4 Joint PSO optimization of TDEM and MT soundings .....	148
8.5 Discussion.....	149
<b>Results from 2D inversion: interpretation and integrated model of the Larderello-Travale field</b> .....	151
9.1 Introduction .....	151
9.2 Meshing .....	153
9.3 Initial models .....	153
9.3.1 Homogeneous halfspace .....	154
9.3.2 A-priori from geological model.....	154
9.3.3 A-priori from PSO models.....	159
9.4 2D inversion: setting parameters .....	159
9.5 Results .....	162
9.5.1 Results from inversion without external constraints.....	162
9.5.2 Results from inversion constrained with geological data .....	163
9.5.3 Results from inversion constrained with PSO resistivity distribution .....	167
9.6 Discussion on the geothermal interpretation and the integrated model .....	169

---

9.6.1 The shallow level of the <i>Lago Boracifero</i> sector: cap-rock and reservoir.....	169
9.6.2 Effect of melting phase on resistivity .....	173
9.6.3 Tectonic implication of the resistivity models.....	174
9.6.4 Correlation with seismic models.....	175
9.6.4 Impact on the conceptual model of the <i>Lago Boracifero</i> area.....	179
<b>Concluding remarks</b> .....	182
10.1 On the probabilistic optimization .....	182
10.2 On the study of the Larderello-Travale geothermal field.....	183
<b>Appendix A:</b> GlobalEM, the Matlab software for optimization of MT data	187
<b>Appendix B:</b> EM soundings.....	200
<b>Appendix C:</b> MT modelling .....	208
<b>References</b> .....	216



## List of Figures

Figure 3.1- Conceptual model of a geothermal system. ....	20
Figure 3.2- Resistivity (and electrical conductivity) ranges for Earth's material .....	23
Figure 3.3- Schematic hydrothermal alteration zones. ....	25
Figure 3.4- Schematic profile of the geothermal systems in Iceland in terms of temperature, resistivity and hydrothermal alteration.....	26
Figure 3.5- Resistivity of dry and wet granite as function of temperature .....	27
Figure 3.6- Bulk resistivities for a two-phase mixing model.....	29
Figure 3.7- Two-phase mixing model with tubes geometry for an ideal basaltic melt (water 6%, 20 MPa, ~1300 °C) in a resistive (2000 $\Omega$ m) rock matrix,.....	31
Figure 3.8- Resistivity as function of pressure .....	32
Figure 4.1- Theoretical MT curves for an ideal 2D Earth's model.....	40
Figure 4.2- Resistivity cross-section compared to the geological model of the Travale sector, (modified from Manzella et al. 2006).....	50
Figure 4.3- Inversion of MT data in the Mt. Amiata geothermal field .....	51
Figure 4.4- Resistivity cross-section in the Termini Imerese test site .....	52
Figure 4.5- Termini Imerese 3D geological model.....	53
Figure 5.1- Geometrical illustration of PSO .....	60
Figure 5.2- Flow-chart of the MT data optimization using the PSO scheme. ....	64
Figure 5.3- Solution on synthetic data. ....	66
Figure 5.4- Solution on synthetic data adopting $\lambda = 0.001$ . ....	67
Figure 5.5- Solution on synthetic data with uniform noise of 5%,. ....	68
Figure 5.6- Occam solution on synthetic data.....	69
Figure 5.7- Sounding AMT6. Occam model. ....	71
Figure 5.8- Sounding AMT8. Occam model .....	72
Figure 5.9- PSO optimization with Occam model of Coprod dataset.....	74
Figure 5.10- A-posteriori resistivity distribution .....	75
Figure 6.1- Study areas for the 3D geological modelling.....	80
Figure 6.2- Schematic geological map.....	84
Figure 6.3- Structural sketch of the Massa Marittima Geological Map.....	86

---

Figure 6.4- Geothermal well Castiglioni-1. ....	91
Figure 6.5- The conceptual model of the Travale-Larderello field.....	93
Figure 6.6- Wells correlation from the <i>Lago Boracifero</i> area. ....	96
Figure 6.7- Overview of input data for 3D modelling. ....	98
Figure 6.8- 3D geological models. In grey-scale format is shown the regional model, in colour-scale are shown the <i>Lago Boracifero</i> and <i>Travale</i> models.....	101
Figure 6.9- Resulting models compared with the stratigraphic well logs.....	102
Figure 7.1- Location of the MT soundings acquired in the frame of previous exploration and research projects.....	110
Figure 7.2- Example of MT response from a site 30 km far from the survey area. .	112
Figure 7.3-Location of the MT and TDEM soundings of old and new datasets available for the study of the <i>Lago Boracifero</i> area.....	113
Figure 7.4- Acquisition layout of MT and TDEM data in the site Lard_2.....	116
Figure 7.5- Time series measured in the “Lard_9” MT site .....	118
Figure 7.6- MT curves of Lard_3 soundings. ....	119
Figure 7.7- TDEM data, site lard_2.The apparent resistivity vs Times is showed. .	121
Figure 7.8-Location of the MT profiles in <i>Lago Boracifero</i> and <i>Travale</i> . ....	122
Figure 7.9- Dimensionality analysis of MT soundings along Profiles 1, 3 and 6....	123
Figure 7.10- Strike analysis at frequency 24 Hz for the <i>Lago Boracifero</i> sector. ...	125
Figure 7.11- Example of theoretical response of TDEM data converted in MT response and overlap with the MT theoretical response for the same model.....	127
Figure 7.12- Joint MT and TDEM analysis for static correction.....	128
Figure 8.1- Histograms from resistivity well log in Radicondoli-7bis .....	132
Figure 8.2- Results of the global optimization of the theoretical data from the <i>Travale-synth-A</i> .....	135
Figure 8.3- Results of the global optimization of the theoretical data from the <i>Travale-synth-B</i> .....	136
Figure 8.4- Results of the global optimization of the theoretical data from the <i>Lago-synth-A/B/C</i> . ....	139
Figure 8.5- Comparison between the optimization using PSO and deterministic inversion for the model <i>Lago-synt-C</i> . ....	140
Figure 8.6- Results from the blocky optimization of the “G6” sounding .....	143

Figure 8.7- Results from the Occam optimization of the “Lard_7” sounding .....	144
Figure 8.8- 1D estimated resistivity models obtained by Occam-like Particle Swarm Optimization. The simplified models are plotted along the Profile 1 of the <i>Lago Boracifero</i> area and the Profile 6 of the <i>Travale</i> area. ....	147
Figure 8.9- Joint Particle Swarm optimization of TDEM and MT data. ....	149
Figure 9.1- Schematic view of the MT profiles selected for the 2D inversion. ....	153
Figure 9.2- Resistivity well log measured along the Radicondoli-7 bis. ....	155
Figure 9.3- Histograms from DLL/IL measurements along six geothermal wells located in the <i>Travale</i> sector. ....	156
Figure 9.4- A-priori model along the Profile 5. It represents a 2D section of the geological model populated with the resistivity values. ....	158
Figure 9.5- A-priori model along the Profile 3. It represents a 2D interpolation of 1D models obtained with the Particle Swarm Optimization procedure. ....	159
Figure 9.6- L-curve graph for the Profile 1.....	161
Figure 9.7- Comparison of different inversions on the same profile. ....	162
Figure 9.8- Resulting models from the 2D inversion of the six MT profiles in the Larderello-Travale geothermal field. Here the homogeneous starting models were used to invert jointly TE and TM polarizations. ....	163
Figure 9.9- Resulting models from the 2D inversion of the six MT profiles in the Larderello-Travale geothermal field. Here the geological information was used to constrain the joint TE and TM inversion. ....	164
Figure 9.10- 2D inversion of single TE mode (on the left) and single TM mode (on the right) of Profile 1.....	166
Figure 9.11- Joint Inversion of TE and TM mode along the Profile 1 (on the left) and Profile 3 (on the right) starting with optimized a-priori models. ....	168
Figure 9.12- Computed electrical resistivity of a partially molten rock as a function of melt fraction following the two phases mixing models by Schmeling (1986b). ....	174
Figure 9.13- MT Profile 1 plotted in 3D and compared with other geophysical data: Comparison between the MT Profile 1 (a) and Profile 3 (b) and the anomaly of seismic low velocity (Batini et al., 1995) here filtered for the values below 5 km/s; b) MT plotted in 3D with the geological map; c) comparison between the Profile 1 and the deep seismic profile CROP 18a (Brogi et al., 2005), particularly the intrusive rocks (MR) imaged by the seismic reflection data are highlighted in red.....	178
Figure 9.14- Comparison between the MT Profile 4 and the LVZ related to a reference model from the inversion of teleseismic travel time (Foley et al., 1992; Batini et	

al., 1995). The seismic model was filtered and the values in the range of -4 to-16% are shown. ....	179
Figure 9.15- Conceptual model of the <i>Lago Boracifero</i> sector from the interpretation of the MT Profile1: 1) productive wells in the proximity of the trace profile (max distance 800 m), 2) main geothermal manifestation, 3) main faults, 4) supposed occurrence of completely cooled intrusion that cannot be imaged by resistivity anomaly, 5) granitic intrusion with residual melt fraction higher than 4%, imaged by a wide resistivity anomaly, 6) Active hydrothermal, vapor-dominated circulation and multi-stage hydrothermal alteration. ....	181
Figure A.1- Structure of the “GlobalEM” software package. Here the PSO workflow is described in detail being the focus of this research, but the Genetic Algorithm was implemented too. ....	189
Figure A.2- Simple GUI for computing the MT theoretical data from user-defined synthetic model. ....	191
Figure A.3- Geometrical illustration of the model parameters update for each particle at each iteration. For details on the symbols the reader is referred to the Chapter 5. ....	194
Figure A.4- Simple GUIs (Dialog boxes) for the setting of the main conditions for the Particle Swarm Optimization of “Blocky” model; i.e. the resistivities and thicknesses are the parameter to be estimated. ....	195
Figure A.5- Matlab function for evaluating the objective function in the Occam-like optimization. A *.mat file is also saved to give the possibility of computing the L-curve analysis for the proper selection of the Lagrangian multiplier. ....	197
Figure B.1- MT curves, acquired in the survey larderello_2016, are showed after La Torraca decomposition, editing and smoothing of the curves and static shift correction (see text for details): a) Lard_2 Site, b) Lard_3 site. ....	200
Figure B.2- MT curves, acquired in the survey larderello_2016, are showed after La Torraca decomposition, editing and smoothing of the curves and static shift correction (see text for details): a) Lard_5 Site, b) Lard_6 site. ....	200
Figure B.3- MT curves, acquired in the survey larderello_2016, are showed after La Torraca decomposition, editing and smoothing of the curves and static shift correction (see text for details): a) Lard_7 Site, b) Lard_8 site. ....	201
Figure B.4- MT curves, acquired in the survey larderello_2016, are showed after La Torraca decomposition, editing and smoothing of the curves and static shift correction (see text for details): a) Lard_9 Site, b) Lard_10 site. ....	201
Figure B.5- MT curves, acquired in the survey larderello_2016, are showed after La Torraca decomposition, editing and smoothing of the curves and static shift correction (see text for details): a) Lard_11 Site, b) Lard_12 site. ....	202

Figure B.6- MT curves, acquired in the survey larderello_2016, are showed after La Torraca decomposition, editing and smoothing of the curves and static shift correction (see text for details): a) Lard_13 Site, b) Lard_14 site.....	202
Figure B.7- MT curves, acquired in the survey larderello_2016, are showed after La Torraca decomposition, editing and smoothing of the curves and static shift correction (see text for details): a) Lard_15 Site, b) Lard_16 site.....	203
Figure B.8- MT curves, acquired in the survey larderello_2016, are showed after La Torraca decomposition, editing and smoothing of the curves and static shift correction (see text for details): a) Lard_17 Site, b) Lard_18 site.....	203
Figure B.9- MT curves, acquired in the survey larderello_2016, are showed after La Torraca decomposition, editing and smoothing of the curves and static shift correction (see text for details): a) Lard_20 Site, b) Lard_21 site.....	204
Figure B.10- MT curve, acquired in the survey larderello_2016, are showed after La Torraca decomposition, editing and smoothing of the curves and static shift correction (see text for details): a) Lard_23. ....	204
Figure B.11- TDEM data: Lard_2, Lard_6, Lard_7, Lard_9.....	205
Figure B.12- TDEM data: Lard_10, Lard_11, Lard_12, Lard_15.....	206
Figure B.13- TDEM data: Lard_16, Lard_17.....	207
Figure C.1- Results from optimization of theoretical data from the <i>Travale-synt-A</i> model.....	208
Figure C.2- Results from optimization of theoretical data from the <i>Travale-synt-B</i> model.....	209
Figure C.3-Results from optimization of measured data in the <i>Lago Boracifero</i> area: Lard_13 site.....	210
Figure C.4-Results from optimization of measured data in <i>Travale</i> area: J2 site....	211
Figure C.5-Example of bad result of optimization procedure on noisy real data..	212
Figure C.6- Example of bad result of optimization procedure on noisy real data ...	213
Figure C.7- Resistivity models extracted from the 3D geological model as 2D slice. These models were used as starting models for the 2D inversion.....	214
Figure C.8- Resistivity models obtained from the interpolation of 1D models computed with Particle Swarm Optimization. ....	214
Figure C.9- Resulting models of 2D inversion for the Profile 1 to Profile 4 MT profiles. Here we tested the a-priori models from the interpolation of 1D PSO models. The TE and TM modes were jointly inverted. ....	215

## List of Tables

Table 3.1-Values of resistivity for few examples of elements, minerals and rocks...	22
Table 5.1- Main features of the synthetic Earth's models, tested by PSO.....	65
Table 5.2- Main setting for the PSO Occam optimization of COPROD dataset. ....	73
Table 6.1- Summary of the input data used for the 3D geological modelling. The model of interest for each source of data is listed. ....	94
Table 6.2- List of units modelled for each area of study. ....	99
Table 7.1- Summary of the previously acquired MT datasets used for the study of the LTGS.....	108
Table 7.2- MT acquisition schedule.....	114
Table 7.3- Brief description of MT and TDEM sites. The coordinates are in WGS1984 UTM 32 N. ....	115
Table 8.1- Main features of the <i>Travale-synt-A</i> and <i>Travale-synt-B</i> models. The model is retrieved from a real stratigraphic well log. The stratigraphy is also reported.	133
Table 8.2- Main settings for the PSO optimization of the MT theoretical data from <i>Travale-synt-A</i> model.....	134
Table 8.3- Main features of the <i>Lago-synt-A/B/C</i> models. The stratigraphy is retrieved from the geological model in the proximity of the <i>Lago Boracifero</i> area. ....	137
Table 8.4- Main settings for the PSO optimization of the MT theoretical data from <i>Lago-synt-A</i> model. ....	138
Table 8.5- Main settings for the PSO optimization of the MT observed data from G6 and Lard_7 soundings. LB=Lower boundary; UP=Upper Boundary. ....	141
Table 9.1- Electrical resistivity values assigned to each stratigraphic unit of the 3D geological models based on the analysis of DLL/IL well logs. ....	156



# Chapter 1

## Introduction

The intrinsic complexity of geothermal systems and the need of an accurate integration of the geophysical parameters with the geological and hydrogeological properties of the systems still represent a challenge of the exploration geophysics. It is in such a scenario, we focused our research on the Larderello-Travale geothermal field (Tuscany, Italy), in order to explore the possibility to relate the results of electromagnetic (EM) surveys with an integrated modelling of the geothermal system.

Larderello is the oldest field under exploitation in the world. Here, the geothermal electricity production, in its modern meaning, was born. Here, one of the most fantastic geothermal resources, with temperature exceeding 350 °C at depth of 3-4 km, is located. A century of industrial and scientific researches were not enough to understand all the geological, chemical and physical features of this complex system, and to solve the critical issues that are currently debated in the scientific community.

The main target of this research is the improvement of the knowledge on the deep structures of the Larderello-Travale field, with a focus on the heat source of the system and deep crustal fluids, the tectonics and its relation with the hydrothermal circulation in the field.

In addition to the new acquisition of magnetotelluric (MT) and Time Domain EM (TDEM) data in a key sector of the field, we also proposed an integrated approach to improve the reliability of the 2D inversion models, by using external

information from the integrated geological modelling of the field as well as an innovative probabilistic analysis of the MT data.

We present our attempt to treat the magnetotelluric inverse problem with a probabilistic philosophy and its application to the geothermal exploration. Here we adopted the Particle Swarm Optimization (PSO), a heuristic method based on the concept of the adaptive behaviour to solve complex problems.

## 1.1 Background

The research moves on the huge amount of previous geophysical and geological studies that were carried out in the Larderello-Travale geothermal area. We took inspiration from the issues they consolidated and above all from the challenges they opened to the scientific community. We particularly refer to the results of previous European projects (I-GET and INTAS) that studied the *Travale* sector by means of electromagnetic (EM) geophysics, as well as (industrial) seismic, geological, petrological and mineralogical studies available in literature.

The *Lago Boracifero* sector of the field represents the focus of our research. It is of interest for a next pioneering deep drilling project of scientific and industrial relevance (DESCRAMBLE project, EU H2020), investigating the possible occurrence of deep-seated fluids at supercritical conditions related to igneous intrusions.

In the frame of this PhD program and of the IMAGE project (Integrated Methods for Advanced Geothermal Exploration; EU FP7), in collaboration with the National Research Council of Italy, we acquired in the *Lago Boracifero* sector new MT and TDEM data. These data add up to previous MT data acquired in the already mentioned EU projects.

This study is based also on a comprehensive and integrated 3D modelling, which included and organized, in Petrel (Schlumberger) environment, a large quantity of data from literature. We analysed hundreds of deep geothermal wells, some geophysical well logs and interpreted seismic data. A large part of the dataset used for the geological modelling is publicly available (in literature or in the National Geothermal Database of Italy). A little part, related to well

stratigraphy and logs from the I-GET project, was provided confidentially by ENEL.

## 1.2 Main objectives

The research has two main objectives:

- From a methodological point of view (merely geophysical), to explore the effectiveness of the probabilistic approach in 1D MT parameter estimation and how this information can be useful to formulate a more constrained modelling in the solution of the 2D MT inversion problem;
- From a geothermal perspective, to improve the knowledge of the geothermal system, formulating an accurate conceptual model of the Larderello-Travale field including its deep roots, with a focus on the *Lago Boracifero* sector, taking into account all the background and the results of the new collected data.

The first objective of the research was to check the effectiveness of the Particle Swarm Optimization (PSO) algorithm. We implemented in Matlab environment the software package “GlobalEM” for the PSO analysis of Magnetotelluric data. The software follows a user-friendly approach for the 1D model parameter estimation from MT data, according to different regularization schemes (including OCCAM) coupled with the possibility to jointly optimize MT and TDEM data.

With regard to the Larderello-Travale geothermal field, the main objective of this research is to obtain a resistivity distribution at depth that can contribute to better understand some of the aspects still debated in literature, such as: *i*) the occurrence of low electrical resistivity anomalies in a vapour-dominated crystalline reservoir, *ii*) the occurrence of shallow partially molten igneous intrusion, *iii*) the role of the faults in the genesis and the evolution of the field.

## 1.3 Thesis outline

The thesis is organized into three parts, in addition to this introduction to the work (*Chapter 1*), the concluding remarks (*Chapter 9*) and the *Appendixes*.

*Part I* describes the theoretical background of the work and consists of four chapters. In *Chapter 2* we introduced the concept of the “Convective Intrusive geothermal play” by reviewing the main features of three case studies: Larderello and Mt. Amiata (Italy) and The Geysers (USA). This category of geothermal play includes some of the most productive fields in the world and its complete review was of main importance for the study of the Larderello field. This chapter is largely based on the published article Santilano et al. (2015a).

In *Chapter 3* the electrical resistivity of Earth’s material is discussed, in consideration that the indirect estimation of resistivity distribution is the aim of the MT and TDEM geophysical surveys. The complexity of the geothermal systems makes the interpretation of data rather difficult. For this reason, we focused on the role of the electrical resistivity in imaging geothermal systems.

In *Chapter 4* we introduce the theoretical bases of the MT and TDEM methods as well as the concepts of processing and analysis of the data. A brief description of the inverse MT problem and the differences between the deterministic and probabilistic philosophies are also provided. Furthermore, the last section of the chapter is aimed to describe some recent case studies in Italy of electromagnetic (EM) geophysics applied to geothermal exploration.

The *Part II*, composed of *Chapter 5*, refers to the probabilistic approach for 1D optimization of magnetotelluric data.

In *Chapter 5* the Particle Swarm Optimization (PSO) algorithm is described as well as its implementation for the optimization of MT data. The tests on numerical simulations as well as the tests on real Audio MT and Long period MT data (COPROD, Jones and Hutton, 1979a) are presented. The COPROD dataset has been used in literature for testing innovative algorithms. The comparison with estimated models by other authors is particularly promising. This chapter is largely based on a scientific article by Godio, A. and Santilano, A., recently submitted to a peer-reviewed journal. In appendix A the Matlab software package GlobalEM, is described in details.

The *Part III* refers to the integrated study of the Larderello-Travale geothermal field. This part is composed by four chapters.

In *Chapter 6* we presented the critical review of an integrated database for the construction of the detailed 3D geological model of the Larderello-Travale geothermal system computed in Petrel (Schlumberger) environment. The

geological model was used to extract information for constraining the MT inversion and also to integrate the resulting resistivity models with other data such as seismic data.

In *Chapter 7* we present the MT and TDEM database including the previous surveys we were allowed to use and the new data acquired in the *Lago Boracifero* sector. The chapter is focused on the detailed description of the acquisition, processing and analysis of the data. An updated state of the art of the EM studies in the Larderello-Travale field is provided, with the aim to clarify the issues still debated in literature.

In *Chapter 8*, we describe the part of the research referring to the probabilistic optimization of the MT data in the Larderello-Travale field. Firstly, we checked the effectiveness of PSO on synthetic data simulating particular conditions of the Larderello-Travale field in order also to retrieve important information on the system. Then, we adopted the PSO for the optimization of the observed MT data in the field, with a focus also on the joint analysis with TDEM.

Finally, in *Chapter 9* we present the results of the 2D MT inversion for the study of the Larderello-Travale field. We focused our effort on the comparison of various a priori models for the inversion, related to geological information (from the geological model) and to the optimized model obtained in Chapter 8. Finally, we present an integrated analysis of the 2D resistivity models with other source of data (in Petrel environment) and its interpretation from a geothermal standpoint.

## *Part I*

# *Electromagnetic geophysics: theoretical background and application to the geothermal exploration*

## Chapter 2

# The concept of geothermal play: the Convective Intrusive type in the frame of Italian and USA fields

### 2.1 Introduction

*This Chapter is largely based on the published article of Santilano et al., (2015a), which focuses on the analysis of different geothermal systems in the frame of the “Convective, Intrusive Geothermal Play” type. Here, we propose the review of the most productive fields in Italy and USA: Larderello, Mt. Amiata (Italy) and The Geysers (USA).*

Geothermal energy is a renewable and eco-compatible resource suitable for base-load power and thermal production. The basic concept of this resource is the use of the Earth’s heat for electrical power production or directly as thermal energy. In the last years this source has been of interest for governments, companies and research institutes worldwide that are working for the increase of geothermal power and heat production.

Although geothermal energy has been exploited for many decades in several countries, a clear and unique classification of geothermal systems has not been accepted worldwide, probably due to the strong variability of geological, geophysical and thermodynamic conditions. We can clearly distinguish

conventional and unconventional geothermal resources, based on the feasibility of the exploitation with current available technologies. Nowadays, the consolidated technologies require the withdrawal of a fluid (i.e. hydrothermal fluid) that efficiently transfers the heat from the underground to the surface; i.e. the conventional resources are found in the hydrothermal systems.

The genesis of geothermal systems can be related to various geological settings and it is challenging to frame the features of these processes in a standardized system.

In the past, many authors proposed a classification of geothermal systems and resources, based mainly on temperature (e.g. Muffler, 1979; Sanyal et al., 2005). Recently Moeck et al. (2014) proposed an alternative scheme to classify geothermal systems, in the frame of “Geothermal Plays”, based on geological characteristics. The “play” concept hails from the oil and gas exploration and corresponds to: “...*model in the mind of the geologist of how a number of geological factors might combine to produce petroleum accumulation in a specific stratigraphic level of a basin*” (Allen P.A. and Allen J.R., 2005). It is hard to import this concept to geothermal exploration due to the possible development of geothermal systems in many geodynamic settings with extremely various geological characteristics worldwide. On the other hand, we agree with Moeck (2014) on the need of a clear and widely accepted new catalogue of Geothermal Plays to support the geothermal exploration activities at least in their very first activities. Merging different opinion and scientific discussions during a recent workshop held by the International Geothermal Association (IGA) in Essen, Germany (IGA, 2013), it has been attempted to classify the Geothermal Plays as follows:

- Convective, volcanic field, divergent margins;
- Convective, volcanic field, convergent margins;
- Convective, Intrusive, extensional;
- Convective, Intrusive, convergent;
- Convective, Extensional domains fault controlled;
- Conductive, Intracratonic basin;
- Conductive, Foreland basin/orogenic belt;
- Conductive, Basement (igneous and metamorphic).

### 2.1.1 Chapter overview

This chapter is aimed to understand: *i)* the common features of Convective and Intrusive Plays since they host some of the most productive geothermal fields in the world, and *ii)* why the Larderello system, the focus in this thesis by EM geophysics, can be attributed to this type of plays. For a detailed description of the Larderello field the reader is referred to the *Part III* of the thesis.

Hereby, we present a critical review and discussion on the structural setting, the heat source and the reservoir characteristics of three important geothermal fields in exploitation since decades:

- Larderello (Italy);
- Mt. Amiata (Italy);
- The Geysers (USA).

We classify them as Convective and Intrusive Play types and we stress the similar geological features that could depict this type of play.

The Larderello and Mt. Amiata fields, both located in Tuscany (Italy), are two large convective geothermal systems with similarities but also many differences. Larderello is one of the few vapor-dominated systems worldwide, where the first geothermal power plant was installed in 1913. The Mt. Amiata geothermal area is located close to the homonymous extinct volcano (0.3-0.2 Ma) and is characterized by a liquid-dominated system. The Geysers field is located in California (USA) close to the Clear Lake volcanic field and is the most productive vapor-dominated geothermal system in the world, exploited since the 1960s.

In the debate regarding the classification and its indicators we argued that these prospective resources are hardly classified on the base of both tectonic setting and stratigraphic features and we proposed other criteria, which will be described.

## 2.2 Structural setting

### 2.2.1 Larderello and Mt. Amiata geothermal fields

The geothermal fields of Larderello and Mt. Amiata (southern Tuscany, Italy) are located in the inner part of the Northern Apennine, a sector of the Apennine

orogenic belt developed as a consequence of the Cenozoic collision between the European (Corso–Sardinian block) and the Adria plates (Boccaletti et al., 2011). The southern Tuscany is characterized by a shallow Moho discontinuity (20-25 km depth), a reduced lithosphere thickness due to uprising asthenosphere and the delamination of crustal lithosphere (Gianelli, 2008). Many authors proposed a tectonic evolution of Northern Apennine due to two main deformational processes: *i*) a first one related to eastward migrating compressional tectonics and *ii*) a subsequent extensional tectonics eastward migrating which affects the inner part of the orogenic belt since at least Early Miocene (Carmignani et al., 1994; Jolivet et al., 1998; Brogi, 2006 and reference therein). Alternative models were proposed to describe the tectonic evolution of inner Northern Apennine (Boccaletti et al., 1997; Bonini and Sani, 2002). These studies revealed a complex tectonic evolution during Miocene-Pleistocene with alternating compressive and extensional tectonics events but suggest a prevalent contribution of compressive tectonics till Pleistocene Epoch, in contrast with an uninterrupted regional extensional tectonics active since at least Early Miocene as suggested by other authors. After Pleistocene, southern Tuscany is characterized by active extensional tectonics as inferred by borehole breakout analysis (Montone et al., 2012). Considering Quaternary tectonics, recent studies suggested an important role of strike-slip faults and step-over zones controlling the magma emplacement in the inner Northern Apennine (Acocella et al., 2006) and in the Mt. Amiata area (Brogi and Fabbrini, 2009). Batini et al. (1985) presented a seismological study of Larderello area, showing an intense seismic activity of low magnitude, partially induced, that could be correlated with seismically active structures.

### **2.2.2 The Geysers geothermal field**

The Geysers-Clear Lake geothermal field is located in northern California, between the San Andreas fault system and the Coast Range thrust (Stanley and Rodriguez al., 1995). This region belongs to the California Coastal Ranges, and its geological features are a consequence of the eastward subduction of the Farallon oceanic plate underneath the North America continental plate since Late Mesozoic time. The tectonic evolution of the region is quite complex. The late Mesozoic subduction system along western North America was replaced, in the Eocene period, by the Mendocino Triple Junction that evolved in the San Andreas transform system (Stanley and Rodriguez, 1995).

The Geysers Geothermal field is located between NW trending right-lateral strike-slip faults that belong to the San Andreas Fault system and exhibits a normal and strike-slip faulting (Boyle et al., 2013). The analysis of seismicity (Oppenheimer, 1986; Boyle et al., 2013) indicates that most of the fault plane solutions show extensional and strike-slip component. However, above 1 km depth reverse component is present.

## 2.3 Heat source and thermal regime

### 2.3.1 Larderello and Mt. Amiata geothermal fields

The geodynamic setting and the magmatic activity produce a huge geothermal anomaly in southern Tuscany with maximum peaks centered in the Larderello and Mt. Amiata areas with values of heat flow up to 1000 mW/m<sup>2</sup> (Baldi et al., 1994). The heat source of Larderello and Mt. Amiata geothermal fields is related to shallow igneous intrusions belonging to the Tuscan Magmatic Province (TMP) according to many authors (see Gianelli, 2008 and references therein). Geophysical data (gravimetry, seismic reflection, seismology and MT) and thermal numerical modelling support the hypothesis of deep buried still molten igneous intrusions below the geothermal systems of southern Tuscany (Foley, 1992; Baldi et al., 1994; Batini et al., 1995; Bernabini et al., 1995; Gianelli et al., 1997; Manzella et al., 1998; Mongelli et al., 1998; Gianelli, 2008). Various models relate the genesis of this magmatic activity in the inner part of Northern Apennines to the west-dipping subduction, delamination and eastward rollback of the Adriatic lithosphere. Both the magmatism and the extensional tectonics migrated from West to East following the eastward migration of the collisional front. The Larderello intrusive bodies, cored in several deep wells, can be classified as two-mica granites ranging in composition from monzogranites to syeno-monzogranites, with ages ranging from 3.8 Ma to 1.3 Ma (Dini et al., 2005). Gianelli and Puxeddu (1994), summarized the geophysical evidence of the batholith beneath Larderello area: *i*) a Bouguer gravity low (20-25 mGal minimum peaks), *ii*) a thermal anomaly (heat flow values >120 mW/m<sup>2</sup>) over an area of 600 km<sup>2</sup>, *iii*) P-wave delays (up to 1 sec), *iv*) lack of hypocentres below 7-8 km and *v*) mineralogical evidence in a deep geothermal well (post-tectonic occurrence of corundum, sanidine and biotite-tourmaline level).

Mt. Amiata is a young (0.3-0.2 Ma) extinct volcano belonging to the TMP made up by trachytes, trachylatites and olivine-latites (Gianelli, 2008). The volcanic edifice hosts an important reservoir of cold and drinkable water and lay

over impermeable, clayey units. As for Larderello, the high-temperature hydrothermal circulation occurs in two deep-seated non volcanic reservoir. Major bodies of intrusive rocks were never crossed by deep wells in Mt. Amiata, but the heat source may be related to shallow intrusions inferred by geophysical data (Bernabini et al., 1995; Manzella et al., 1998; Finetti, 2006). This allows us to consider this geothermal play as intrusive.

### **2.3.2 The Geysers geothermal field**

The heat source of The Geysers geothermal field corresponds to a Quaternary pluton complex ( $>100 \text{ km}^3$ ) of batholithic dimension known as “felsite” that occurs only in the subsurface and is clearly affiliated geochemically and mineralogically with the Cobb Mountain volcanic centre of the Clear Lake volcanic field (Hulen and Nielson, 1996; Dalrymple et al., 1999). Movement of the Mendocino Triple Junction is widely believed to be the cause of northward migrating, late Tertiary and Quaternary volcanism in the California Coast Ranges (Stanley and Rodriguez, 1995). A slab window is assumed to favour asthenosphere upwelling and basic magmas emplacement that in turn have fractionated, melted or assimilated continental crust producing felsic magma (Hulen and Nielson, 1996). According to Dalrymple et al. (1999), the Geysers Plutonic Complex (GPC) crystallized at 1.18 Ma and suggests a further heat source, in addition to the intrusive mass of the GPC, to explain the observed thermal evolution of the complex. Based on deep wells data, Hulén and Nielson (1996) distinguished three type of rocks constituting the igneous body: *i*) granite, *ii*) microgranite porphyry and *iii*) late granodiorite. The presence of batholith is supported by: *i*) a Bouguer gravity low (-24 mGal minimum peaks), *ii*) a thermal anomaly with heat flow values greater than  $168 \text{ mW/m}^2$  over an area of  $750 \text{ km}^2$  and values in the range  $335\text{-}500 \text{ mW/m}^2$  over an area of  $75 \text{ km}^2$  centered on the field, *iii*) P-wave delays (up to 1 sec), *iv*) lack of hypocentres below 5-7 km depth and *v*) the occurrence of a thick aureole of biotite-tourmaline rich hornfels around the felsite (Walters and Combs, 1989; Gianelli and Puxeddu, 1994; Nielson and Moore, 2000 and reference therein).

Both the huge vapor-dominated reservoir and the upper portion of the “felsite” are oriented NW-SE, sub-parallel to the right-lateral San Andreas Fault and related wrench faults. In fact, Hulén and Norton (2000) considered the emplacement of the “felsite” possibly related to pull-apart extension. The presence of a batholith or multiple silicic magma chambers at depth are supported

by geophysical evidence, but a shallow intrusion cyclically replenished by new magma (at least each 500,000y) is required to keep the present-day heat-flow and thermal anomaly (Erkan et al., 2005).

## **2.4 Reservoir characteristics**

### **2.4.1 Larderello and Mt. Amiata geothermal fields**

There are differences and similarities between the Larderello and Mt. Amiata geothermal reservoirs. Both areas host two reservoirs, the shallow being hosted in sedimentary units and the deep in crystalline rocks. At Larderello superheated steam is present to depth over 3.5 km and with temperatures exceeding 350°C, whereas the deep reservoir of the Mt. Amiata geothermal fields is in two-phase (liquid+vapour mixture) state with temperatures of 300-350°C (Barelli et al., 2010). In the upper levels (shallow reservoir), the Larderello reservoir consists of several rock types: sandstone, marls, radiolarites, and, more commonly, Mesozoic micritic limestone and anhydrite dolostone. The deep reservoir consists of phyllite, micaschist, skarn, hornfelses and granite. Similar rocks form the reservoir of the Mt. Amiata geothermal field: Mesozoic limestone and anhydrite dolostone (shallow reservoir) and phyllite, quartzite and dolomitic marbles (deep reservoir) (Pandeli et al., 1988). Strong reflectors in the metamorphic complexes have been explained with rock fracturing and presence of fluids (Batini et al., 1983; Cameli et al., 1995). Gianelli and Bertini (1993) report the occurrence of a hydrothermal breccia at 1090 m depth and suggest that natural hydraulic fracturing could have been occurred within the system. Hydraulic fracturing may also be a present day mechanism of rock fracturing at Larderello. Also at Mt. Amiata, in the deep reservoir, the occurrence of hydrothermal breccias (Ruggieri et al., 2004), lead us to assume a similar process of permeability enhancement. Coupled with this process it is clear that faults and densely fractured zones play a fundamental role for the permeability of the reservoir, considering that primary permeability is extremely low. Barelli et al. (2010) highlights that the shallow and deep reservoirs of Mt. Amiata system are in piezometric equilibrium as pointed out by the hydrostatic pressure distribution. Thermal springs and diffuse gas discharge are abundant in both Larderello and Amiata geothermal fields and surrounding areas, with fierce manifestations in Larderello (Duchi et al., 1986; Minissale et al., 1991; Minissale et al., 1997; Frondini et al., 2009).

### **2.4.2 The Geysers geothermal field**

At The Geysers the geothermal fluids are hosted principally by highly deformed, late Mesozoic age, subduction-trench-related metasedimentary and meta-igneous rocks of the Franciscan complex. The system is disrupted by high-angle generally northwest-trending faults related to the still-active San Andreas fault and low- to moderate-angle thrust faults. The Franciscan rocks at The Geysers are intruded by a northwest-trending, Plio-Pleistocene, multi-phase, felsic pluton, which actually hosts a portion of the steam reservoir, and underwent further mineral recrystallization due to the intrusion and related fluids. The configurations of the felsite and reservoir coincide, strongly suggesting that the intrusion critically influenced steam-field evolution (Hulen and Nielson, 1993). The two reservoirs (shallow and deeper “High Temperature Zone”) produce steam at temperatures in the range 235-342°C at depth of approximately 500-2500 m b.g.l. and the permeability is mainly related to rock fractures. Recent experimental redrilling and deepening of an abandoned well were able to significantly increase the flow rate of a low permeability level at 3350 m depth and 400°C temperature, and, practically, create an EGS demonstration project into the High Temperature Zone (Garcia et al., 2012). Geothermal surface manifestation are widely diffused counting several thermal springs in the surrounding area (Donnelly-Nolan et al., 1993).

## **2.5 Discussion**

In our opinion a worldwide-accepted temperature-based classification of geothermal resources is needed, because it provides a quantitative evaluation of power production. On the other hand, in agreement with the definition of geothermal play of Moeck (2014), in the first stage of exploration it is useful to take into account a catalogue of plays based on geological features. But we argue: are geological features clear enough for characterizing favourable conditions for geothermal resources?

The comparison of the main geological conditions among the Larderello and Mt. Amiata (Italy), The Geysers (USA) geothermal fields, led us to identify common features that may characterize the Convective and Intrusive Play. The most important common feature of this type of Play is the effectiveness of the heat source represented by shallow plutonic intrusions, although nowadays for the Mt. Amiata field the magmatic contribution is only inferred, as it was inferred in

Larderello and The Geysers at the beginning. This is a crucial point and the term Intrusive for a play is not so immediate to apply. For example: recent acidic intrusions are considered to be the heat source of Larderello and Mt. Amiata geothermal systems (Bertini et al., 2006; Gianelli, 2008), whereas in the conceptual model of the Larderello geothermal area of Brogi et al. (2003, and references therein) the geothermal area is located in a “basin and range”-like structure, the magmatic contribution as heat source being minimized and depicting an overall scenario of a fault-controlled system.

The efficacy of the heat source is a leading issue. In fact, with regard to the Italian and American fields the available information nowadays endorses the effectiveness of buried intrusion older than 1 Ma. Mathematical models exclude the possibility that intrusions of any reasonable, even large, size can supply enough heat and are able to feed large geothermal systems for more than 1 Ma (Norton and Knight, 1977; Calore et al. 1981; Cathless and Erendi, 1997). A continuous magma, and therefore heat, feeding is therefore necessary to maintain a geothermal system of the size of Larderello or The Geysers. In our opinion, the term “Intrusive” should be accompanied by the term “Young”. We can define young an intrusion at least coeval, or younger than the last tectonic phase affecting the geothermal area and if isotopic dating is available it should be younger than approximately 1Ma.

The age of the magmatism is used also for the catalogue of geothermal play proposed by IGA and IFC (2014), which, however, lacks a clear distinction of volcanic and intrusive plays. In our opinion a system fed by young intrusions with the geothermal reservoir hosted into the associated volcanites has different features with respect to a “convective, intrusive” play, with reservoir hosted in sedimentary and crystalline units. The geothermal plays characterized by intrusions approximately older than 1 Ma and without evidence of partial melt in the upper crust could be included into a “amagmatic play”, to be eventually sub-classified. Geochemical data on surface manifestations should be considered for supporting the cataloguing activities because they provide useful information about the hypothesis of magmatic contribution helping in discriminating the intrusive and amagmatic systems.

Of course, large or composite batholiths are better heat source than small dikes or laccoliths, which cannot induce thermal anomaly for a long period of time. The volume of the intrusion, however, is not a good discriminating parameter, because during the exploration it is difficult to define its size. So, to

further distinguish the intrusive plays on the basis of the size of the intrusion is in our opinion of not practical use.

Another important issue is the convective heat transfer that implies the circulation of a thermovector fluid. This condition distinguishes the conventional system exploitable by the current technologies from the conductive unconventional geothermal systems that require engineering stimulation. The three geothermal systems, here considered, are classified as Convective since they show a wide and effective hydrothermal circulation, even complex, considering the presence of more than one reservoir for each field. In our analysis we could count on geophysical data and well logs for fields in operation. Considering an initial stage of exploration for a play, without geophysical data, it is difficult to assess the regime of heat transfer at depth. A preliminary indication could be provided by the number and type of geothermal manifestations in the surrounding areas. Surface manifestations (e.g. hot-springs and gas discharge) are common in the three fields of interest, disregarding the fluid phase in the reservoir (steam-dominated in Larderello and The Geysers and liquid-dominated in Amiata). In the considered cases, the low permeability layer acting as cap-rock is a low permeability sedimentary or crystalline unit, and the abundance and distribution of natural manifestations, as well as the hydraulic head of steam or brine, are strictly related to the depth of the reservoir and the faults and fractures regime.

Attempts at evaluating the steam fraction in geothermal reservoir have been proposed by D'Amore and Truesdell (1979) but its applications before drilling and during the geochemical survey of natural manifestation is problematic. In any case the presence of steam phase is not a discrimination for intrusive or a fault-controlled geothermal systems. For example Mt. Amiata is an intrusive geothermal system with liquid-dominated reservoirs.

The comparison of these fields drove us to exclude lithological and stratigraphic conditions as key parameters to classify the plays. A geothermal reservoir can be hosted in various typologies of sedimentary and crystalline rocks. What really matters is the rock permeability.

What makes things even more complex is the geodynamic and structural setting, which may spatially vary in stress regime (from compressive to extensional or strike slip) and in time (polyphasic tectonic). In areas rich of data such as those we analysed the tectonic evolution is still under debate in the

scientific community. We have shown that Larderello and Mt. Amiata are located in the inner sector of an active orogenic belt that undergone extensional tectonic since Miocene or Pleistocene (non univocal consensus about timing) and some authors suggested the importance of recent strike-slip faults during the emplacement of plutons that represent the heat source.

The main elements in common in the three fields, which we used for the classification are the hydrothermal circulation and the known or inferred plutonic heat source respectively identifying the convective and intrusive terms. We observe that there are two other common parameters in the four areas: *i*) relevant seismic activity and *ii*) high heat flow. It is known that geothermal fields are common in tectonically active areas and earthquake swarms could be associated to areas of recent volcanic or geothermal activity (Sibson, 1996). The heat flow values depict huge thermal anomalies in the surrounding areas of the Larderello, Mt. Amiata, and The Geysers fields with maximum values centred on the field in exploitation.

## **2.6 Summary**

We compared the main geological features of Larderello, Mt. Amiata and The Geysers geothermal fields in order to describe the common elements that could be useful for the classification of Geothermal Plays based on the terminology proposed for the IGA Workshop held in Essen, Germany (IGA, 2013). We classified these fields as Convective and Intrusive Plays. The first term would indicate the presence of a reservoir suitable for economically exploitation with current technologies without engineering stimulation. The Intrusive term is correlated with the plutonic heat source that feeds wide and highly productive geothermal systems. We do not adhere to the proposal to split this play in different kinds, depending on the tectonic setting. Considering that a play should be defined in an unambiguous way, and should help in classifying resources and planning exploration decisions, we conclude that recognized resources, such as those we analysed, and even more so the prospective resources, can hardly be classified on the base of tectonic setting. We explained that geodynamic and structural setting are still debated in such well known fields, and a tectonics-based classification of Geothermal Plays couldn't simplify the exploration planning. The structural survey remains a milestone in a geothermal exploration project to understand tectonics evolution and to assess the faults and fractures systems that

control hydrothermal circulation. Indeed, tectonic processes are of main importance in the genesis and evolution of a geothermal system.

With regard to the classification of Geothermal Plays we suggest to simplify the classification of the Convective Plays distinguishing Volcanic, Young Intrusive and Amagmatic. The role of the tectonic settings is reduced for our classification purposes, which can be subjective and therefore leading to ambiguous conceptual models. Beside highlighting the importance of geochemical data for inferring magmatic heat source, we identify two more features that are common in the four field: *i)* they are seismically active and *ii)* they show high heat flow values and wide thermal anomalies. These features might be used for a sub-classification.

## Chapter 3

# The role of electrical resistivity in the geothermal exploration

### 3.1 Introduction

The geothermal resources can be regarded as part of very complex systems where different physical and chemical processes continuously and simultaneously occur.

Considering the hydrothermal systems, which are the conventionally exploited systems, the main constituting elements are (figure 3.1): *i*) a heat source represented by a recent magmatic intrusion or high heat flow due to particularly geodynamic settings, *ii*) a reservoir hosting the hydrothermal circulation and usually characterized by secondary permeability due to faults and fractures and *iii*) the cap-rock, an impermeable volume of rocks that avoids the dissipation of heat on surface.

The indirect estimation of physical parameters of a geothermal system is the aim of the geophysical exploration, but in such complexity the interpretation of data is quite difficult. The role of the electrical resistivity is of primary importance, although considering the integration of different dataset the best practice for modelling this complexity. The electromagnetic (EM) methods play a fundamental role in the geothermal exploration due to the particular sensitivity of the subsurface electrical resistivity to hydrothermal circulation, thermal regime and rocks alteration. Many papers have been published on the study of geothermal

areas by EM methods worldwide (Meju, 2002; Spichak and Manzella, 2009; Muñoz, 2014 and references therein). In this chapter, the main factors controlling the electrical resistivity of the system are briefly introduced.

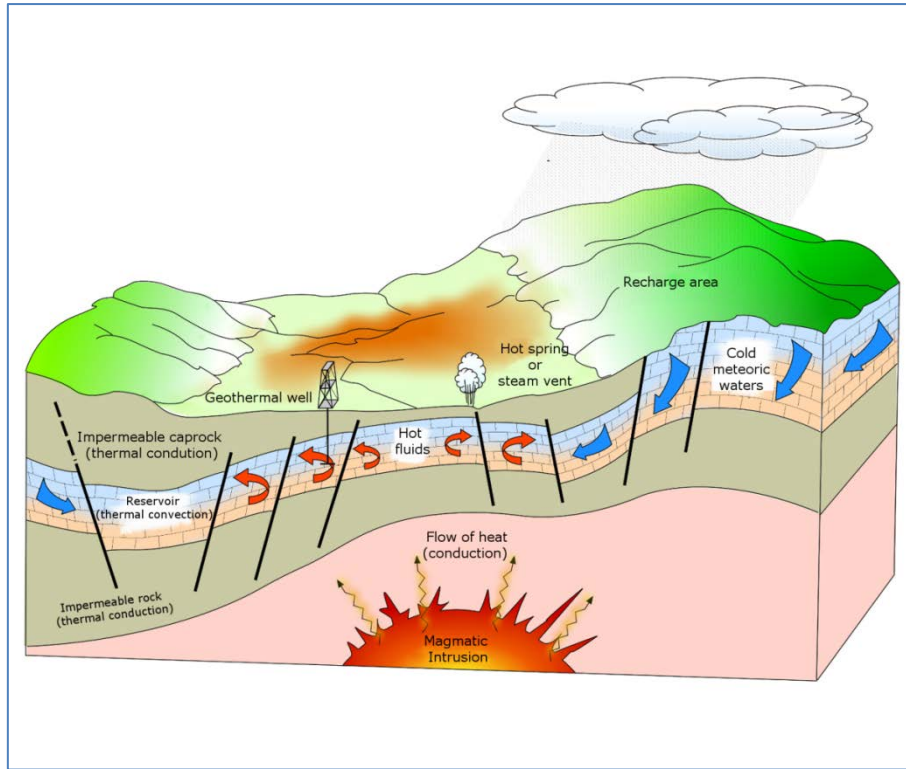


Figure 3.1- Conceptual model of a geothermal system (from Dickson and Fanelli, 2004).

### 3.2 Electrical resistivity of Earth's materials

Detailed reviews on the electrical properties of the Earth's material are given in several papers (e.g. Olhoeft, 1981a, Telford et al., 1990; Zhdanov and Keller, 1994; Evans, 2012; Karato and Wang, 2013)

The electrical resistivity (hereafter also resistivity)  $\rho$  ( $\Omega\text{m}$ ) is the property that quantify how the medium opposes the flow of electrical currents. Considering a solid of length  $L(\text{m})$  and section  $A(\text{m}^2)$  (Telford et al., 1990):

$$\rho = \frac{RA}{L} \quad [\text{Eq.3.1}]$$

$$R = \frac{V}{I} \quad [\text{Eq.3.2}]$$

where  $R$  ( $\Omega$ ) is the resistance,  $V$ (V) the voltage and  $I$  (A) is the electric current. The electrical conductivity (hereafter also conductivity) is the reciprocal of resistivity ( $\sigma=1/\rho$ ).

The conduction processes in the Earth are referred mainly to the transport of different charge carriers such as (Evans, 2012): *i*) electrons, *ii*) electron “holes” and *iii*) ions. The electronic conduction for free electrons occurs in metals that are characterized by very high conductivity in the order of  $10^8$  S/m (Table 3.1). However, such process of electronic conduction occurs also in the graphite mineral, producing very low resistivity similar to those of metals. The occurrence of metals and graphite, depending upon the interconnection grade, strongly influence the bulk resistivity of a rock systems composed of several components.

The conductivity in the Earth is in the range of many orders of magnitude. The indirect imaging of the resistivity distribution by EM methods can lead to interpret the variations in terms of certain geological, geophysical and geochemical conditions, useful for geothermal exploration. Most of the minerals in the Earth behave like semiconductors (or insulator), with the conduction due to point defects in the crystal lattice that allow mobile charged particles (Karato and Wang, 2013). This process is strongly dependent upon temperature, pressure and oxygen fugacity (Evans, 2012). The most common minerals and rocks show very high resistivity, e.g. Quartz, Calcite, Anhydrite, Granite etc. (Table 3.1).

Some important minerals are generally connected to hydrothermal and metasomatic processes characterized by very low resistivity such as Pyrite. The role of these ore minerals can dramatically influence the bulk resistivity of the rock system and can be index of active hydrothermal process or fossil epithermal deposits.

Table 3.1-Values of resistivity for few examples of elements, minerals and rocks.

<b>Material</b>	<b>Resistivity (<math>\Omega\text{m}</math>)</b>
<b>Aluminium*</b>	$2,5 \cdot 10^{-8}$
<b>Copper*</b>	1,2 to $30 \cdot 10^{-8}$
<b>Iron*</b>	$9 \cdot 10^{-8}$
<b>Silver*</b>	$1,5 \cdot 10^{-8}$
<b>Graphite*</b>	$>28 \cdot 10^{-8}$
<b>Pyrite**</b>	$2,9 \cdot 10^{-5}$ to 1,5
<b>Chalcopyrite**</b>	$1,2 \cdot 10^{-5}$ to 0,3
<b>Quartz**</b>	$4 \cdot 10^{10}$ to $2 \cdot 10^{14}$
<b>Calcite**</b>	$2 \cdot 10^{12}$
<b>Rock salt**</b>	30 to $10^{13}$
<b>Mica**</b>	$9 \cdot 10^2$ to $10^{14}$
<b>Biotite**</b>	$2 \cdot 10^2$ to $10^6$
<b>Anhydrite**</b>	$10^9$
<b>Graphitic slate**</b>	0,3
<b>Granite**</b>	$4,5 \cdot 10^3$ (wet) to $1,3 \cdot 10^6$ (dry)
<b>Clays**</b>	1 to 100
<b>Sea water**</b>	0,2
<b>Saline waters (20%)**</b>	0,05
<b>Meteoric waters**</b>	30 to $10^3$

source from \* Zhdanov and Keller, 1994; \*\* source from Telford et al., 1990

Different mineral assemblages and lithologies produce a large variation of resistivity, as depicted in figure 3.2.

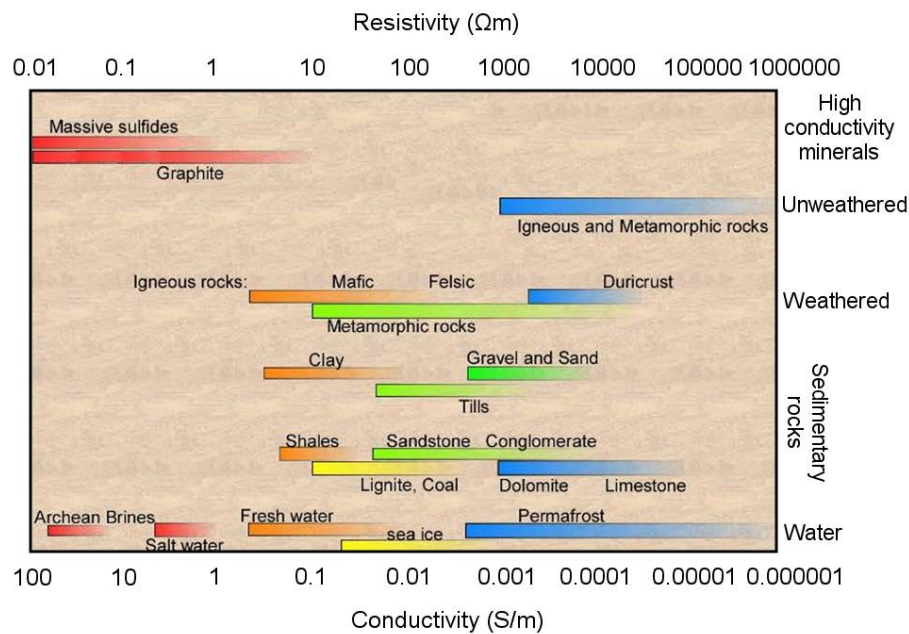


Figure 3.2- Resistivity (and electrical conductivity) ranges for Earth's material (modified from Palacky, 1987 and Miensopust, 2010).

On the other hand, the electrolytic conduction is of main importance considering that the transfer of ions in fluids circulating in the pores and fractures of rocks strongly controls the bulk resistivity values. Indeed, in the Earth a common situation is the occurrence of a two-phase system with a high resistive solid phase and a relative conductive fluid phase.

A particular conduction process, called "Surface Conduction", occurs in the fluid/grain interface, where additional charge carriers are able to conduct electricity (for details see Revil and Glover, 1998). This process is intense in clay minerals, commonly part of alteration assemblages in geothermal areas, depending also on their CEC (Cation Exchange Capacity).

### 3.3 The role of mineralogy

Hereby we highlight the fundamental role of mineralogy in the electrical resistivity of geothermal system, comparable for importance with that of circulating fluids. The magmatic and/or hydrothermal activity in geothermal field are coupled with a more or less intense rock alteration with mineral parageneses that should be taken into account for the interpretation of bulk resistivity.

For a detailed review of the hydrothermal systems and mineral processes the reader is referred to Pirajno (2009). The author described the main ore deposits type. The most common in geothermal environment are the intrusion-related such as Epithermal and Porphyry deposits. Porphyry ore systems originate from high-temperature magmatic-hydrothermal fluids.

The Epithermal systems were firstly defined by Lindgren (1933) as: *“Metalliferous deposits formed near the surface by ascending thermal waters and in genetic connection with igneous rocks”*. Pirajno (2009) considered epithermal the deposits originated at low temperature (50-300°C) and low pressure from fluids of meteoric origin with minor magmatic components, distinguishing also fossil (ancient geothermal systems) and active (active geothermal systems). The hydrothermal alteration is a complex process of water-rocks interaction that causes mineralogical, chemical and textural changes. A great variety of alternation mineral assemblages can be present as function of temperature and chemical composition of the fluids and the nature of the host rocks. The concept of hydrothermal alteration zones is quite important with typical mineral assemblages as function of temperature and chemical conditions (figure 3.3). Their imaging (also by resistivity) can provide information on the thermometry of the hydrothermal circulation (active or fossil). It should be noted that these deposits remain (more or less) stable also when the thermal regime changes (in term of cooled fossil systems) and the direct relation with active circulation is misleading.

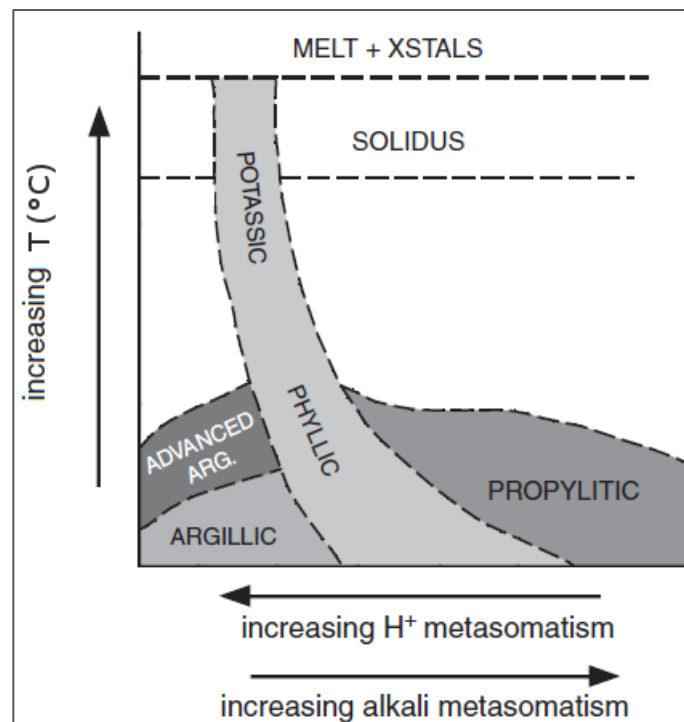


Figure 3.3- Schematic hydrothermal alteration zones as function of temperature and alkali or Hydrogen activity (modified from Pirajno, 2009).

In volcanic setting, where the metasomatism of the fluids is very high, the well defined electrical resistivity of hydrothermal alteration zones was used in the years for targeting hydrothermal reservoir. Indeed, the Argillic alterations (e.g. Kaolinite, Illite-Smectite, Pyrite etc.) usually originates at low temperatures and shallow depth, causing a low permeability zones that prevent the dissipation of heat and fluids. This zones correspond to the cap-rock generated for “self-sealing” process. These secondary clays and sulphides minerals provide very low electrical resistivity. With the increase of temperature at depth, other typical assemblages such as Phyllic (e.g. Sericite, Quartz, Pyrite etc.) and Propylitic (Epidote, Chlorite, Apatite etc.) are usually recognized with relative higher resistivity. The permeability in the latter zone is not completely reduced and the high temperature circulation can be present. In figure 3.4 the schematic hydrothermal alteration profile of Iceland system is given. It is shown that a shallow clayey, electrically conductive zone overlay a more resistive core (epidote-chlorite) characterized also by pore fluids circulation.

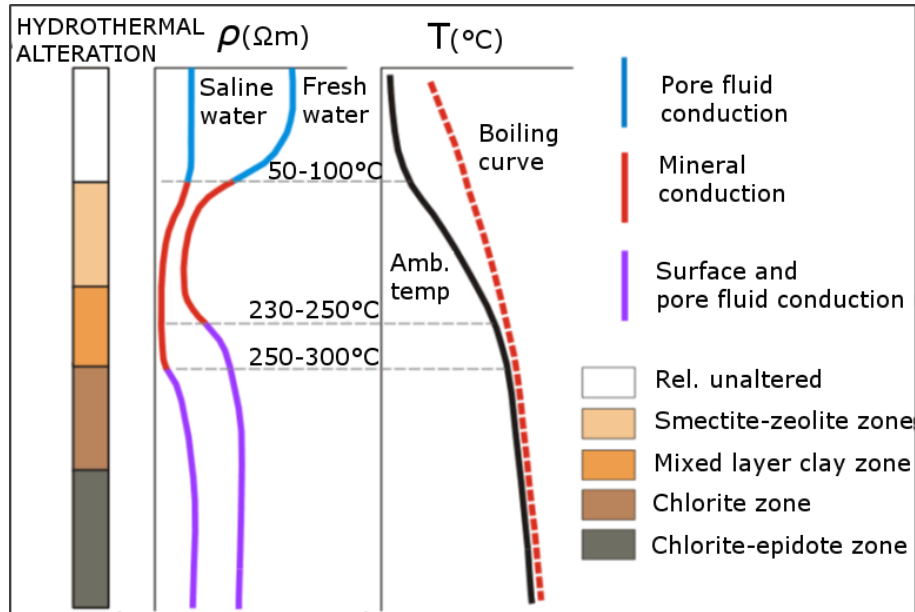


Figure 3.4- Schematic profile of the geothermal systems in Iceland in terms of temperature, resistivity and hydrothermal alteration (from Flovenz et al., 2005 as modified by Hersir and Árnason, 2010).

### 3.4 The role of temperature

Different authors studied the role of temperature in the resistivity of geothermal system (e.g. Flóvenz et al., 1985; Kummerow and Raab, 2015). The temperature influences both the electrolytic conduction and the resistivity of the solid matrix. There is an inverse proportionality between the temperature and the resistivity of the circulating fluid thus contributing to the reduction (in case of higher temperature) of the bulk resistivity of the rocks. It should be noted that melt fraction related to high temperature conditions reduce the bulk resistivity.

The temperature dependence of the resistivity of the solid phase (rock matrix) are given by the Arrhenius relation (as described in Caldwell et al., 1986):

$$\rho = \rho_0 e^{E/kT} \quad [\text{Eq.3.3}]$$

where  $\rho_0$  is the resistivity at theoretical infinite temperature,  $E$  is the activation energy for the conduction process,  $k$  is the Boltzmann's constant and  $T$  is the

temperature. We report, as example in figure 3.5, the resistivity values for dry and wet granite as function of temperature (from Olhoeft, 1981b). The role of temperature is quite important but the occurrence of a fluid phase reduces the resistivity of orders of magnitudes also at low temperatures.

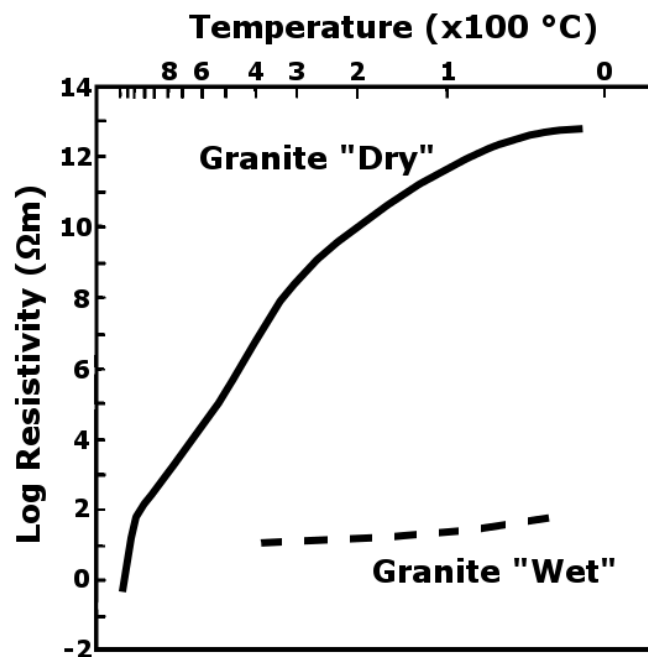


Figure 3.5- Resistivity of dry and wet granite as function of temperature after experimental analyses by Olhoeft, 1981b (modified picture).

## 3.5 The role of multiple phase systems

As commonly occurring in the Earth, the bulk conductivity of the rock is related to the contribution of different phases. In geothermal environment two most common cases occur (Evans, 2012): *i*) solid matrix with hydrothermal fluids circulating in pores and fractures and *ii*) solid matrix with partial melt.

### 3.5.1 Aqueous fluids

The occurrence of water at liquid phase circulating in the rocks dominates the bulk resistivity. As previously introduced, the geothermal energy production by conventional technology implies necessarily the extraction of the hot fluids from a

reservoir; i.e. the hydrothermal circulation represents the target of the geothermal exploration.

The main factors affecting the electrical behaviour of this rock system are:

- Resistivity of the fluid phase, strongly controlled by its salinity and temperature;
- Mineralogy of the solid matrix and occurrence of clay minerals;
- Porosity (and permeability);
- Pressure;
- Saturation.

The conduction in this case is mainly due to the ions that are free to move in the solution. Therefore, the resistivity of the fluid is fundamental as well as its phase. For example, vapour-bearing strata theoretically can show high resistivity due to the extremely low conductivity of the vapour. Instead, if we consider a liquid phase, the higher is the salinity, the higher is the ions concentrations and the lower is the resistivity.

A pioneering study on the relation of the factors controlling the bulk resistivity  $\rho$  was provided by Archie (1942) in terms of electrical conductivity of fluid, saturation and porosity.

$$\rho = a \rho_w \Phi^n S_w^m \quad [\text{Eq.3.4}]$$

where  $\rho_w$  is the resistivity of the water,  $\Phi$  is the porosity,  $S_w$  is the saturation;  $a$ ,  $m$  and  $n$  are empiric constants. Further modifications were proposed in literature considering a more complex system. Waxman and Smith (1968) proposed a model taking into account also the term of surface conduction related to the amount of clays in the rock (in sand formation) affecting the bulk conductivity  $\sigma_b$ :

$$\sigma_b = \frac{1}{F} (\sigma_e + \sigma_w) \quad [\text{Eq.3.5}]$$

where  $F$  is the shaly-sand formation factor, and  $\sigma_e$  and  $\sigma_w$  are the specific conductances related to the clays and the aqueous solution, respectively.

In Caldwell et al. (1986 and reference therein), based on the model by Waxman and Smith (1968), the following equation is proposed for computing the bulk resistivity  $\rho$ , in geothermal prospects:

$$\rho = \rho_w \Phi^n S_w^m (1 + kC\rho_w)^{-1} \quad [\text{Eq.3.6}]$$

$C$  is the proportion of clay minerals and  $k$  is a constant depending on the clay mineralogy. In consideration of the specific purpose of geothermal exploration, the abundance of alteration clayey minerals (and other high conductive minerals), is an aspect to be considered in geothermal areas. A modified Archie's law that considers  $n$ -phases (e.g. solid matrix, fluid, clay and sulfides) were proposed by Glover et al. (2010).

The high temperatures of the hydrothermal fluids coupled with particular chemical-physical conditions favour the water-rocks interaction contributing to increase the salinity of the circulating fluids. These fluids differ in terms of resistivity with respect to freshwater that in a geothermal system are found in recharge area (i.e. low temperature sector). The possibility to distinguish hydrothermal circulation, dry zones and recharge areas is fundamental for reducing the mining risk. The figure 3.5 points out the magnitude of the resistivity decrease for dry or wet granite. In figure 3.6 (Ussher et al., 2000) we show the bulk resistivity of a rock as function of porosity and temperature using the Archie's Law.

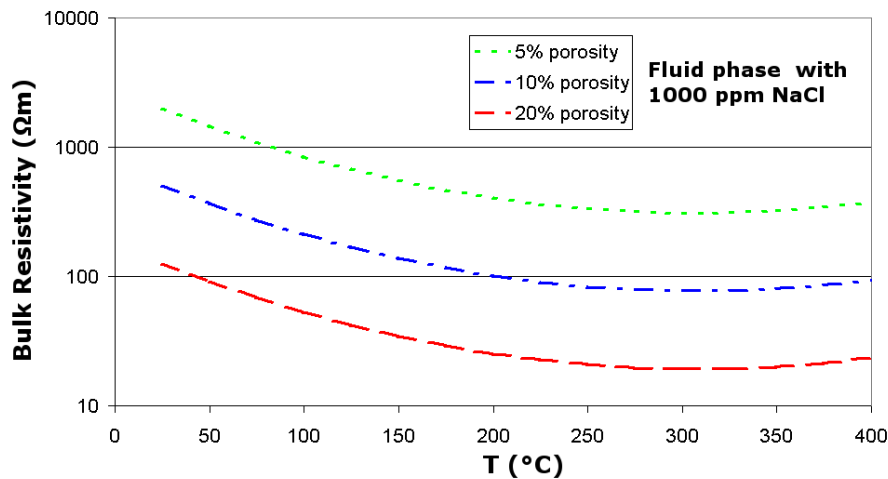


Figure 3.6- Bulk resistivities (using Archie's Law) for a two-phase mixing model with "clean" rocks and a brine fluid phase containing 1000 ppm of NaCl (from Ussher et al., 2000).

### 3.5.2 Melt

The role of the electrical conductivity of melts have been studied by several authors in relation to low resistive anomalies at level of Mid and Lower Crust and Mantle (e.g. Jödicke et al., 2006; Wannamaker et al., 2008; Pommier et al., 2010). The conductivity of silicate liquids ranges from  $10^{-2}$  to  $10^1$  (S/m) (Gaillard et al., 2005 and reference therein), as function of physical and chemical properties (Pommier and Le-Trong, 2011) such as temperature, pressure, water content and composition (e.g.  $\text{SiO}_2$  and  $\text{Na}_2\text{O}$ ). Being order of magnitude higher than the conductivity of the solid phase, the melts strongly influence the bulk resistivity of the rocks in a two-phase system. Given the conductivity of liquid and solid phases, the role played by melt fraction and grade of interconnection is fundamental. The theoretical basis of the electrical conductivity in partially molten rocks were treated in Waff (1974) with a focus on the statistical model of liquid connectivity in Schmeling (1986a).

In literature many two-phase mixing models were proposed based on particular geometries. For example, the modified Archie's law from Glover et al., (2000), the HS-bound model (Hashin and Shtrikman, 1962) and the wetted (Film) grain and cubes models (Waff, 1974) are commonly used.

We report the simple formula for computing the bulk conductivity of a two-phase system that considers the geometry of the melts connection as equally spaced tubes (from Schmeling, 1986b and reference therein):

$$\sigma_b = \frac{1}{3} \beta \sigma_l + (1 - \beta) \sigma_s \quad [\text{Eq.3.7}]$$

where the bulk conductivity is function of the melt fraction  $\beta$  and the conductivity of the melt  $\sigma_l$  and solidus  $\sigma_s$ . The role of the melt fraction is graphically explained in figure 3.7.

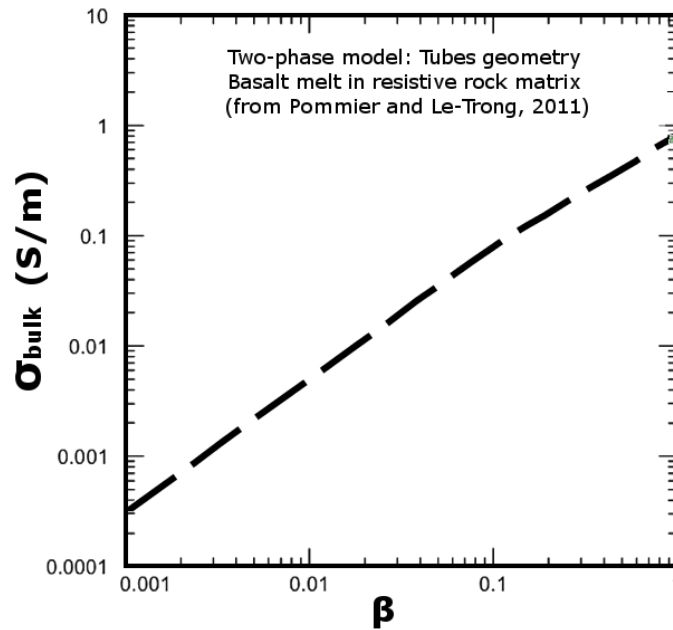


Figure 3.7- Two-phase mixing model with tubes geometry for an ideal basaltic melt (water 6%, 20 MPa,  $\sim 1300$  °C) in a resistive ( $2000 \Omega\text{m}$ ) rock matrix, from Pommier and Le-Trong (2011). The bulk conductivity is plotted as function of the fraction melt  $\beta$ .

It should be noted that very useful tools were implemented in the web-based software SIGMELTS, published by Pommier and Le-Trong, (2011), for obtaining information on the electric properties of partially melted systems with a focus on EM geophysics applications.

### 3.6 The role of pressure

Early studies on the role of pressure by Brace et al. (1965) and Brace and Orange (1968) described the increment of electrical resistivity for higher pressure in crystalline rocks, similar to other observation on clastic rocks. This response is mainly due to the reduction of the porosity (figure 3.8).

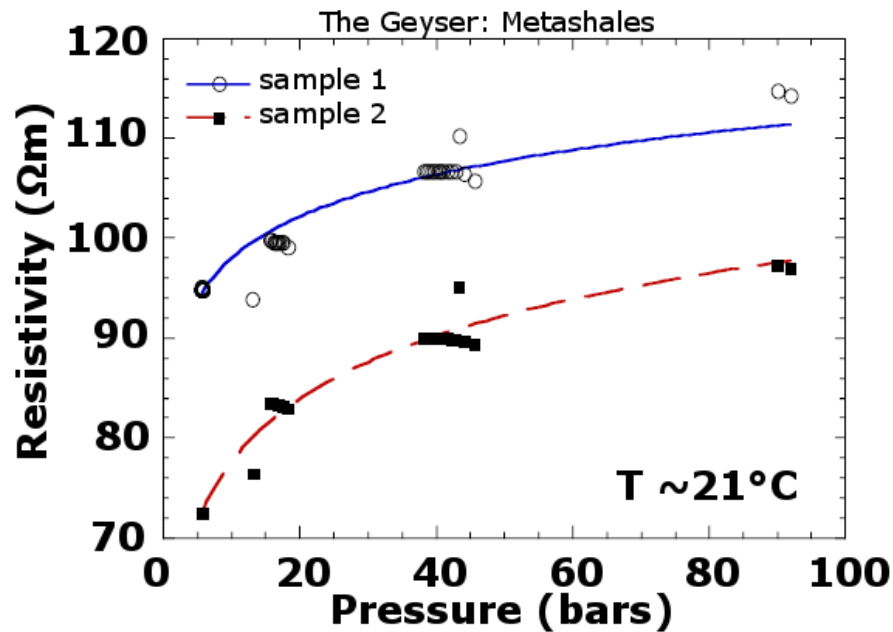


Figure 3.8- Resistivity as function of pressure for metashales samples from The Geyser geothermal field (modified from Al Duba et al., 1997).

The role of pressure is usually less considered in the contribution of the bulk resistivity of a rock systems, due to much stronger control of the properties of fluids and mineralogy. In some particular situations the pressure conditions are of primary importance, related also to geothermal systems. We refer for example to the unconventional geothermal resources in the context of geopressed systems. Briefly, the geopressed resources are suitable for trigeneration of power from: *i*) kinetic energy (well-head overpressure), *ii*) thermal energy (stored in the water) and *iii*) chemical energy (hydrocarbons combustion). The geopressed systems commonly occur in siliciclastic sedimentary basins as those of the Gulf of Mexico. Here, the target is the “Hard geopressed zones” in sandstones (gradient of 0.7 Psi/ft; i.e. about 1.6 Bar/10m) that are well imaged by geophysical measurements for the increase of electrical resistivity (Loucks et al., 1981).

Regarding the high temperature geothermal fields, we highlight the role of pressure reduction in phase changes of hydrothermal fluids. As previously mentioned, considering an aqueous solution the liquid phase usually provides the decrease of bulk resistivity; conversely, it is increased for vapour phase. The possibility to image steam-rich from water-filled zones is of help in geothermal exploration and monitoring (Al Duba et al., 1997; Roberts et al., 2002).

### **3.7 Additional remarks**

The fundamental role of the electrical resistivity in geothermal exploration relies on the fact that the factors controlling the bulk values of this parameter are strictly related to the characteristics of the main constituting elements of a geothermal system. The distribution of electrical resistivity at depth in geothermal systems is really complex and a unique relation between resistivity anomalies and hydrothermal fluid circulation cannot be established. For instance, beside hydrothermal fluids, also self-sealing, mineral alteration processes and metalliferous ore deposits can provide very low resistivity structures in these systems. The conceptual model for Iceland is valid for the geothermal exploration of certain geothermal plays (e.g. volcanic), but in other areas is quite different: for example in the Mt. Amiata play. Volpi et al. 2003 demonstrated that the low resistivity anomalies, in carbonate and crystalline rocks, are related to the hydrothermal circulation zones in the water dominated geothermal reservoir (see Section 4.7).

## Chapter 4

# Magnetotelluric (MT) and Time Domain EM (TDEM) methods: Theoretical Background

### 4.1 Introduction on the MT method

The Magnetotelluric (MT) is a geophysical electromagnetic (EM) passive method for determining the subsurface electrical resistivity from the near-surface to hundreds kilometres deep by measuring the natural magnetic and electrical fields on the Earth's surface. The method is commonly used for Earth-resources exploration and studies on the Earth's Crust and Mantle.

The theory has been proposed for the first time in the 50's simultaneously in different countries by Tikhonov (1950) in the USSR, Cagniard (1953) in France, Kato, Kikuchi (1950a,b) and Rikitake (1951) in Japan as cited by Chave and Jones (2012). Impressive scientific researches have been conducted in these decades contributing to the improvement of the methodology, that is nowadays of interest for scientific and industrial purposes. Detailed descriptions of the theory of the MT method as well as of the best practices for data acquisition and analysis, were recent published in exhaustive books by Simpson and Bahr (2005), Berdichevsky and Dmitriev (2008), Zhdanov (2009) and Chave and Jones (2012), on which the following theoretical background is mainly based.

Furthermore, the Magnetotelluric scientific community is used to meet since 1972 each two years for the “EM Induction Workshops”, where invited review papers are presented and published in important scientific Journals. The reader is referred to the complete list of these reviews, available at the MTnet (website), that greatly depict the ongoing scientific innovations.

## 4.2 Basic theory and assumptions behind the method

The most important physical assumptions behind Magnetotellurics are hereby listed as summarized in Simpson and Bahr (2005):

- Maxwell’s equations are obeyed;
- The Earth does not generate electromagnetic energy, but only dissipates or absorbs it;
- All fields may be treated as conservative and analytic away from their sources;
- The natural occurring EM source fields utilised in MT may be treated as uniform, plane-polarised waves with a near-vertical incidence angle on Earth surface (at least at mid-latitudes);
- No accumulation of free charges is expected in a 1D layered Earth. In a multi-dimensional Earth, charges can accumulate along discontinuities causing galvanic phenomena;
- The Earth acts as an ohmic conductor;
- Quasi-static approximation; i.e. time-varying displacement currents are negligible compared with time-varying conduction currents. This issue is really important because allows the treatment of EM induction in the Earth purely as a diffusion process;
- The variation in the electrical permittivities and magnetic permeabilities of rocks is assumed negligible compared with variations in bulk rock conductivities.

Magnetotellurics is a passive method in the sense that the energy source corresponds to the natural time-varying electromagnetic waves generated in the atmosphere and magnetosphere by different physical processes. The high frequency signal ( $> 1$  Hz) is generated by distant lightning storms that propagate in the Earth’s ionosphere. The low frequency signal ( $< 1$ Hz) is generated by the interaction between the Earth’s magnetosphere and the solar wind plasma (Garcia and Jones, 2002). The currents above the Earth’s surface are the primary sources,

while the Earth acts as a secondary source due to the currents induced in the conducting ground (Viljanen, 2012). The total field measured at the surface is influenced by the Earth's resistivity structure.

The well known Maxwell's equations (1861, 1865) mathematically represent the fundamentals of electricity and magnetism and their relations, as follow in the differential form (with notation from Chave and Weidelt, 2012):

$$\nabla \cdot \mathbf{D} = \rho_e \quad [\text{Eq.4.1}]$$

$$\nabla \cdot \mathbf{B} = 0 \quad [\text{Eq.4.2}]$$

$$\nabla \times \mathbf{E} = - \frac{\partial \mathbf{B}}{\partial t} \quad [\text{Eq.4.3}]$$

$$\nabla \times \mathbf{H} = \mathbf{J} + \frac{\partial \mathbf{D}}{\partial t} \quad [\text{Eq.4.4}]$$

where  $\mathbf{D}$  is the electric displacement,  $\mathbf{B}$  is the magnetic induction,  $\mathbf{E}$  is the electrical field,  $\mathbf{J}$  is the electric current density,  $\mathbf{H}$  is the magnetic field and  $\rho_e$  is the electric charge density. The Gauss's law for electricity (Eq.4.1) describes the behaviour of the electric field around electric charges. The amount of charge inside a volume is equal to the electric displacement through the closed surface of that volume and the divergence is non-zero. The Gauss's law for magnetism (Eq.4.2) states that the divergence of the magnetic induction is zero through a volume, that is source-free and that the monopoles do not exist. The Faraday's law (Eq.4.3) describes the coupling of an induced electric field in a closed loop due to a time varying magnetic field. Finally, the Ampere's Law (Eq.4.4) describes the magnetic fields produced by the vector sum of electric currents and time-varying electric fields.

### 4.2.1 EM induction

We can describe the propagation of EM fields into conductive media through the electromagnetic diffusion. The behaviour is mathematical and physical treated in Zhdanov (2009); hereby a brief summary is reported. Firstly, we recall the diffusion equations, as follow:

$$\nabla^2 \mathbf{E} - \mu\sigma \frac{\partial \mathbf{E}}{\partial t} = 0 \quad [\text{Eq.4.5}]$$

$$\nabla^2 \mathbf{H} - \mu\sigma \frac{\partial \mathbf{H}}{\partial t} = 0 \quad [\text{Eq.4.6}]$$

where  $\sigma$  is the electrical conductivity of the medium and  $\mu$  is the magnetic permeability. Let introduce an important parameter, the complex wave number  $k$ :

$$k = \sqrt{i\omega\mu_0\sigma} \quad [\text{Eq.4.7}]$$

with  $\omega$  the angular frequency,  $\mu_0$  the magnetic permeability of free-space. The wave number of a medium is quite important in determining the behaviour of a EM field in the medium. This notation is valid for the frequencies we deal with MT as diffusion propagation. At higher frequencies an additional term related to the displacement currents is dominant and the propagation is by radiation (for details see Zhadanov and Keller, 1994). Considering a very simple problem of the propagation of planar EM waves in a homogeneous medium, we have first of all the following condition:

$$\frac{\partial \mathbf{E}}{\partial x} \equiv \frac{\partial \mathbf{E}}{\partial y} \equiv \frac{\partial \mathbf{H}}{\partial x} \equiv \frac{\partial \mathbf{H}}{\partial y} \equiv 0 \quad [\text{Eq.4.8}]$$

with the fields attenuating in the  $z$  direction. The general solutions of the *one-dimensional Helmholtz equations* are:

$$H = H^+ e^{ikz} + H^- e^{-ikz} \quad [\text{Eq.4.9}]$$

$$E = E^+ e^{ikz} + E^- e^{-ikz} \quad [\text{Eq.4.10}]$$

with  $H^{+-}$  and  $E^{+-}$  arbitrary constant vectors.

At the frequencies used in Magnetotellurics, the electromagnetic fields are governed by a diffusion equation. In a uniformly conducting medium, the skin depth is considered the distance over which the electromagnetic field decays by  $1/e \approx 0.37$ , and is given by:

$$\partial_{sd} = 503 (\rho T)^{0.5} \quad [\text{Eq.4.11}]$$

Considering the case of travelling plane EM waves, vertically incident, into a flat  $N$ -layered Earth, with uniform  $\sigma$  in each  $j^{\text{th}}$ -layer we have:

$$\mathbf{H}_x(z) = -\frac{k_j}{\omega\mu_0} (E_{Yj}^+ e^{ik_j z} - E_{Yj}^- e^{-ik_j z}) \quad [\text{Eq.4.12}]$$

$$\mathbf{H}_y(z) = \frac{k_j}{\omega\mu_0} (E_{Xj}^+ e^{ik_j z} - E_{Xj}^- e^{-ik_j z}) \quad [\text{Eq.4.13}]$$

### 4.2.2 Transfer function, apparent resistivity and phase

The MT transfer function represents the frequency-domain relationship between observed electric and magnetic time series. In order to retrieve information on the electrical resistivity of the investigated Earth, the MT transfer function is to be estimated.

The fundamental parameter in the MT method is the electrical impedance, the ratio of the measured electric and magnetic orthogonal fields measured on the Earth's surface, in the form of a complex second-rank tensor  $\mathbf{Z}$  (frequency-dependent):

$$\mathbf{E} = \mathbf{Z} \mathbf{H} \quad [\text{Eq.4.14}]$$

$$\begin{pmatrix} E_x \\ E_y \end{pmatrix} = \begin{pmatrix} Z_{xx} & Z_{xy} \\ Z_{yx} & Z_{yy} \end{pmatrix} \begin{pmatrix} H_x \\ H_y \end{pmatrix} \quad [\text{Eq.4.15}]$$

For mathematical details on the transfer function we refer the reader to the concept of Schmucker–Weidelt transfer function (Weidelt, 1972; Schmucker, 1973). The observed tensor is dependent on the frequency and the electrical conductivity profile in the Earth. Therefore the essence of MT is the measuring on the Earth surface of the impedance over a spectrum of frequencies in order to determine the conductivity of the Earth as a function of depth. The tensor allows the computation of the apparent resistivity and phase for each frequency and component acquired, as follow:

$$\rho_a = \frac{1}{\omega\mu_0} |\mathbf{Z}|^2 \quad [\text{Eq.4.16}]$$

and

$$\Phi = \arctan\left(\frac{\text{Im } \mathbf{Z}}{\text{Re } \mathbf{Z}}\right) \quad [\text{Eq.4.17}]$$

What is really important to highlight is that the measured impedance tensor is strongly affected by the dimensionality of the investigated Earth structure; e.g. the

1D case occurs when the conductivity changes only vertically without any lateral variation, as for horizontally stratified earth. Following we summarize the impedance tensor in the three cases:

$$\mathbf{Z}_{1D} = \begin{pmatrix} Z_{xx} & Z_{xy} \\ Z_{yx} & Z_{yy} \end{pmatrix} = \begin{pmatrix} 0 & Z_{xy} \\ -Z_{xy} & 0 \end{pmatrix} \quad [\text{Eq.4.18}]$$

$$\mathbf{Z}_{2D} = \begin{pmatrix} Z_{xx} & Z_{xy} \\ Z_{yx} & Z_{yy} \end{pmatrix} = \begin{pmatrix} 0 & Z_{xy} \\ Z_{yx} & 0 \end{pmatrix} \quad [\text{Eq.4.19}]$$

$$\mathbf{Z}_{3D} = \begin{pmatrix} Z_{xx} & Z_{xy} \\ Z_{yx} & Z_{yy} \end{pmatrix} \quad [\text{Eq.4.20}]$$

This issue has great impact on the interpretation of a MT sounding, and the dimensionality should be carefully retrieved through specific MT data analysis. Let consider for example an ideal 2D Earth structure (figure 4.1), with a vertical contact being investigated by MT (from Simpson and Bahr, 2005). Physically, the current density must be conserved across the boundary, implying a discontinuity of the electric field. The response is decoupled into two independent modes. The Transverse Electric (TE) mode describes currents flowing parallel to the strike while the Transverse Magnetic (TM) mode describes currents flowing perpendicular to the strike.

Obviously, the decoupling into two modes, in the proximity of lateral discontinuities, affects the impedance tensor and therefore the apparent resistivity and phase. In figure 4.1, the theoretical MT soundings are plotted as function of the distance with the 2D contact. It is shown that as long as the structure is 1D the MT curves measured in a sounding along XY and YX directions coincide, while the effects of the 2D structure produce different TE and TM apparent resistivity and phase curves.

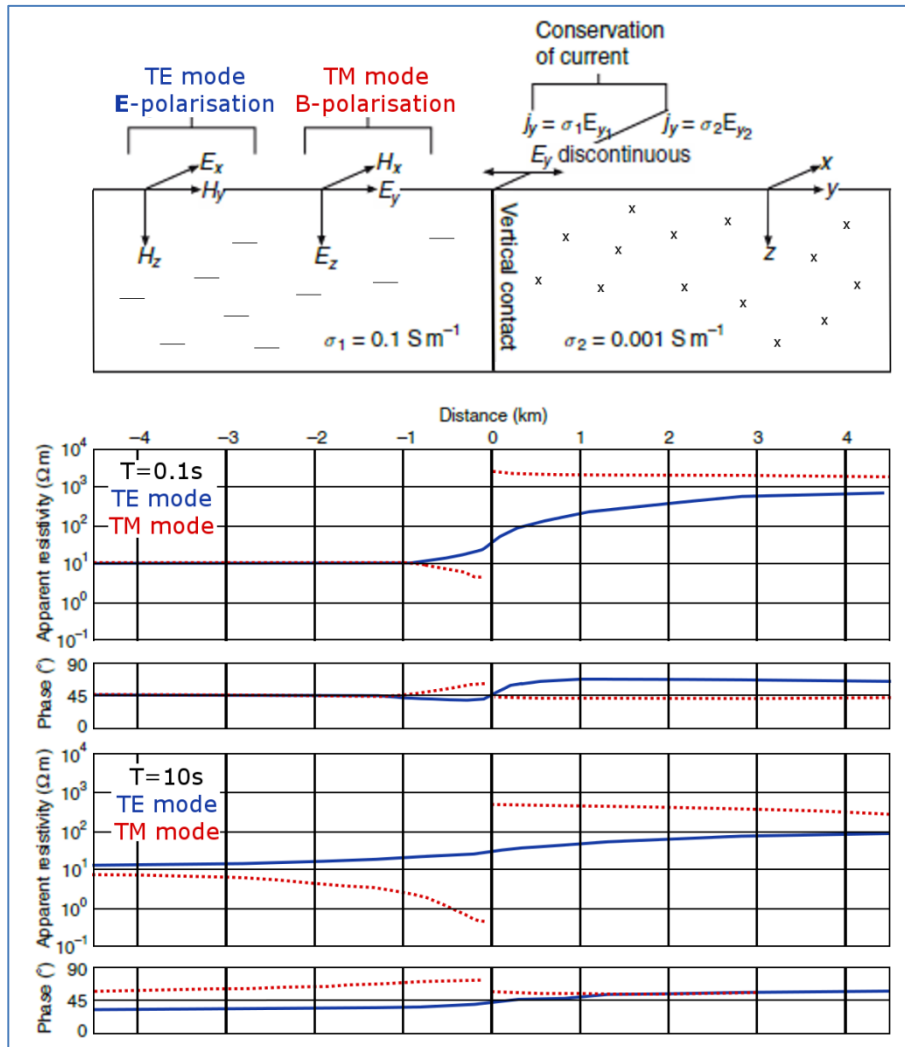


Figure 4.1- Example of 2D Earth's model with a vertical contact (modified from Simpson and Bahr, 2005). The theoretical MT curves are plotted for the periods 0.1s and 10 s as function of the distance with the vertical contact. The TE mode is shown in blue and the TM mode in red.

### 4.3 The concepts of MT data acquisition and processing

On the basis of measured frequency bands, MT methods are classified as Audio MT (AMT) from  $10^4$  to  $10^1$  Hz, and Long-period MT (LMT) from  $10^0$  to less than  $10^{-5}$  Hz (Chave and Jones, 2012). Broadband instrumentations (BBMT) allow the measuring of high and low frequencies. Usually the lowest frequency measured

for deep geothermal exploration is about  $10^{-2}$  or  $10^{-3}$  Hz while shallow geothermal exploration can be carried out by using the AMT frequency range. The instrumentations for the acquisition of MT data are quite simple in the sense that the transmitters are not required due to the natural origin of signals. The common layout is the simultaneous acquisition of the two horizontal perpendicular magnetic and electric fields on surface, usually with one direction parallel to the magnetic North (x-direction for MT convention). The electric fields  $E_x$  and  $E_y$  are measured with two dipoles (with grounded electrodes). Two magnetometers are duly grounded for the acquisition of the magnetic fields  $H_x$  and  $H_y$ . In addition the vertical component of the magnetic field  $H_z$  can be measured, too. The receivers are used to record the time series with recent 24 to 32 bit A/D conversion systems.

Only a small part of the time series collected during a MT sounding contains information related to the transfer functions. The procedure aimed at reducing the great amount of collected data is called "Data processing". Considering that the MT is a passive method and the energy sources cannot be controlled, the procedure of filtering that part of data related to noise is a quite complex procedure. Very briefly, the main steps are the pre-processing of the data (e.g. time series preparation), the Fourier transformation in frequency domain and finally the robust transfer functions estimation. The estimation of the transfer function represents a critical issue in MT and has been the focus of many researches. Different methods of MT data processing have been implemented and compared in literature (e.g. Egbert and Booker, 1986; Chave and Thompson, 1989; Jones et al., 1989; Larsen et al., 1996; Oettinger et al., 2001). Since the remote reference method has been proposed in Gamble et al. (1979), it became a best practice in the MT acquisition and processing due to the possibility of process the local time series with time series simultaneously acquired in a remote site with very high signal to noise ratio. This procedure strongly improves the reduction of the noise. An exhaustive explanation of the processing of correlated or uncorrelated noise is given in Larsen et al., (1996). Particularly interesting (and tricky) is the correlated noise produced by the DC electrified railways with an estimated response similar to that of the near-field with an artificial rise of  $45^\circ$  of the apparent resistivity curves coupled with phase values tending to zero (see details in Szarka, 1988).

## 4.4 MT data analysis

### 4.4.1 Distortion

Further analyses on the estimated impedance tensor are required in order to overcome some of the main problems affecting the MT method: the distortion of the impedance tensor. Jones (2012) in his review of the distortion effects considered the distortion of regional electric fields by local structures the greatest bane in magnetotellurics.

A well known frequency-independent galvanic effect is the “static shift”. The effect is a shift of the apparent resistivity curve for an unknown multiplier (constant on a logarithmic scale) without affecting the phase (Jones, 1988). The effect is caused by heterogeneities in the properties of the rocks/soils at the location of the electrodes or by topography. In order to correct the static shift several approaches have been proposed such as inversion algorithms that consider MT shift a parameter to be solved (DeGroot-Hedlin, 1991). Due to the fact that the TDEM measurements are not affected by such distortions, the joint analysis of MT and TDEM data became a commonly accepted way to correct the MT static shift (e.g. Sternberg et al., 1988; Arnason, 2015). In our research we explored a procedure of joint analysis of MT and TDEM data (see Chapter 8).

Different schemes have been proposed in literature for the identification of the type of distortion and its removal. The work of Groom and Baily, (1989) provided a complete description of the galvanic distortion as well as a method to separate the effects of 3D channeling from those of 2D induction. The method is based on the decomposition of the impedance tensor, that can be factorised as follow:

$$\mathbf{Z}_{obs} = \mathbf{R} \mathbf{C} \mathbf{Z}_2 \mathbf{R}^T \quad [\text{Eq.4.21}]$$

where  $\mathbf{Z}_{obs}$  is the measured impedance tensor,  $\mathbf{R}$  is a rotation matrix (angle between the measured reference and the 2D geoelectric strike) and  $\mathbf{Z}_2$  is the regional 2D response tensor.  $\mathbf{C}$  is the distortion tensor that can be factorised:

$$\mathbf{C} = g \mathbf{T} \mathbf{S} \mathbf{A} \quad [\text{Eq.4.22}]$$

where  $g$  is a scalar (called *site gain*),  $\mathbf{T}$   $\mathbf{S}$  and  $\mathbf{A}$  are the *Twist*, *Shear* and *Anisotropy* tensors. The decomposition allows the recovering of the principal impedances and the geoelectric strike.

Smith (1995) proposed another parametrization of the distortion matrices used to identify the distortion of electric fields by near-surface inhomogeneities. LaTorraca et al. (1986) implemented a different approach based on Singular Value Decomposition (SVD) in order to define eight parameters, describing the impedance tensor, to be interpreted in terms of three-dimensional conductivity structures. Their analysis of  $Z$ , yields to the computation the following parameters: two singular values (maximum and minimum  $|E//H|$ ) and two phases, the principal axis directions for  $E$  and  $H$  vectors and two ellipticities.

#### 4.4.2 Dimensionality

In Jones (2012) the dimensionality distortion is also taken into account, occurring when: "...*MT responses have an intrinsically higher dimension than is being used in their interpretation*". With regard to the dimensionality (and directionality) analysis of MT data, many approaches have been formerly proposed in literature, such as the analyses of the Skew (Swift, 1967), Ellipticity and Polar diagrams. Recent and widely accepted rigorous methods were published by Weaver et al. (2000) and Marti et al. (2005). Weaver et al. (2000) based their work on the analysis of seven independent parameters ( $I_1$ - $I_7$ ) and the parameter  $Q$ , that are invariant under a rotation of the horizontal axes. The authors provided a physical interpretation of the properties of these parameters in terms of the dimension of the investigated Earth. For example the pure 1D case is identified for  $I_3=I_4=I_5=I_6=0$ . Different types of galvanic distortion of a 2D structure can be also discriminated as well as pure 2D or 3D cases. In certain cases the regional strike direction can be estimated, too. Marti et al. (2005) proposed a new method for the dimensionality analysis by integrating parameters used in Bahr (1991) method with those used in Weaver et al. (2000).

### 4.5 The relation between MT data and Earth's model parameters: Forward and Inverse problems

In magnetotellurics the complete understanding of the physics behind the method allows to relate the MT data to the Earth's model parameters. This issue led us to introduce two fundamental problems in geophysics: the forward problem and the inverse problem. These problems are continuing to be the objective of scientific research for geophysics; in literature many articles and books were published (e.g; Tarantola, 2005; Menke; 2012; Aster et al., 2013).

### 4.5.1 MT forward problem: the 1D case

The MT forward problem is to find the theoretical data (apparent resistivity and phase)  $d_{theor}$  given certain Earth's model parameters  $m$ , throughout solving a set of functions (mathematical model) called "Forward functional"  $G$ , that describes the physical process of EM induction:

$$\mathbf{d}_{theor} = G(\mathbf{m}) \quad [\text{Eq.4.23}]$$

The numerical simulation schemes available in literature are able to solve the forward problem in 1D, 2D and 3D (e.g. Madden, 1972; Mackie, et al., 1993; Farquharson and Miensopust, 2011; Weiss, 2012). A resistivity model is discretised and the basic equations of MT are solved.

Hereby, a brief description of the 1D forward solution as proposed in Sims and Bostick (1969) is reported for a  $n$ -layered model lying above a homogeneous halfspace. This scheme is based on a recursive formula for the computation of the surface impedance  $Z_i$  at the top of each  $i^{th}$  layer. Stated the continuity of the tangential fields as boundary conditions and the solutions of the Helmholtz equations, the impedance  $Z_i$  looking down from the top is from (Sims and Bostick, 1969):

$$Z_i = Z_{0i} \frac{1 - R_i e^{-2k_i h_i}}{1 + R_i e^{-2k_i h_i}}; i = 1, 2 \dots n - 1 \quad [\text{Eq.4.24}]$$

Instead for the halfspace is:

$$Z_n = Z_{0n} \quad [\text{Eq.4.25}]$$

where  $h_i$  is the thickness of the  $i^{th}$  layer,  $k_i$  is the wave number and  $R_i$  is the reflection coefficient as:

$$R_i = \frac{Z_{0i} - Z_{i+1}}{Z_{0i} + Z_{i+1}} \quad [\text{Eq.4.26}]$$

the characteristic impedance  $Z_{0i}$  is:

$$Z_{0i} = \sqrt{\frac{i\omega\mu_0}{\sigma_i}} \quad [\text{Eq.4.27}]$$

Starting from the halfspace, the impedance at the top of the first layer  $Z_1$ , i.e. on the Earth's surface, is computed recursively and the apparent resistivity and phase are retrieved as function of frequency according to [Eq.4.16, 4.17]. This scheme of forward modelling was implemented in the probabilistic optimization discussed in this thesis.

### 4.5.2 MT inverse problem: the deterministic and probabilistic approaches

Conversely, the inverse problem is to find the model parameters  $m$  given certain observed data  $d$ :

$$G(\mathbf{m}) = \mathbf{d}_{obs} \quad [\text{Eq.4.28}]$$

Solving the inverse problem allows the geophysicist to indirectly estimate the subsoil physical parameters (i.e. the resistivity model of the investigated Earth) from the analysis of the MT data measured at surface. The problem is ill-posed due to its instability; for details see Berdichevsky and Dmitriev (2002) that described MT in terms of ill-posed problems.

It is possible to define two main philosophies for solving the inverse problem: *i)* the deterministic and *ii)* the probabilistic approaches. The deterministic methods represent the conventional way for estimating the resistivity models. As previously described, magnetotellurics suffers of dimensionality problem. In literature many consolidated schemes of 1D, 2D and 3D inversions are available, even if the 3D inversion is continuing nowadays to be the focus of the scientific research. In general the model parameters are solved iteratively by minimizing a functional operator according to a derivative approach. These methods usually require to solve less complex problem by linearizing the model. There is the possibility that the procedure reaches a local minimum of the functional operator, depending also how the starting model is near to the global minimum. Two of the most common schemes in MT are the Occam inversion (Constable et al., 1987; Degroot-Hedlin and Constable 1990) and Non-Linear Coniugate Gradients (Rodi and Mackie, 2001). For the mathematical review of MT inversion algorithms see Siripunvaraporn, (2012).

Conversely, the probabilistic approach is less convention and is yet matter of research. The probabilistic methods do not imply any derivative approach but the model space is sampled randomly or according to some strategies. Furthermore, this approach does not need any starting model that can influence the success of the inversion procedure.

Simply, many Earth's models are proposed and the theoretical data compared with the observed data and directly the minimization function is estimated, in order to retrieve the best model. The philosophy of the probabilistic approach, that can be considered as an optimization procedure, is the exploration of wider space solution, seeking for a global solution to the problem. In spite of theoretical demonstration, the MT inverse problem is non-unique mainly due to the occurrence of noise, finite number of frequencies (Grandis et al., 1999), and anisotropy (Yin, 2003). Different schemes are available in literature known as Global Optimization Algorithms; for a complete description of such methods applied to geophysics we refer to Sen and Stoffa (2013). The random sampling of the model space is the concept at the base of the *Monte Carlo methods*. This algorithm, firstly proposed by Metropolis and Ulam (1949), has been yet used for solving geophysical inverse problems (Sambridge and Mosegaard, 2002) and also the MT problem (e.g. Jones and Hutton, 1979b; Grandis et al., 1999).

In the last decades, in order to solve non-linear problems, artificial intelligence algorithms were proposed in literature based on the concept of adaptive behaviour. Recently, such application were used also to solve the geophysical inverse problem. Common algorithms are: *i*) Genetic Algorithms (GA) and *ii*) Simulated Annealing (SA).

The GAs were firstly proposed by Holland (1975) based on the analogies with biologic evolution. The algorithm starts with a population of models that are iteratively evaluated and updated following the main steps of coding, selection, crossover, and mutation. This procedure allows the combination of the best models, in terms of misfit functions, till the final optimized model is achieved. Examples of GA applications in MT are given in Everett and Schultz (1993), Pérez-Flores and Schultz (2002). The SA (Kirkpatrick et al., 1983) is a probabilistic optimization method that is based on the simulation of the thermodynamic processes of annealing and statistical mechanics. The method was applied in MT; an example is given in Dosso and Oldenburg (1991).

More recently Kennedy and Eberhart (1995) presented a heuristic method called Particle Swarm Optimization (PSO) that is based on swarm intelligence and evolutionary computation. The swarm represents a population of Earth's models. At each iteration the PSO updates the model parameters of the swarms throughout an artificial intelligence behaviour. In spite of its high velocity convergence and the widespread use in engineering, few applications were performed in geophysics and less in MT (e.g. Shaw and Srivastava, 2007).

The PSO algorithm is implemented and used for the MT inverse problem in this thesis. The detailed mathematical explanation is given in Chapter 5 whereas the Matlab implementation is described in Appendix A.

## 4.6 The TDEM method

Time Domain or Transient EM (TDEM or TEM) method (Ward and Hohmann, 1988; Spies and Frischknecht, 1991) has been widely applied in geological, engineering and environmental fields. The principle of TDEM resistivity sounding is based on the diffusion of EM fields in the Earth. A static magnetic field is established in the Earth while a transmitter current is on. When this field is changed (usually by abrupt interruption, with current reduced to zero), the electromotive force generated according to the Faraday's law causes the flow of eddy currents in the ground. At the instant  $t_0$  of turnoff, the eddy currents reproduce the static magnetic field then decays rapidly inducing new currents in the ground at greater depth. Secondary magnetic fields decay quickly in poor conductors and slowly in good conductors. The measurements of the decay of the magnetic fields as function of time allows the estimation of the electrical resistivity distribution of the investigated Earth. The recorded voltage is firstly converted in apparent resistivity response versus time, accordingly to standard approach (e.g. Nabighian, 1979). Particularly, the apparent resistivity is related to the voltage signal and to the time decay, as follow:

$$\rho_a(t) = \frac{k_{tem} M^{2/3}}{t^{5/3} e(t)^{2/3}} \quad [\text{Eq.4.29}]$$

where  $k_{tem}$  is a constant of the equipment,  $M$  is the magnetic dipole moment;  $t$  is the time and  $e(t)$  is the recorded TDEM signal. The estimation of the resistivity model from TDEM data represents a geophysical inverse problem that we previously introduced.

The characteristic of TDEM has been a key advantage in sounding near-surface conductive layers on Earth. Measuring the response at later times means a greater depth of penetration  $\partial_{ad}$ .

$$\partial_{ad} = 36 (\rho t)^{0.5} \quad [\text{Eq.4.30}]$$

where  $t$  is the delay time of TDEM (seconds) and  $\rho$  the resistivity of the medium.

The method was implemented both for ground or airborne measurements (Christiansen et al., 2009). The ground TDEM soundings are made by laying out a loop of wire usually with a side length in the range of 20-200 meters and pulsing a controlled current. Different field configurations imply a receiver loop in the same centre (central geometries) or at certain distance (offset geometries). The decay characteristic of the voltage in the receiver is determined for a number of time gates, each measuring and recording the amplitude of decaying voltage. We consider important to highlight some aspects (from Barrocu and Ranieri, 2000):

- The penetration depth is proportional with resistivity;
- The mean resolution is about 1/10 of the loop side;
- The TDEM technique is not effective to image layers with very high resistivity.

## **4.7 Electromagnetic methods for shallow and deep geothermal exploration in Italy: case studies**

In Italy, many exploration projects have been carried out in the last decades for assessing shallow and deep geothermal resources. Obviously, the most famous high temperature fields such as Larderello-Travale, Mt. Amiata, Phlegrean Fields (Southern Italy) were the focus of many projects, but recently many industrial and scientific projects were also carried out in central and southern Italy. The basic and applied research is quite active in this field as proven by the recent Italian and European Projects as INTAS, I-GET, ENGINE and VIGOR projects (VIGOR web site) and the ongoing IMAGE project (IMAGE web site). In this Section we reported the brief description of some cases study in Italy, available in literature, as reviewed by Santilano et al., (2015b).

### **4.7.1 MT method in geothermal exploration: case studies in Italy**

In geothermal exploration, MT is applied worldwide contributing to the characterization of the geological, hydraulic conditions of geothermal systems and their heat sources.

In Italy MT industrial surveys are nowadays carried out in the frame of many exploration permits (e.g. Caranova et al. 2015). In the last decades, important researches have been carried out in Italy for improving the MT methodology for geothermal exploration (Larsen et al. 1995, 1996; Di Maio et al. 1998; Manzella, 2004; Volpi et al. 2003 and reference therein). As example of MT case studies in Italy, we briefly described the studies carried out in southern Tuscany by Manzella et al. (2006) and Volpi et al. (2003), respectively for exploring the Larderello-Travale and Mt. Amiata systems.

The exploration and exploitation in this areas are nowadays mainly targeted at the deep reservoir hosted in crystalline rocks. High and low frequency MT data, were acquired and used for the modelling. The high level of noise was overcome by robust remote reference processing. The MT data were inverted with different algorithms (Spichak and Popova, 2000; Rodi and Mackie, 2001) to achieve the resistivity models. Figure 4.2 shows the resistivity model obtained in the Travale sector compared to the geological model (Manzella et al., 2006). A fault zone has been resolved on the SW part of the profile. The most important feature is a low resistivity anomaly in the crystalline basement at depth of 1.5 km up to 3 km, where the deep fractured and highly productive reservoir is under exploitation. This interpretation is not widely accepted due to the vapour dominated nature of the geothermal reservoir and represent an open challenge in the frame of this field. A deeper low resistivity anomaly is detected at depth of 6 km, below the seismic marker known as K-horizon. This horizon is interpreted in literature as an indicator of the brittle-ductile rheological transition or as a possible reservoir at supercritical conditions (see Chapter 6).

The MT studies carried out at Travale led Spichak and Zakharova (2015a) to define the relationship between electrical resistivity values and deep temperature using their electromagnetic geothermometer.

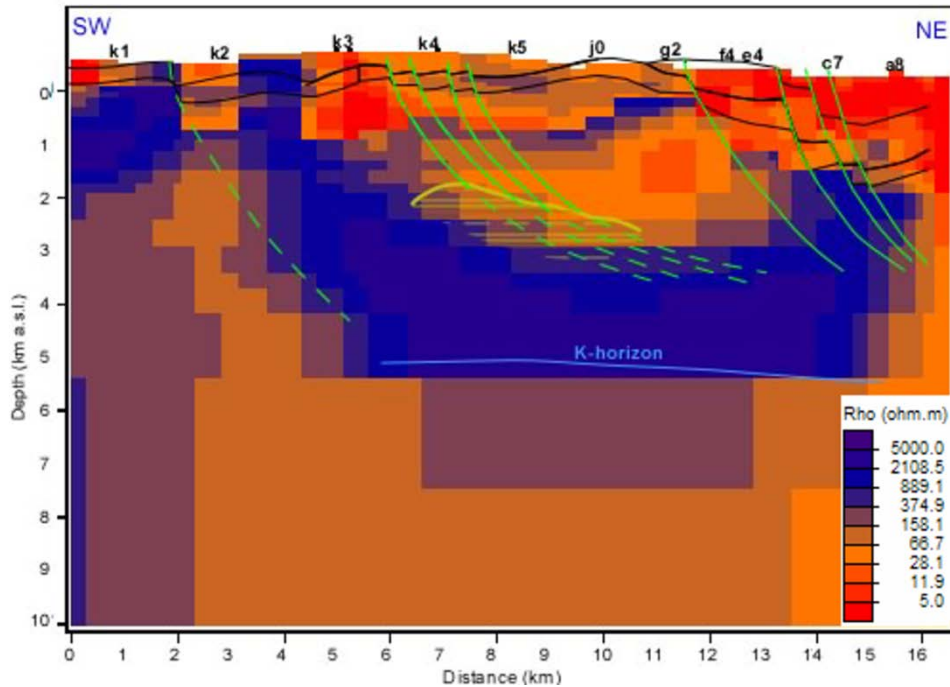


Figure 4.2- Resistivity cross-section compared to the geological model of the Travale sector, (modified from Manzella et al. 2006). Black lines are the main geological unit interfaces; green lines are faults; yellow line is the H horizon (corresponding to a high productive zone); K horizon is the white line. Inversion of TE and TM mode of a part of the dataset that is nowadays available starting from a resistivity model from geology.

In figure 4.3, the resistivity model for the Mt. Amiata geothermal field (inverting TM mode) is shown. As previously described, in spite of the occurrence of an extinct volcano the hydrothermal circulation in Mt. Amiata occurs at depth in carbonate and crystalline rocks (above an inferred igneous intrusion). Volpi et al. (2003) demonstrated that the low resistivity anomalies, in carbonate and crystalline rocks, are related to the hydrothermal circulation zones in the water dominated geothermal reservoir.

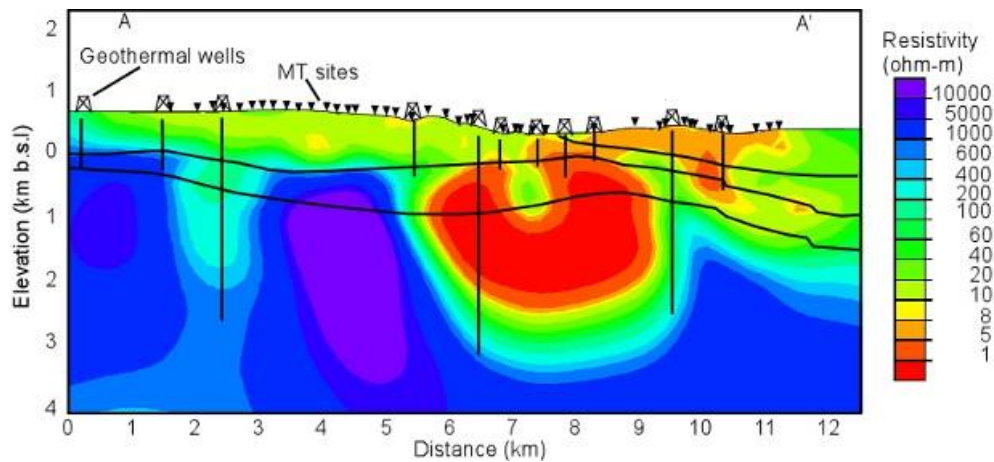


Figure 4.3- Inversion of MT data (TM mode) in the Mt. Amiata geothermal field coupled with the main stratigraphic interface and productive deep geothermal wells, located in the proximity of low resistive anomaly (from Volpi et al. 2003).

#### 4.7.2 TDEM methods in geothermal exploration: case studies in Italy

Some cases of TDEM studies for geothermal resources applications have been reported by Kauahikaua (1981), Wright et al. (1985), Pellerin et al. (1996), and Menghini et al. (2002). TDEM method has been also used for the “static shift” correction of MT soundings, in the case of deep geothermal surveys (e.g. Pellerin and Hohmann, 1990). The possibility of directly detecting a geothermal reservoir by TDEM is possible only for shallow geothermal resources.

A case-study reported by Menghini et al. (2010), utilized TDEM method in an area close to Viterbo town in Central Italy, to detect the presence of the direct faults, which allows the rising of mineralized waters to the surface, as occurs with natural hot springs. The study also pointed out the importance of reconstructing the detailed structural features of the survey area, in order to understand the hydrothermal model. For example, a secondary geothermal reservoir was inferred within the more permeable and shallower layers (in this case calcareous turbidites).

Recently, progress in TDEM airborne systems (Siemon et al. 2009), allows to investigate wide areas (in the order of hundreds of square-km) and yielding the same lateral resolution of the ground-based survey. The TDEM equipment, e.g.

transmitter and receiver, can be mounted directly on an aircraft or carried as an external sling load (e.g. on a helicopter). The principles of operation are basically the same as previously described for the ground-based TDEM.

In the frame of the VIGOR project, Santilano et al. (2016a) exploited Airborne EM data for estimating the geothermal energy that is exchanged by a ground volume unit. The study was based on the characterization of electrical and thermo-physical properties of rocks over large areas in western Sicily (Italy) by integrating Airborne Electromagnetic (SkyTEM system) data and laboratory measurements on rock thermal conductivity of samples. This is relevant to design GCHP (Ground-Coupled Heat Pump) systems, used to exploit the ground as a thermal energy source and sink.

Public well data useful to reconstruct the complex geological and hydrogeological setting were limited, and the AEM prospection was applied to define a 3D distribution of resistivity values. Three-dimensional modelling were performed as well as laboratory measurements in order to model the 3D distribution of the thermal conductivity. Figure 4.4 shows an interpreted resistivity profile extracted by the 3D resistivity model of the Termini Imerese test site.

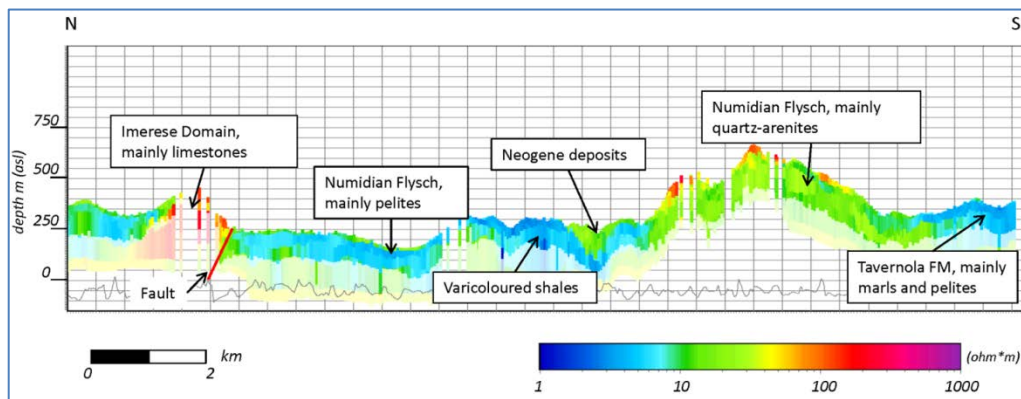


Figure 4.4- Resistivity cross-section along one of the flight lines in the Termini Imerese test site (Profile N-S 2). A schematic interpretation is provided (picture from Santilano et al., 2015b, for details see Santilano et al., 2016a).

The integration of geological information and 3D resistivity models allowed to identify the lithological units that could be distinguished by their electrical resistivity contrast (Litho-Electrical Units) that were modelled in 3D (figure 4.5). Laboratory measurements of thermo-physics parameters on rock samples permitted to assign a thermal conductivity value to each Litho-Electrical Units.

The 3D distribution of subsurface thermal conductivity represented the main input for assessing the rate of thermal energy exchanged with ground up to 250 m b.g.l. according to the empirical method by Galgaro et al. (2015).

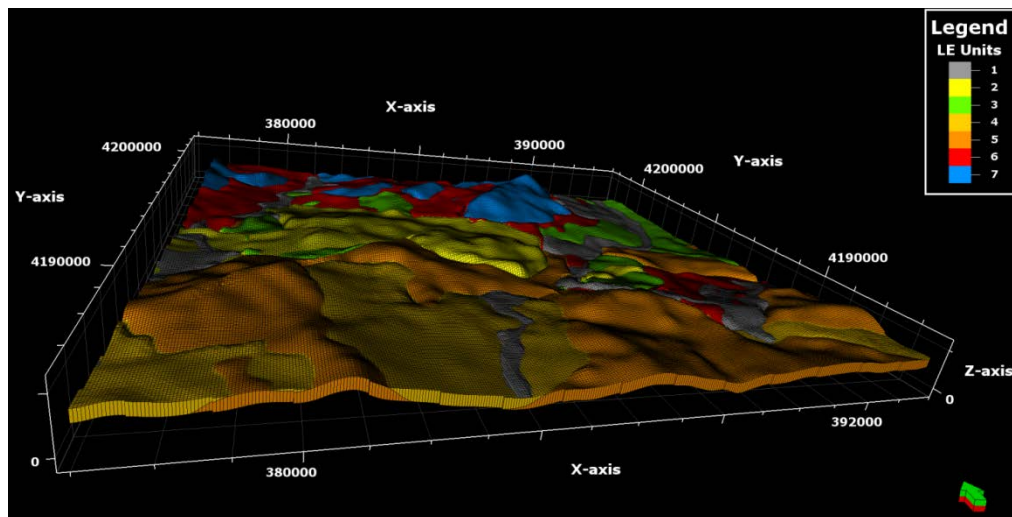


Figure 4.5- Termini Imerese 3D geological model from integrated analysis with 3D Airborne EM model. 1) Quaternary deposits LE Unit, 2) Termini Imerese Neogene LE Unit, 3) Sicilide LE Unit, 4) Tavernola LE Unit, 5) Numidian Flysch, Geraci Siculo LE Unit, 6) Numidian Flysch, Portella Colla LE Unit, 7) Imerese LE Unit. (from Santilano et al., 2016a).

## *Part II*

# *On the probabilistic optimization of EM data*

## Chapter 5

# The Particle Swarm Optimization (PSO) algorithm: application to magnetotelluric data

### 5.1 Introduction

*This Chapter is largely based on the article we prepared for the submission to a scientific peer-reviewed journal:*

- *Godio, A. and Santilano, A. On the optimization of electromagnetic geophysical data: application of the PSO algorithm*

#### 5.1.1 Foreword of PSO application in geophysics

In geophysical application, ill-posedness, ill-conditioning and non-uniqueness of the solution make the use of optimization process based on evolutionary algorithms like Particle Swarm Optimization (PSO) extremely challenging. Hereby, we discuss through synthetic and real data the PSO algorithm for the optimization of Magnetotelluric (MT) data. Its application to the study of the Larderello field is described in Chapter 8.

The 1D interpretation requires to solve the model parameters distribution (resistivity and thickness of each layer) starting from the spectra of apparent

resistivity and phase. The problem is usually ill-posed, can suffer of non-uniqueness and the experimental uncertainties have a great impact on the stability of the model parameters. The 1D problem is usually solved by means of inversion procedures; several approaches have been presented and widely adopted in literature to solve the 1D problem in magnetotellurics since decades (see Chapter 4 for details). The high non-linearity of the problem requires many cares in the inversion procedures and constraints and boundaries are usually introduced. The deterministic inversion methods (e.g. gradient-based) are usually able to find local minima of the functional operator.

The stochastic approaches can explore wider space solution, randomly (Piatti et al. 2010), or according to some strategies such as the evolutionary algorithms (Godio, 2016), seeking for a global solution to the problem. The adoption of PSO in geosciences is still limited to a few cases in hydrogeology and in geophysical inversion (e.g. Shaw and Srivastava, 2007; Yuan et al., 2009; Fernández Martínez et al., 2010a).

In this research, we propose an overview on the PSO for solving 1D MT problems with the aim to explore the capability of the probabilistic and evolutionary approach. Beside the application of PSO in MT, the novelty is related to the use of the metaheuristic for the minimization of different objective functions and their comparison, including also an Occam-like approach (following Constable et al., 1987). The innovative approach can be of help for the joint optimization of different geophysical datasets (as proposed in Chapter 8) with the possibility of the analysis of a-posteriori distribution of estimated parameters.

Hereby, the reliability of the PSO metaheuristic approach is tested on synthetic, real AMT and Long Period MT (COPROD) data. The geological interpretation of the resulting models from real MT data is not the aim of this Chapter. In the *Part III* of this thesis we adopted this algorithm for the geothermal study of the Larderello-Travale area.

### **5.1.2 Introduction on GlobalEM: the software for 1D optimization of EM data**

We implemented in Matlab environment the software package “GlobalEM” for the analysis of Magnetotelluric data. The software follows a user-friendly approach in order to estimate 1D model parameters by Particle Swarm

Optimization (PSO). The package is composed of routines programmed in-house coupled with routines modified from open-source codes available in literature.

The structure is really simple, being composed of few fundamental blocks, with their functions, that are called from the “Main” program:

- Conversion module
- 1D Forward module
- MT data analysis modules
- PSO Optimization module: from theoretical or measured MT data
- Print results module

Each module was implemented with Graphical User Interfaces (GUIs) allowing the users the proper setting of the main parameters. The whole workflow can be accomplished without any modifications of the source scripts. Indeed, we decided to implement also a *Conversion module* in order to convert the MT data stored in standard \*.EDI files in \*.MAT files. The user can run dimensionality and directionality analyses according to different literature approaches as well as tensor decomposition (described in Chapter 4). The input MT data, to be used for the optimization, can be also computed via numerical simulation and perturbed with a certain noise level in the *1D Forward module*.

The *PSO Optimization module* allows the user to obtain optimized resistivity models by Particle Swarm Optimization from theoretical or real measured data. The main setting parameters of the algorithm can be duly inserted by the user throughout specific GUIs. Finally, the results are properly plotted in the *Print results module*. If many n-trials were chosen, the a-posteriori distribution and statistical parameters can also be computed.

For a complete description of the software the reader is referred to the Appendix A.

## 5.2 The PSO method

PSO is a heuristic optimization method proposed by Kennedy and Eberhart (1995) and is based on two main concept: *i*) simulation of the swarm intelligence and the behavior of flocks of bird and fish and *ii*) evolutionary computation. The algorithm is widely adopted in several fields such as optimization processes, model classification, machine study, neural network training (Mohana et al.,

2014). The elements (or "particles"), that compose the swarm, explore the solution space of the problem; the particle with best *fitness* value, which corresponds a high quality solution, will be the leader of the group around which other particles will move. The process starts from a population with low fitness and, after successive evolutions, arrives to a solution with higher fitness value according to an adaptive behaviour of the swarm.

The population (or "swarm") is initialized with random solutions. The particles, i.e. the members of the swarm representing a potential model, "fly" through the problem space following the current optimal particles (Sen and Stoffa, 1995). Thus, PSO searches for optima by updating each particle according to certain parameters called position and velocity. Movement of particles is not entirely random; each particle is attracted towards both its own personal best position, in terms of fitness of the solution, and the swarm's best position of particles, which are vectors in the parameter space. These particles are able to move inside the boundaries of the parameter space.

The movement of a particle is realized for each iteration by adding a displacement vector, called velocity. Following Engelbrecht (2007), the velocity consists of three terms: *cognitive*, *social* and *inertia or previous velocity*. The *cognitive component* holds the individual experience of particles, the *social component* holds shared information of the swarm's best solution and the *inertia component* means the previous position in the space domain (Engelbrecht 2007). These terms, and their weighting, play a very important role for determining how wide is the search. Higher influence of the social term causes a more limited search, whereas the inertia term promotes wider search of the space.

### **5.2.1 PSO theoretical background**

PSO follows a specific procedure to solve geophysical problem, that is summarized as follow. The space  $M$ , with  $N$  dimensions, of admissible models is a priori defined with the following features:

$$l_k \leq x_{jk} \leq u_k \quad [\text{Eq.5.1}]$$

$$1 \leq k \leq n \quad [\text{Eq.5.2}]$$

$$1 \leq j \leq N \quad [\text{Eq.5.3}]$$

where  $l_k$  and  $u_k$ , are the lower and upper limits for the  $k^{\text{th}}$  parameter of the  $j^{\text{th}}$  particle. The initial population is composed by  $N$  individual model solution  $j$ ; i.e. the particles of the swarms. Each particle is represented by a  $n$ -sized vector of model. In 1D magnetotellurics inversion problem, the parameters to be optimized are the electrical resistivities and the thicknesses of the layered Earth (or only resistivities).

For every particle of the swarm, the solution of the forward problem is computed according to a non-linear forward functional  $F(x_j)$ . Particularly, the forward problem is solved using the approach based on a recursive formula associated with the  $j^{\text{th}}$  model parameters as described in Chapter 4. The PSO optimization process pursues the minimization of an objective function dependent on the computed theoretical response  $F(x)$  and observed data ( $d$ ). An additional term of regularization is usually added to minimize a functional on model parameters.

To start, a swarm of particles is selected randomly from the pre-specified parameter search space, and the velocity of each one is initialized to zero. Local and global bests for the initial swarm,  $l_j(0)$  and  $g(0)$ , are then calculated. The same procedure is performed for next generation, for all the particles in the swarm.

The algorithm updates positions,  $x_j(t)$ , and velocities,  $v_j(t)$ , of the individuals as follow (Engelbrecht, 2007):

$$\mathbf{v}_j(t+1) = \omega \mathbf{v}_j(t) + c_1 r_1 (\mathbf{l}_j(t) - \mathbf{x}_j(t)) + c_2 r_2 (\mathbf{g}(t) - \mathbf{x}_j(t)) \quad [\text{Eq.5.4}]$$

$$\mathbf{x}_j(t+1) = \mathbf{v}_j(t+1) + \mathbf{x}_j(t) \quad [\text{Eq.5.5}]$$

The speed and the locations are updated according to Eq.5.4 and Eq.5.5, as graphically described in figure 5.1.

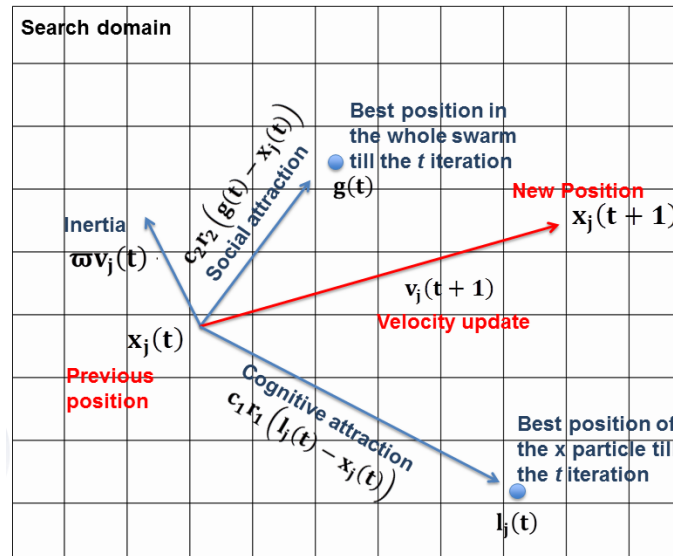


Figure 5.1- Geometrical illustration of the model parameters update for each particle at each iteration of PSO, modified after Ebbesen et al. (2012).

At the  $t^{\text{th}}$  iteration ( $t=0..T$ , where  $T$  is the maximum number of generation) each particle  $j$  of the swarm samples the search space according to its own misfit history,  $l_j(t)$ , and its companions searching experience,  $g(t)$ . The factors  $\omega$ ,  $c_1$ ,  $c_2$  are coefficients, whereas  $r_1$  and  $r_2$  are random values.

The speed vector is updated based on the "memory" gained by every individual, conceptually resembling an autobiographical memory, as well as the knowledge gained by the swarm as a whole. This is the base of an intelligent and adaptive (artificial) behaviour; i.e. learning from experience and adapting for the future.

Three terms of the velocity play different roles in Eq.5.4. The first one is the *previous velocity*, where  $\omega$  is the *inertia weight* ( $0.8 \leq \omega \leq 1.2$ ) as proposed by Shy and Eberhart (1998), responding for keeping the particle moving in the same direction. Generally, lower values of  $\omega$  speed up the convergence of the swarm promoting local exploitation, while higher values encourage exploration of the entire search space. The second term is the *cognitive component*, containing the *cognitive attraction coefficient*  $c_1$  ( $0 \leq c_1 \leq 2$ ); this term acts as the particle's memory, causing it to draw back to the region of the search space in which it has experienced own best solution. The third term is the *social component* and

contains the *social attraction coefficient*  $c_2$  ( $0 \leq c_2 \leq 2$ ); it causes the particle to move to the best region found by the particle's neighborhood.

The random values  $r_1$  and  $r_2$  cause a stochastic influence on the velocity update, for each particle, controlled by the its individual and global (of the swarm) best solutions. The stability of the swarm is usually kept according to the follow inequalities (Ebbesen et al, 2012):

$$0 < c_1 + c_2 < 4 \quad [\text{Eq.5.6}]$$

$$\frac{c_1+c_2}{2} - 1 < \omega < 1 \quad [\text{Eq.5.7}]$$

### 5.2.2 Search space's constraints and boundaries

Hereby, the constraints to be placed upon the search space are discussed. Different distinct constraints handling methods are usually implemented: *i*) penalize, *ii*) absorb, *iii*) nearest (for details see Ebbesen et al, 2012). In such a context we used the penalize method. The method penalizes particles violating constraints by assigning a high objective function value. Particles are free to move across the constraints but are yet attracted to the feasible region in which they can eventually re-enter.

For the geophysical applications, a priori information of the search space can be introduced (if available) to reduce the ambiguities of the solutions. They usually refer to additional information on geological features (depth of contacts, layer thickness) or on values of geophysical parameters values, i.e. the electrical resistivity of rocks for EM soundings. They can be included into the PSO algorithm through different ways (Fernández-Martínez, 2010b): *i*) as a particle which is introduced into the swarm to influence the oscillation centre, *ii*) by including in the minimization function a regularization term in addition to the norm used in the data space; in this case a Lagrangian multiplier ( $\lambda$ ) is introduced to defines the amount of regularization that is chosen in the model construction and *iii*) by adding a *force* term into Eq.5.4 for updating the velocities. In addition it is possible to reduce the search domain for specific layers.

## 5.3 Minimization function

The optimization process to estimate the model parameters from the magnetotelluric soundings focus on the discussion of the functional to be

minimized. The minimization function  $\Psi$  usually consists of different terms (e.g. Aster et al., 2013; Sen and Stoffa, 2013).

We firstly introduce the general functional:

$$\Psi(\mathbf{m}) = \left( a \|\boldsymbol{\rho}_{a,o} - \boldsymbol{\rho}_{a,p}\|_2 + b \|\boldsymbol{\phi}_{a,o} - \boldsymbol{\phi}_{a,p}\|_2 \right) + \lambda^2 \|\mathbf{m} - \mathbf{m}_r\|_2 \quad [\text{Eq.5.8}]$$

The first term of Eq.5.8 is related to the misfit of the model's forward response as the Euclidean (data) norm of the misfits between the observed experimental data and the theoretical predicted data (apparent resistivity  $\rho_{a,o-p}$  and phase  $\phi_{a,o-p}$ ). In order to constrain and regularize the optimization process, a second term is added to the functional as the Euclidean (model) norm of the misfits between the model parameters  $m$  and the parameters of a reference model  $m_r$ . In this case the model parameters vector  $m$  consist of the electrical resistivities and the thicknesses of a few-layered Earth model, or “blocky” model. The coefficients  $a$  and  $b$  are used to weight the influence of the apparent resistivity and phase for computing the misfit on data. The Lagrangian multiplier  $\lambda$ , is a trade-off parameter that controls the effect of the reference model ( $m_r$ ) in the optimization process. The number of layers is a priori selected.

The minimization of Eq.5.8 allows the use of a-priori information in the optimization. This means that geological features or values of geophysical parameters can be included into the reference model of the second term. Furthermore, an unconstrained optimization can be computed by setting to zero the trade-off parameter.

Smith and Booker (1988) published pioneering studies describing effective approaches to invert 1D MT data by minimizing the structure. The minimum structure can be measured in terms of the derivative of the model. Hereby we tested an minimization function Eq.5.9 for PSO by following an “Occam-like” regularization as proposed by Constable et al. (1987). We minimize for the roughness of the model, defined as the integrated square of the first derivative of the model with respect to depth, in order to achieve the “smooth” model. A second derivative can be also used (here not implemented).

$$\Psi(\mathbf{m}) = \left( a \|\boldsymbol{\rho}_{a,o} - \boldsymbol{\rho}_{a,p}\|_2 + b \|\boldsymbol{\phi}_{a,o} - \boldsymbol{\phi}_{a,p}\|_2 \right) + \lambda^2 \|\partial m\|_2 \quad [\text{Eq.5.9}]$$

The model roughness represents the second term of the functional and is computed by applying a differencing operator  $R$  to the elements of the model vector  $m$ ; a Lagrangian multiplier  $\lambda$  is used. The proper selection of  $\lambda$  is not trivial; here a L-curve criterion is adopted (for a review see Farquharson and Oldenburg, 2004). The L-curve, in a plot data norm vs model norm, represents the value of the trade-off parameter that properly balance the two terms of the minimization function. In this case the model parameters vector  $m$  consist only of the electrical resistivities for a many-layered Earth model with fixed thicknesses. We discretize the models as function of depth and frequency of measured EM fields in order to take into account the loss of resolving power, according to the skin depth concept. This approach allows to find the model as smooth as possible which fits the observed data.

Finally, the minimum structure approach can include an additional term for the measure of the difference of the model  $m$  respect to an a-priori reference model  $m_r$ :

$$\Psi(\mathbf{m}) = \left( a \|\rho_{a,o} - \rho_{a,p}\|_2 + b \|\phi_{a,o} - \phi_{a,p}\|_2 \right) + \lambda_1^2 \|\mathbf{m}_p - \mathbf{m}_r\| + \lambda_2^2 \|\partial m\|_2 \quad [\text{Eq.5.10}]$$

This approach allows to find the smoothest model fitting the observed data, considering also a-priori geological or geophysical information, if available. The use of a reference model from the interpretation of near soundings is known as laterally constrained optimization (Auken and Christiansen, 2004).

## 5.4 Flow chart of the geophysical optimization

The PSO algorithm was developed by modifying the original structure of the code by Chen (2009), in order to be implemented in the software “GlobalEM” (for details see Appendix A). We briefly illustrate the procedure we implemented to optimize the magnetotelluric data by using PSO algorithm (figure 5.2):

- to select the objective function to be minimized;
- to set the reference model if a priori information about stratigraphy or geophysical parameters is available; to set properly the space boundaries. For the few-layers optimization the space boundaries refer to thickness and resistivity of layers while for the “Occam-like” optimization the space boundaries refer to the resistivity.

- to tune the values of coefficients into Eq.5.4 and initialize the PSO algorithm with a set of particles, randomly distributed throughout the space domain, with positions  $x_j(t=0)$ ;
- to get the theoretical data by solving the forward problem for each Earth's model corresponding to each particle at  $t^{\text{th}}$  iteration;
- to evaluate the objective function for each particle at  $t^{\text{th}}$  iteration;
- to update the particles positions and velocities using Eq.5.4 and Eq.5.5 at iteration  $t+1$ , compute theoretical data and evaluate the minimization function. This step is repeated for the maximum number of iterations  $T$ .
- to obtain the model parameters, i.e. thicknesses and resistivities of layers for few-layered optimization or resistivities of layers for “Occam-like” optimization.

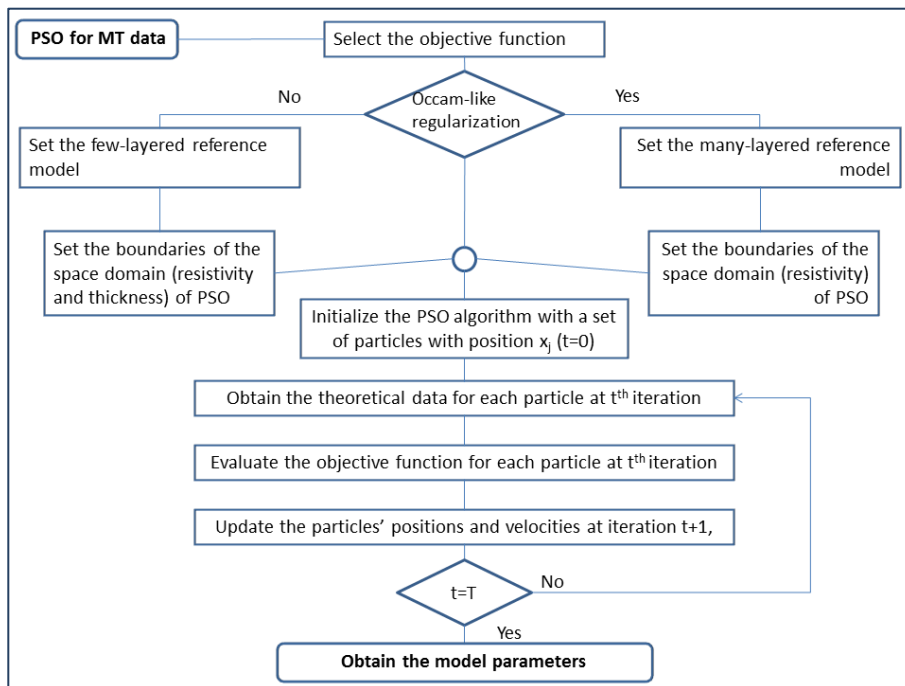


Figure 5.2- Flow-chart of the MT data optimization using the PSO scheme.

## 5.5 Results

Analysis on synthetic data allowed us to evaluate the sensitivity of the main factors affecting the reliability and convergence of the PSO. We refer to synthetic datasets of AMT data in the frequency range between 1 to  $10^4$  Hz. Results on real AMT and Long Period MT data are then discussed. We would stress that the optimization procedure, based on stochastic and evolutionary approach, results in a resistivity model. The repetition for a certain number of times (trials) of the optimization procedure on the same data and with the same setting parameters allows the analysis of a-posteriori distribution.

### 5.5.1 Test on synthetic data

Test on synthetic MT data refers on the approach to minimize the functions Eq.5.8 and Eq.5.9. The main features of the synthetic models are summarized in Table 5.1.

Table 5.1- Main features of the synthetic Earth's models, tested by PSO.

Model n.1		Model n.2	
Resistivity ( $\Omega$ m)	Thickness (m)	Resistivity ( $\Omega$ m)	Thickness (m)
100	200	100	100
20	100	50	100
200	200	10	50
1000		200	100
		1000	

Initially, we check the reliability of the approach on a dataset of AMT in the frequency range between 1 Hz and 10000 Hz, considering Model n.1. Equivalence and low sensitivity to the third layer yield to a challenging problem.

Figure 5.3 refers to the solution obtained by minimizing the functional Eq. 5.8 i.e. "blocky optimization", with a Lagrangian multiplier equal zero; this means that no model constraints are adopted. It can be noted that solutions are well gathered, and the resistivity of the second layer is correctly detected. The space domain was properly chosen, i.e. upper and lower boundaries of resistivity and thickness for each layer. For example the algorithm searched, in this case, the solution in the range of 1-2000  $\Omega$  m.

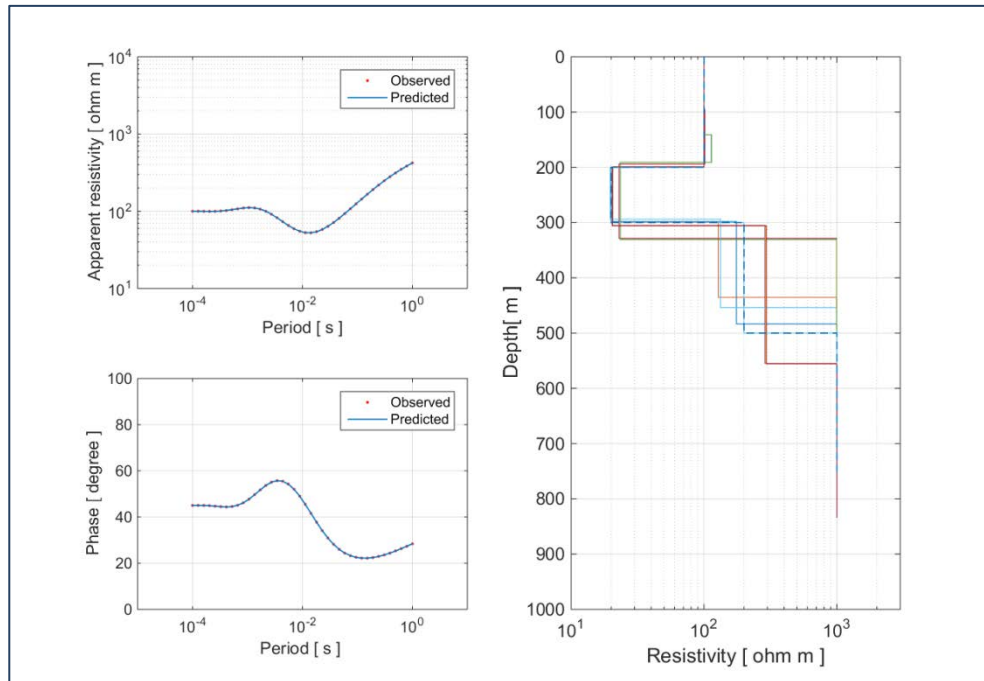


Figure 5.3- Solution on synthetic data adopting 350 generations and population size of 1000, (Cognitive attraction = 1 and Social attraction = 1.5). On the left the synthetic response of apparent resistivity and phase for the best optimized and synthetic models are shown; on the right the computed response with PSO for several trials.

The convergence is usually obtained with 250 generations or less, considering a population size of 200 elements. The effect of the cognitive and social parameters plays a rule in controlling the convergence; higher values usually means a faster convergence but this is not always considered a benefit because the solution space is explored less accurately.

Figure 5.4 refers to the solution obtained by adopting a Lagrangian multiplier for the introduction of a reference model as external constrains in the “blocky optimization”. The constraint is the “synthetic model” perturbed of about  $\pm 20\%$ .

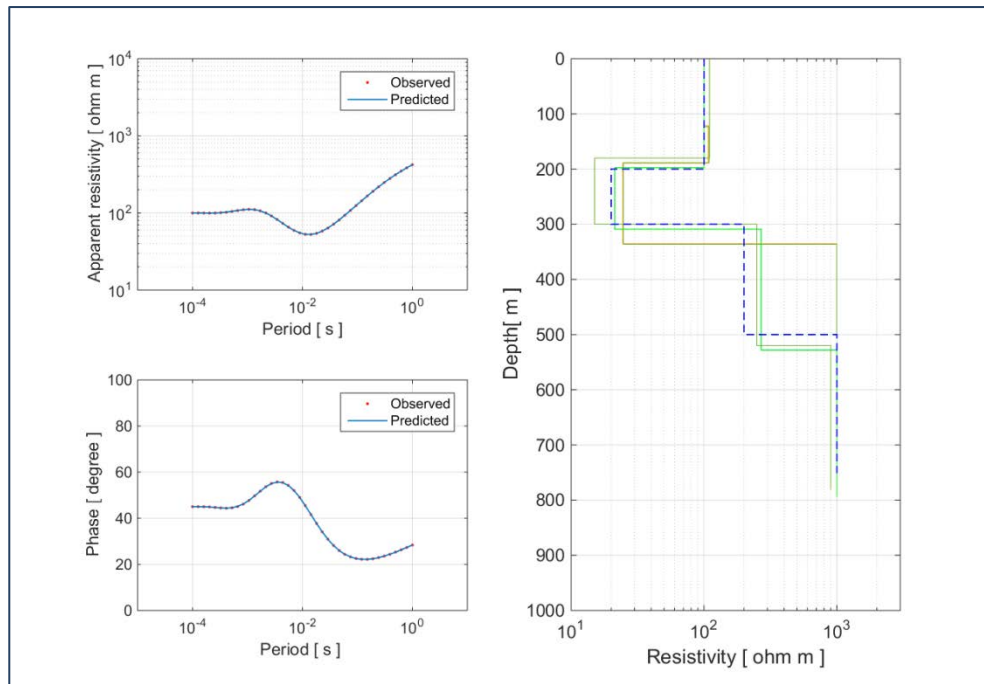


Figure 5.4- Solution on synthetic data adopting 150 generations and population size of 500. On the left the synthetic response of apparent resistivity and phase for the best optimized and synthetic models are shown; on the right the computed response with PSO for several trials, by considering a Lagrangian multiplier  $\lambda = 0.001$ .

For the same synthetic model we tested the optimization by fixing the features of the bedrock (halfspace) and by perturbing the theoretical MT data with 5% uniform noise (figure 5.5), in order to check the effectiveness of the algorithm for noisy data. The error level was chosen in accordance with the intermediate level (among 1-5-20%) used by Smith and Booker (1988) in testing their inversion scheme.

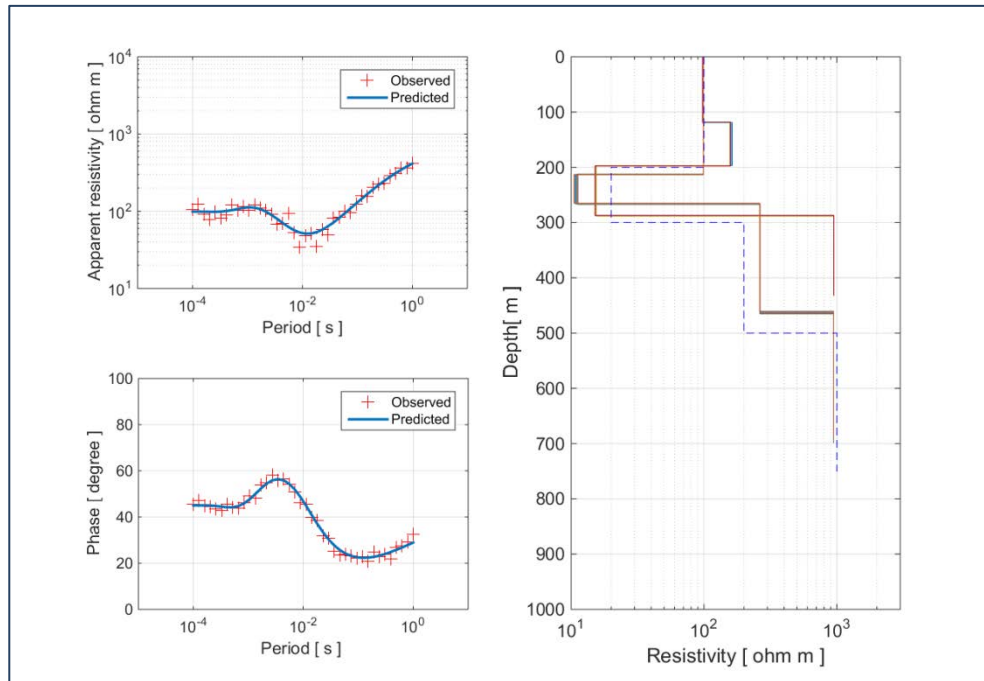


Figure 5.5- Solution on synthetic data with uniform noise of 5%, adopting 150 generations and population size of 500 (Cognitive attraction = 0.5 and Social attraction = 1.25). On the left the synthetic response of apparent resistivity and phase for the best optimized and synthetic models are shown; on the right the computed response with PSO for several trials, by considering a Lagrangian multiplier  $\lambda = 0.001$ .

A second synthetic dataset, related to the Model n.2 (Table 5.1), has been generated in order to check the effectiveness of the Occam solution by PSO. We solved the optimization problem with a model of 25 layers (figure 5.6), with the minimum structure approach; i.e. the second term of Eq.5.9 takes into account for the minimization of the model roughness. This allow us to retrieve a smoothed model of the “true” structure according to the Occam method.

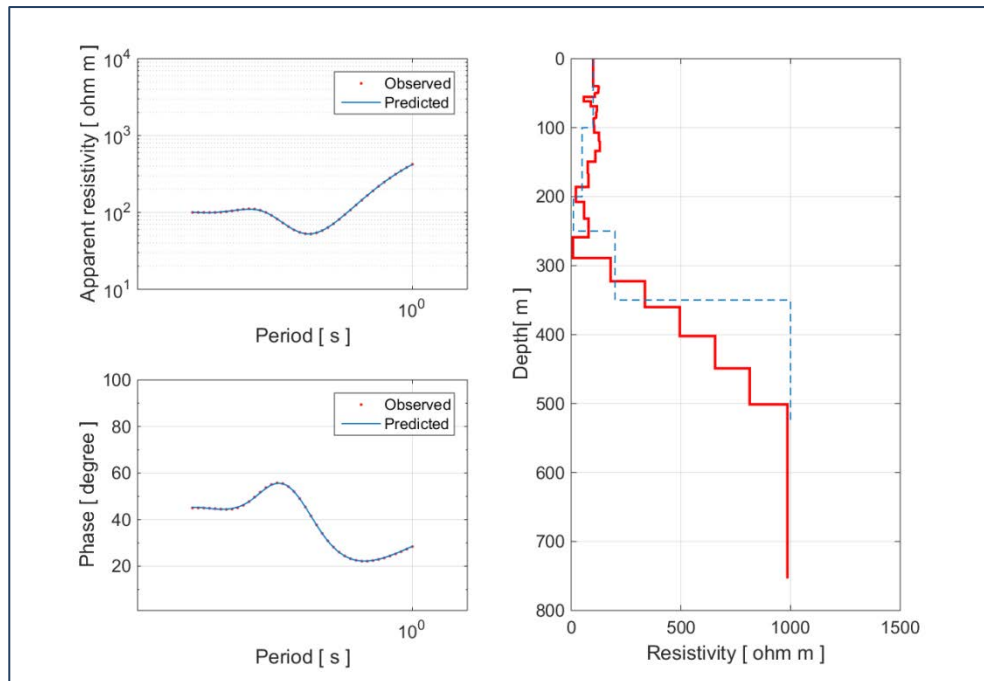


Figure 5.6- Occam solution on synthetic data, adopting 150 generations and population size of 750 (Cognitive attraction = 1 and Social attraction = 1.5). On the left the synthetic response of apparent resistivity and phase for the best optimized and synthetic models are shown; on the right the computed response with PSO, by considering a Lagrangian multiplier  $\lambda = 0.0001$ .

The proper selection of the Lagrangian multiplier was accomplished by the L-curve criterion. The plot of the Data Misfit (first term) versus the Model Misfit (second term) of Eq.5.9 for several trials with different values of  $\lambda$  indicates that the optimal compromise between the smoothness of the model and the fitting of the data is given for a value of  $\lambda=0.0001$ , corresponding to the flexural point of the curve.

The results of the Occam-like optimization procedure are quite promising in the sense that the main layers were recognized. The examples on synthetic response refer to a challenging problems where equivalence of the conductive layer lead to a strongly ill-posed problem.

### 5.5.2 Application to real AMT data

Application on real AMT data refers to dataset composed by 34 soundings (aligned along 5 profiles), in an active geothermal area in Tuscany, in the

proximity of Mt. Amiata. Here, we focused on the reliability of Particle Swarm Optimization on real AMT data; the interpretation of the results in term of shallow geothermal exploration in this area is not the aim of the research.

MT data have been acquired in the frequency range of  $10^4 - 10^1$  Hz using a MTU\_A Phoenix equipment with two electrical dipoles and 2 magnetometers (AMTC-30). The geological formations are characterized by high resistivity contrast with a presence of multidimensional anomalies and complex discontinuities. A dimensionality analysis has been performed by the method of invariants (Weaver et al. 2000) to select the soundings that can be interpreted in a reliable way using 1D approach. The dimensionality was higher than 1D for low frequencies and hence we considered the determinant average impedances (Berdichevsky and Dmitriev, 1976).

We adopted the Occam-like procedure minimizing Eq.5.9 for the optimization. Hereby we show the results from two selected soundings (AMT6 and AMT8) aligned along the same profile. According to a preliminary analysis of the optimal Lagrangian multiplier, we selected a values of 0.001. The PSO has been applied with several trials and the best 11 results are here reported. Particularly we adopted a PSO with a population size of 250, a number of generations equal to 250 and cognitive and social attraction 1 and 1.5, respectively.

The Occam optimization of AMT 6 (figure 5.7) depicts an uppermost resistive layer at the depth of 50 m, followed by a marked decrease of resistivity down to  $10 \Omega \text{ m}$  at the depth around 100 m. For deeper layers, we observe a slight increase of the resistivity up to  $50 \Omega \text{ m}$ . This is consistent with the trend of the apparent resistivity and phase curve. The data fitting looks rather good with except for the period range in AMT dead-band 1-5 kHz .

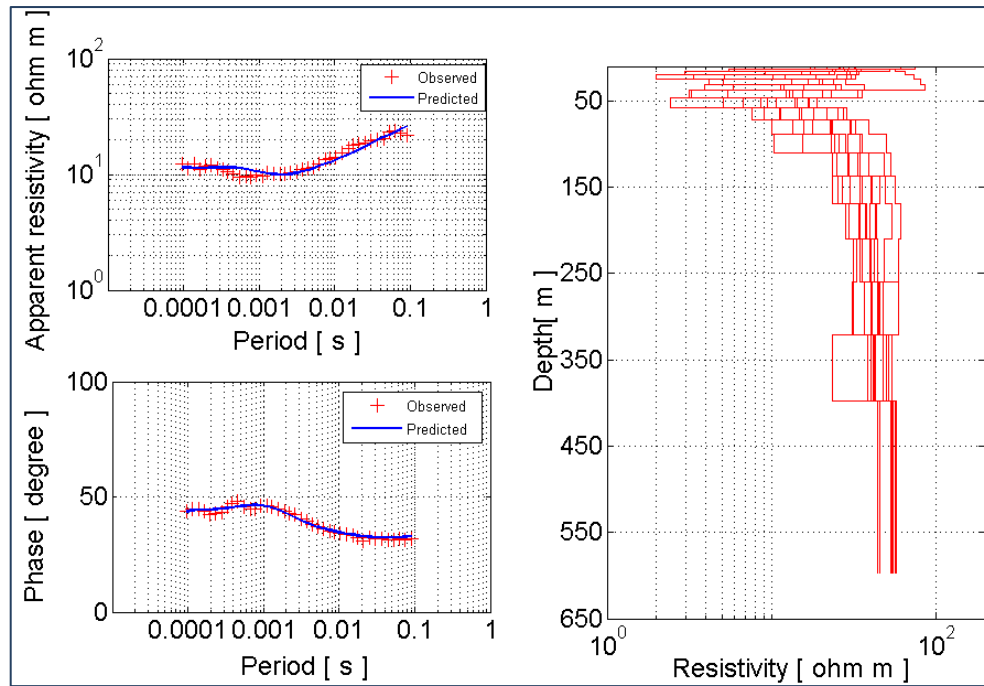


Figure 5.7- Sounding AMT6. Occam model with 25 layers and a  $\lambda$  equal 0.001; Population size equal 250 – Generation: 250 – Cognitive attraction= 1 and Social attraction= 1.5.

The sounding AMT8 (figure 5.8) shows a marked increase of the apparent resistivity for periods from  $10^{-3}$  up to  $10^{-1}$  s. The optimized model shows a relative maximum of the resistivity (100  $\Omega$  m) at the depth of about 70 m and a conductive layer at the depth of 150 m. At deeper levels, we observe a increase of the resistivity higher than 100  $\Omega$  m. We also observe a good matching of the apparent resistivity curves (predicted and observed), with except for AMT dead-band.

It should be noted that the results from both the two soundings show higher uncertainties in the model parameters at shallow depth; the sparse distribution of the shallow strata is evident.

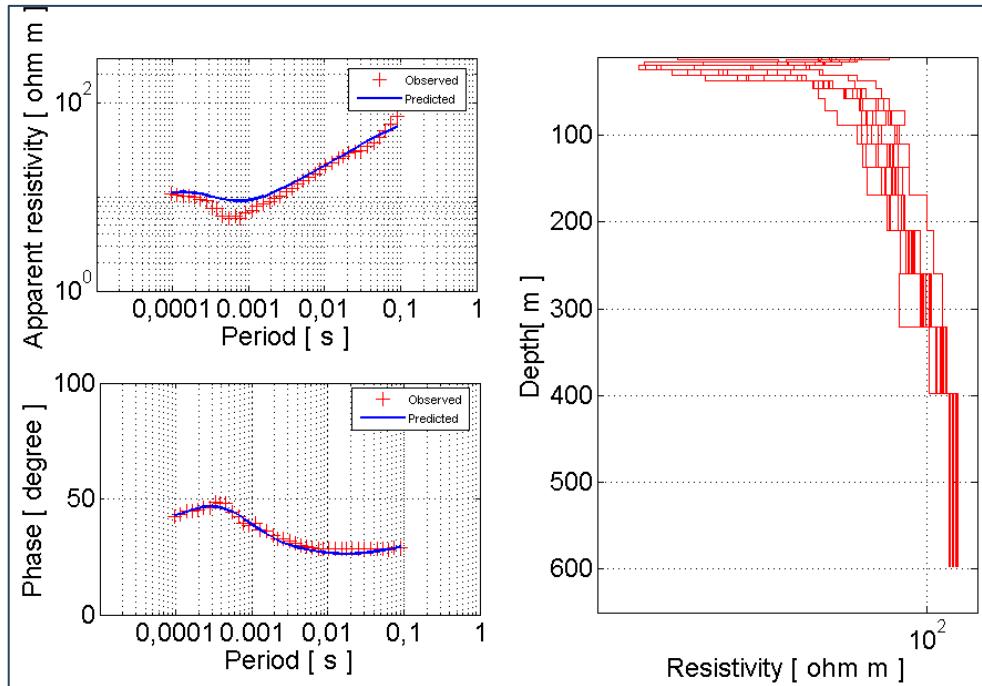


Figure 5.8- Sounding AMT8. Occam model with 25 layers and  $\lambda$  equal 0.001; Population size equal 250 – Generation: 250 – Cognitive attraction.= 1 and Social attraction= 1.5.

### 5.5.3 Application to real Long Period MT data

Hereby, we tested the effectiveness of the PSO scheme for the parameter estimation from Long Period MT data. We considered appropriate to use real MT data yet published and at disposal of the scientific community for testing the 1D inversion algorithms; i.e. the COPROD dataset by Jones and Hutton, (1979a). The data were acquired in S. Scotland in the period range of 28.5 to 1960.7 seconds. The depth of investigation is order of magnitude larger of previous tests. The discretization was set on the basis of the skin depth concept for 19 layers with fixed thicknesses.

The minimization function Eq.5.9 was used in order to achieve the smoothest model fitting the data. In Table 5.2 the main settings for the PSO optimization are summarized.

Table 5.2- Main setting for the PSO Occam optimization of COPROD dataset.

<b><i>PSO (Occam-like): Lower (LB)/Upper boundary (UB)</i></b>		
<b><i>Layer</i></b>	<b><i>Resistivity (<math>\Omega m</math>)</i></b>	<b><i>Thickness</i></b>
1	LB=1; UP=1000	200m
2-20	LB=1; UP=5000	logarithmic increase from 200 m to 350 km
<b><i>PSO: settings</i></b>		
Initial population	300	
Particle Inertia	0,9	
Cognitive		
Attraction	0,5	
Social Attraction	1,5	
Generations (Iterations)	200	
Trials	25	
<b><i>PSO: Objective function</i></b>		
$a$ (weight on $\rho_a$ )	0,6	
$b$ (weight on $\Phi$ )	0,4	
$\lambda$ (Lagrangian multiplier)	$10^{-4}$	

We performed the optimization of the COPROD dataset for 25 trials in order to check the validity of the estimated model parameters or the inconsistency of some layer of the resulting model. A simple computation allows us to estimate the number of forward model calculations: one complete optimization required 300 models for 200 generations (iteration), the repeatability of the procedure was tested 25 times.

In literature the dataset was used to test different inversion schemes and many models were presented. In figure 5.9 we presents the resulting 25 models obtained from Particle Swarm Optimization and the model obtained with the median values of resistivity among the 25 trials. In addition we plotted also the inversion models published by Jones and Hutton, (1979b) and by Constable et al. (1987) for the comparison with the most common algorithm in MT (Occam inversion), that inspired also part of our study.

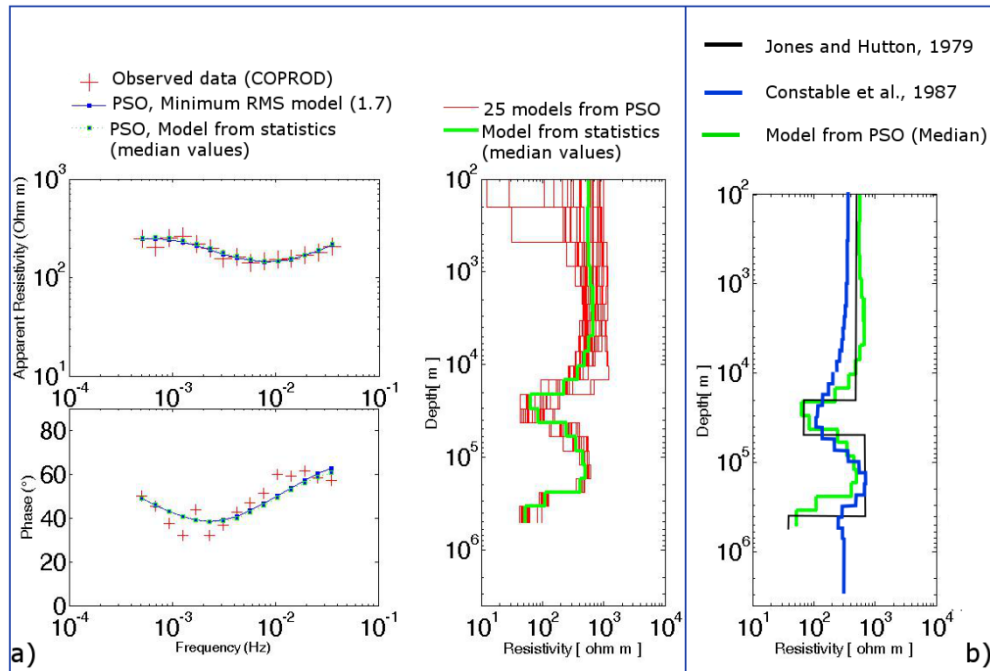


Figure 5.9- PSO optimization with Occam model of Coprod dataset. a) 25 optimized model by PSO and MT data responses from the minimum RMS model, the Model from statistics (median values among 25 trials) and observed data; b) Optimized model by PSO compared with Monte Carlo method (Jones and Hutton, 1979b) and deterministic Occam method (Constable et al., 1987).

The results of PSO are quite consistent with the model proposed in literature. Our results depicted the middle conductor, its depth (20 km) and resistivity (about  $60 \Omega \text{ m}$ ) as well as the resistor at depth of 45 km (about  $400 \Omega \text{ m}$ ) similarly to the other models. With respect to the deterministic Occam model by Constable et al. (1987) we observed differences in the determination of the resistivity of the upper level of the model and above all in the resistivity of the deepest conductor (the depth is instead consistent). On the other hand, these resistivity values of the upper and deeper levels are coherent with the model published by Jones and Hutton (1979b). Our results among 25 models seems indicate a large uncertainties in the determination of the resistivity in the upper levels, while the resistivity of the deepest conductor is coherent. Indeed, the a-posteriori distribution for each layer is particularly useful in the sense that an unimodal distribution of the estimated resistivity can point out the validity of the solution. On the other hand a multimodal distribution is index of poorly resolved model. In figure 5.10 we show

the a-posteriori distribution related to high consistent results (layers 17 and 8) and a poorly resolved layer (layer 2). We observed the highest uncertainty in the upper part of the resulting model.

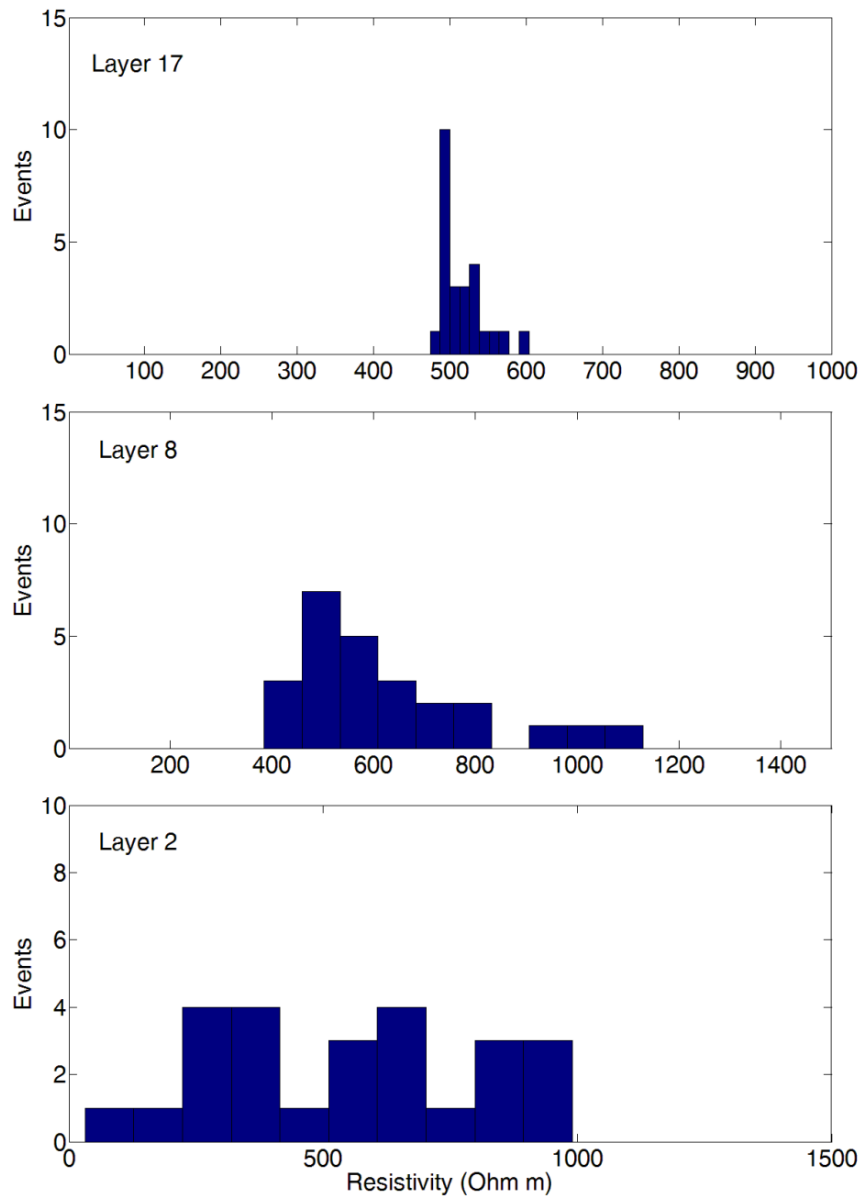


Figure 5.10- A-posteriori resistivity distribution of some layers from example of figure 5.9 (after 25 trials).

## 5.6 Discussion

The application of PSO is very promising also for the possibility to introduce a priori information in the optimisation process. Particularly, a priori information can be easily included into the second term of Eq.5.8 of the fitness functions for blocky optimization (eventually also in a third term of Eq.5.10 for Occam; here not presented). We have only explored the possibility to include a priori information in the overall process by adding additional terms in the minimization process. Future research should be oriented to the exploration of the feasibility of introducing a-priori information directly as special particle in the swarm.

The optimization process is able to manage complex non-linear, ill-posed problem in an effective way in terms of reliability of the solution and offering the capability to explore the whole space's parameters. The process can be enhanced in term of computing efficiency by acting on the cognitive attraction and social attraction. By increasing the values of these parameters, the convergence is usually faster even if the whole space parameters could be not explored completely. For the specific problem we have verified that a good trade-off between convergence and global optimization search is to adopt cognitive value less than one 1 and social attraction of 1.5. The particle inertia plays a relevant role in the convergence behaviour, acting as the trade-off between global and local exploration abilities of the swarm; a high inertia increases global exploration. We considered appropriate equal to 0.9-1.

It is straightforward that by increasing the populations size a better global search is performed, despite the computation time is increased. The computation effort is strongly dependents on the complexity of the forward modelling and on the efficiency in repeating the forward modelling for several thousand of times. The optimization of the COPROD dataset allow us to consider the PSO approach suitable for the model parameter estimation from 1D MT data according to a stochastic and evolutionary approach. Indeed, the reliability of the model is clear in term of error between observed and predicted data and in term of comparison with literature models on the same dataset. Slight differences with the deterministic smoothed inversion were recognized in the resistivity values of the upper and deepest levels of the model.

The distribution of the model parameters (a-posteriori) is explored by performing several trials; for each trial we adopt the same population size and

generation number and the same coefficients for the velocity update. The a-posteriori distribution analysis includes several effects: the propagation of the data uncertainties and the error inherent and the conditioning of the optimisation process. This latter point includes also the assumption on the initially random distribution of the population forming the swarm.

## 5.7 Final remarks

The application of PSO on MT data is rather novelty and it is suggested because the relative high speed of convergence (few minutes for each optimized model) with respect to other probabilistic method (obviously very slow compared to deterministic one) and the possibility to check the repeatability of the results with the a-posteriori distribution. Application on the synthetic dataset allows us to analyse the relevance of the setting parameters, and to select the optimal solutions when a priori information or additional constraints are introduced. We demonstrated how PSO could be an effective approach in MT data optimization. In addition we were able to implement a smoothed Occam-like optimization based on probabilistic and evolutionary approach.

Furthermore, the direct minimization of the objective function, without complex mathematical manipulation, favours the implementation of constraint optimization (e.g. to constrain a specific layer). Moreover the method is suitable for introducing multi-objective minimization processes for simultaneous or joint inversion (e.g. optimization of TDEM and AMT data sets simultaneously, as described in Chapter 8). The approach is also promising for interpreting 2D datasets; the stability of the solution must be checked in detail when a huge amount of model parameters is introduced. In the Part III of the thesis we adopted the PSO algorithm for the study of the Larderello geothermal field.

## *Part III*

*The Larderello-Travale geothermal field (Italy): improvement on the knowledge of the geothermal system by electromagnetic study*

## **Chapter 6**

# **The 3D geological model of the Larderello-Travale geothermal system**

### **6.1 Introduction**

The geological modelling represents an essential activity in the frame of the geothermal exploration of a play. The reliability of the model is strictly related to the quantity and quality of the direct (geological and well) data and indirect geophysical data.

The main objective of this chapter is to describe the 3D geological modelling of the Larderello geothermal system that we performed in Petrel (Schlumberger) environment. Particularly, we reviewed and integrated various datasets available in literature or kindly provided by ENEL Green Power.

Geological structures are three-dimensional and the fully 3D geological modelling improves significantly the integration of different sources of data and their interpretation. Considering the geophysics and in particularly MT, it is important to constrain the inverse problem with a reliable model. Once estimated the geophysical parameters, the integrated geological model is of help for the interpretation, and allows to consider the system as a whole.

In our opinion, an essential technical issue for the correct modelling of geological bodies is the pre-processing of available data to be suitable for the integration in a 3D environment. This activity is challenging in plays with really complex geology with available datasets that often differ in terms of original interpretation by different authors. Indeed, the main effort was the homogenization of the different source of data (discordant, in some cases) that have been proposed in the last decades of exploration of the Larderello field. Our dataset refers mainly to stratigraphic well logs, geological profiles and interpreted seismic data.

### 6.1.1 Overview on the study areas

The model can be divided into three different sectors (figure 6.1):

- Regional model
- Travale-Radicondoli model (hereafter also Travale)
- Lago Boracifero model

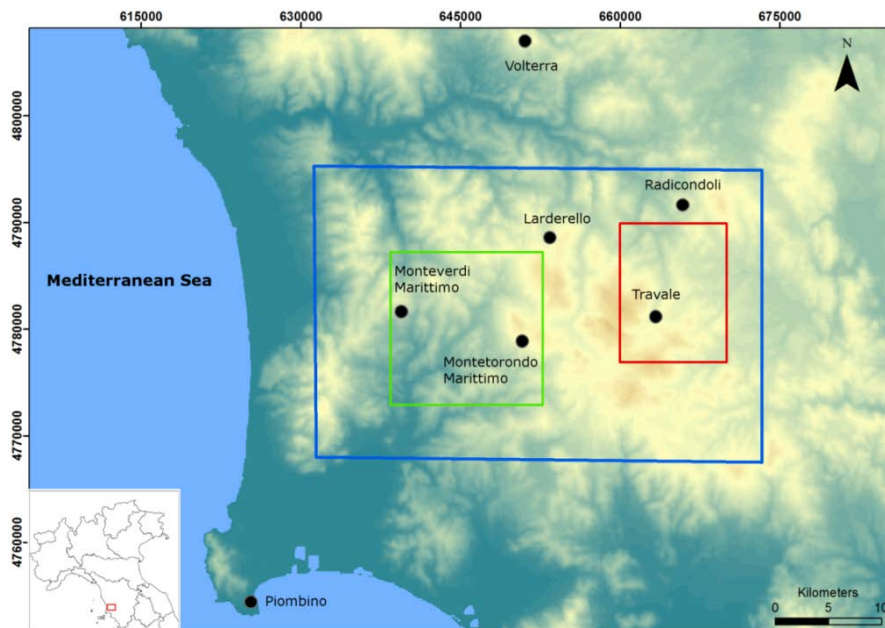


Figure 6.1- Study areas for the 3D geological modelling. The blue area represent the regional model, the red area represents the *Travale* model and the green area represents the *Lago Boracifero* model. The coordinates are in WGS1984-UTM32N.

We built the *regional model* in order to realize a first-order approximation of the geology over wide areas in southern Tuscany. This model was used as a-priori information for the inversion of the old MT dataset, acquired by ENEL GP in 1992 for crustal studies across southern Tuscany, that has been re-processed and inverted in this research and published in Santilano et al. (2015c).

*Travale-Radicondoli* and *Lago Boracifero* (Boraciferous Lake) correspond to the eastern and south-western sectors of the Larderello field, respectively. The models of these two areas were used as a-priori information for the inversion of the recent MT datasets and then for the geothermal interpretation. These areas represent two of the most productive zones of the whole field. The *Lago Boracifero* represents the main area of study where a new MT dataset was acquired. The *Travale* model was built due to the availability of underground data and geophysical data.

## 6.2 Historical perspective of the field

Larderello is a small town located in southern Tuscany (Italy) along the “Colline Metallifere” (Metalliferous Hills), an important mining and industrial area of the Tuscan “Maremma” geographic area. Here, the geothermal energy, in its modern meaning, was born.

The impressive geothermal manifestations of this area and its Earth resources favoured early human settlements. Many historical studies described the strict relationship among the inhabitants and the geothermal energy since the Pre-historic Time (Burgassi, 1987). During this period, the Etruscans and the Romans after, exploited the thermal energy (e.g. balneology) and the epithermal deposits (mines and quarries).

In historical time, during a survey for natural resources prospecting, the scientist Targioni Tozzetti (1769) published the first description of the “Lagoni” (steaming pool): “*They are places where water pool, coupled in the Earth interior with volatile mineral acids, Sulphur, Alum, Vitriol and salt...absorb a great heat and spring out boiling in a terrifying way, with horrible noise, with hot and wet vapour, dense as fog, with sulphur smell...*”. After this description, in 1777, the chemist U.F. Hoefer discovered the boric acid by analysing the water from the “Lagoni” of Monterotondo Marittimo (Ciardi and Cataldi, 2005).

The exploitation of the boric acid from hydrothermal fluids can be considered the first industrial utilization of geothermal energy, economically sustainable since 1812. Allegrini et al. (1992) identifies three main periods of industrial use: *i*) hydrothermal fluids as raw material, *ii*) hydrothermal fluids as source of thermal energy for the production cycle of boric acid and *iii*) hydrothermal fluids as source for thermal energy and for electrical power production.

In 1904 the experiment designed by Piero Ginori Conti was successful turning on five lamps using the thermal energy of the hydrothermal fluids from a well drilled in Larderello. In 1913 the first geothermal power plant in the world was in operation with the name of “Larderello 1”.

Nowadays, the exploitation of the geothermal resources for power production in the Larderello-Travale field (LTGS) is carried out by ENEL GP on six mining leases. The research and technological progresses drove the exploration deeper into the Earth. The exploitation started from the shallow carbonate reservoir and continued into the deeper crystalline geothermal reservoir, after pioneering deep drilling projects in the ‘80s. The field is one of the few examples of superheated steam system on Earth with about 50 °C of superheating (Bertani, 2005). The scientific research and the exploration is now focused on the possibility to exploit deep-buried hydrothermal fluids in supercritical conditions.

In these decades the quality of data increased significantly, starting from the first geothermal wells handmade drilled in the XIX Century to the recent directional drilling up to 4500 meters deep. The geophysical resistivity measurements evolved in this period from Direct Current (DC) surveys to the MT soundings for deeper imaging of the electrical resistivity. Regarding seismic, the acquisition of 2D seismic profiles was substituted with the acquisition of wide 3D seismic surveys that allowed a significant reduction of the mining risk, i.e. the drilling of dry unsuccessful wells. Other geophysical data have been acquired, e.g. gravimetry, passive seismic and thermometry.

Superheated steam at Larderello feeds an installed capacity of 795 MWe (Bertani, 2015). Since 2010, after regulation modifications, many research permits have been released by Tuscany Region to other operators around the present mining leases at Larderello as well as in the Mt. Amiata geothermal field (about 75 km far from Larderello).

## 6.3 The integrated database

An enormous amount of geological and geophysical data have been acquired by the private operators (mainly ENEL GP) and research institutes, for this field. In order to compute the integrated 3D geological model of the Larderello-Travale field, we firstly designed and developed a database in GIS environment (ArcGIS, ESRI), as much as possible comprehensive, considering topographic, geological and geophysical data (figure 6.2).

A wide and detailed bibliographic search was accomplished for collecting the data available in scientific literature. The part of the Italian Geothermal Database (BNDG), that is managed by the CNR-IGG (Barbier et al., 2000; Trumpy and Manzella, 2016, Geothopica website), covering the study areas was included. In addition, we included the dataset, kindly and confidentially provided by ENEL GP in the frame of European projects. During this stage, proper coordinate transformations and spatial operations were performed. Topographic bases (ISPRA web site; Tuscan Region web site; Minambiente web site) were firstly organized.

With regard to geology, the database includes different geological maps at different scales, both raster and vector, such as the geological cartography of the Tuscan Region at scale 1:10.000 (Tuscan Region web site). The geological maps of the CARG (Geological CARTography) Project at scale 1:50.000 (ISPRA web site) were used, too.

We also reported the traces of geological or interpreted seismic profiles that have been analysed from literature. Vector contour maps of the geometry of geological or seismic surfaces were computed. Geological surfaces from the interpretation of 3D seismic data were considered for the *Travale* area (kindly and confidentially provided by ENEL).

The main source of data that allows a constrained 3D reconstruction of the geological structures at depth are the stratigraphic well logs, that represent the only direct underground information. Our GIS database counts 195 deep geothermal wells, located in the *Travale* and *Lago Boracifero* areas; the main data e.g. well head coordinates, year of drilling, total measured depth, stratigraphy were stored.

The well dataset from the Italian Geothermal Database partially lack the information on the deviation paths. For this reason, we considered only the wells data coupled with deviation paths or pseudo-vertical wells whose vertical and horizontal off-set is supposed to be negligible. The well data provided confidentially by ENEL GP and complete of deviation path and geophysical logs are located mainly in the *Travale* area. It is worthwhile to highlight that the stratigraphic logs are actually the synthetic stratigraphic well logs reported in the BNDG or provided by ENEL GP, whereas the original data, i.e. the master logs, are not available.

Finally, the database includes the information about the Magnetotelluric and TDEM dataset acquired or used in this study.

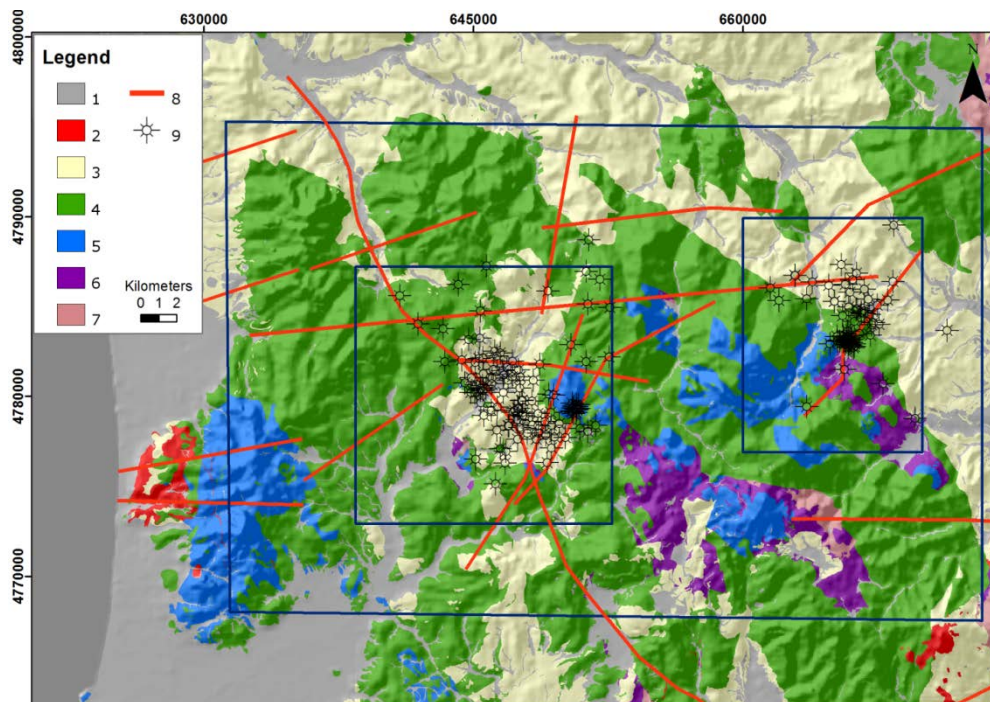


Figure 6.2- Schematic geological map, modified from the geological maps at scale 1:10000 (Tuscany Region website) and overview of the information layers of the GIS database. 1) Quaternary deposits; 2) Igneous rocks; 3) Neoautochthonous terrigenous deposits (Miocene-Pliocene); 4) Ligurian and sub-Ligurian Flysch complex (Jurassic-Eocene); 5) Tuscan Nappe formations (Upper Triassic-Miocene); 6) Calcare Cavernoso and anhydrites (Triassic); 7) Metamorphic Units (Triassic-Paleozoic); 8) Traces of geological or geophysical profiles; 9) Deep geothermal wells. The coordinates are in WGS1984-UTM32N.

## 6.4 The conceptual model

### 6.4.1 Geothermal background, tectonics and heat source

We considered the Larderello-Travale (LTGS) as a “Convective intrusive geothermal play” following the classification from Moeck (2014). For a detailed description of the concept of geothermal play and the geological background of the Larderello-Travale system we refer to the Chapter 2. Hereafter, we summarize the main geological features with a focus on the *Lago Boracifero* sector.

The field is located in the inner part of the Northern Apennine, a sector of the Apennine. The tectonic pile locally crops out along ridges separated by Neogene late-to post-orogenic basins filled with continental to marine sediments (hereafter referred also as “Neoautochthonous or M-P-Q”, from Miocene, Pliocene and Quaternary). The Apenninic tectonic pile includes the Ligurian and sub-Ligurian oceanic units (Jurassic–Eocene), hereafter referred also as “Ligurids or Ligurian Complex”, overlying the “Tuscan Nappe” and “the Tuscan metamorphic units”, derived from the deformation of the Adriatic palaeomargin, Palaeozoic to Miocene in age (Bertini et al., 2006). The Tuscan Nappe in southern Tuscany, particularly in Larderello, is strongly delaminated locally completely absent.

The productive areas of Larderello and Travale, in the West and East respectively, are located approximately 15 km apart and are characterized by similar geological setting. With regard to the deep geothermal system, they represent two exploited areas of an enormous unique vapour-dominated reservoir hosted in crystalline rocks, with an approximated horizontal extension of 400 km<sup>2</sup>.

We would briefly focus on the tectonics of the study area in the proximity of the *Lago Boracifero* sector. According to the model proposed by Carmignani et al. (1994) after the collisional event, a subsequent extensional tectonics eastward migrating affected the inner part of the orogenic belt since at least Early Miocene. An essential role is supposed to be played during this period by crustal transfer faults of regional importance that accommodated the Apennines extension processes (Liotta, 1991), throughout Wrench tectonics. Many authors claimed the possible role in controlling the magma emplacement in the inner Apennines along the transfer zones (e.g. Dini et al., 2008). In figure 6.3 we showed a simplified structural map of southern Tuscany in which are highlighted the dominant extensional structures parallel to Apennine strike (N130E) and the

Antiappenninic-transverse faults. In Lazzarotto (1967) for the first time the possible occurrence of segments of such transfer faults were recognized in the Larderello area in proximity of the Cornia River. In the years the presence or the importance of this fault in the evolution of the geothermal fields of Larderello were quite disregarded. In Costantini et al. (2002), as results of the drawing of the CARG geological map of Italy, the authors supposed that a fault in the proximity of the Cornia River could be a segment of a transfer fault.

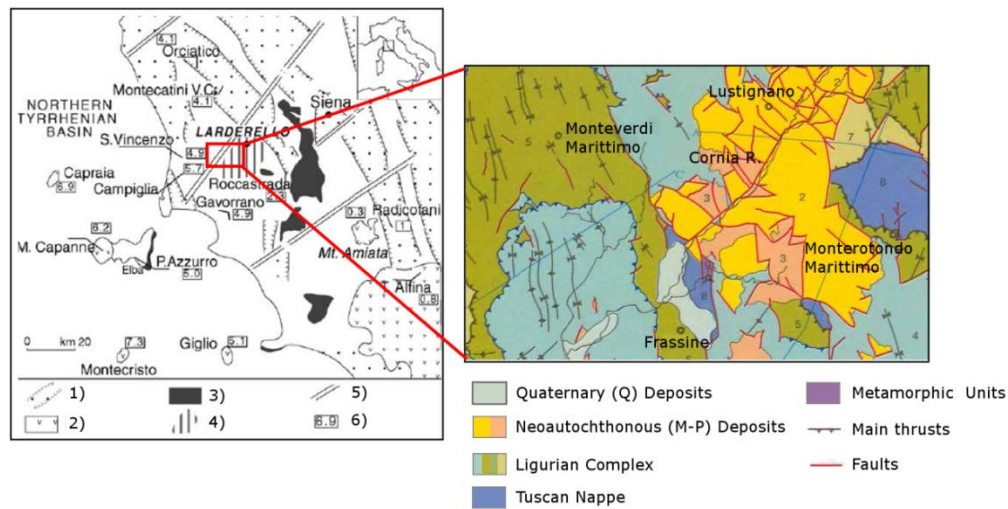


Figure 6.3- On the left, simplified structural map (modified from Brogi et al., 2005) of southern Tuscany showing: 1) the main extensional structures forming the Neogene Basins; 2) the magmatic rocks, 3) the metamorphic units, the 4) Miocene and Pliocene transfer zones and 5) the ages of the main magmatic bodies. A zoom on the right is shown from the structural sketch of the Massa Marittima Geological Map (CARG Project, Costantini et al., 2002).

The geodynamic setting and the Neogene to Quaternary magmatic activity produced a huge geothermal anomaly in southern Tuscany, with maximum peaks centred in the Larderello area with values of heat flow up to  $1000 \text{ mWm}^{-2}$  (Baldi et al., 1994). It should be noted that the peaks of heat flow, geothermal gradient and also of the Helium isotope ( $R/R_a$ ) values are centred in the *Lago Boracifero* sector (Magro et al., 2003; Bellani et al., 2004), i.e. the study area of this thesis. Geophysical data and thermal numerical modelling support the hypothesis of deep buried still molten igneous intrusions (see Chapter 2)

The LTGS is one of the few examples in the world of vapour-dominated system, being characterized by superheated steam at depths over 3500 meters

b.g.l. with temperature exceeding 350 °C and pressure up to 70 bar (Romagnoli et al., 2010). The hydrothermal circulation occurs into two geothermal reservoirs. The shallow reservoir consists of several rock types, but Mesozoic limestone and anhydrite dolostone are predominant. The deep reservoir consists of phyllite, micaschist, gneiss, skarn, hornfels and granite.

The primary porosity of the rocks hosting the hydrothermal circulation is almost homogeneous and very low (1-5%), whereas the secondary permeability is strongly heterogeneous, due to the variability of the fracture networks and can locally reach values greater than 5 mD (Arias et al., 2010).

Strong seismic reflectors in the metamorphic complex have been explained with rock fracturing and the presence of fluids (e.g. Casini et al., 2010a). 2D seismic and recent 3D seismic surveys clearly detected two important seismic markers: *i*) H-horizon and *ii*) K-horizon. The H-horizon is a discontinuous high amplitude reflector, bright-spot type, corresponding to highly productive intervals (Bertini et al., 2006) and represents the mining target. Indeed, its detailed imaging allowed the abrupt decrease of the mining risk.

The K-horizon is a high amplitude and locally bright-spot type reflector, more continuous and deeper than the H-horizon. The origin and nature of the K-horizon is still debated in literature; a recent interpretation suggests the presence of supercritical fluids at the top of young igneous intrusion (Bertini et al., 2006, Gianelli, 2008). It was not yet drilled, but it represents the target of a deep exploration project, inside the *Lago Boracifero* area as possible deep-seated supercritical reservoir. The San Pompeo-2 geothermal well is supposed to have reached the proximity of the K-horizon, when a main blow-out of the well occurred and forced the operator to close the borehole.

The enormous amount of thermal energy is efficiently stored into the deep-seated reservoirs, thanks to the cap-rock of the system. At Larderello, the seal is composed by sedimentary rocks belonging to the Ligurian/Sub-Ligurian domain (Jurassic-Eocene), that tectonically overlay the carbonates and the crystalline rocks, and by the Neoautochthonous basin deposits.

Isotopic studies on discharged steam at Larderello indicated a predominant meteoric origin. The recharge supplies 1/3 of the steam production in the field, while the rest comes from the boiling of deep seated fluids (Panichi et al., 1974; Celati et al., 1991).

Few considerations are summarized below in order to point out the scientific relevance of the *Lago Boracifero* sector:

- High temperature hydrothermal circulation is here exploited, with temperature up to 350 °C;
- A regional culmination of the seismic K-horizon occurs in this sector reaching depths of about 3-4 km;
- Very high temperature and high pressure systems possibly at supercritical condition are inferred at or close the depth of K-horizon, and are shallow enough to be explored with current technologies; expected temperature > 400°C and pressure > 290 bar.

### 6.4.2 Stratigraphy

An up-scaling of the stratigraphic features was necessary to improve the modelling. We followed the concept of Litho-Electrical units proposed by Santilano et al. (2016a). We grouped the geological units considering first of all similar lithological and tectono-stratigraphic evidences and then the electrical resistivity of rocks. This approach is useful for using the geological model as a-priori information to constrain Magnetotelluric inversion.

The tectono-stratigraphic complexes, occurring in southern Tuscany, were abundantly studied in literature (e.g. Cameli et al., 1993; Batini et al., 2003; Brogi et al., 2005 and reference therein). The main features of the stratigraphic setting at Larderello-Travale are widely accepted in the scientific community. Some issues are still matter of debate and for the computation of the 3D models we had to critically analyse the available data and try to validate our assumptions. We refer particularly to the boundary between the sedimentary “Tuscan Nappe” and the Paleozoic “Tuscan metamorphic units” (hereafter also referred as “metamorphic basement or basement”). For this particular aspect, we analysed the stratigraphic logs of selected wells from the *Lago Boracifero* and *Travale* areas and literature data. A pioneering study by Gianelli et al. (1978), firstly recognized the Tectonic Wedges Complex (hereafter referred also as TWC) as tectonic wedges of Paleozoic phyllites, metamorphic Triassic “Verrucano” and carbonates. At a regional scale in Tuscany, the dolostone and anhydrites of “Burano Formation” are considered the base of the Tuscan Nappe. Our analysis drove us to consider suitable for the modelling the stratigraphic setting proposed by Pandeli et al. (1991), specifically for the area of interest. The concept is that, at Larderello, the Triassic dolostone and anhydrites similar to “Burano Fm.” and “Calcere

Cavernoso” are included into the TWC. This complex seems to be related to the main structural highs of the geothermal reservoir (corresponding to our study areas) and is embedded between the Tuscan Nappe or Ligurids and the “basement”.

Hereby, we described the simplified stratigraphy that we adopted as benchmark for the 3D geological modelling areas:

- Neautochthonous Complex (Miocene - Quaternary);
- Ligurian Complex (Jurassic - Oligocene);
- Tuscan Nappe (Triassic to Miocene);
- Tectonic Wedges Complex (Paleozoic-Triassic);
- Metamorphic Basement (Pre-Cambrian? – Paleozoic):
  - Phyllitic Complex
  - Micaschist Complex
  - Gneiss Complex
- Intrusive Complex (Pliocene – Quaternary?)

The *Neautochthonous* units are composed by Miocene to Quaternary deposits, mainly related to marine, lacustrine and to continental environments, represented by conglomerates, sandstone, clays, marls and evaporites. The origin and nature of this basins is still debated in literature, if caused by extensional or compressive (thrust-top basins) tectonics. This aspect is out of the aim of the thesis and for a detailed description we refer to (Carmignani et al., 1994; Bonini et al., 2001 and reference therein). The analysis of the stratigraphic well logs revealed up to 670 meters of Neautochthonous deposits along the V.C.-4 geothermal well in the *Lago Boracifero* area. In the *Travale* area more than 1100 meters has been reported in the well logs near Radicondoli.

Many studies have been carried out on the *Ligurian Complex* (Nirta et al., 2005; Pandeli et al., 2005; Marroni and Pandolfi, 2007 and reference therein). The genesis is related to the convergence tectonics that caused the closure of the Ligurian-Piedmont Ocean since Late Cretaceous. Due to the polyphased tectonics the tectono-stratigraphy is really complex. The units widely crop out in southern Tuscany and in literature they are divided into three main domains, geometrically from the top downward: *i*) Internal unit; *ii*) External unit and *iii*) Sub-ligurian units. The Internal domain is mainly represented by the Jurassic ophiolite sequence of Jurassic age representing the base of a sedimentary cover. The External units and the Sub-ligurian units represent the ocean-continent transition.

The main lithologies are shales, siliceous limestones, marly limestones and calcareous arenites. For the modelling purposes, these three domains can be modelled as a whole complex, due to the general behaviour as impermeable cap-rock and a low electrical resistivity response in the areas of study.

The *Tuscan Nappe* represents a sedimentary succession deposited since Triassic to Miocene on the continental paleomargin of the Adria Plate. The succession was strongly delaminated by tectonic processes (the so called “Serie Ridotta”). The scientific community is still debating on the nature of this processes, if related to compression or extensional tectonics (e.g. Decandia et al., 1993; Finetti et al. 2001). The issue is not a central topic of this study, but the matter of fact, for the 3D modelling, is that the Tuscan Nappe has a complex geometry at depth. Usually, the Nappe is characterized by locally large thicknesses that abruptly decrease laterally up to the complete tectonic omission, showing a well known boudinage-like shape.

In southern Tuscany, the base of the sedimentary Tuscan Nappe is composed by Triassic evaporites, dolostone and limestone (Burano Fm. and Calcare Cavernoso). As described previously, in the study areas these units were included in the TWC complex, for tectonic considerations. The Rhaetian-Liassic formation of the Tuscan Nappe was rarely involved in the TWC, and for this reason our conceptual model considers this layer the base of the Tuscan Nappe. The succession continues upward with the shelf limestone Jurassic in age. Pelagic deposits, Jurassic to Oligocene, end with the marls and clays of the “Scaglia Toscana Fm”. Siliciclastic turbidite deposit, Miocene in age, known as “Macigno Fm” represents the higher unit of the Nappe. The wide outcrops of the Tuscan Nappe carbonates occur near the Travale and Montieri towns in the *Travale* area, and near Monterotondo Marittimo for the *Lago Boracifero* area. These outcrops are supposed to be the local recharge of the geothermal system.

The *Tectonic Wedges Complex* is widely present in the two study areas and is embedded between the Tuscan Nappe or Ligurids and the “basement”. It is composed by a pile of alternating tectonic slices (wedges) of Burano and Calcare Cavernoso-like sedimentary rocks and low-grade metamorphic clastic sequences, Triassic (Verrucano) and Paleozoic in age (Pandeli et al., 1991). This complex has been widely cored by the deep geothermal wells. As exhaustive example for the two areas of *Lago Boracifero* and *Travale*, we reported the stratigraphy from the geothermal well Castiglioni-1 (figure 6.4). In this case the Tuscan Nappe is absent (due to tectonic processes) and at the base of Ligurids a succession of tectonic

wedges in direct (tectonic) contact occurs. The TWC succession starts with a 20 m thick layer of Burano-like rocks and continues up to the involvement of the Paleozoic basement.

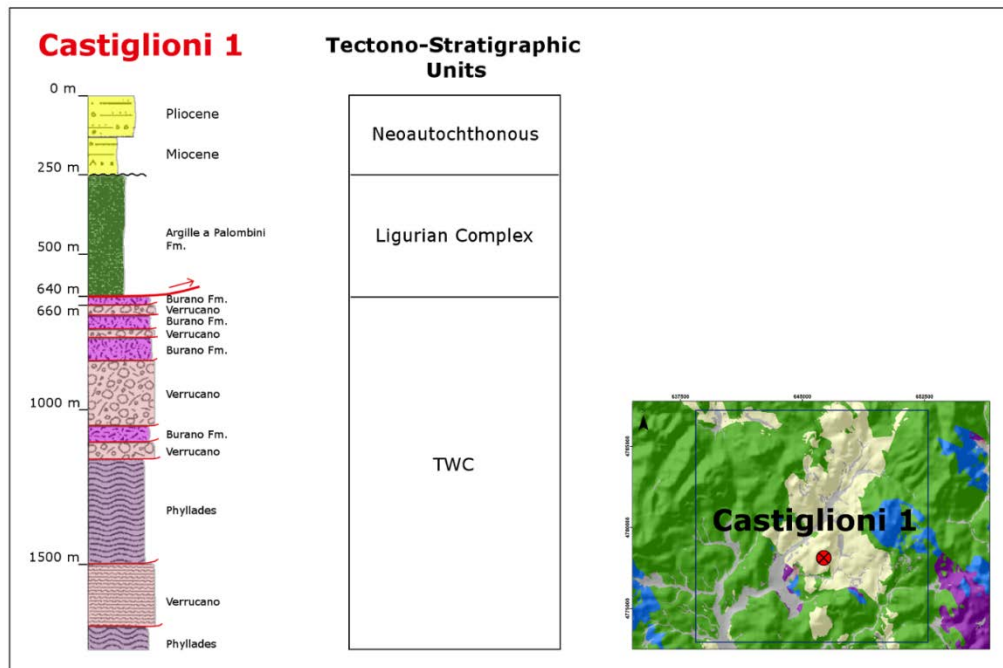


Figure 6.4- Geothermal well Castiglioni-1. The stratigraphy is that of Pandeli et al. (1991) and Italian Geothermal Database. The related Tectono-stratigraphic units and the location of the well are reported.

The *Metamorphic basement* is composed by three main complexes: *i*) Phyllitic Complex; *ii*) Micaschist Complex and *iii*) Gneiss Complex. The lithological characteristics are described in the review of the geological features of the Larderello field proposed by Bertini et al. (2006).

Phyllitic Complex is composed mainly by metagreywacke and subordinately by carbonate–siliciclastic metasediments (Cambrian–Devonian). Micaschist Complex, consisting of micaschist with minor amphibolite, is probably Precambrian to Early Palaeozoic in age. This first two complexes have been recognized as part of the Monticiano-Roccastrada Unit by other authors (e.g. Brogi et al., 2005). The Gneiss Complex, includes gneisses with minor amphibolite layers probably Precambrian to Early Palaeozoic in age.

With regards to the *Intrusive Complex*, the Larderello igneous bodies have been cored in several deep wells. The rocks range in composition from monzogranites to syeno-monzogranites, with ages ranging from 3.8 to 1.3 Myr (Dini et al., 2005); present partially melted igneous intrusions possibly occur (see Chapter 2). The interpretation of some authors implies the presence of a very large recent batholite (e.g. Romagnoli et al., 2010; Arias et al., 2010).

In figure 6.5 we summarized the principal characteristics of the LTGS in order to depict the conceptual model.

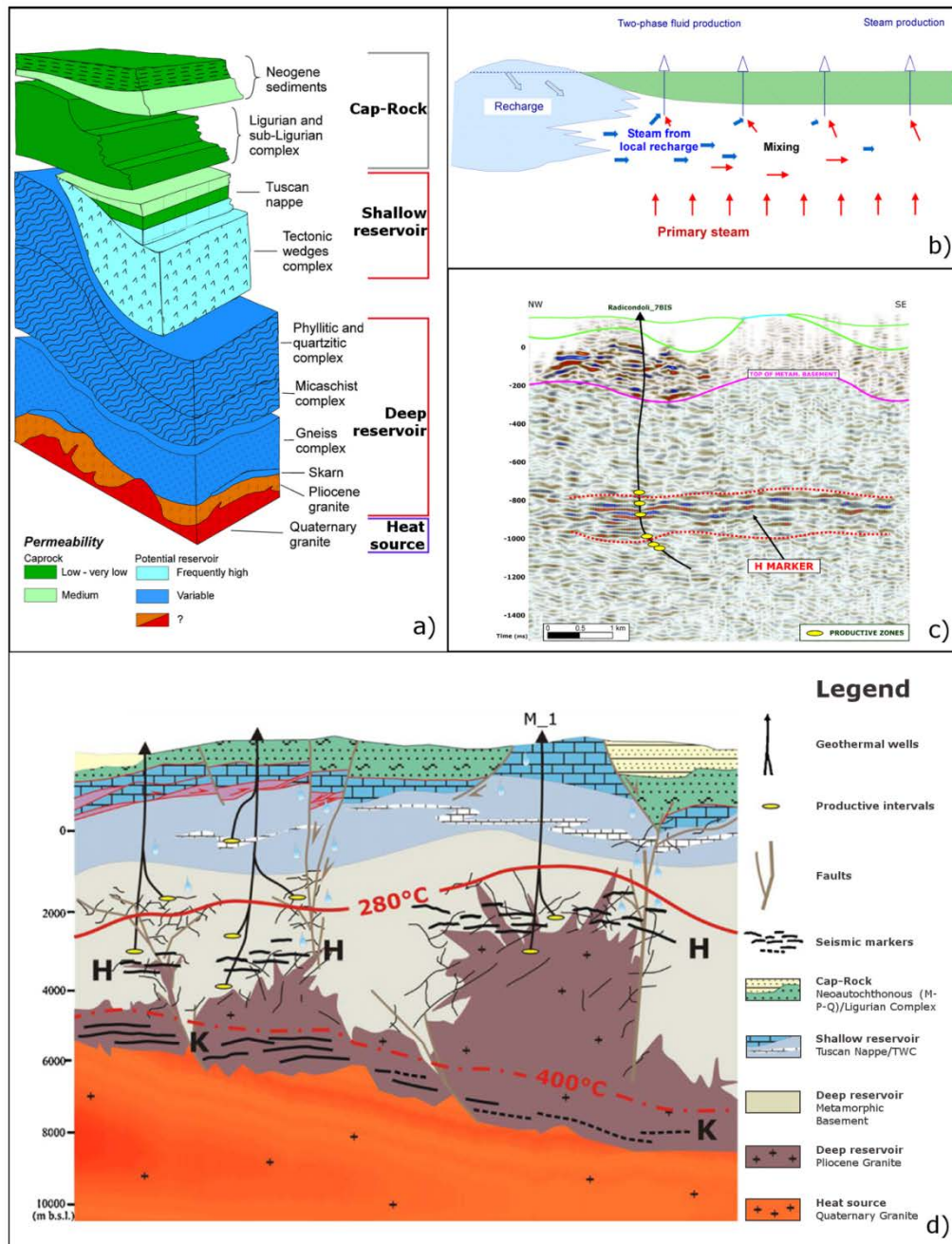


Figure 6.5- The conceptual model of the Travale-Larderello field. a) Schematic sketch of the tectono-stratigraphic and hydrogeological complexes (modified from Arias et al., 2010 and Romagnoli et al., 2010). b) Schematic cross-section of the interference between the local recharge and the deep primary steam and its influence on the steam discharged by the geothermal wells at Larderello-Travale (from Romagnoli et al., 2010). c) Seismic reflections related to the highly productive H-horizon within the metamorphic

basement (from Casini et al., 2010b). d) Schematic conceptual model of the *Travale* area (modified from Casini et al., 2010b).

## 6.5 The 3D modelling

### 6.5.1 Input data

The 3D geological models of the study areas were computed in Petrel environment (Schlumberger), a software commonly adopted for the exploration and management of oil and gas fields and secondarily deep geothermal fields. Part of the database, designed in 2D GIS environment and briefly described in Section 6.3, was processed in order to develop a 3D database. The data used as input for the 3D geological modelling are listed in Table 6.1.

The workflow is conceptually very simple, being composed by the following steps:

- develop a 3D database
- set the constrain points from the input data
- computation of the top of each unit by 3D geostatistical tools
- build the 3D geological model, based on the 3D reconstruction of the top of the units

Table 6.1- Summary of the input data used for the 3D geological modelling. The model of interest for each source of data is listed.

DATA	TYPE	SOURCE	MODEL
DEM	Vector (from raster)	Geoportale Nazionale (Minambiente web site)	Regional-Lago B-Travale
Geological map 1:10.000	Vector	Tuscan Region web site	Regional-Lago B-Travale
Geological maps 1:50.000	Raster	CARG Project (ISPRA web site)	Lago B.
Top of the metamorphic basement	Vector	Bertani et al., 2005	Regional
Top of the Carbonate reservoir	Vector	Geothopica web site	Regional
Top of K-Horizon	Vector (from raster)	Cameli et al., 1998	Regional
Geological cross-sections	Raster	Scientific articles, CARG	Lago B-

		Project (ISPRA web site)	Travale
Interpreted deep seismic profile CROP 18A	Raster	Brogi et al., 2005	Lago B.
Top of Phyllitic and Igneous Complexes from 3D seismic data	Vector	ENEL GP (confidentially in the frame of European Projects)	Travale
K-Horizon from 3D seismic data	Vector	ENEL GP (confidentially in the frame of European Projects)	Lago B- Travale
Well data and stratigraphic well tops (101)		BNDG (Barbier et al. 2000, Trumpy and Manzella, 2016)	Lago B.
Well data stratigraphic well tops (89)		ENEL GP (confidentially in the frame of European Projects)	Lago B- Travale

Technically, one of the main effort was the homogenization of the different source of data that we collected. Let examine the principal source of data, i.e. the stratigraphic well logs, that represents the only direct information on the subsoil. The database counts 195 deep geothermal wells, located in the *Travale* and *Lago Boracifero* areas. The oldest well in database, San Edoardo 1, was drilled in the late '20s and some other wells in the '30s. Most of the wells were drilled in the '60s, '70s and '80s and some wells in the '90s. It is clear that different interpretation could result. The scientists that managed the Italian Geothermal Database accomplished a first attempt to homogenize the dataset, but in this study we tried to frame the stratigraphies, reported in the BNDG into our conceptual stratigraphy (figure 6.6).

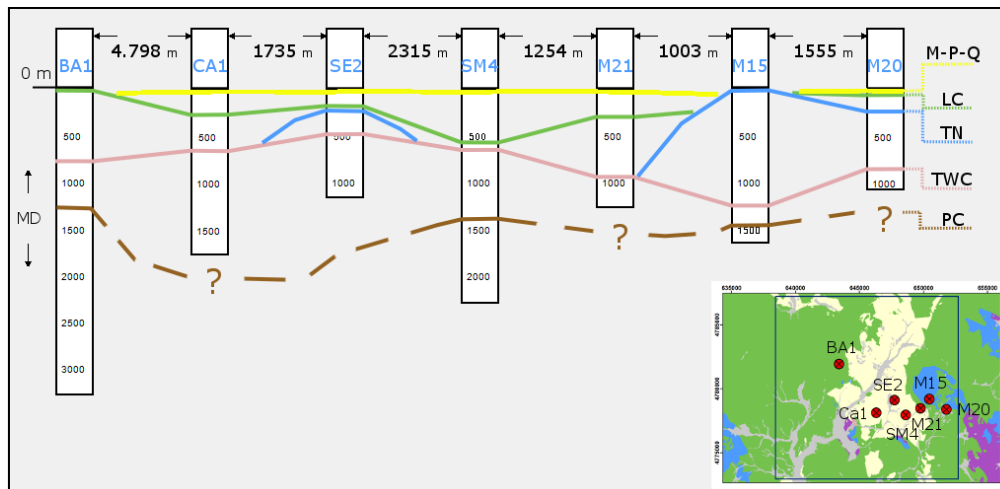


Figure 6.6- Wells correlation from the *Lago Boracifero* area. Seven wells (from Italian Geothermal Database) are considered: Badia 1 (BA1), Castiglioni 1 (CA1), San Edoardo 2 (SE2), San Martino 4 (SM4), Monterotondo 21-15-20 (M21-M15-M20). See the map for location. The simplified stratigraphy is plotted: Neoauchthonous (Miocene to Quaternary, M-P-Q), Ligurian Complex (LC), Tuscan Nappe (TN), Tectonic Wedges Complex (TWC), PC (Phyllitic Complex). The horizontal distance between wells is shown in meters as well as the Measured Depth.

Each well was imported in Petrel coupled with the data on stratigraphy known as “well tops”, i.e. the depth of the top of a unit (figure 6.7a). The “well tops” are considered the data that mostly control the interpolation for computing each tops. Most of the wells has maximum measured depth MD less than 2000 meters, whereas about 50 wells are deeper than 2000 meters up to 4500 meters (MD).

Mainly for the *Travale* area, ENEL GP provided in a confidentiality agreement the more detailed well stratigraphies, coupled with the information on the deviation well path. In addition, we were allowed to use also as input data the 3D reconstruction of the top of the K-horizon, the top of wide igneous intrusion, and the top the Phyllitic Complex. These geometries were the results of a wide 3D seismic survey described in Casini et al. (2010a-b).

Different sources of data have been used for constraining the reconstruction at depth of the 3D geometries (figure 6.7b-c). With regard to the *Lago Boracifero* model, we imported in 3D the deep geological cross-sections available in literature. We refer for example to the CROP 18A, a deep seismic profile, interpreted by Brogi et al. (2005) or the integrated geological profiles by

Romagnoli et al. (2010). Other information available in literature such as the contour maps of geological and seismic surfaces was used, too.

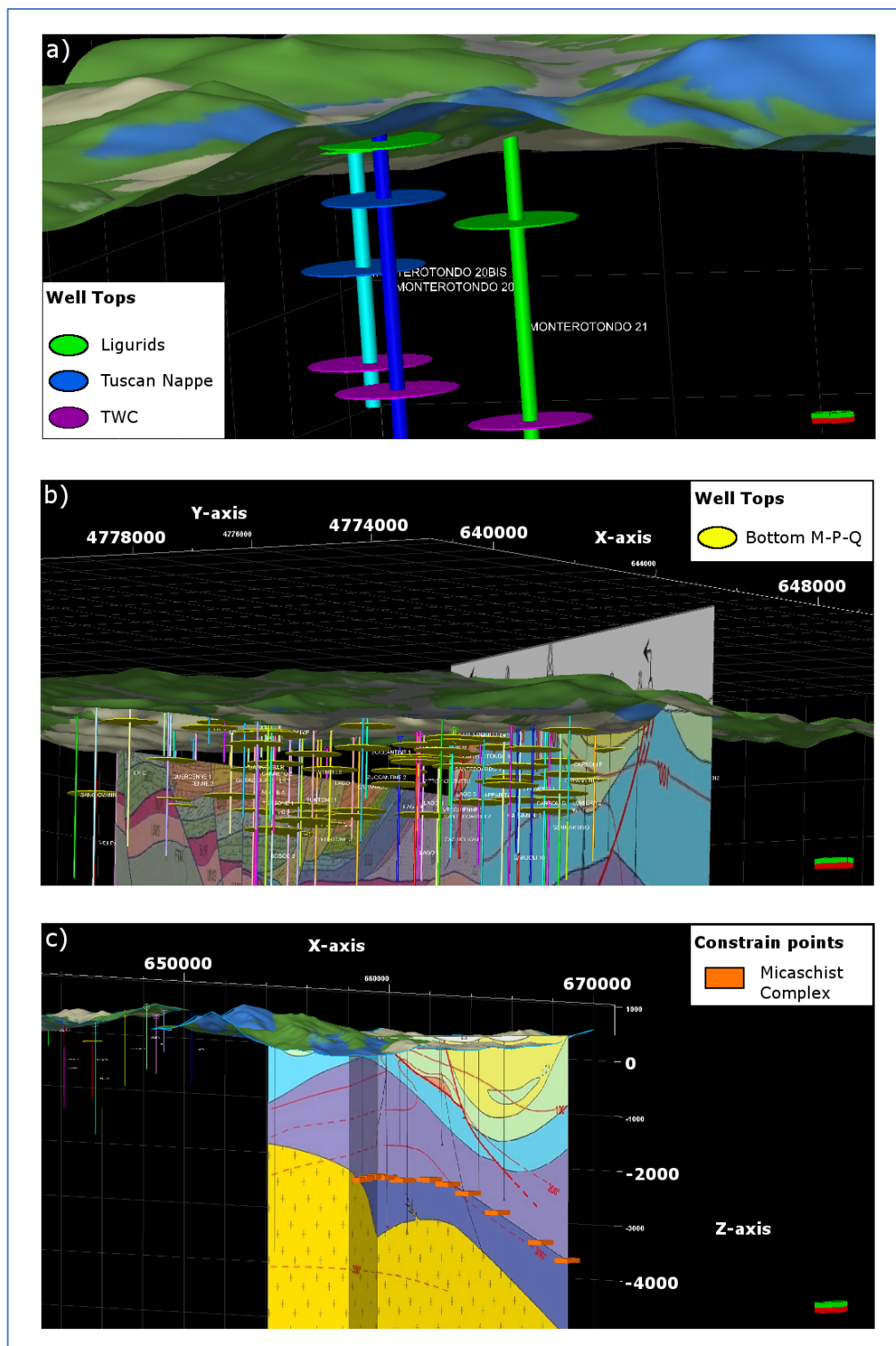


Figure 6.7- Overview of input data for 3D modelling. a) Example of stratigraphic

well tops near Monterotondo Marittimo town. b) Different source of input data (*Lago Boracifero* area): Well tops for the bottom of Neoautochthonous Complex, on the right the integrated geological cross-section (from Romagnoli et al., 2010; and on the left the geological cross-section of the geological map 1:50.000 “Foglio 306, Massa Marittima” (ISPRA web site). c) Conversion from raster data to constrain points: example from the *Travale* area for the top of Micaschist Complex (the section is from Romagnoli et al., 2010).

Coupled with the underground information, we implemented also the dataset on surface. The vector geological map, simplified according to our classification, was used to create the constrain points of the outcropping units.

### 6.5.2 Horizons interpolation and 3D Grid

In Table 6.2 we listed the units modelled for the three areas: *Travale*, *Lago Boracifero* and *regional model*. Briefly, for the *regional model* we realized a first-order approximation of the geology over wide areas in southern Tuscany. We considered the K-horizon (from Cameli et al., 1998) as lower boundary, then we modelled the metamorphic basement (from Bertani et al., 2005) and the top of the Tuscan Nappe (from BNDG). The topography represented the top of the impermeable cap-rock (Ligurian Complex and Neoautochthonous) except for the local outcrops of the Tuscan Nappe or the basement.

The *Lago Boracifero* and *Travale* models represent the detailed reconstructions of the complex geology of the two sectors of the LTGS field. The whole stratigraphy, from the Neoautochthonous to the Intrusive Complex, has been modelled by integrating different sources of data, previously described.

Table 6.2- List of units modelled for each area of study.

UNIT	MODEL
Neoautochthonous Complex	Lago B-Travale
Ligurian Complex	Lago B-Travale
Tuscan Nappe	Lago B-Travale
TWC	Lago B-Travale
Phyllitic Complex	Lago B-Travale
Micaschist Complex	Lago B-Travale
Gneiss Complex	Lago B.
Igneous Complex	Travale
K-Horizon (base of the model)	Regional-Lago B-Travale

Neoautochthonous and Ligurian Complexes (Imperable cap-rock)	Regional
Tuscan nappe + TWC (Shallow reservoir)	Regional
Metamorphic basement (Deep reservoir)	Regional

The computing of the top of a unit implied the interpolation of the input data (constrained points). As previously stated, the main input data are represented by the stratigraphic well tops. The tool “global adjustment by well tops“ in Petrel allows the use of different interpolation methods for reconstructing the surface (corresponding to the top of the unit). We preferred to use the “convergent method”, that is the general algorithm used to build most of the surfaces in Petrel. Only for some surfaces the adoption of the “moving average” algorithm produced more reliable results, e.g. for the tops of the Micaschist Complex for the two areas. This is based upon an inverse distance weighting; we adopted the quadruple inverse distance, giving higher weight to points near to the grid nodes. The grid resolution for the tops of the tectono-stratigraphic units is 250 meters.

The last step was the reconstruction of the 3D grids; i.e. the 3D geological models. Different methods can be used for the 3D gridding in Petrel environment, some of them requiring the reconstruction of faults geometries (e.g. Santilano et al., 2016a). For our purposes, the “simple grid” method appeared suitable. The tools take into account the geometries of the tops of each units and the stratigraphic role: *i*) “base”, to truncate the above horizons, *ii*) “erosional”, to truncate the below horizons, *iii*) “discontinuous”, acting both as base and erosional and *iv*) “conformable”, truncated by other horizons.

Finally, the 3D geological models at regional scale and of the *Travale* and *Lago Boracifero* areas were computed with a resolution of 250 meters (figure 6.8).

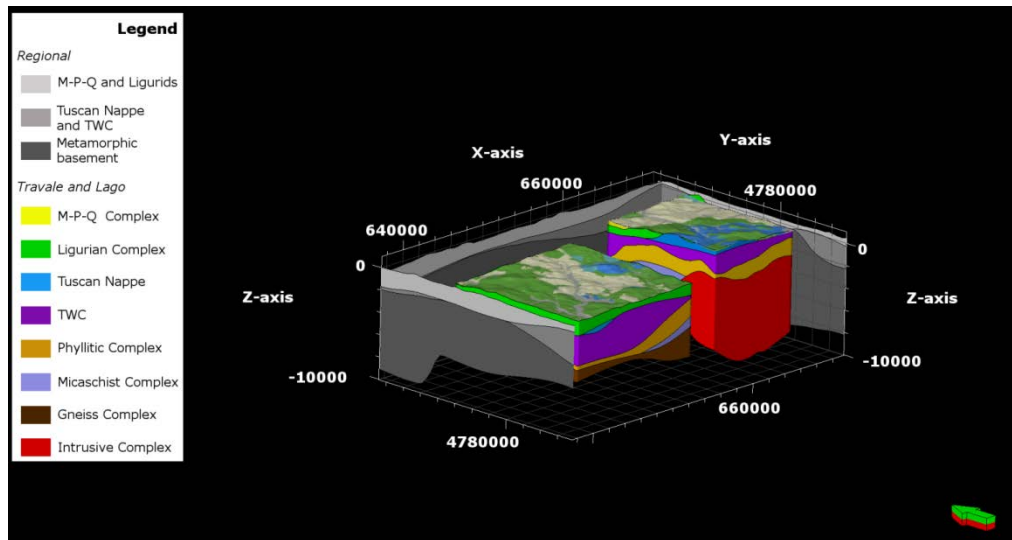


Figure 6.8- 3D geological models. In grey-scale format is shown the regional model, in colour-scale are shown the *Lago Boracifero* and *Travale* models.

## 6.6 Discussion on the 3D models

Some clear evidences can be pointed out from the 3D modelling. Firstly at regional scale, the structural high of the metamorphic basement occurs below the two sectors of the field, *Lago Boracifero* and *Travale*. Secondly and most important, the dome-like shape of the seismic K-horizon reaches its lowest depth below the *Lago Boracifero* area that is in one of the hottest sector of the field with the highest heat flow values.

With regard to the two areas of study, it can be stated that the integration of the different source of data produced reliable 3D geological models in a complex tectono-stratigraphic setting. In figure 6.9 we show an example of resulting geometries from the gridding, with respect to the direct information of well tops along two profiles. We stress that the boudinage-like geometry of the Tuscan Nappe, widely discussed in literature, was also depicted in our models.

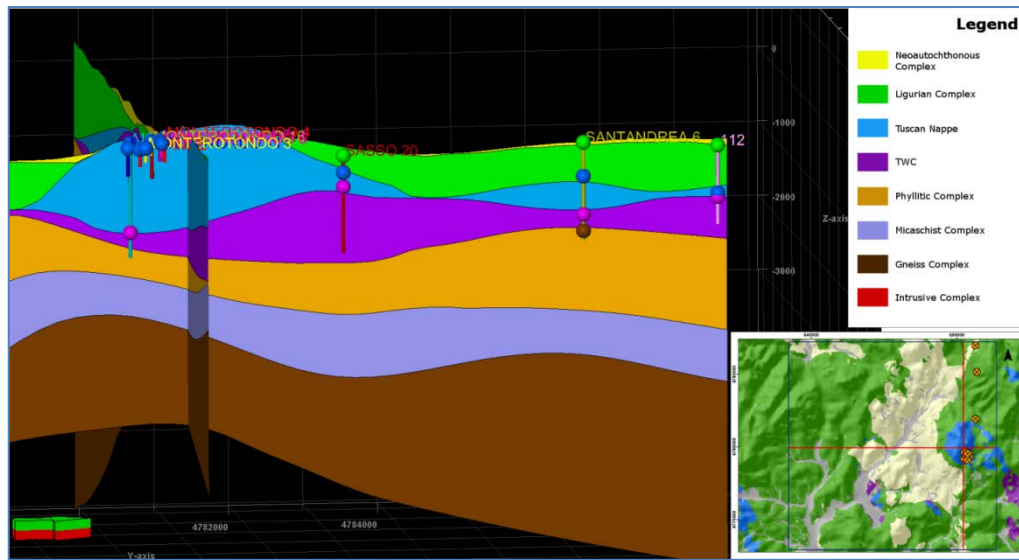


Figure 6.9- Resulting models compared with the stratigraphic well logs. The location of wells and the traces of the two perpendicular profile are shown.

In the *Travale* area the Gneiss Complex was not modelled due to a wide Pliocene (probably to Quaternary) igneous intrusion (cooled in the shallow level) that was intruded in the proximity of this complex. The size of this intrusion is highly debated in the scientific community. The database in this sector is that of ENEL that considers a very wide intrusion at depth. Most probably the structure is that of a very complex composite batholite. The lowest Gneiss Complex was drilled in very few wells in the *Travale* area, and the distinction between Intrusive and Gneiss complex is out of the resolution of our model. Conversely, in the *Lago Boracifero* area the Gneiss Complex was drilled abundantly and we modelled all the units except for the Intrusive Complex. Indeed, in this area the intrusion seems to occur mainly close or below the K-horizon that represents the base of the model.

Finally, we highlight that the models do not consider at the moment the faults, although we recognize the role of the fault modelling in geothermal exploration. With the quality and quantity of data used for implementing the models, the resulting surfaces accommodate the displacement of the main structures. The final models are reliable and suitable to be used as a-priori information for the Magnetotelluric inversion and for the further data interpretation.

## Chapter 7

# The MT study of the Larderello-Travale geothermal system: the EM dataset

### 7.1 Introduction

The EM geophysical study carried out in the Larderello-Travale field is here presented. In this chapter we described in details the acquisition and the processing of the new MT and TDEM dataset acquired in the *Lago Boracifero* area, in the frame of the FP7 IMAGE Project and of this PhD program as well as older datasets.

Despite 100 years of exploitation and exploration, many issues are still debated on the physics of the geothermal processes in this field. The analysis of the new dataset can contribute to the understanding of this issues. We particularly refer: *i)* to the anomalous low electrical resistivity values that were estimated locally in the reservoir and *ii)* to the uncertainties on the deep structures of the field in the proximity of the “Boraciferous Lake” (*Lago Boracifero*) and *iii)* the role of faults in the hydrothermal circulation.

The geophysical study counted the analysis of old and new MT dataset for a total amount of 146 soundings in the whole field. The *Lago Boracifero* area is to be considered the main target of this study and despite its prominent geothermal

features, this sector was not widely investigated by Magnetotellurics. Some considerations on the scientific relevance of this sector are summarized in Subsection 6.4.1.

The new dataset, acquired in *Lago Boracifero*, was integrated with other MT datasets previously acquired in the surrounding areas and in the *Travale* sector. We considered crucial the analysis of the old MT datasets that were previously acquired in the frame of old geothermal exploration activities and research projects. The importance of this data relies first of all on the possibility to compare the data with other information such as the geophysical well logs that is available only in few sectors of the Travel area (kindly and confidentially provided by ENEL GP). Here, the analysis of these MT soundings highlighted specific problematics to be taken into account for the organization of the MT survey we carried out in this study, e.g. static shift effects and strong near field effect (DC railways). Furthermore, the analysis of the MT soundings acquired along two very long profiles across southern Tuscany from the coast to the Travale field (Fiordelisi et al., 1998), results in estimated resistivity models at regional scale very important for preliminary information on deep structures (see Subsection 7.2.2).

In the *Lago Boracifero* area, the TDEM soundings have been acquired at the same sites of selected MT soundings, and used for static shift correction of the MT data. We tested different approaches to achieve optimal correction by a joint analysis. In the next chapters we discussed also the application of a simultaneous probabilistic optimization of MT and TDEM soundings for a more accurate initial model for 2D interpretation of MT data.

## **7.2 State of the art and open challenges in the EM exploration of the Larderello-Travale field**

### **7.2.1 Previous EM studies and open challenges**

Hereby, an updated state of the art of the EM exploration activities and research projects in the Larderello field is described as well as the open challenges that the EM geophysics can contribute to solve. Since 1913, the exploration and exploitation of the field was continuously directed toward deeper levels of the systems, focusing on the deep crystalline reservoir. The geophysical exploration evolved in this period as long as the industrial target was the shallow reservoir,

the DC methods, were used to image the top of carbonates being more resistive than overlying cap rocks. After collecting thousands of soundings in the area, these methods, were partially abandoned due to the difficulty to image the resistivity of deep targets. Magnetotellurics was therefore adopted to obtain information on the resistivity distribution at depth of the geothermal reservoir and the inferred heat sources.

Early experiments were conducted in the '70-'80s, e.g. Mosnier and Planson (1985). The authors used the “differential magnetic soundings” method in order to detect the channelling of the natural telluric currents by conductive electric structures. They observed strong conductors below the *Travale* area and linked this behaviour to the geothermal activity, and mentioned also the expected resistive behaviour due to the vapour state of the geothermal fluids. In the same period, other groups acquired MT data in the *Travale* area (Duprat and Gole, 1985; Hutton, 1985; Schwarz et al., 1985), observing a highly coherent noise affecting the low frequency data in the whole area.

Since the early '90 to the 2009, many Magnetotelluric studies have been carried out in southern Tuscany and specifically in the Larderello-Travale field in the frame of industrial exploration or in the frame of research projects. Fiordelisi et al. (1998) and Manzella (2004), obtained first indication on the deep resistivity distribution in Southern Tuscany, along very long MT profiles. The strong heterogeneity of the resistivity distribution is the main feature that all these studies highlighted, coupled with the strong EM noise and other important issues such as the widespread low resistive responses at the depth of the reservoir and low resistivity at higher depth interpreted as due to the occurrence of partial melt. Here the first open challenges: Why low electrical resistivity occurs in a vapour-dominated reservoir? Could the deep-buried resistivity anomalies (below the reservoirs) correspond to igneous and still melted intrusions and can be estimated a first-order approximation of their geometries?

With regard to the imaging of such resistivity anomalies in the deep geothermal reservoir, further detailed magnetotelluric studies have been carried out in the *Travale* sector in the frame of the INTAS and I-GET European Projects during the period 2004-2009. Many MT data were acquired and multidisciplinary studies were accomplished in order to depict in details the resistivity anomalies and to understand the physics behind these electrical responses in *Travale* but a unique explanation was not figured out.

Manzella et al., (2006) described the results coming from the analysis of the first part of the MT dataset that is nowadays available for the *Travale* area. In particular, this study was focused on the correlation with the main active faults and the electrical resistivity distribution. The authors recognized low resistivity anomalies that were interpreted to be related to higher permeability zone with circulating fluids strongly controlled by the structural setting. The occurrence of a relevant fault is imaged by low resistivity that can be related to the hydrothermal alteration of active hydrothermal circulation (see figure 4.2).

In Giolito et al. (2009) and Manzella et al. (2010) the authors proposed an extremely interesting multidisciplinary approach that provided for the integrated analysis between the whole MT dataset and mineralogical analysis on cuttings and cores of the deep geothermal wells and geophysical well logs in the *Travale* sector. The aim of this study was the understanding of the cause of the reduction in the resistivity in the vapour-dominated crystalline reservoir, that in this area was recognized up to few  $\Omega\text{m}$  in crystalline rocks. The results highlighted an inverse correlation between the amount of phyllosilicates and the resistivity measured in wells. The authors did not consider this correlation the cause of the widespread low resistivity anomaly detected by MT in the vapour-dominated reservoir, suggesting a role played by liquid phase in the reservoir occurring in small pores (although never highlighted by production tests).

It should be mentioned that Spichak and Zakharova (2014; 2015a; 2015b) completely differed from the above described interpretations. The authors analysed the same MT dataset in the *Travale* area, with a different approach based on the joint analysis of the resistivity and temperature models. They concluded that the heat transport accounts only for monophasic vapour hydrothermal circulation also at supercritical conditions and related it to the high resistive zone of the *Travale* field. Furthermore, the authors applied electromagnetic geothermometry technique (Spichak and Zakharova, 2015b) for estimating the temperature model from MT data.

The difficulty to interpret low resistivity anomalies in dry-steam reservoirs, led also a part of the scientific community to consider questionable the quality of MT data and not excluding a bias or a noise effect (personal communication from A. Manzella). The last issue was taken into account in the frame of the IMAGE Project. Coupled with the MT survey in the *Lago Boracifero* area described in this study, an experimental surface-hole deep ERT (Electrical

Resistivity Tomography) was designed along the Venelle-2 deep geothermal well by the researchers of the CNR-IMAA (see details of the experiment design in Capozzoli et al., 2016; Santilano et al., 2016b). The resistivity models estimated with a controlled source DC method, yet unpublished, show a very strong reduction of resistivity values in the metamorphic rocks in the *Lago Boracifero* area, confirming also that the MT responses in the LTGS field can be taken into account for studying the field.

### **7.2.2 Recent re-analysis of old dataset in southern Tuscany**

In this Subsection we would also mention the results that were achieved in the very early stages of this research published in Santilano et al., (2015c), by re-analysing the old MT soundings (acquired by ENEL in 1992) along a profile crossing the southernmost parts of the Larderello and Travale field. The inversion results were constrained with the starting model extracted from the 3D regional model. The resulting 2D resistivity model was compared with other geophysical data (e.g. seismic tomography) and geological data. Its preliminary information highlighted the widespread low resistivity of the TWC and Phyllitic Complex while a resistivity interface seemed to occur in proximity of Micaschist, Gneiss and intrusive complex. Furthermore, low resistivity anomalies locally occurred within these high resistivity units and a widespread low resistivity behaviour are again recognized at depth > 6-8 km.

### **7.2.3 Additional issues on the deep levels of the field**

What is evident from the state of the art is that the contribution of the main elements affecting the subsoil bulk resistivity, i.e. mineralogy, temperature and physical-chemical features of fluids are still to be fully investigated. Furthermore, many MT studies were conducted in the *Travale* sector whereas poor information was available for the *Lago Boracifero*.

It is worth to mention also some particular aspects on the deep level of the geothermal system where the heat sources, i.e. recent acidic igneous intrusions, are supposed to be seated. Different conceptual models were proposed in literature. Bertini et al., 2006 and Casini et al., 2010a-b in their models interpreted the K-horizon as the top of a recent Quaternary granitic intrusion. This implied very large volume of melt. Brogi et al. (2003) and Liotta and Ranalli (1999) minimized the contribution of the magmatic activity depicting an overall scenario

of a fault-controlled system, particularly they interpreted the K-horizon as kinematic shear zones with entrapped fluids in fractured levels. The conceptual model proposed by Gianelli (1994) imply the emplacement of a composite granitic batholith below the LTGS with local bodies still partially melted. It is evident that this aspect is not trivial; beside the scientific interest, the differences among the models have important implication for the industrial exploration. All the models, however, consider reliable the occurrence of deep-seated supercritical fluids at the depth of the k-horizon.

Another important issue is the role of the faults in the geothermal system, i.e. if these structures represent preferred pathway for hydrothermal circulation. It should be noted that the geothermal operator of the field is targeting the directional drilling toward the “bright spot” seismic reflections, although a clear understanding of its relation with tectonics is still missing.

## 7.3 The EM data in the Larderello-Travale geothermal field

### 7.3.1 Overview of the old MT datasets

A brief description of the old MT data that were acquired in the frame of exploration and research projects is presented; i.e. the MT soundings previously acquired that we were kindly allowed to use in this study. In Table 7.1 we summarized some information about this part of the MT dataset, composed by three sub-dataset.

Table 7.1- Summary of the previously acquired MT datasets used for the study of the LTGS.

Dataset	Sites	Area	Frequency range	Operator	Year	Project
S-Tuscany_92	34	Larderello-Travale	BBMT	ENEL GP	1992	Industrial
Trav-Rad_04	55	Travale	BBMT-AMT	CNR-IGG and EU consortium	2004	INTAS Project
Trav-Rad_07	34	Travale	LMT-AMT	CNR-IGG	2006-2007	I-GET Project

The “S-Tuscany\_92” was part of a larger MT survey carried out by ENEL for the exploration of the geothermal systems in southern Tuscany. Among many MT soundings acquired in the '80 and '90 we selected only the survey that was designed with a remote reference mode (figure 7.1). Indeed, the single sites or local-remote referenced sites were biased by the EM noise. The 34 soundings were acquired using Phoenix V-5 systems along two very long profiles crossing in East-West direction the whole field of Larderello-Travale. A remote reference processing technique (Gamble et al., 1979) and a processing code described by Larsen et al. (1996) were used with the remote site located in the Island of Capraia (Tuscan Archipelago). The EM impedances were measured in the frequency ranged of  $3 \cdot 10^2$  to  $10^{-3}$  Hz. The first two western sites of the North and South profiles have been neglected for the modelling due to the very high level of EM noise. Further details of these soundings are reported in Fiordelisi et al. (1998) and Manzella (2004). The “Trav-Rad\_04” and “Trav-Rad\_07” constitute an important MT dataset acquired in the *Travale* sector in the frame of previous European projects (figure 7.1). The soundings belonging to “Trav-Rad\_04” were acquired using the Phoenix V-5 with impedances measured in the frequency range of  $3 \cdot 10^2$  to  $10^{-3}$  Hz. With regard to the “Trav-Rad\_07” the dataset counts LMT soundings acquired using NIMS or LEMI systems with impedances measured in the frequency range of  $5 \times 10^0$  to  $10^{-3}$  Hz. High frequency ( $10^3$  to  $10^{-1}$  Hz) AMT data were recorded partially in the same place of LMT sites by using the Stratagem system. As previously stated, the EM noise in southern Tuscany, and particularly in exploited geothermal field, is relevant and the remote reference processing technique was adopted, except for the AMT soundings. The remote stations were installed either in Sardinia and Capraia Islands respectively for the “Trav-Rad\_04” and “Trav-Rad\_07” surveys. The acquisition lasted at least 12 hours overnight for BBMT and LMT soundings. The whole dataset was processed with the algorithm described in Larsen et al. (1996).

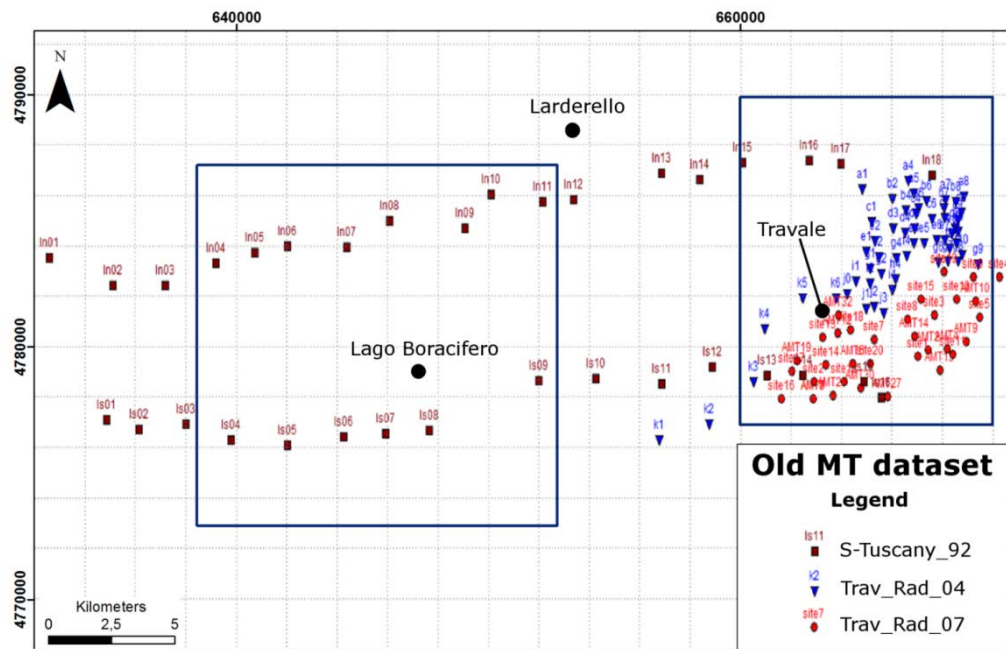


Figure 7.1- Location of the MT soundings acquired in the frame of previous exploration and research projects. The two areas in the blue squares correspond to the *Lago Boracifero* and *Travale* 3D geological models.

We stress that the analyses of old data have been performed by using the MT transfer function tensors as estimated by the authors, and reported in Manzella et al., (2006; 2010), after robust data processing. Furthermore, we performed post-processing analysis such as tensor decomposition, editing of MT curves (e.g. smoothing), dimensionality and directionality analysis, static shift, etc. The static shift problems, affecting some of the soundings, were corrected by the authors using independent geophysical data (e.g. VES and TDEM) that were not anymore available. Few soundings, affected by static shift and lacking of independent geophysical data, have been corrected in this study by integrated analysis with the geology.

The geographical distribution of the old MT data clearly indicates the lack of information in the sector of interest of this study in proximity of the *Lago Boracifero*.

### **7.3.2 MT measurements in the Lago Boracifero sector: the new survey**

In the frame of the FP7 IMAGE Project and of this PhD program, a new MT survey was carried out in the *Lago Boracifero* area coupled with the acquisition of TDEM data. The fieldwork was divided in three parts: *i)* to search a site suitable for installing the remote MT station in the Tuscany mainland, *ii)* to accomplish the MT survey and *iii)* to accomplish the TDEM survey.

Despite the area of interest is still quite “wild”, many man-made sources of noise perturb the natural occurring EM fields. The main problem is due to DC electrified railways, active on the west of the area (along the coast) and on the East. The analysis of previous MT dataset highlighted the impossibility to use MT data acquired in single site as well as in local-remote mode in the geothermal fields of Southern Tuscany, due to the strong correlated noise affecting the low frequency bands. In order to overcome this problem only a remote reference technique (Gamble et al., 1979) should be used. The site of Capraia Island was already proved to be effective in previous MT surveys (Fiordelisi et al., 1998; Volpi et al., 2003). Considering the logistic difficulties to manage a remote station in an island, we have dedicated special care to locate a site in the Tuscan mainland with high signal to noise ratio to be used for the remote reference processing. For this purpose, we implemented a database in GIS environment with the vector elements of possible EM noise source: i.e. power lines, power plants, railways etc. We selected the site as far as possible to the possible sources. The results were not encouraging in the fact that the near-field and correlated noise of the DC railways affected the MT data recorded also tens kilometres far; see for example in figure 7.2 the MT curves in a site near the town of Volterra affected by such kind of near-field effect.

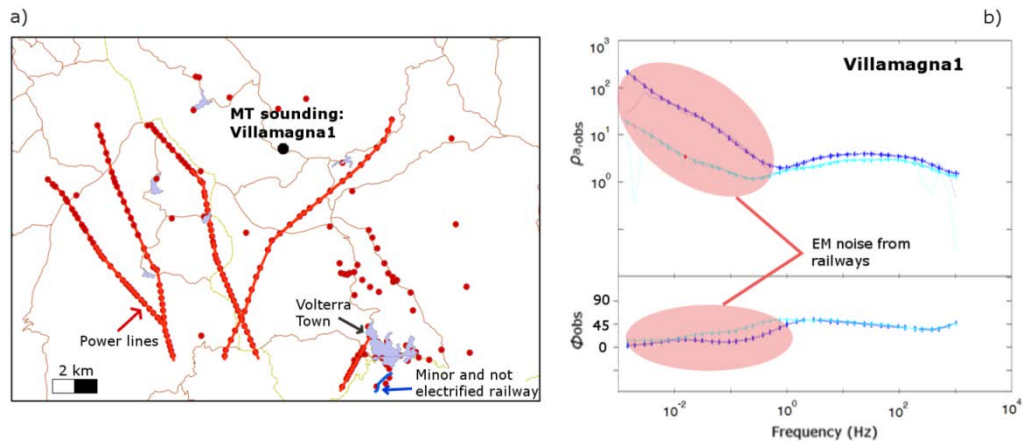


Figure 7.2- Example of MT response from a site 30 km far from the survey area. a) Vector elements of EM sources of noise plotted in GIS environment, the location of the Villamagna1 MT soundings is shown, too; b) MT curves for the Villamagna1 soundings, the effects of railways is highlighted at frequencies lower than  $10^0$  Hz.

After various attempts in 2015, we decided to install the instrumentation on the Capraia Island, stated the impossibility to find a suitable site on the mainland. Capraia is a volcanic island located 50 km far from the coast and 80 km from the survey area. It is quite wild with very steep topography and few roads only in the proximity of the little town and harbour while the rest of the Island is accessible only by (hard) walking. Fortunately, we were allowed to install the permanent MT station in a (wonderful) winery located in the unique little flat valley of the Island, easy reachable.

In March-April 2016 we have carried out a new broadband magnetotelluric survey in the western sector of the Larderello field centred in *Lago Boracifero* coupled with a TDEM survey acquired in July 2016 (figure 7.3). The MT data acquisition lasted 30 days and is also briefly described in Santilano et al., 2016b. The available equipment was suitable to install two synchronous MT sites, i.e. one permanently installed as remote and one daily moved site by site in the survey area. The instruments were tailored by Zonge International Inc. and consisted of:

- two ZEN receivers (high-resolution, multi-channel 32-bit receivers) able to record broadband time-series from  $10^{-4}$  to  $10^3$  Hz;
- Four magnetometers of the type ANT/4;

- Non-polarizable electrodes (Pb-PbCl) specifically for geophysical resistivity measurements.

The new dataset, we called “Larderello\_2016” counts 22 MT soundings. Some of the sites required the repetition of the acquisition due to technical problems such as boars “playing” with the electrodes or cutting the cables.

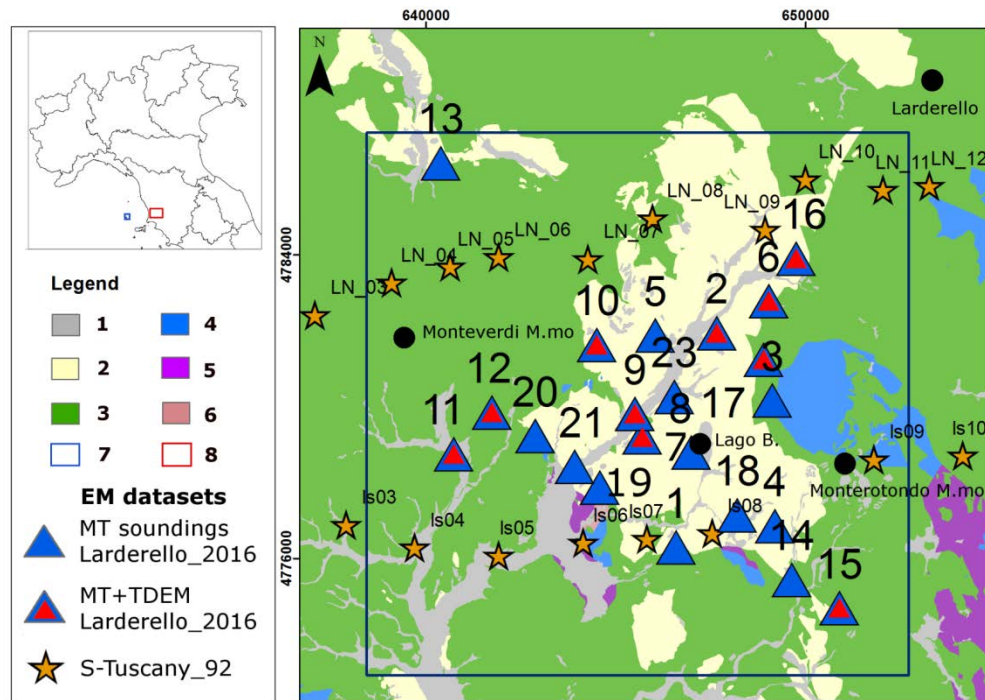


Figure 7.3-Location of the MT and TDEM soundings of old and new datasets available for the study of the *Lago Boracifero* area: 1) Quaternary deposits; 2) Neoautochthonous terrigenous deposits (Miocene-Pliocene); 3) Ligurian and sub-Ligurian Flysch complex (Jurassic-Eocene); 4) Tuscan Nappe formations (Upper Trias-Miocene); 5) Calcare Cavernoso and anhydrites; 6) Metamorphic Units (Paleozoic); 7) Remote MT site in the Capraia Island; 8) Survey area in the *Lago Boracifero* sector of the Larderello field.

The layout of the MT stations was a L-shape configuration to measure four components of the MT fields ( $E_x$ ,  $E_y$ ,  $H_x$ ,  $H_y$ ). The electrodes were duly connected to the receiver to establish a pair of orthogonal dipoles for measuring the  $E_x$  and  $E_y$  components of the electric fields with a distance between electrodes of 100 meters (only for two sites the length was shorter due to logistic

barriers). Two magnetometers were used to measure the horizontal perpendicular magnetic fields  $H_x$  and  $H_y$ . For each site the two components of E and H were measured parallel/perpendicular to the magnetic North (figure 7.4). The MT convention is used to consider the X component parallel to the North and the Y component parallel to the East. The a-priori knowledge of the geoelectrical strike is quite impossible in a very complex system such as the area of interest. For each MT site, we measured the signals overnight by setting a standard acquisition schedule synchronous with the remote station; see details in Table 7.2, whereas in Table 7.3 a brief description of the sites is reported.

Table 7.2- MT acquisition schedule.

<b>MT schedule</b>	
<b>Duration of acquisition (minutes)</b>	<b>A/D rate (Hz)</b>
15	4096
60	1024
1020 (at least)	256

### **7.3.3 TDEM measurements in the *Lago Boracifero* sector: the new survey**

In July 2016 we carried out a TDEM survey with the aim of correcting the MT soundings affected by static shift effects and for testing innovative joint optimization of MT and TDEM data by using the PSO algorithm. After estimated the transfer function of all the MT soundings we selected 10 sites, with clear static effects, for TDEM data acquisition. The equipment was a TEM-FAST 48 (AEMR company), a highly portable system based on advanced TEM-FAST technology (see details in Ranieri, 2000 and Barsukov et al. 2015). The TDEM soundings were acquired by laying out a rectangular loop of wire 50x50 meters and 100x100 meters and pulsing it with a controlled current. The configuration was a coincident loop: i.e. same loop for transmitting and receiving. The voltages produced by the decaying magnetic field are recorded at successively later times. The measurements of the current flow provided information of the electrical resistivity of the Earth at increasingly depths. The decay of the voltage in the receiver is determined for a number of time gates, each measuring and recording the amplitude of decaying voltage. In Table 7.3 a brief description of the TDEM sites is reported (see Appendix B for the TDEM data).

Table 7.3- Brief description of MT and TDEM sites. The coordinates are in WGS1984 UTM 32 N.

<b>X</b>	<b>Y</b>	<b>Altitude (m)</b>	<b>Name MT site</b>	<b>Locality</b>	<b>Data</b>
646585	4776296	309	Lard_1	Campagnelli	MT
647665	4781944	296	Lard_2	Podere Florestano	MT+TDEM
649126	4780168	464	Lard_3	Fattoria Vecchienne	MT
649194	4776864	305	Lard_4	Podere Real Ponte	MT
646043	4781881	267	Lard_5	Podere Galletto	MT
649032	4782786	397	Lard_6	Podere Il bagno	MT+TDEM
645700	4779201	295	Lard_7	Pozzo Venelle-2	MT+TDEM
646987	4778797	298	Lard_8	Podere S. Giulio	MT
645498	4779816	194	Lard_9	Fiume Cornia	MT+TDEM
644496	4781640	354	Lard_10	Podere Le Piscine	MT+TDEM
640731	4778759	143	Lard_11	Podere Sant'Agnese	MT+TDEM
641729	4779853	234	Lard_12	Pod Cà al Colle	MT+TDEM
640391	4786422	213	Lard_13	Tenuta Canneto	MT
649643	4775445	266	Lard_14	I Boschetti	MT
650894	4774698	414	Lard_15	Poggio Carlo	MT+TDEM
649748	4783912	406	Lard_16	La Leccia	MT+TDEM
648897	4781248	465	Lard_17	Podere Adarbia	MT+TDEM
648200	4777147	280	Lard_18	Rio secco	MT
644572	4777871	247	Lard_19	Podere Monti Leo	MT
642877	4779236	273	Lard_20	Podere Castellacce	MT
643912	4778422	171	Lard_21	Botro Guardigiano	MT
646542	4780269	245	Lard_23	Podere Le Gorghe	MT

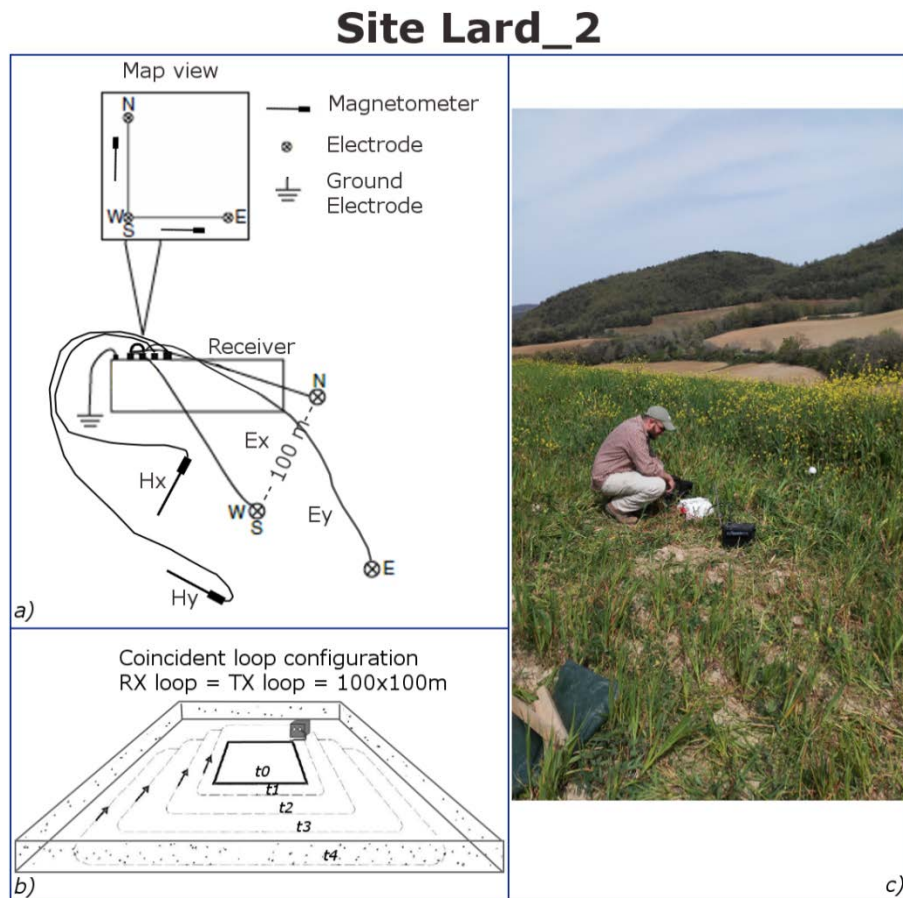


Figure 7.4- Example of acquisition layout for both MT and TDEM data in the site Lard\_2 in the proximity of the Podere Florestano: a) L-shaped layout of MT station (modified from Simpson and Bahr, 2005), b) Coincident loop layout of TDEM station (modified from Ranieri, 2000). The arrows indicate the flowing current at later times and c) picture form fieldwork during the installation of the MT station.

### 7.3.4 MT in the *Lago Boracifero* sector: Data processing

With regard to MT data processing, for each local site we measured four components (Ex, Ey, Hx, Hy) of the MT fields in the frequency range of  $10^3$  to  $10^{-3}$  Hz coupled with the simultaneous measurements of the two horizontal components of the magnetic field (Hx and Hy) in the remote site. The frequency spectra ensured an investigation depth suitable to image our targets, i.e. the deep structures of the field.

The processing procedure for estimating the impedance tensors ( $Z$ ), was carried out by using the following codes provided by Zonge International Inc. that are based on conventional algorithm commonly used in the scientific community:

- MTFT24, a time series processing tool;
- MTEdit, a tool for the transfer function estimation

We stress that in the frame of a geothermal exploration survey in Belgium (Coppo et al., 2016; Manzella et al., 2016), a comparison among the transfer functions estimated with these commercial codes and with conventional codes from Egbert G.D. & Booker J.R. (1986), proved the similarity of results.

Through the “data processing” it is possible to reduce the contribution in the signal of the sources of EM noises. The survey area is not intensely urbanized but many power lines and power plants are present and the correlated noise coming from the electrified railways affects the area. These issues required necessarily the use of robust statistical estimators coupled with remote reference technique processing. We used the “MTFT24” code to process the time series performing cascade decimation to Fourier transform from the time domain to the frequency domain. Some of the noisy data could be filtered at this stage such as the signals at 50 Hz (and harmonics) from the power lines by applying a notch filter. In figure 7.5 the time series before and after the removing of the power lines signals are shown from the site “Lard\_9”. it is also evident the problem affecting the channel 1 (Ey) in the last two hours of acquisition (electric cable cut by animals); these segments were not taken into account for computing the impedance tensor.

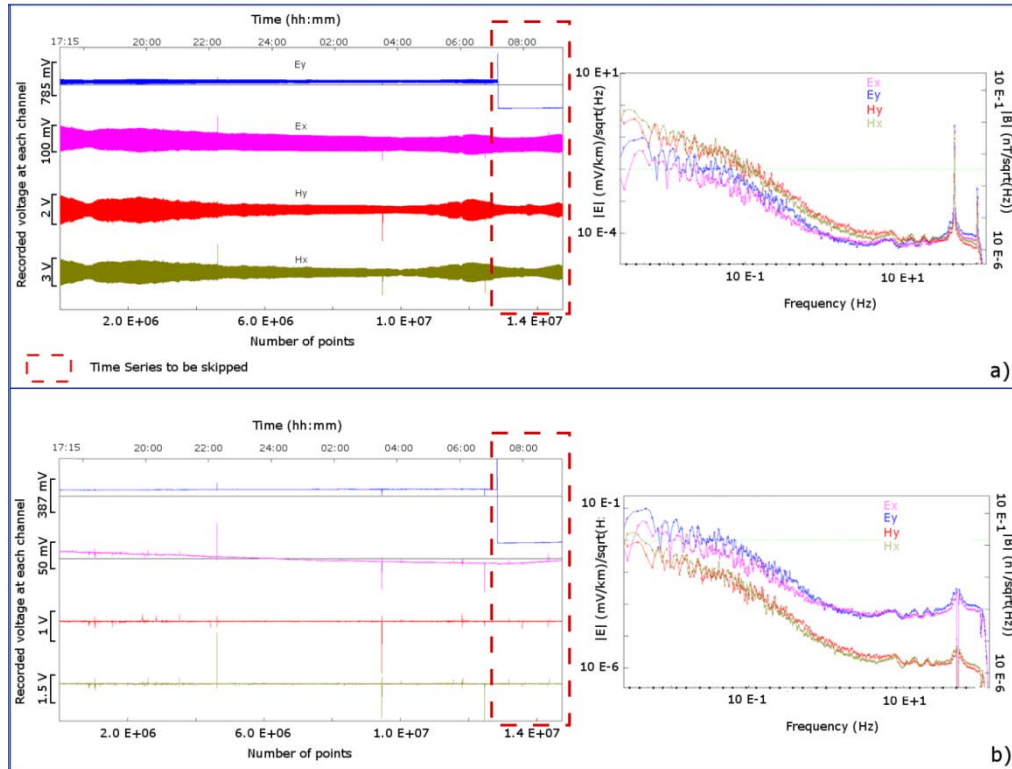


Figure 7.5- Time series measured in the “Lard\_9” MT site: a) On the left the time series before the application of filters and on the right the related spectra amplitude plot of the four MT fields components (Ey, Ex, Hy, Hx). b) On the left the time series after the application of the notch filter at 50 Hz (and harmonics) and on the right the related spectra amplitude plot. The recorded voltage at the receiver is shown; for the Hy and Hx components after the correction with the response curve the values will be reported in nT or A/m respectively for H and B.

As previously mentioned in Chapter 4, the datum we use in Magnetotellurics is the frequency-dependent tensor  $\mathbf{Z}$  that connects the two components of horizontal electric and magnetic fields measured in the Earth’s surface. The spectral coefficients were used as input files for the estimation of the impedance tensor with “MTEdit”. The commercial code is described in its manual and briefly in Zonge (2016). In addition, a threshold of 0.6 for the coherency, between the electric and magnetic fields, was selected to filter the data with lower values and a manual QC controls was accomplished on the estimated MT curves.

The apparent resistivities and impedance phases were computed for each soundings and for the two components  $\rho_{a,xy}$ ,  $\rho_{a,yx}$ ,  $\Phi_{,xy}$ ,  $\Phi_{,yx}$  (from the secondary diagonal of  $Z$ ) that represent the MT data to be used for the model parameter estimation.

As expected, the MT data appeared very noisy. The highest levels of noise were observed at frequencies lower than  $10^{-1}$ - $10^{-2}$  Hz due to the previously described railways effect. In many soundings this problem was successfully solved with the remote processing technique (figure 7.6) but in some cases the lowest frequencies ( $<10^{-2}$  Hz) were disregarded. Furthermore, we observed very high noise levels in the frequency range known as MT Dead Band particularly from 0.1 to 1 Hz. Furthermore, in some soundings, the electric signal appeared to be strongly polarized. It should be mentioned that the site Lard\_4 was totally corrupted by noise, probably due to the short distance with the Carboli power plant, and was not taken into account for the MT analysis, modelling and inversion. The frequencies lower than 1 Hz were disregarded for the site Lard\_1 due to technical problems with the remote site that did not allow the remote reference processing.

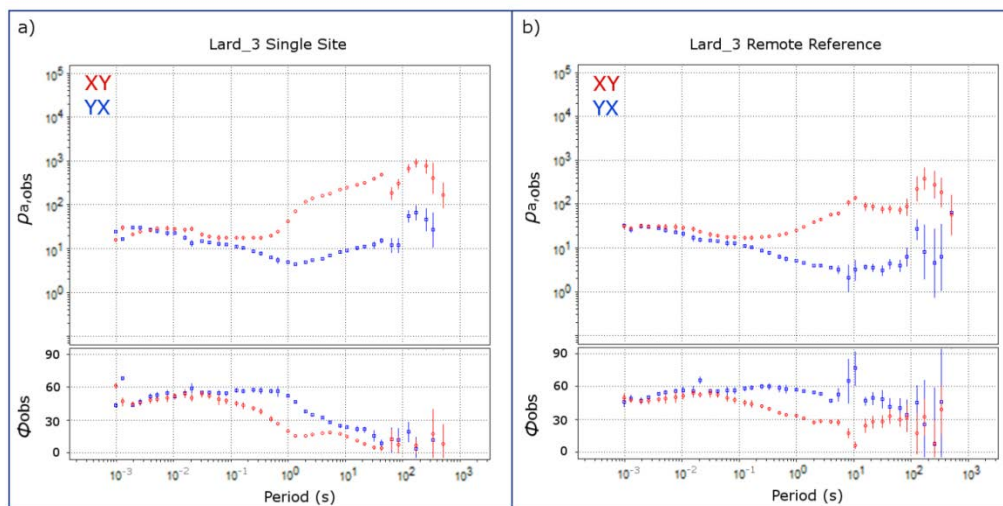


Figure 7.6- MT curves of Lard\_3 soundings. The raw data are shown (no manual editing or smoothing): a) MT curve estimated in single site mode; b) MT curve estimated in Remote Reference mode.

The estimated impedances were imported in the commercial software “WingLink” (Geosystem) for the analysis. MT data analysis was also performed through the own codes in Matlab environment (see Appendix A).

The most important issue to be faced was the identification of the distortion of MT data. We further processed the estimated transfer functions by carrying out a SVD of the impedance tensor that enabled us to compute the eigenstate analysis as proposed by LaTorraca et al. (1986). The principal directions for E and H were computed, too. It should be noted that the MT curves were smoothed by using the “D+” solution (Beamish and Travassos, 1992). In Appendix B all the MT curves of the Larderello\_2016 survey, already corrected for the static shift, are shown.

### **7.3.5 TDEM in the *Lago Boracifero* sector: Data processing**

With regard to the TDEM survey, the acquisition system was set to transmit current up to 3 A with active time gates from 4  $\mu$ s to 2.024 or 4.048 ms and a stacking time of some minutes. Measurements were repeated several times at each sounding location, to minimize aliasing effects due to high-frequency noise. The ratio of “current on” versus “current off” time was equal to 3/1. The time window (current off time) extended from 4  $\mu$ s to 4 ms with 48 signal integration channels. The normalised voltage (V/I) and the errors were given for each channel. The repeatability of the TDEM data was assessed by using different acquisition configurations (time windows, stacking and amplification). A low background noise and a good repeatability of the measurements were observed; we discharged only few data for acquisition times higher than 2 ms. The observed values of the voltage decay with errors higher than 10% were removed from raw data.

The recorded voltage was converted in apparent resistivity response versus time, according to standard approach as suggested by Nabighian (1979) and described in Chapter 4. The data we obtained with the TDEM is the apparent resistivity at increasing time, i.e. at increasing depths, as showed in figure 7.7 for the site Lard\_2.

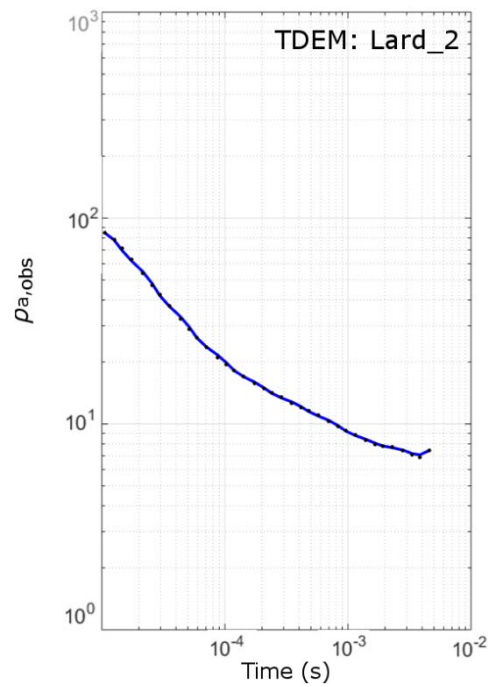


Figure 7.7- TDEM data, site lard\_2. The apparent resistivity vs Times is showed.

## 7.4 Data analysis

### 7.4.1 Dimensionality and Directionality from MT data

For the study of the *Lago Boracifero* sector we selected four MT profiles, three of them being about E-W oriented and one, Profile 1, NW-SE oriented. The latter was chosen with the aim to understand if the Cornia River can be correspond to a fault (that some authors suggested). In addition, in the *Travale* sector, we selected two MT profiles in order to understand the MT response in that area where many direct data (e.g. well logs) are available (figure 7.8).

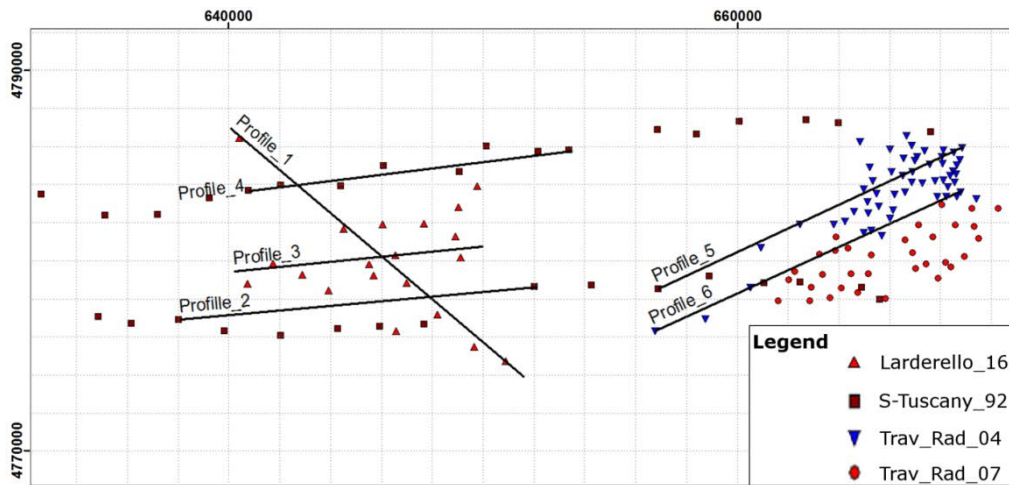


Figure 7.8-Location of the MT profiles in the *Lago Boracifero* and *Travale* sectors.

The dimensionality analysis is a main step of data analysis and is aimed to understand if the MT response is related to 1D, 2D or 3D Earth structure. Many approaches have been proposed in literature. The dimensionality tools available in WingLink such as Skew (Swift, 1967) and Polar diagrams can provide a first-order approximation; the presence of noise can lead unreliable interpretations. We analysed also the dimensionality with the more robust methodologies named “WAL” and “B-Q” proposed respectively by Weaver et al. (2000) and Marti et al. (2005) that we implemented in Matlab environment as tool of “Global EM”. As proposed in Marti et al., (2009) we considered appropriate the use of different threshold values (beneath which the invariants are considered to be zero) in the range of 0.1-0.2. In Marti et al., (2005) the approach provided for the combined use of different parameters used in Bahr (1991) and Weaver et al. (2000). We highlight that the results from the two approaches “WAL” and “B-Q” unexpectedly differed, mainly at long periods probably due to higher levels of noise in the data. In figure 7.9 the results of B-Q analysis for the MT soundings acquired both in the *Lago Boracifero* and *Travale* sectors are showed.

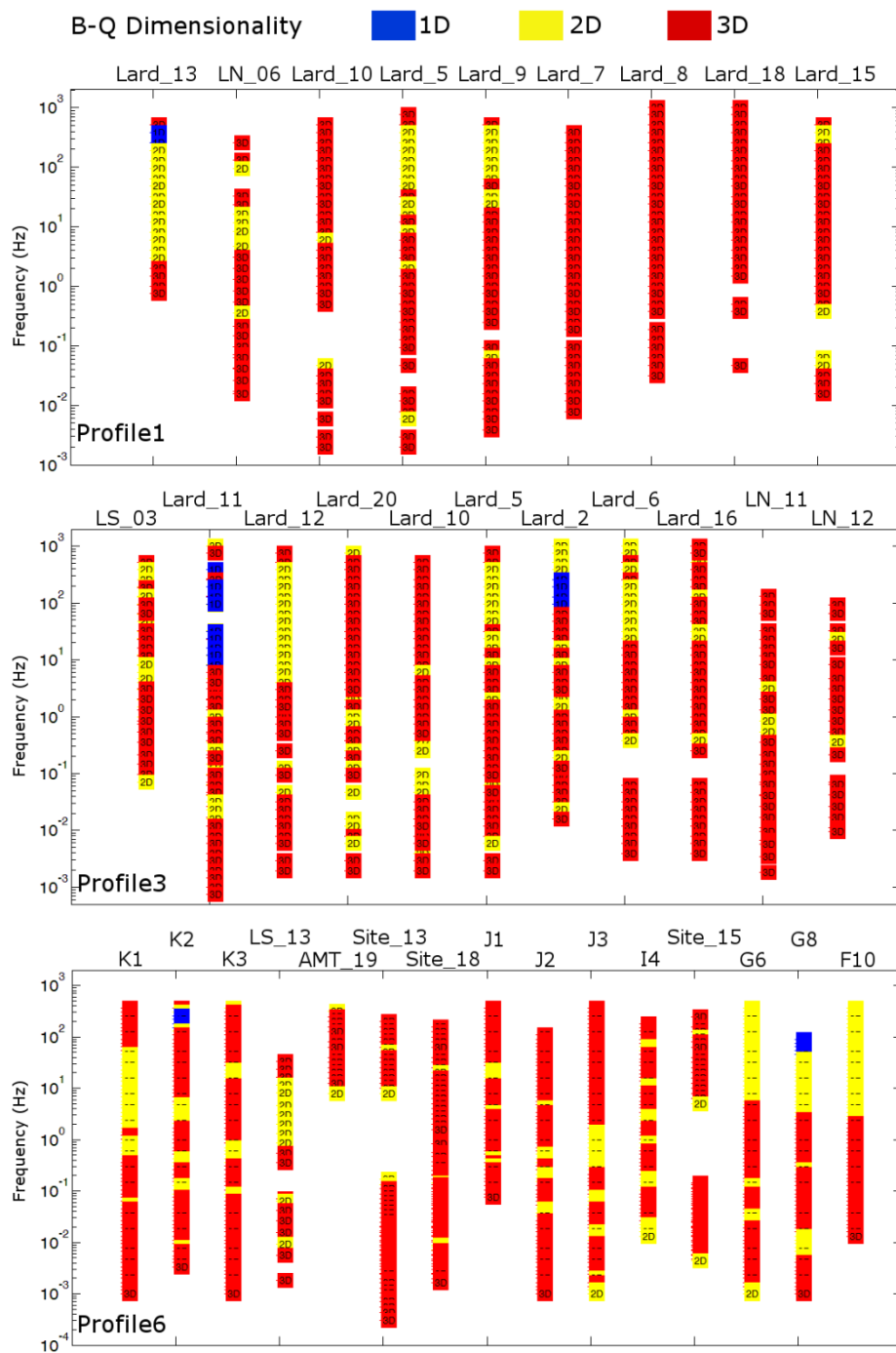


Figure 7.9- Dimensionality analysis of MT soundings along Profiles 1, 3 and 6 from *Lago Boracifero* and *Travale* area with the B-Q Method (Marti et al., 2005).

As expected, the analysis showed a very complex structure of the Larderello-Travale geothermal field. It is clear that 2D dimension can locally occur, but the Earth structure in this area is mainly 3D. An important two-dimensional structure can be pointed out in the Profile 6 at the high frequencies of the last three soundings (G6-G8 and F10) perfectly corresponding to the well known structural basin of Radicondoli. In the *Lago Boracifero* sector and particularly in the central part of the study area (Lard\_5 and Lard\_9), in the proximity of the Cornia River, a two-dimensional geoelectric structure was recognized at high frequencies (up to  $10^1$  Hz) while at lower frequencies the 3D structure is again predominant. We checked the strike values computed by different analyses: *i*) by using the approach proposed in Swift (1967), *ii*) observing the direction of principal electric and magnetic fields obtained by tensor decomposition (LaTorraca et al., 1986) and *iii*) by the analysis of invariant parameters Weaver et al. (2000). With regard to the *Travale* sector particularly for the 2D structure pointed out with the dimensionality analysis, the strike direction at periods of 0.1 s up to 1 s is clearly N40W, perfectly in accordance with the tectonics, i.e. the Radicondoli basin. Regarding to the *Lago Boracifero* area, particularly those soundings showing 2D response, the strike direction ranged from N30W to N30E. It is clear that in proximity of the Cornia River the geoelectric strike is usually from N10E to N30E, in accordance with the strike of the supposed faults being located along the river. In figure 7.10 the strike direction is showed for frequency 24 Hz for those soundings showing a 2D response; the direction was obtained by following Weaver et al. (2000).

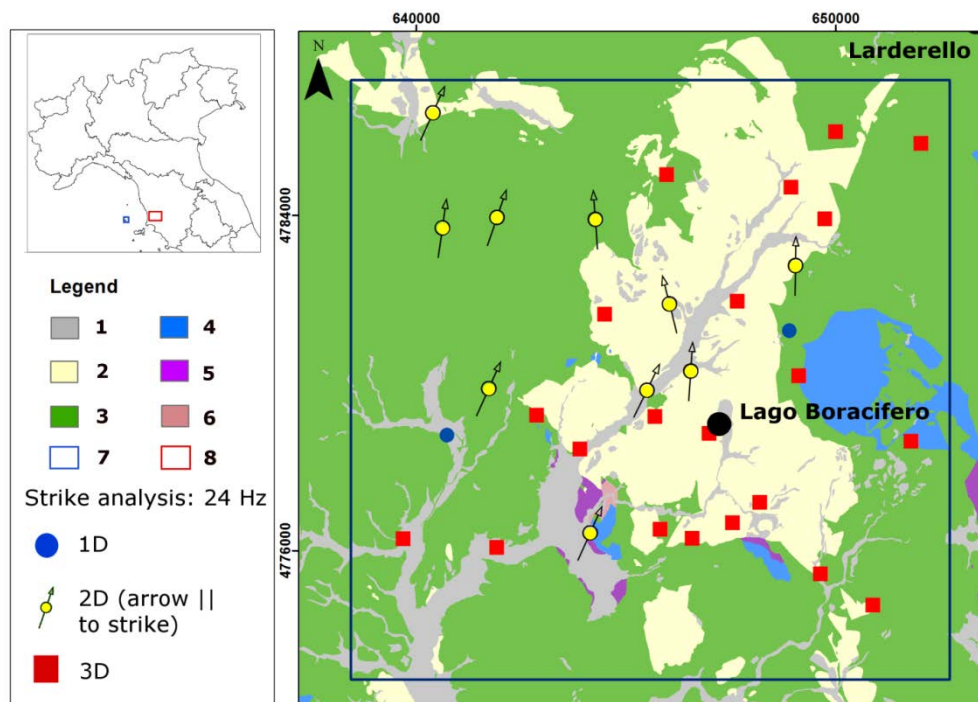


Figure 7.10- Strike analysis at frequency 24 Hz for the *Lago Boracifero* sector. For the legend 1-8 see the figure 7.3.

### 7.4.2 Integration of TDEM and MT data for static shift correction

The measured MT data can be affected by a kind of distortion commonly referred to as static shift. The effect is a shift of the apparent resistivity curve. Due to the fact that the TDEM measurements are not affected by such distortions, the joint analysis of MT and TDEM data become a commonly accepted way to correct the MT static shift.

In this study we explored two procedures of joint analysis of MT and TDEM data:

- by converting the TDEM curves in frequency domain and overlaying on the MT curves, as proposed by Sternberg et al. (1988);
- by inverting the results of TDEM soundings and computing the theoretical response of magnetotellurics to be used for the shift of the real observed MT data, as proposed by Pellerin and Hohmann (1990).

With regard to the first procedure we firstly introduce the concept of the diffusion depth for TDEM that is the analogous to the skin depth in the frequency domain for MT. The TDEM measurements are collected at a sequence of times following transmitter turnoff. The transition from near to far field can be accomplished simply by measuring the response at later times, rather than requiring transmitter-receiver separation. In other words, the early-time (near-field) depth of investigation is geometric, whereas the late-time (far-field) depth of investigation is parametric. The investigation depth depends on the characteristics of the transmission and of the subsurface.

The MT static shift correction is performed by converting TDEM data to an apparent resistivity curve, which is then compared to the MT curves. The TE and/or TM curves are then shifted to match the TDEM curve. The method is based on the relationship between the TDEM diffusion depth  $\delta_{dd}$  (see Eq. 4.30) and the MT skin depth  $\delta_{sd}$  (see Eq. 4.11). At the same depth of penetration we assume that TDEM delay time ( $t$ ) must be equivalent with MT period ( $T$ ). The conversion factor  $cf$  can be approximated as (Sternberg et al., 1988):

$$cf = 194 \quad [\text{Eq. 7.1}]$$

The value is in accordance with the conversion described in. Finally, the TDEM signal has been converted in an equivalent MT-period by multiplying the time of the TDEM signal for the conversion factor. For each site, the TM and TE curves were shifted in accordance with the TDEM converted curve. Obviously, the overlapping of the two apparent resistivity curves (TDEM, MT) occurs only for the higher periods of the TDEM curve, due to the shallower investigation depth of the converted TDEM rather than MT.

We tested the accuracy of this conversion by analyzing the synthetic response of TDEM 1D model, computed by a forward modelling of the voltage decay, and the theoretical response of the same model computed using the forward modelling of MT. For the test a simple 4-layered synthetic model was considered with the following thicknesses and resistivities: 200m and 100  $\Omega\text{m}$ , 100 m and 20  $\Omega\text{m}$ , 200m and 200  $\Omega\text{m}$  and a halfspace of 1000  $\Omega\text{m}$ .

The MT theoretical data were computed by using the forward modelling implemented in “GlobalEM” software package (see Appendix A) whereas the TDEM forward problem was for a central-loop configuration, as proposed by Ingeman-Nielsen and Baumgartner (2006). The code is developed in Matlab

environment and it computes the 1D forward modelling response based on the Hankel transforms occurring in the field equations. Finally the TDEM times were converted in period using the conversion coefficient described in this paragraph. The overlap between the two data set is rather satisfactory even a smoother trend of TDEM data is shown (figure 7.11).

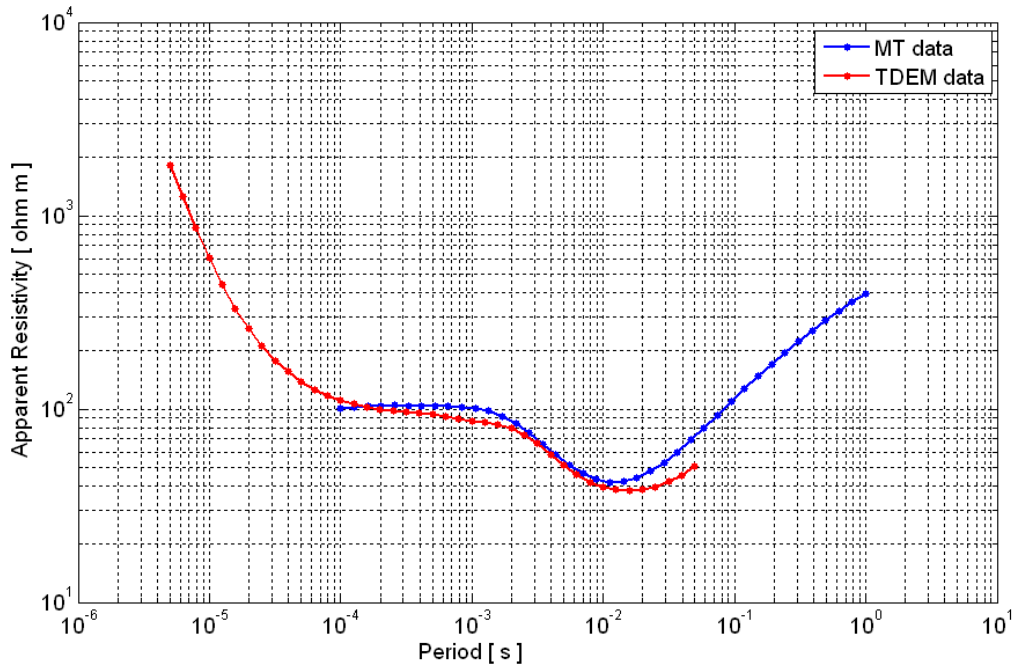


Figure 7.11- Example of theoretical response of TDEM data converted in MT response and overlap with the MT theoretical response for the same model

We stress that this approach was also used to create a unique dataset MT-TDEM to be jointly optimized with Global Optimization Algorithm in order to constrain the very shallow part of the investigated Earth (see Chapter8, figure 8.9).

We tested also an alternative approach to correct the static shift of MT data by computing a MT theoretical response on the model obtained from the inversion of TDEM sounding. The obtained theoretical MT curve is compared with the observed MT data and the curves can be properly shifted. In order to retrieve a smoothed 1D profile from TDEM data, we have applied a direct transformation (pseudo-gradient transform) adapting the Niblett-Bostick transform (Bostick 1977; Meju, 1998). Once obtained the TDEM inverted model, the MT forward

problem can be solved and the theoretical data can be compared with real one on the same site. In figure 7.12 we show the results of a test on the Lard\_10 site. Particularly in figure 7.12c the raw observed MT data are shown, with a clear static shift of the YX component. The comparison with the theoretical data allowed the easy correction (shift) of the MT curve.

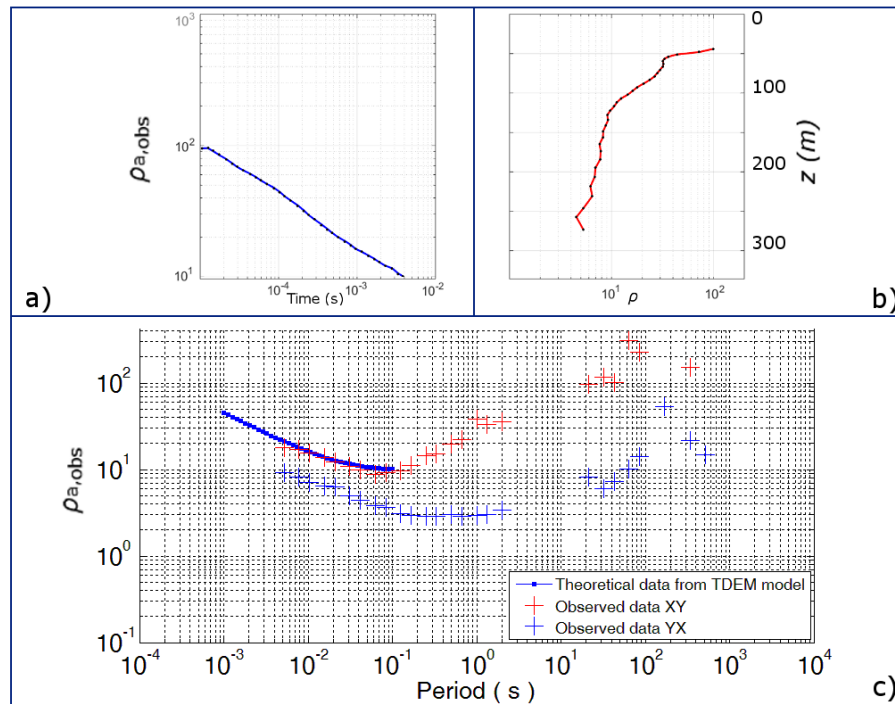


Figure 7.12- Joint MT and TDEM analysis for static correction: the example of the site Lard\_10; a) TDEM response (apparent resistivity vs times); b) Smoothed inversion model from TDEM sounding; c) Raw observed XY and YX MT data coupled with the MT theoretical response referred to the inverted model.

The results of the two approaches were both quite consistent. The joint analyses of TDEM and MT were applied on the 10 sites belonging to the Larderello\_2016 dataset in order to properly correct the static shift problems.

## Chapter 8

# Global Optimization of the EM geophysical data from the Larderello-Travale field

### 8.1 Introduction

Hereby, we describe that part of the research that refers to the global optimization of MT data for the possibility of finding a solution of the inverse problem as near as possible to the global minimum of the objective function. Decades of advanced research on deterministic inversion in 1D to 3D of MT data, provided well-performing algorithms, that are able to solve strongly non linear and ill-posed problem. Such methods require usually the computation of the partial derivatives of the synthetic data with respect to model parameters, through a local search of the domain.

The stochastic approaches can explore wider space solution, randomly (Piatti et al. 2010) or according to some strategies such as the evolutionary algorithms (Godio, 2016).

In order to obtain preliminary information on the electrical responses at depth in the Larderello-Travale geothermal field we achieved 1D Earth-layered models by optimizing the observed MT data in the area. We adopted the Global

Optimization Algorithm (GOA) described in this study; the Particle Swarm Optimization (PSO).

We are aware that the MT parameter estimation in 1D is strictly limited by the dimensionality problem. Indeed, the dimensionality analysis on the dataset, highlighted complex structures. In spite of this consideration, a first-order approximation of the electrical resistivity response can be obtained by optimizing in 1D the MT curves in TE, TM modes and as determinant averages impedance.

Firstly, we tested the optimization on synthetic data considering stratigraphic models and resistivity from geothermal well logs. The comparison among the results on numerical modelling and observed data, is of help to state if the optimized models can represent an important source of data for the study of the geothermal field. The synthetic data were used also to check the effectiveness of PSO in addition to the experimental results in Chapter 5.

In the *Travale* area we selected some MT soundings to be optimized, acquired near deep geothermal wells for which the resistivity well logs were available. The complete MT dataset along the 2D profiles in the *Lago Boracifero* area was optimized. Beside the intrinsic information of the 1D optimized layered-models, we interpolated the estimated parameters along 2D profiles to be used as a-priori information for the 2D deterministic inversion (Chapter 9). In this case we tested the idea that optimized models can provide important information rather than using a homogeneous starting model for constraining the inversion, especially in geothermal areas where subsoil data are not available (the so called green-fields).

The Larderello-Travale system is a perfect geothermal play for testing such approaches due to the availability of subsoil data that can be used to validate the results.

## 8.2 Test on synthetic data

The optimization process to estimate the model parameters from the magnetotelluric soundings focuses on the discussion of the functional to be minimized (see details in Chapter 5). The PSO was adopted for obtaining both “blocky” few-layered and “Occam-like” smooth model. The “blocky” optimization takes into account a first term in the Eq. 5.8 related to the Euclidean norm of misfit on data ( $\rho_a$  and  $\Phi$ ). Assigning a value of  $\lambda$  (Lagrangian multiplier)

different to zero, the second term related to the model misfit is also considered; the minimization with  $\lambda$  equal to zero is unconstrained and only the data misfit is considered. In the case of “blocky” models the parameters to be estimated are  $\rho$  of the layers and their thickness; the number of layers is a-priori fixed. The “Occam-like” optimization is for the first time (to our knowledge) applied to PSO for MT modelling. In addition to the first term related to data misfit, the procedure minimize the roughness of the model, according to the minimum structure approach (Eq. 5.9); the Lagrangian multiplier controls the effects of the model structure on the minimization. In this case the parameters to be estimated are  $\rho$  of the layers while thicknesses are fixed, usually according a logarithmic increase along  $z$ .

We tested the effectiveness of the PSO on numerical simulations related to the real Earth stratigraphy of the Larderello-Travale geothermal field. This test can point out important information on the electrical structure at depth because we refer the simulation to an area where stratigraphic, resistivity logs and measured MT soundings are available.

### 8.2.1 Test on synthetic data: simulating the *Travale* sector

The first test refers to an Earth model “*Travale-synt*” depicted from the stratigraphic well log of Radicondoli-7bis, located in the Travale area. Two synthetic data  $\rho_{a,th}$  and  $\Phi_{th}$  were generated, “*Travale-synt-A*” and “*Travale-synt-B*”, respectively considering the stratigraphy with  $\rho$  values from literature (usually assigned for such kind of rocks) and values from the resistivity well log of Radicondoli-7bis.

It is not trivial that the DLL/IL (Dual Lateral Log/Induction Log) in-hole measurements deny the expected very high electrical resistivity for rocks such as micaschist, granites and limestone, in the area of the Radicondoli-7bis. For example, the statistical analysis on deep resistivity well logs at level of buried Micaschist Complex and Intrusive Complex clearly stated the very low resistive response with median values of about 1000  $\Omega\text{m}$  (figure 8.1).

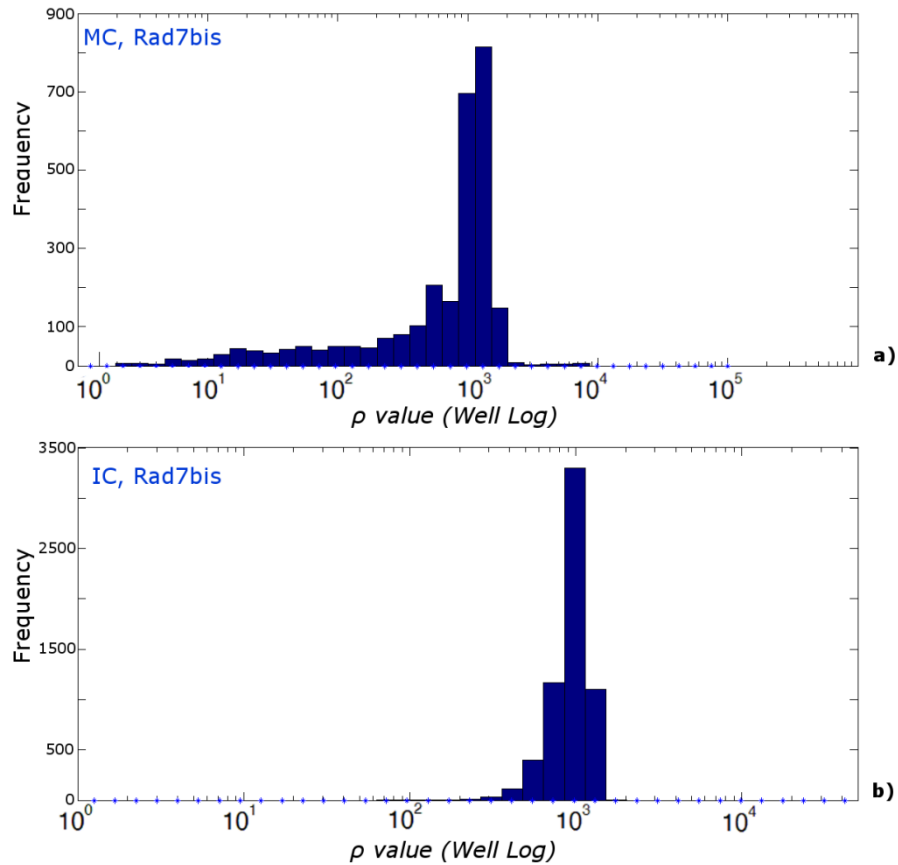


Figure 8.1- Histograms from resistivity well log measurements in Radicondoli-7bis. a) Resistivity values for the Micaschist Complex (MC), b) Resistivity values for the Intrusive Complex (IC).

The 1D synthetic model is composed by 6 layers, including a homogenous halfspace at the bottom, representing a typical stratigraphy in this area, with the tectonic delamination of the Tuscan Nappe.

The *Travale-synt* model takes into account a value of  $\rho$  assigned from literature data (e.g. Telford et al., 1990) considering a reference lithologic pattern for each stratigraphic unit. The resistivity values for the *Travale-synt-B* were retrieved from a statistical analysis of the resistivity well log. We considered the values of resistivity inside each unit, about a measurement every 0.1 m, and the median values were taken into consideration. We stress that the resistivity well logs in the *Travale* area suggested only slight low resistivity anomalies but the response along the Radicondoli-7bis is much lower probably due to very local

conditions. A value of 100  $\Omega\text{m}$  was assigned to the halfspace simulating the Lower Crust and part of the Mantle.

In Table 8.1 we reassumed the main features of the *Travale-synt-A* and *Travale-synt-B* synthetic models. On these models we computed the 1D forward modelling, generating the theoretical  $\rho_{a,th}$  and  $\Phi_{th}$  data in a frequency range of  $10^{-3}$ - $10^3$  Hz; the synthetic dataset was used for testing the PSO. We perturbed the synthetic data with a random error increasing with period.

Table 8.1- Main features of the *Travale-synt-A* and *Travale-synt-B* models. The model is retrieved from a real stratigraphic well log. The stratigraphy is also reported.

$n_l$	$\rho$ ( $\Omega\text{m}$ ) <i>Travale-synt-A</i>	$\rho$ ( $\Omega\text{m}$ ) <i>Travale-synt-B</i>	Thickness (m)	Corresponding Unit
1	15	5	750	Ligurian Complex
2	3000	230	15	TWC
3	1000	730	1577	Phyllitic Complex
4	3000	870	254	Micaschist Complex
5	6000	950	10000	Granite
6	100	100	halfspace	

The module of GlobaleM “PSO Optimization; theoretical data” was used for testing the PSO algorithm on the generated synthetic dataset from the models *Travale-synt-A* and *Travale-synt-B*. In this case, we tested the “blocky” optimization with number of layers  $n_l=6$  including the halfspace; i.e. the variables to be optimized are the  $n_l$  resistivity plus the  $n_l-1$  thicknesses. In Table 8.2 we summarized the main settings for computing the PSO optimization of the MT theoretical data from *Travale-synt-A* model. Firstly, we defined the space domain for the algorithm to search the solution; i.e. the lower and upper boundaries of possible values of thicknesses and resistivities. The objective function we minimized Eq.5.8 takes into account two coefficients to be set for weighting the apparent resistivity and the phase, respectively  $a$  and  $b$ . We stress that the Lagrangian multiplier  $\lambda$  was set to zero; i.e. only the misfit on data is considered and no-apriori information is used. The initial population size, the particle inertia, the cognitive and social attractions and the number of iteration were set, too. Theoretically, only one trial can be enough to find a reliable solution. We computed the optimization 100 times (number of trials) in order to define a posteriori model parameter distribution.

Table 8.2- Main settings for the PSO optimization of the MT theoretical data from *Travale-synt-A* model.

<b>PSO (Blocky): Lower (LB) /Upper boundary (UB)</b>		
$n_l$	$\rho$ ( $\Omega m$ )	$Tk$ (m)
1	LB=1; UP=200	LB=10; UP=1000
2	LB=1; UP=10000	LB=10; UP=1000
3	LB=1; UP=10000	LB=10; UP=1000
4	LB=1; UP=10000	LB=10; UP=10000
5	LB=1; UP=10000	LB=1000; UP=15000
6	LB=1; UP=10000	halfspace
<b>PSO: settings</b>		
Initial population		1000
Particle Inertia		0,9
Cognitive Attraction		0,5
Social Attraction		1,75
Generations (Iterations)		150
Trials		100
<b>PSO: Objective function</b>		
$a$ (weight on $\rho_a$ )		0,6
$b$ (weight on $\Phi$ )		0,4
$\lambda$ (Lagrangian multiplier)		0

The results refer to the unconstrained optimizations and are shown in details in Appendix C. Let's first have a look to the synthetic model *Travale-synt-A*. In figure 8.2a the 100 optimized models are shown. The model with the minimum RMS (0.6), considered as the final model, is highlighted as well as the model coming from the statistics; i.e. the median value for each layer among all the trials. The results are quite promising, considering for example that the depth of the first resistive layer and the resistivity of the first layer are exactly modelled with misfits less than 6 meters and 1  $\Omega m$ , as well as the depth and resistivity of the halfspace. Also the resistive layer above the conductive halfspace is exactly depicted. The sensitivity on the third layer is not optimal and the resistivity of the high resistive layer is overestimated. The a-posteriori analysis helps in the identification of low sensitivity layers by recognizing multimodal distributions. For example, the first and the last layers are characterized by Gaussian distributions whereas the third layer shows a strongly multimodal distribution

(figure 8.2b-8.2c). Briefly, the optimization recognized an overall high resistive response at depth for this real stratigraphy with resistivity assigned from literature.

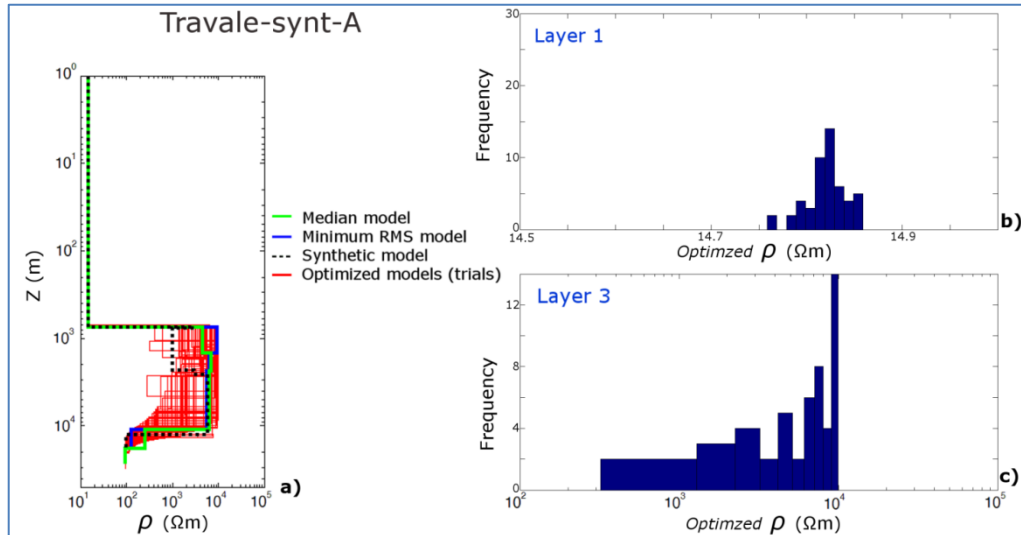


Figure 8.2- Results of the global optimization of the theoretical data from the *Travale-synth-A*. a) Estimated parameters, in red the 100 optimized models, in blue the minimum RMS model, in green the model from statistics and in black the synthetic model is also shown. b) Histograms of estimated parameters from the models for the layer 1 and for c) the layer 3.

The optimization process, with similar settings to the previous, has been performed on the perturbed theoretical data from the synthetic model *Travale-synth-B*, i.e. with the stratigraphy and resistivity from well logs of the Radicondoli-7bis.

The results show that all the 100 optimized models were able to almost perfectly recognize the depth of the first resistor and the last conductor, i.e. the halfspace, and the resistivity values of the first and the halfspace (figure 8.3). The sensitivity of the mid-layers is quite low for the resistivity but not for the thickness. We decided to maintain a wide space domain, to search the solution, but considering the MT curve of synth-B we could have use smaller intervals of UB and LB.

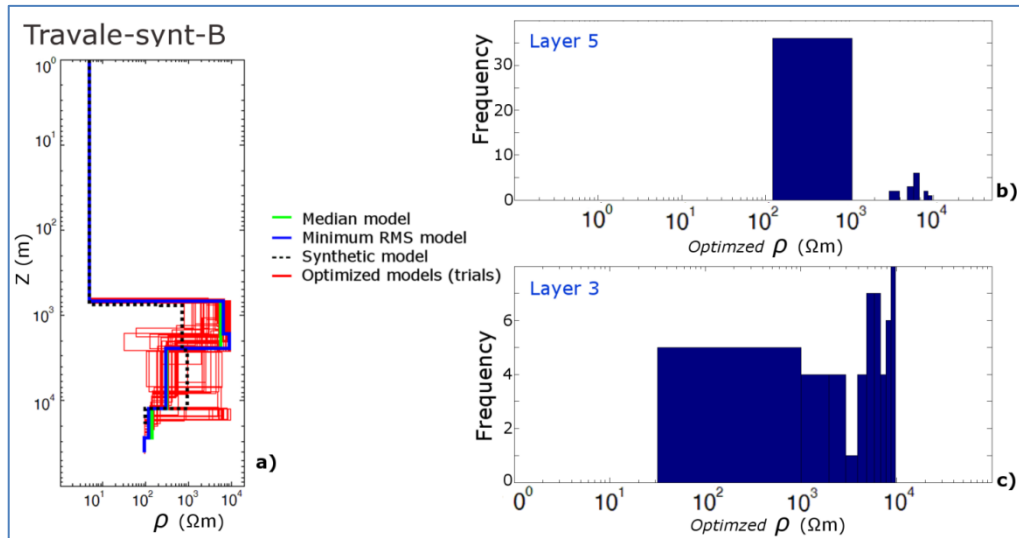


Figure 8.3- Results of the global optimization of the theoretical data from the *Travale-synth-B*. a) Estimated parameters, in red the 100 optimized models, in blue the minimum RMS model, in green the model from statistics and in black the synthetic model is also shown. b) Histograms of estimated parameters from the models for the layer 5 and for c) the layer 3.

In this case as well as the previous optimization, the a-posteriori analysis helps in the identification of low sensitivity layers for their multimodal distributions; i.e. the 3<sup>rd</sup> layer, while the layer above the halfspace is mainly characterized by a unimodal distribution.

### 8.2.2 Test on synthetic data: simulating the *Lago Boracifero* sector

The second numerical test refers to a synthetic MT dataset “*Lago-synth*” computed from the geological model in the area of *Lago Boracifero*. In addition to the stratigraphy we added a deep conductive body whose top corresponds to the seismic K-horizon. A sensitivity analysis was accomplished by modifying the thickness of this layer from 300 meters to 1000 meters and finally 4000 meters, respectively the *Lago-synth-A,B* and *C*. This sensitivity analysis is relevant to define the capability of the PSO to image the resistivity models from MT data. Furthermore, this analysis has important practical application to the study of the Larderello field, due to the fact that we are simulating a geothermal reservoir below the K-horizon as suggested in literature (see Chapter 2). The synthetic resistivity models *Lago-synth-A/B/C* are described in Table 8.3. The selection of

the area is driven by the fact that this sector is very promising, one of the hottest of the field, where the K-horizon reaches the lowest depth. The shallow stratigraphy is known from many stratigraphy logs. Here, the delamination of the Tuscan Nappe is complete and the Ligurian Complex is directly (tectonically) in contact with the TWC. Neogene-Quaternary deposits occur in the area, too. The last two layers of the synthetic models correspond to the Lower Crust and the Mantle. The  $\rho_{a,th}$  and  $\Phi_{th}$  curves for the three models were computed with the “1D forward module” in a frequency range of  $10^{-3}$  to  $10^3$  Hz with five measures for decade.

Table 8.3- Main features of the *Lago-synt-A/B/C* models. The stratigraphy is retrieved from the geological model in the proximity of the *Lago Boracifero* area.

$n_l$	$\rho$ ( $\Omega\text{m}$ ) <i>Lago-synt-A/B/C</i>	Thickness (m) <i>Lago-synt-A</i>	Thickness (m) <i>Lago-synt-B</i>	Thickness (m) <i>Lago-synt-C</i>	Corresponding Unit
1	15	650	650	650	M-P-Q/ Ligurian Complex
2	700	2000	2000	2000	TWC/ Phyllitic Complex
3	2000	500	500	500	Micaschist Complex
4	100	300	1000	4000	Simulated deep- geothermal reservoir
5	3000	8000	8000	8000	Gneiss
6	100	10000	10000	10000	
7	30	Halfspace	halfspace	halfspace	

In this case, we tested the “Occam-like” optimization with a number of layers  $n_l=20$  including the halfspace. In this case the variables to be optimized are the  $n_l$  resistivities while the thicknesses of the  $n_l-1$  layers are fixed. In Table 8.4 we summarized the main settings of the PSO optimization.

The objective function we minimized, Eq.5.9, takes into account two coefficients to be set for weighting the apparent resistivity and the phase, respectively  $a$  and  $b$ . The structure is minimized by considering the roughness of the model; i.e. the second term of Eq.5.9. The influence of the regularization is related to the choose of the Lagrangian multiplier  $\lambda$ . We stress that the “Occam-like” regularization implies the a-priori discretization of the model. Our experiences suggested that the correct setting of the layer thicknesses is really

important for obtaining reliable models. We took into account the skin-depth of the highest and lowest frequencies and we set a logarithmic increase of the thicknesses into this range. The number of trials in this test and for each model *Lago-synt-A/B/C* was 25.

Table 8.4- Main settings for the PSO optimization of the MT theoretical data from *Lago-synt-A* model.

<i>PSO (Occam-like): Lower (LB)/Upper boundary (UB)</i>		
$n_l$	$\rho$ ( $\Omega m$ )	$Tk$ (m)
1	LB=1; UP=200	200
2-20	LB=5; UP=10000	logarithmic increase from 200 to 31000 m
<i>PSO: settings</i>		
Initial population	250	
Particle Inertia	0,9	
Cognitive Attraction	0,5	
Social Attraction	1,75	
Generations (Iterations)	200	
Trials	25	
<i>PSO: Objective function</i>		
$a$ (weight on $\rho a$ )	0,7	
$b$ (weight on $\Phi$ )	0,3	
$\lambda$ (Lagrangian)	$10^{-4}$	

The “Occam-like” regularization provided very promising results for the imaging of the 1D resistivity models. The results of the sensitivity analysis are shown in figure 8.4.

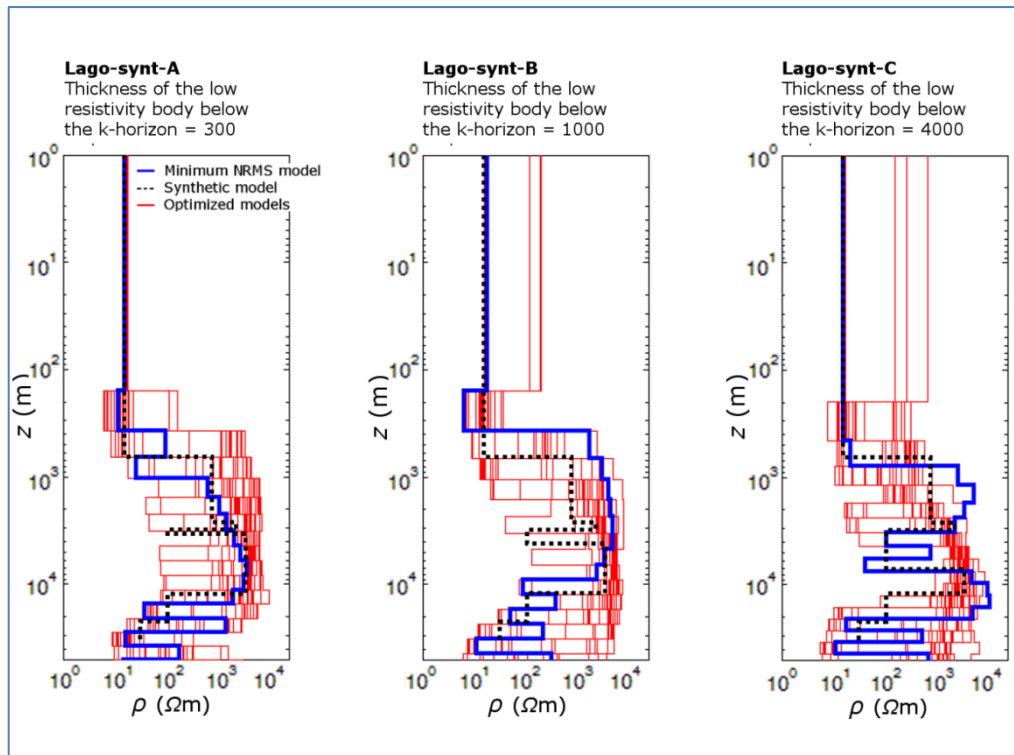


Figure 8.4- Results of the global optimization of the theoretical data from the *Lago-synth-A/B/C*. Estimated parameters: in red the 25 optimized models, in blue the minimum RMS model, the synthetic model is black.

The first evidence is that in the three models, the resistivity of the first layer is perfectly depicted with a misfit between modelled and theoretical apparent resistivity less than  $1 \Omega\text{m}$  and  $2.1 \Omega\text{m}$ , respectively for the *Lago-synth A/C* and *B*. The depth of the first resistive layer, the second layer with resistivity of  $700 \Omega\text{m}$  was detected with an error of about 100 meters in the *Lago-synth-C* while in the other two models the second layer was depicted with a good approximation but with higher misfits. The parameters related to the resistive layers, the 2<sup>nd</sup>, 3<sup>rd</sup> and 5<sup>th</sup>, in the three models were imaged within an acceptable error. With regard to the conductive body in the proximity of the K-horizon, it seems that 300 meters, or even 1000 meters are not accurately detected by optimization.

The PSO algorithm is sensitive to the conductive layer with thickness of 4000 meters and is able to recognize the depths of its top and bottom interbedded into two resistive layers. It should be noted that this conductive layer was recognized in the minimum NRMS (Normalized Root Mean Square) model, but was not

correctly imaged by all the trails due to equivalence problems. That issue must be taken into account for interpreting the resistivity data in the Larderello-Travale Geothermal field. The depth of the high conductivity halfspace was recognized in all the models but at this deep level the structure of the models is not enough minimized. The optimized models with minimum NRMS were taken into account with values of 0.01, 0.15 and 0.03, for the *Lago-synth-A/B/C* respectively. The RMS is normalized for the difference between the highest and lowest values of apparent resistivity and phase.

We stress that the Occam deterministic inversion (Constable et al., 1987) is really effective to invert 1D MT data, with impressive results with a very low computation time. In the case of the model *Lago-synth-C*, the comparison of the deterministic inversion and PSO showed that the inversion clearly and precisely detected the parameters of the conductive body but it was not able to detect the resistivity values of the two resistive layers above and below our target as imaged by PSO (figure 8.5).

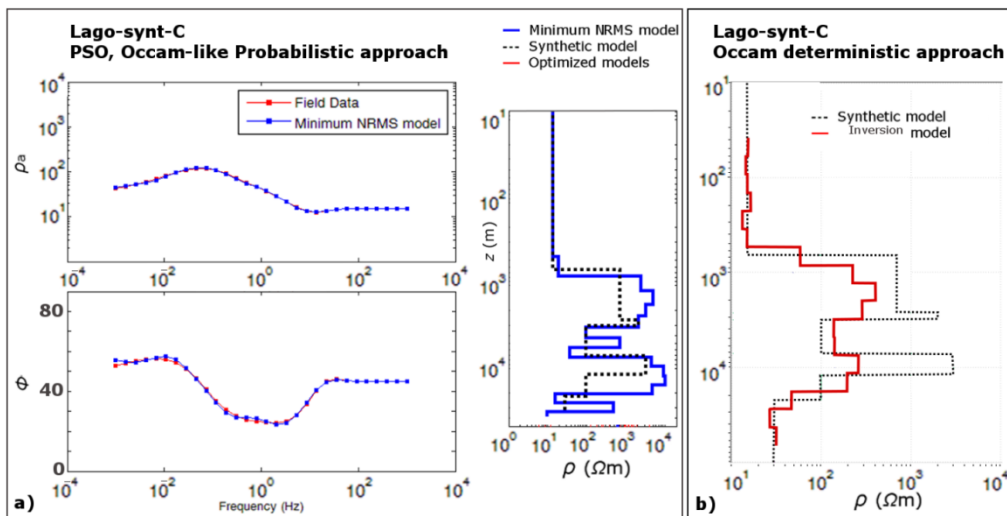


Figure 8.5- Comparison between the optimization using PSO and deterministic inversion for the model *Lago-synth-C*. a) In blue the minimum NRMS optimized model and its MT curve are shown while the red MT curve is referred to the theoretical data, b) Results from deterministic inversion using Occam algorithm.

## 8.3 Optimization of observed MT data from the Larderello-Geothermal field

### 8.3.1 Optimization of observed MT data: insights from the “G6” and “Lard\_7” soundings

Firstly, we present the results coming from the “G6” (Trav\_Rad-04 dataset) and the “Lard\_7” (Larderello\_2016 dataset) MT soundings located in the proximity of the Radicondoli-7bis and Venelle-2 geothermal wells, representing the two synthetic models *Travale-synt* and *Lago-synt*, respectively. A six-layers “blocky” resistivity model was estimated from the observed data in G6, whereas an “Occam-like” optimization was computed from the Lard\_7 site (see details in Table 8.5). The determinant average curves were considered for both soundings. The apparent resistivity and phase were considered in the optimizations with weight of 0.6 and 0.4, respectively.

Table 8.5- Main settings for the PSO optimization of the MT observed data from G6 and Lard\_7 soundings. LB=Lower boundary; UP=Upper Boundary.

<i>Lard_7</i>			<i>G6</i>		
<i>PSO (Occam-like)</i>			<i>PSO (Blocky)</i>		
$n_l$	$\rho$ ( $\Omega m$ )	$Tk$ (m)	$n_l$	$\rho$ ( $\Omega m$ )	$Tk$ (m)
1	LB=1; UP=200	200	1	LB=1; UP=200	LB=10; UP=750
2-3	LB=1; UP=1000	logarithmic increase from	2	LB=1; UP=2000	LB=50; UP=1500
4-20	LB=1; UP=10000	200 to 40000 m	3	LB=1; UP=2000	LB=100; UP=3000
			4	LB=1; UP=2000	LB=100; UP=1000 0
			5	LB=1; UP=2000	LB=1000; UP=1500 0
			6	LB=1; UP=2000	halfspace
<i>PSO(Occam-like): settings</i>			<i>PSO: settings(Blocky)</i>		
	Initial population	200		Initial population	200
	Particle Inertia	0,9		Particle Inertia	0,9
	Cognitive Attraction	0,5		Cognitive Attraction	0,5

Social Attraction	1,5	Social Attraction	1,75
Generations (Iterations)	200	Generations (Iterations)	200
Trials	25	Trials	100
<b><i>PSO(Occam-like): Objective function</i></b>		<b><i>PSO(Blocky): Objective function</i></b>	
$a$ (weight on $\rho a$ )	0,6	$a$ (weight on $\rho a$ )	0,5
$b$ (weight on $\Phi$ )	0,4	$b$ (weight on $\Phi$ )	0,5
$\lambda$ (Lagrangian)	$5 \cdot 10^{-4}$	$\lambda$ (Lagrangian)	0

In figure 8.6 the estimated blocky model from the G6 sounding is shown. The sounding was acquired in the frequency range of  $3.6 \cdot 10^2$  to  $10^{-3}$  Hz. Considering that the dimensionality analysis stated a very complex structure 2D/3D for this sounding, the 1D model is not completely reliable and can be considered only a first-order approximation. Among the 100 trials, the optimization itself is statistically quite consistent. As expected, the first layer is the most robust with a standard deviation, on 100 trials, of 0.9 for resistivity and a strong unimodal distribution. Other layers showed a-posteriori distribution that can be approximated as unimodal except for some outliers with values away from the mean. We considered the resulting model with the minimum RMS model correspondent to 0.01.

The results indicate an overall low resistivity electrical response for the whole investigated crust. The model is as far as possible to the high resistivity synthetic model *Travale-synt-A* that took into account only the stratigraphy and resistivity values typically assigned for those rocks. The synthetic model *Travale-synth-B* that took into account the resistivity values from the resistivity well logs is also quite higher than the measured MT data. Essentially the MT curves in G6 do not show any high resistivity response in the crystalline rocks, being the estimated values always lower than 100  $\Omega\text{m}$ .

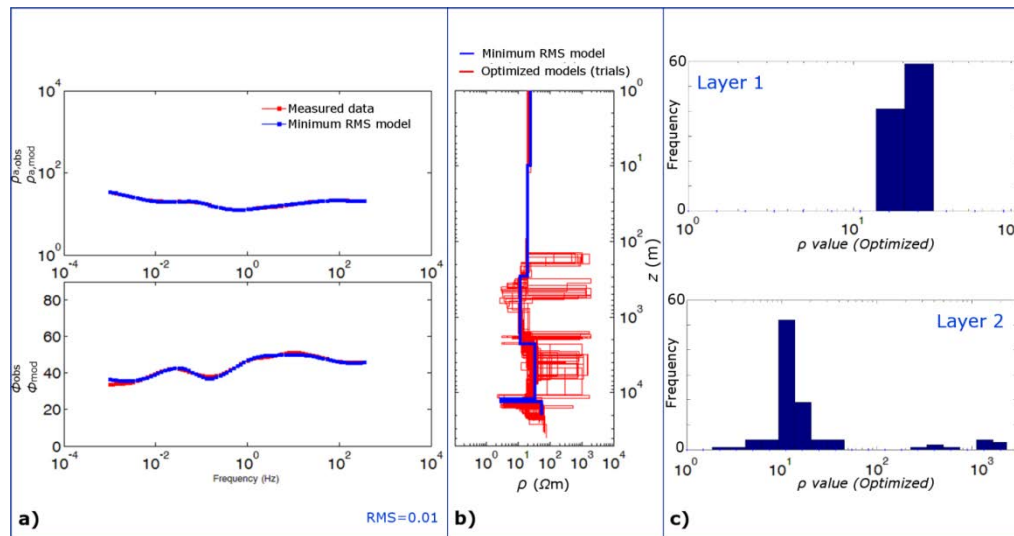


Figure 8.6- Results from the blocky optimization of the ‘‘G6’’ sounding: a) MT data, apparent resistivity and phase, referred to the minimum RMS model, b) 100 optimized model, the model with minimum RMS is highlighted in blue, c) Histogram of the 100 optimized resistivity value for layers 1 and 3.

With regard to the numerical test *Lago-synt*, from the stratigraphy of Venelle-2 well, we analysed the real MT data of the sounding Lard\_7, acquired very near to the well. The sounding is in the frequency range of  $3.8 \cdot 10^2$  to  $6.24 \cdot 10^2$  Hz. In this case the Occam optimization highlighted higher resistivity for the crystalline basement at depth of the Micaschist Complex with values of about 1000  $\Omega m$ . The resistivity response of the TWC and Phyllitic Complexes was much lower resistive than expected ( $< 100$   $\Omega m$ ). We underline that a low resistivity behaviour is also estimated at depth of about 8 km. The model we took into account was that with the minimum RMS (1.2) among 25 trials (figure 8.7).

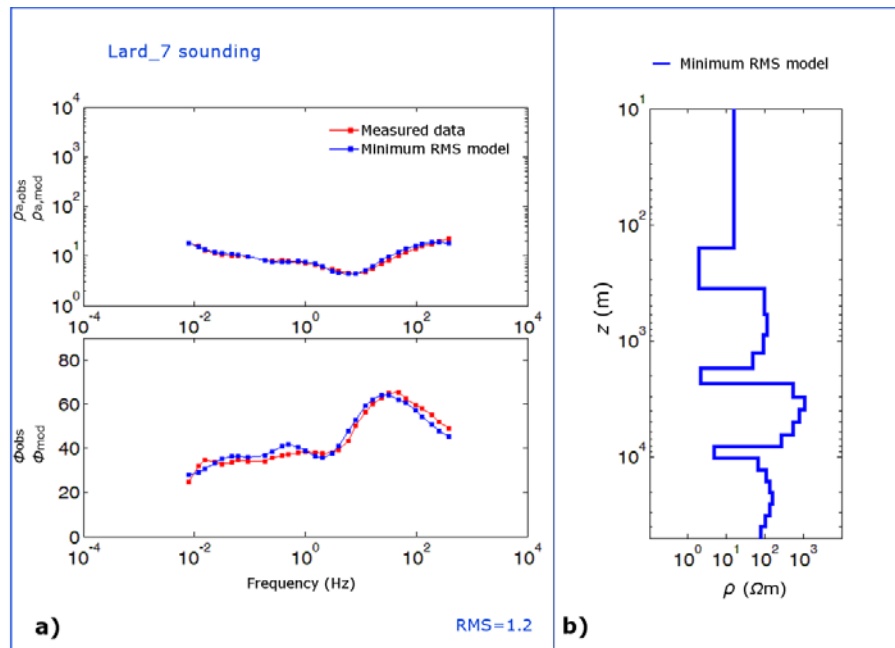


Figure 8.7- Results from the Occam optimization of the “Lard\_7” sounding: a) MT data, apparent resistivity and phase, referred to the minimum RMS model, b) estimated model.

### 8.3.2 Optimization of observed MT data: insights from the complete dataset

The optimization of measured MT soundings refers to the whole MT dataset available for this study in the *Lago Boracifero* area and selected stations in *Travale*. Hereby, we present the 1D resistivity smooth “Occam-like” models from the MT curves of stations located along the profiles 1 and 6 (also P1 and P6). We decided to use the Occam optimization, so avoiding a fixed and restricted number of layers of the estimated model. Our tests on synthetic models stated the effectiveness of this approach.

The analysis of MT soundings in the *Travale* area was accomplished in order to retrieve important information from the comparison with the available resistivity well logs.

We stress that all the optimizations we performed along the two selected profiles are unconstrained in the sense that only the contribution of the observed

data and the term related to the minimum structure were taken into account; no external constraints were used. We chose also to consider appropriate upper and lower boundaries of electrical resistivity in order to search the solution in a space domain as global as possible. It should be noted that it is possible to drive and accelerate the convergence to a solution by narrowing the search domain. Only for the first layers for whom direct information was available (outcropping rocks and TDEM), the search domain was considered smaller in our study, whereas for the other layers the algorithm was allowed to search in a wider domain.

In the Occam inversion procedure, the layer discretization, i.e. the fixed thicknesses, was accomplished by taking into account a logarithmic increase of the thickness of 19 layers whose sum was coincident with the skin depth of the lowest frequency for an average resistivity of 100  $\Omega\text{m}$ . For example the different investigation depth of the soundings “AMT19”, along the P6, is due to the fact that was acquired in the frequency range of Audio MT. For few soundings, e.g. “Lard\_13”, the investigation depth is reduced since the high level of EM noise impeded the correct computation of the determinant average curve; the lowest frequency with an acceptable level of noise was considered.

In figure 8.8 the resulting 1D Occam models were simplified in few layers models and were projected along the profiles, respectively the P1 and P6. For each sounding we took into account the model with the lowest NRMS among at least 25 trials.

Considering the *Lago Boracifero* area (Profile 1, figure 8.8), low resistivity features seem to occur at depth of 7-8 km in the optimized model for the Lard\_7 sounding. As first-order indication from the 1D analysis, with its limitations, the soundings along the Profile 1 seem to be characterized by widespread low resistivity response in the crystalline units. This reduction of resistivity is well depicted in the central part of the profile in the proximity of the Cornia River. In the NW and SE corners the resistivity distribution highlights higher resistivity responses at depth of crystalline rocks rather than the central sector, as estimated in the LN\_06 and Lard\_15 soundings.

With regard to the *Travale* area, the estimated resistivity models along the Profile 6 show an overall low resistivity response at depth up to 6000 m in the crystalline units with values usually < 1000  $\Omega\text{m}$ . Particularly impressive is the estimated model of the “G6” sounding where values never are higher than 100

$\Omega\text{m}$  (mainly  $< 50 \Omega\text{m}$ ). Interesting information regarding productivity (flow rate of geothermal fluids) derives from the geothermal well in the proximity of the “G6” soundings; they are possibly related to a dense fracture network. Other magnetotelluric soundings, showing particularly anomalous conductive behaviour, are in the central sector of the Profile 6. For instance, the “LS13” and the “K3” sites show at depth of 8 km with values lower than  $50 \Omega\text{m}$ .

The estimated models with PSO for very noisy MT sounding, are characterized by high misfit among modelled and measured data, in particular for the phase. This may represent a limit of the algorithm, or could also provide information on the uncertainty of the resulting models. In Appendix C (figure C.3-C.4) we show examples of very low misfits (consequently very low RMS values) and in Appendix C (figure C.5-C.6) we show models with higher errors due to a high uncertainty on the data, for the *Lago Boracifero* and *Travale* area.

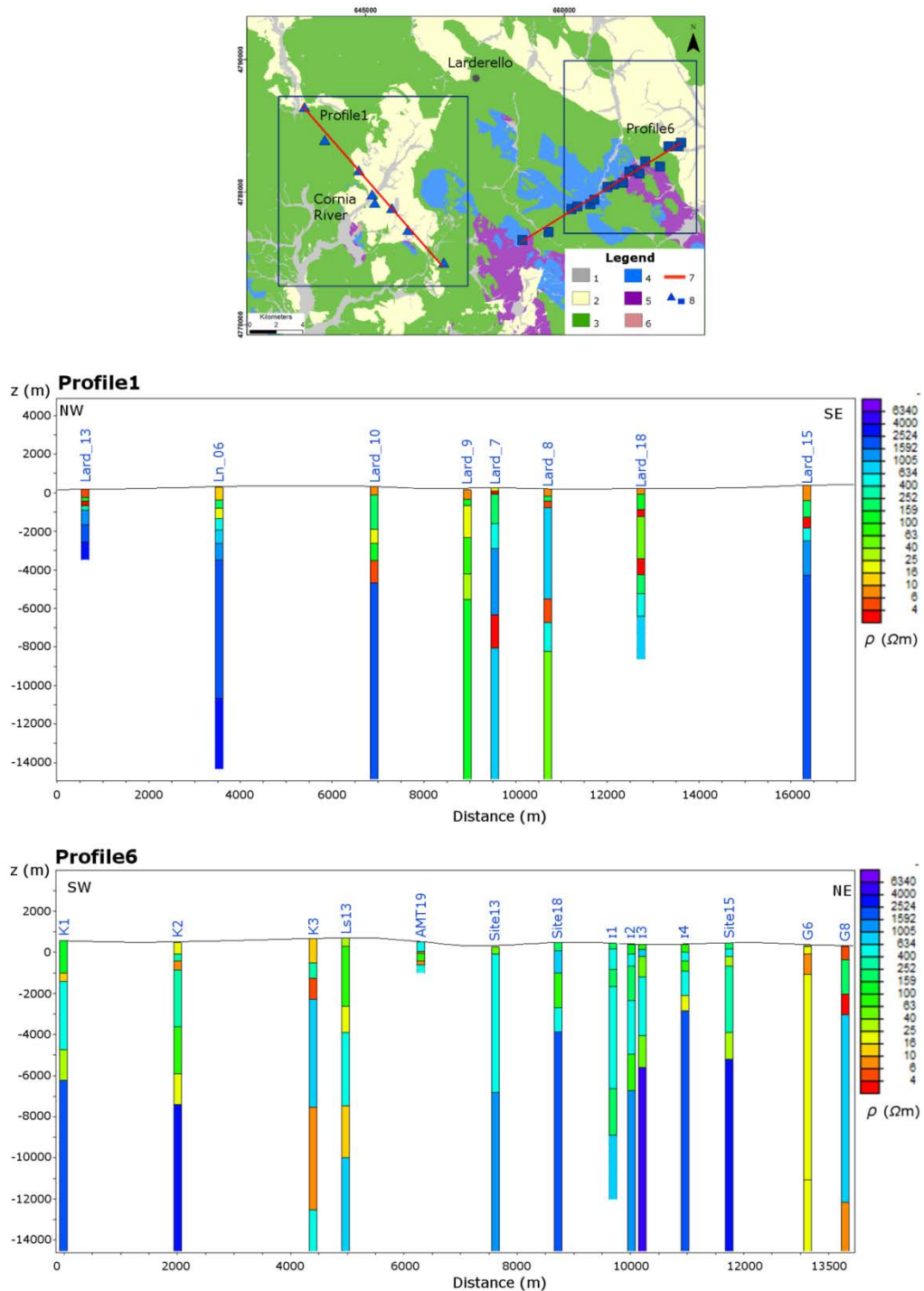


Figure 8.8- 1D estimated resistivity models obtained by Occam-like Particle Swarm Optimization. The simplified models are plotted along the Profile 1 of the *Lago*

*Boracifero* area and the Profile 6 of the *Travale* area. The traces of the profiles and the location of the MT stations are shown in the geological map: 1)-2)-3)-4)-5) (see figure 6.2); 7) Traces of MT profiles; 8) MT soundings.

## 8.4 Joint PSO optimization of TDEM and MT soundings

Different schemes and algorithms have been proposed in literature for computing joint inversion of TDEM and MT datasets (e.g. Meju, 1996). In this section we explore the possibility to constrain and refine the estimated 1D models by implementing a PSO scheme able to optimized jointly the MT and TDEM datasets. The procedure is based on the conversion of the TDEM response in a frequency domain MT curve; the assumptions and the mathematics beyond the approach are discussed in Chapters 4 and 7.

The result of the conversion step is a dataset of a MT curve, corrected for eventual static problems effects, merged with the low period TDEM response. The same procedure of PSO optimization was then applied to the merged TDEM/MT curves.

In figure 8.9 the results from the Lard\_16 “La Leccia” site are shown. The merged MT/TDEM apparent resistivity curve lies on a very broad band from  $3 \cdot 10^2$  to almost  $10^{-5}$  seconds (period). The theoretical apparent resistivity from the minimum RMS model is very close to the observed curve. It should be noted that the implemented algorithm allows the weight of the phase only for periods related to MT data; i.e. for the TDEM data the phase was not taken into account. The approach seems quite consistent in order to jointly analyse the two EM datasets in the same site, and allows the estimation of a well constrained (near surface) resistivity model.

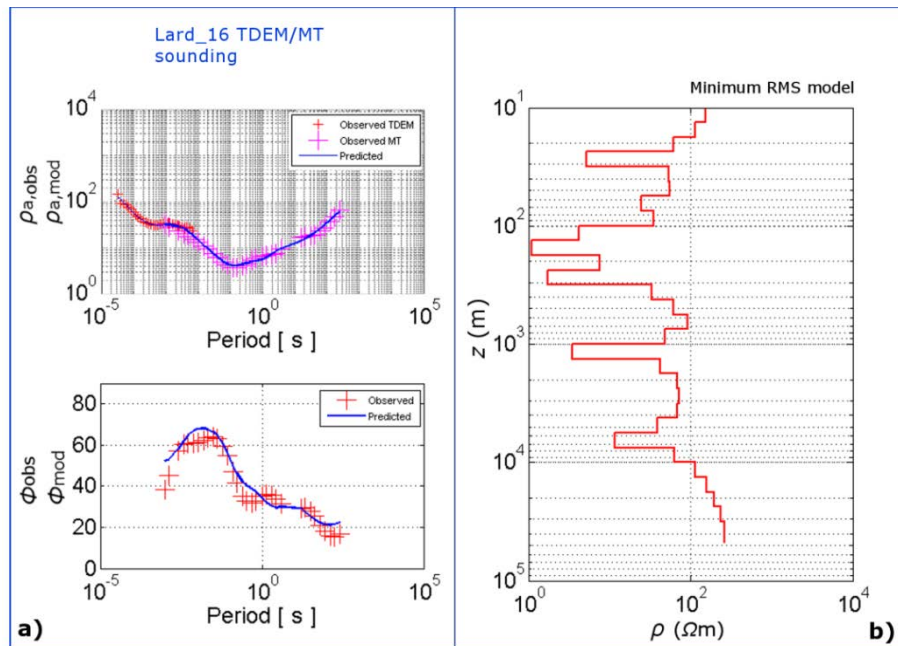


Figure 8.9- Joint Particle Swarm optimization of TDEM and MT data, example from the Lard\_16 site. a) Observed and modelled TDEM and MT apparent resistivity. The observed and modelled phase is related only to the MT dataset; b) The estimated resistivity model, with the minimum RMS (among 21 trials), is shown.

## 8.5 Discussion

Important information was retrieved from the optimization of the synthetic data, simulating the stratigraphy of the field, and their comparison with real observed MT data. Furthermore, the comparison among the MT soundings acquired in the proximity of the geothermal wells, used as benchmark for the synthetic models, coupled with the DLL/IL data can provide very useful information on the features at depth of the geothermal field.

This aspect is not trivial and the differences among the previous resistivity MT models defined in some sectors of the field (e.g. Manzella et al., 2010) and the DLL/IL values was matter of debate in literature, and yet nowadays is still controversial. Our 1D analysis states that the consideration of typical literature values of resistivity for each unit of the field cannot be reliable to describe the real resistivity distribution at depth; an accurate analysis on the MT data should be considered. Very impressive anomalous high conductive responses were depicted in various sectors of the Larderello-Travale field such as in the proximity of the

“G6” sounding where values lower than 50  $\Omega\text{m}$  were estimated at depth of micaschist. It should be noted that the drilling of the well Radicondoli-7bis, located near this sounding, was characterized by total mud circulation loss in the crystalline rocks indicating a possible wide fractured zone with related hydrothermal circulation (vapour dominated).

We stress that the sector below the *Lago Boracifero*, seems to be characterized by low resistivity values in contrast with the soundings at the margin of the area.

With respect to the MT data measured in *Travale*, the PSO optimization of the MT soundings acquired in the *Lago Boracifero* area resulted much more complex. The hypothesis is that a higher level of EM noise affected the measurements, decreasing the efficiency of the PSO. In spite of this consideration we think that the resulting resistivity models can represent important preliminary information on the electrical resistivity distribution at depth in the field.

The information gained, by global optimization in 1D, can be useful for the deterministic data inversion in 2D since a more reliable a-priori model has been provided in order to get a more constrained solution.

Furthermore, we implemented a scheme for the joint global optimization, with PSO, of TDEM and MT soundings. The results were very promising and we were able to constrain the shallow part of the estimated resistivity model. In such a way the static shift problem of MT data can be minimised.

## Chapter9

# Results from 2D inversion: interpretation and integrated model of the Larderello-Travale field

### 9.1 Introduction

For the study of the Larderello-Travale field we estimated the electrical resistivity distribution at depth along selected magnetotelluric profiles by using a common 2D deterministic inversion algorithm implemented in the WinGLink software package. The dimensionality analyses (see Chapter 7) pointed out a very complex 3D structure dominating the field, in particular at low frequencies, but important 2D structures were found in the proximity of the Cornia River (*Lago Boracifero* sector) and in the Radicondoli Basin (*Travale* sector). The 2D analysis of 3D data has limits that should be taken into account. Only a wise 2D interpretation of 3D MT data can be suitable for a reliable geological interpretation; for a review of this issue we refer the reader to the work of Ledo (2005).

The inversion schemes are iterative procedures that allow the estimation of model parameters, starting from an a-priori model. Berdichevsky and Dmitriev (2002) stated that to get a solution of MT inversion closed to the global minimum

as much as possible, the reliability of the a-priori model appears to be important. This particular aspect is also related to the function to be minimized having different local minima where the solution can possibly converge.

We focused on the understanding of the reliability of the a-priori model for the inversion procedure. For this reason we implemented and tested the 2D inversion starting from three sets of a-priori models: *i*) homogeneous, *ii*) geological (i.e. geologically-constrained) and *iii*) interpolation of 1D optimized models.

A strength of our study is the use of a detailed 3D geological model that was populated with resistivity values coming from the quantitative analysis of resistivity well logs.

It should be noted that the information on resistivity from well logs refers to a very small volume of rocks investigated in the surroundings of the borehole. The MT methods, treating the EM induction in the Earth as diffusive, returns an average response of electrical properties on wide investigate volumes. Differences among the resistivity models from well logs and the MT estimated models from MT were recognized in some previous studies in the area (e.g. Manzella et al., 2010) but a unique explanation was not figured out. For this reason, we tested the a-priori information from an accurate analysis on the collected EM data throughout the PSO approach .

It is interesting to compare the 2D inversion models in these three cases, since each one is referred to a different level of information. A-priori model from data analysis (in this case from PSO optimized model) can be useful for the prospecting of geothermal greenfield, for whom no subsoil data are available. In figure 9.1 a schematic view of the selected MT profiles is shown coupled with some toponyms that will be used in the following description and discussion.

A focus on the *Lago Boracifero* is hereby presented being the main area of interest.

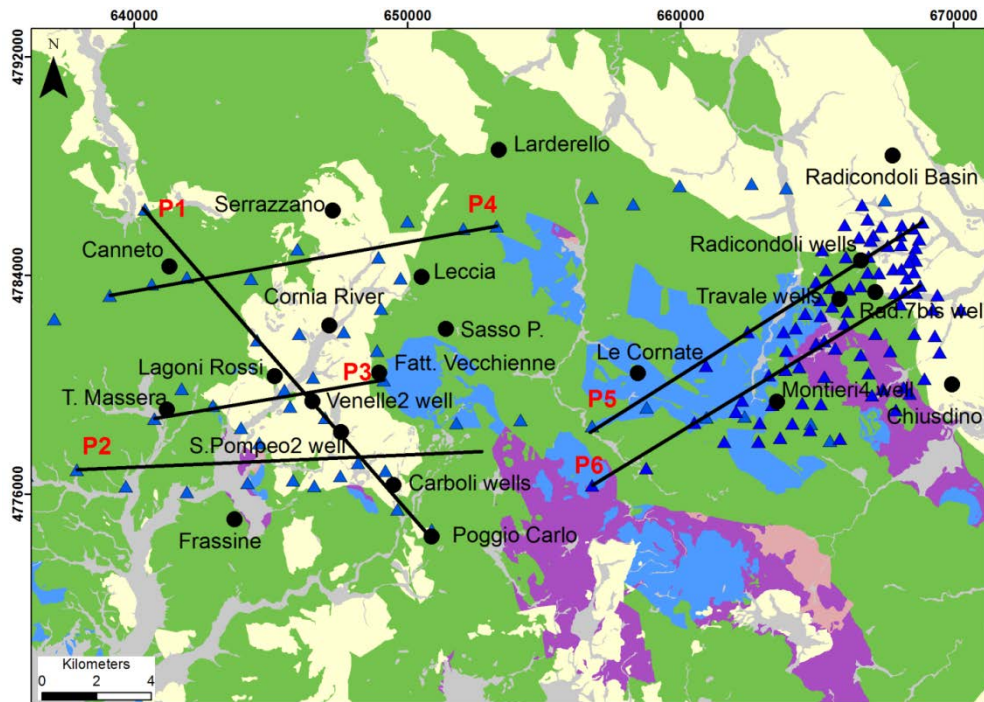


Figure 9.1- Schematic view of the MT profiles selected for the 2D inversion. Toponyms and some wells are shown. For detail on the geological maps the reader is referred to the figure 6.2.

## 9.2 Meshing

The 2D meshes were generated with finer size of cells in the central and detailed zone (between the first and last MT soundings), incorporating also the topography. The boundary effects were removed by extending laterally and downwards the meshes with an increasing size of the cells. The effects of the Mediterranean Sea, located from 20 km to 40 km from the study areas, were taken into account in each model with a electrical resistivity of  $0.3 \Omega\text{m}$ .

## 9.3 Initial models

For each MT profile, three resistivity models were implemented and tested as starting model for the 2D inversion:

- Homogeneous halfspace;

- Resistivity distribution by assigning resistivity values to different units of the geological model (later Geological model);
- 2D model obtained from interpolation of 1D resistivity distribution of PSO optimization (later PSO model).

### 9.3.1 Homogeneous halfspace

The homogeneous a-priori model is a halfspace with a homogeneous electrical resistivity of 100  $\Omega\text{m}$  (with except for the Mediterranean Sea) implemented on the previously described 2D mesh.

### 9.3.2 A-priori from geological model

The implementation of the a-priori models from geological information required some effort. First of all, the detailed 3D geological models for the *Lago Boracifero* and *Travale* area were built (see detail in Chapter 6). Six slices, corresponding to the MT profiles, were extracted from the 3D models. At this stage the available information was strictly related to the geometry of the geological units. The assignment of a resistivity value for each unit was required.

We have verified that the range of resistivity values commonly adopted in literature for such kind of rocks (particularly the crystalline rocks) are not suitable for the MT study of the Larderello system (Chapter 8). For this reason, we accomplished a detailed analysis on the resistivity logs acquired in deep geothermal wells located in the *Travale* sector. As an example, the deep resistivity well log of Radicondoli-7bis well is shown in figure 9.2; this log was previously published in Giolito et al., (2009). The other well logs used in this research are available confidentially and cannot be shown here.

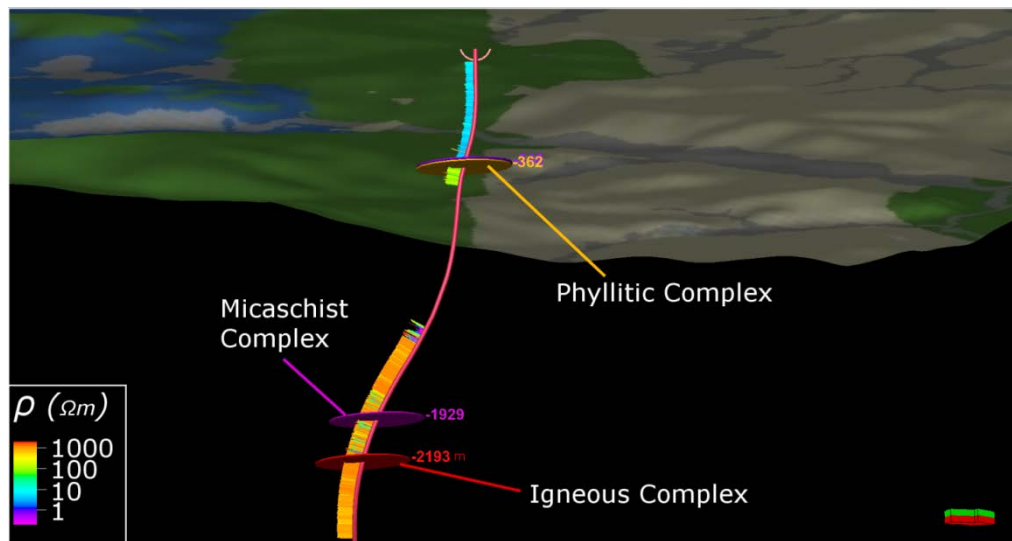


Figure 9.2- Resistivity well log measured along the Radicondoli-7 bis. The well tops are shown, too.

The resistivity log of the Radicondoli-7bis is quite peculiar since very low resistivity values were measured along the borehole with mean values of Granite and Micaschist complexes lower than  $1000 \Omega m$ . This response cannot be considered representative for the granites of the whole field, since higher values were measured along other boreholes.

The dataset of resistivity logs consists of DLL/IL measurements, with resolution of the centimetres order, that we imported and visualized in 3D (Petrel environment), along the deviated path of six boreholes: Radicondoli-20-29-7bis, Montieri-4, Travale Sud-1 and Chiusdino-4. Therefore, we extracted from the whole geophysical logs, those resistivity values inside a certain stratigraphic unit modelled in three-dimensions. We computed simple statistical parameters among the values measured in the boreholes and belonging to a certain unit (figure 9.3).

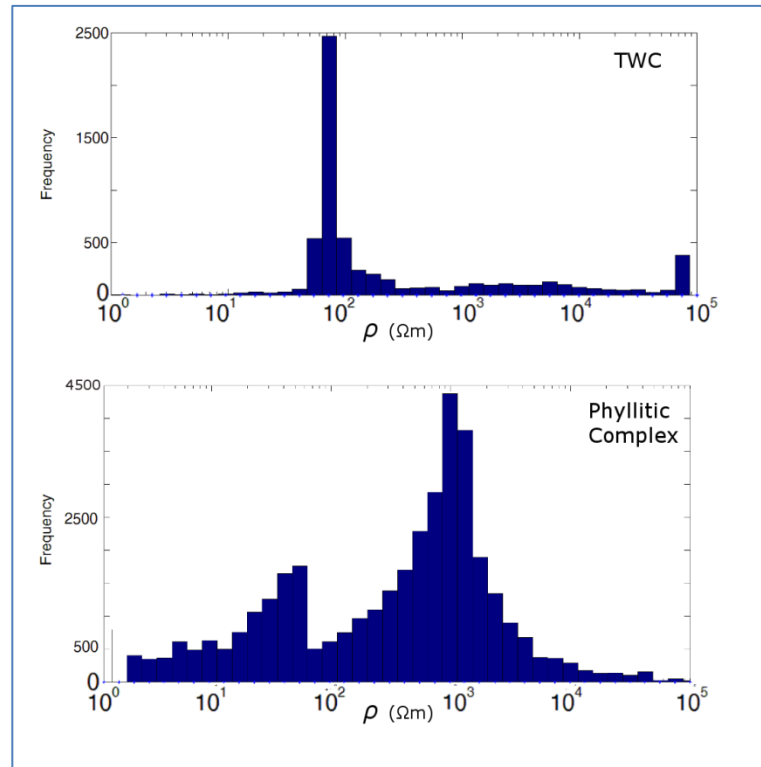


Figure 9.3- Histograms from DLL/IL measurements along six geothermal wells located in the *Travale* sector. The resistivity values for the TWC and Phyllitic Complex are shown.

This analysis allowed the definition of data-driven value, the median in this case, to be assigned to each stratigraphic unit (Table 9.1).

Table 9.1- Electrical resistivity values assigned to each stratigraphic unit of the 3D geological models based on the analysis of DLL/IL well logs.

Unit	Resistivity ( $\Omega\text{m}$ )
Neoautochthonous Complex	3
Ligurian Complex	15
Tuscan Nappe	100
TWC	600
Phyllitic Complex	700
Micaschist Complex	2000
Gneiss Complex	3000

---

Igneous Complex	3000
-----------------	------

---

It is clear that some factor, such as mineralogy, temperature and hydrothermal circulation, operates for the decreasing of the overall resistivity, particularly evident in the TWC (Tectonic Wedges Complex) and Phyllitic Complex.

With regard to the Phyllitic complex, high (expected) resistivity values occurred with interbedded thin layers having resistivity lower than 1-3  $\Omega\text{m}$ , probably related to the presence of graphite (e.g. see Pandeli et al., 1991 for the mineralogical composition of the geological unit). In figure 9.2, along the Radicondoli-7bis, an interval with very low resistivity values ( $< 1 \Omega\text{m}$  at about -1800 m) is observed in the Phyllitic Complex. According to the synthetic well logs stratigraphy this unit is characterized by layers of graphitic phyllites and a productive fracture. More recently, in the frame of a H2020 Project (DESCRAMBLE), a resistivity well log was acquired in the Venelle-2 (centre of the *Lago Boracifero* area) and the results revealed very low resistive response in the Phyllitic complex. Since the Venelle-2 logs were available only after we finished the models, this information was used only as confirmation of our analysis.

With regard to the Micaschist Complex, the only DLL/IL available was recorded in the Radicondoli-7bis in a short interval with total loss of circulation (with productive fractures) and an intense decrease of resistivity occurred. Following the indication of ENEL GP within the I-GET EU Project and based on their analysis of other resistivity logs, we used a value of 2000  $\Omega\text{m}$  for our inversions, which is slightly higher than the median value computed from available well logs.

Regarding the Igneous Complex, the resistivity values distribution is multimodal demonstrating a strong heterogeneity in this unit. No data were available for the Gneiss Unit and taking into account the lithology and literature data, a reasonable value of electrical resistivity, i.e. 3000  $\Omega\text{m}$ , was assigned.

The geological profiles were extracted from the 3D models, and populated with the computed resistivity values. They defined the a-priori models (from geology) for the 2D inversion of MT data. As an example, the model for the Profile 5 is shown in figure 9.4; the other models are shown in Appendix C.

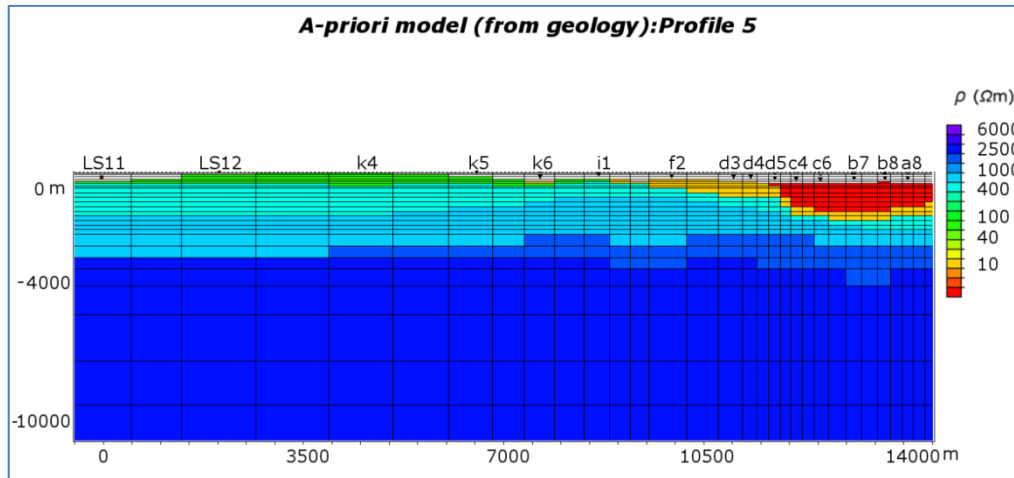


Figure 9.4- A-priori model along the Profile 5. It represents a 2D section of the geological model populated with the resistivity values.

Due to the very deep extension of the mesh grid along  $z$ , we simulated two cases. In the first case the Crust-Mantle (Mohorovičić) discontinuity was taken into account with a value of  $30 \Omega\text{m}$  at a depth of 22 km. In the second case we added also the Upper-Lower Crust discontinuity with a resistivity of  $100 \Omega\text{m}$  at a depth of 12 km. The depth of these two surfaces were retrieved from studies on the geodynamics of Appennines and the resistivity values from general tectonophysics studies (Jones, 1992; Armadillo et al., 2001; Accaino et al., 2006; Korja, 2007; Di Stefano et al., 2011). We did not insert in the model also the K-horizon interface since at the moment we do not have any clear physical information about its nature (only its bright-spot seismic response). Considering the K-horizon as a possible target for our geophysical study, we decided to not constrain the inversion with some a-priori (not validated) information on this marker.

We must keep in mind that the investigated volume of geophysical well logs is orders of magnitude smaller than that of Magnetotellurics, and the attributed resistivity values must be considered only as starting value for our inversion. The response of MT measurements is indicative of the volumetric averages of the Earth resistivities due to the diffusive propagation of EM fields. Indeed, in many cases a strict relation among the two kinds of resistivity (DLL/IL and MT) measurements can be misleading.

### 9.3.3 A-priori from PSO models

As a way to constrain the inversion using only MT information we also tested the use of a-priori models based only on the MT data and not on geology. Here we adopt the result of the 2D sections (from interpolation of 1D) to be used as a-priori models for the deterministic 2D inversion. In figure 9.5 the interpolation of PSO models is shown for the Profile 3; other models are shown in Appendix C.

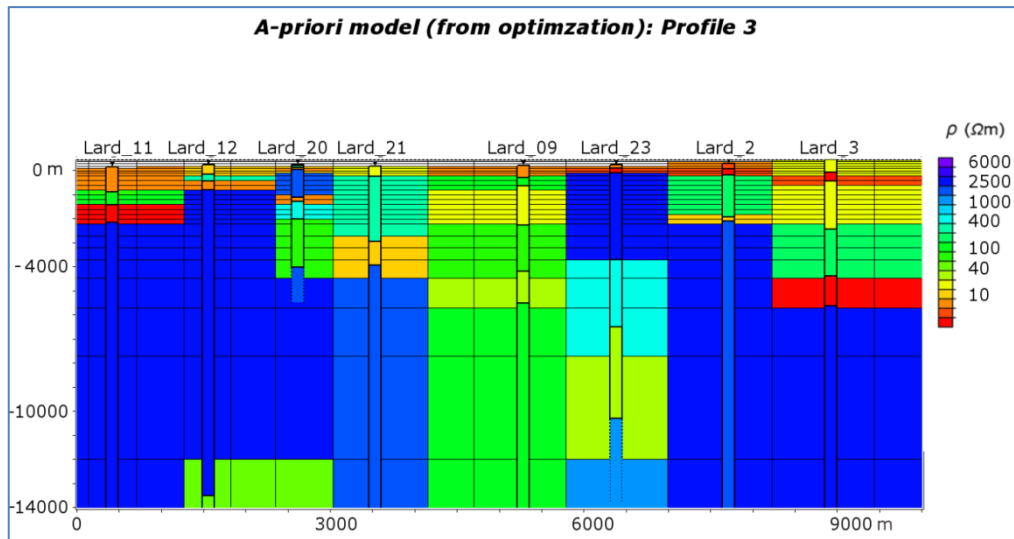


Figure 9.5- A-priori model along the Profile 3. It represents a 2D interpolation of 1D models obtained with the Particle Swarm Optimization procedure.

## 9.4 2D inversion: setting parameters

The 2D inversion was performed along six profiles crossing the available EM datasets (S-Tuscany\_92, Trav-Rad\_04/07, Larderello\_2016) by using the inversion algorithm published in Rodi and Mackie (2001) and implemented in the WinGLink software package. The algorithm employs a nonlinear conjugate gradients (NLCG) scheme and solves the not quadratic objective function discarding the iterated linearized approach and applying a NCLG variant. The algorithm proposed in Rodi and Mackie (2001) computes a regularized solution (Tikhonov and Arsenin, 1977) as the model minimizes the following objective function  $\Psi$ :

$$\Psi(\mathbf{m}) = (\mathbf{d} - F(\mathbf{m}))^T \mathbf{V}^{-1} (\mathbf{d} - F(\mathbf{m})) + \lambda \mathbf{m}^T \mathbf{L}^T \mathbf{L} \mathbf{m} \quad [\text{Eq. 9.1}]$$

where  $\mathbf{V}$  is the error variance matrix and  $\lambda$  is the Lagrangian multiplier.  $\mathbf{L}$  can be a first or second order operator, for example  $\mathbf{L}\mathbf{m}$  can represent the gradient or the Laplacian of resistivity.  $F$  is the forward operator; i.e. the nonlinear system of equations that describe the MT field for certain model parameters.

The numerical simulation; i.e. the forward modelling, is computed by finding 2D finite difference solutions to Maxwell's equations as described in Mackie et al. (1988). Obviously, Maxwell's equations decouple into Transverse Electric (TE) and Transverse Magnetic (TM) polarizations. Before proceeding with the modelling, we must distinguish the TE and TM polarities for the XY and YX component of  $\mathbf{Z}$  for each sounding. We accomplished this aspect by taking into account the strike direction ranging from N30W to N30E for the *Lago Boracifero* sector (see details in Chapter 7) and N40W for *Travale* with the further information in some cases of the direction of principal E and H fields obtained by tensor decomposition (La Torraca et al., 1986).

We provide hereafter a brief description of the user-defined parameters we set for the 2D inversion of the six profiles in the *Lago Boracifero* and *Travale* sectors. Among the three kinds of a-priori models the main difference in the inversion parameters setting is that for the homogeneous starting model we chose to solve for the smoothest model while for the inversions with starting models from PSO and geology we chose to solve for the smoothest variation away from the a-priori model. The role of the Lagrangian multiplier is fundamental in the regularized 2D inversion. The parameter represents the trade-off that properly balances the two terms of the minimization function; i.e. fitting the data, achieving the minimum difference between modelled and observed data and the effect of the reference model. The proper selection of  $\lambda$  is not trivial; here a L-curve criterion is adopted and a value  $\lambda = 3$  was chosen. In figure 9.6 we show the L-curve graph obtained for the Profile 1. Of course, larger values of  $\lambda$  produced smoother models with a worse data fit and higher NRMS values.

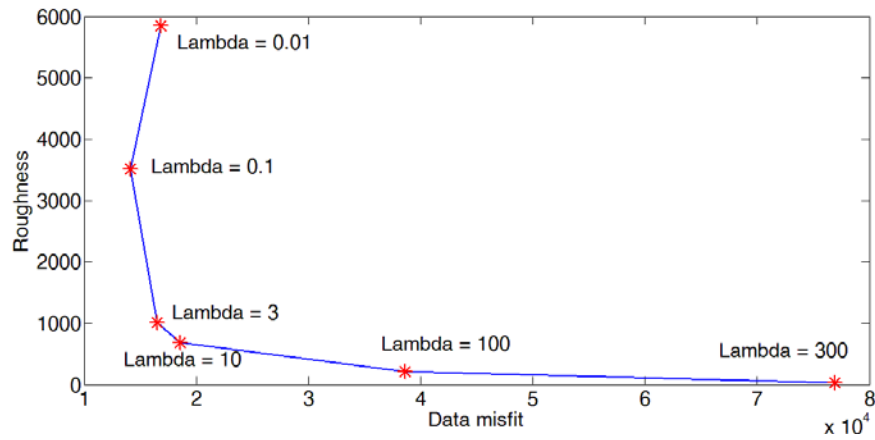


Figure 9.6- L-curve graph for the Profile 1. The roughness of the model is plotted versus the data misfit for six inversion with different Lambda ( $\lambda$ ) value. The maximum curvature indicates the optimal trade-off between the terms of the objective function.

The regularization can be accomplished by minimizing the integral of the Laplacian  $|\nabla^2(m)|^2$  or the Gradient  $|\nabla(m)|^2$  of the model specifying uniform (equal dimensions of the model) or standard grid; the uniform grid produces smoother results. We ran different inversions in order to test the effectiveness of such regularization parameters, observing in few cases significant differences. The results from the minimization of the Gradient of the model and the use of standard grid seemed to be the most reliable, also in terms of RMS, and were chosen for the interpretation of inversion models. In figure 9.7, the comparison among different settings is showed for the Profile 3.

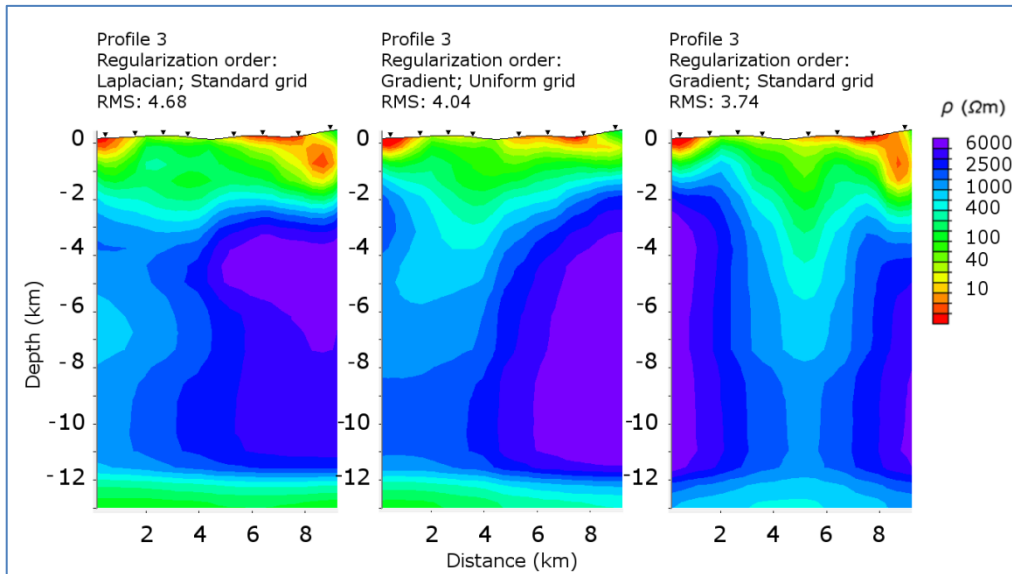


Figure 9.7- Comparison of different inversions on the same profile. On the left the Laplacian is minimized (Standard grid), in the middle the Gradient (Uniform grid) as well as on the right with a Standard grid. The corresponding RMS values are shown.

Six decades of data were inverted, with lowest frequency of  $10^{-3}$  Hz. The error threshold for apparent resistivity and phase was set to 5%. The inversions iterated at maximum 100 times (or less if a RMS threshold was reached).

## 9.5 Results

### 9.5.1 Results from inversion without external constraints

Let first analyse the results of the 2D inversion along the six profiles starting from a homogeneous halfspace of  $100 \Omega\text{m}$ . The joint TE and TM inversions are shown in figure 9.8.

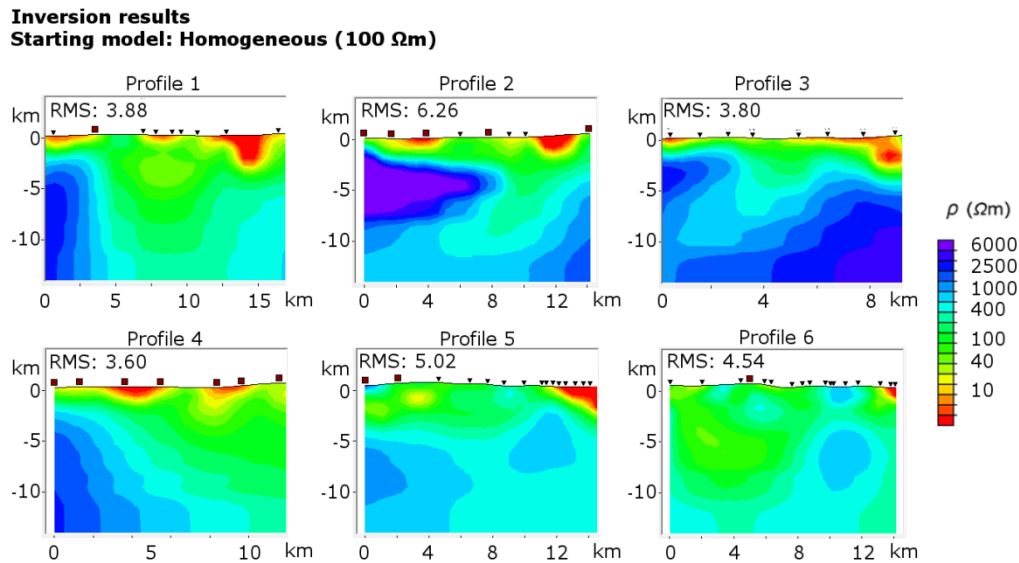


Figure 9.8- Resulting models from the 2D inversion of the six MT profiles in the Larderello-Travale geothermal field. Here the homogeneous starting models were used to invert jointly TE and TM polarizations. The RMS values are also shown.

The resulting models appear very smooth and lack the necessary resolution for imaging the subsurface, especially in complex structures such as in Larderello. It is clear that to fit the data a strong reduction of resistivity is required along the profiles also at depth of crystalline rocks. With regard to the *Lago Boracifero* an important structure with a decrease of resistivity to 50-100  $\Omega\text{m}$  is highlighted, located mostly in the central part of the profiles. Some other shallow low resistivity structures coincident with Neogene basins seems to be oversized. In the *Travale* sector (Profiles 5 and 6), the Radicondoli Basin is duly imaged and a general low resistivity is imaged along the whole Profiles, with slight higher values in Profile 5.

### 9.5.2 Results from inversion constrained with geological data

As previously described, in order to constrain the inversion and improve the resolution for imaging the deep structures, models from the 3D geology were used as a-priori information. For each MT profile two hypotheses were tested: with or without a high conductive Lower Crust. We preferred to consider the models without the Lower Crust interface, since they produced lower RMS. In figure 9.9 the results are shown for the constrained inversion using geological a-priori information and inverting jointly TE and TM polarizations.

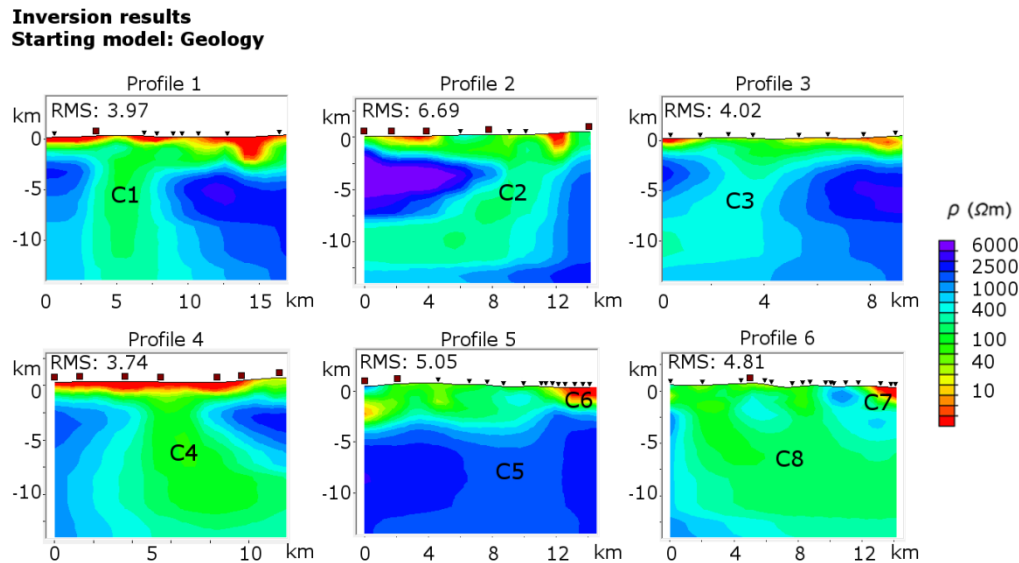


Figure 9.9- Resulting models from the 2D inversion of the six MT profiles in the Larderello-Travale geothermal field. Here the geological information was used to constrain the joint TE and TM inversion. The RMS values are shown as well as indication of low resistivity anomalies (C1-C8).

The resistivity models clearly indicate that low resistivity anomalies occur at depth of the vapour-dominated reservoir hosted in crystalline rocks and also at deeper level in spite of we constrained the inversion with deep high resistivity layers. With regard to the *Lago Boracifero* sector, i.e. the profiles 1-4, four main sub-horizontal layers can be recognized with the following resistivity: 1) 3-30  $\Omega\text{m}$ , 2) 40-200  $\Omega\text{m}$ , 3) 2500-5000  $\Omega\text{m}$ , 4) 100-400  $\Omega\text{m}$ . As expected, the low resistivity shallow layer, with values in the range of 3-30  $\Omega\text{m}$ , corresponds to the Neoautochthonous and Ligurian Complexes. In the right-end side of Profile 1 and 2 the size of this layer is overestimated, probably due to the large distance between the MT stations.

The underlying layer, characterized by resistivity values in the range of 40-200  $\Omega\text{m}$ , is located at a structural level coincident with the Tuscan Complex, TWC and most of the Phyllitic Complex. The bottom of this layer is located at a depth quite variable with an average of 2500 m b.g.l.

The third layer, characterized by resistivity values in the range of 2500-5000  $\Omega\text{m}$ , corresponds mainly to the Micaschist, Gneiss and Intrusive complexes. In

this latter case, we observed a good match between the MT response and the average resistivity value estimated from geophysical well logs.

Finally, at depth higher than 7 km, a general decrease of resistivity is observed with values locally lower than 400  $\Omega\text{m}$ .

All the MT profiles in the *Lago Boracifero* sector show a very important sub-vertical structure cross-cutting the main layers previously described and characterized by low resistivity, with average values of about 150  $\Omega\text{m}$ . In figure 9.9 this vertical structure is indicated as C1 to C4. For example, sub-vertical structure, in the Profile 1 (C1), is mainly located below the Lagoni Rossi and the Cornia River clearly cross-cutting the high resistive third layer. At deeper levels the low resistivity anomaly seems to occur also below the zones of Venelle-2 and San Pompeo-2 geothermal wells (figure 9.1, for location).

In the Profile 4 the anomaly seems wider at depth compared to the other profiles. We further investigated this important sub-vertical structure, by inverting single TE or TM mode, taking as example the Profile 1. With regard to the 2D interpretation of 3D data, Ledo (2005) stated that the polarization less affected by 3D effects depends on the relative position between the 3D structure with respect to the regional 2D strike. In our case the 3D body is parallel to the regional 2D strike direction and the TM mode is the less prone to error, according to Ledo (2005). For the *Lago Boracifero* sector the assumption of the occurrence of a 3D body elongated parallel to the strike direction is based not only on the MT data analysis but is also supported by the analysis of independent data (e.g. seismic data, see Section 9.6). Briefly, an anomalous low velocity (P waves) and low density body is recognized at mid crustal level in the area of interest by seismological and gravimetric studies (e.g. Baldi et al., 1994; Batini et al., 1995), being interpreted as partially melted body. Information on its elongation can be retrieved by analysing the depth of the K-horizon (Cameli et al., 1998), NE-SW elongated in the area, parallel to the supposed Cornia Fault and to the 2D strikes from MT dimensionality analysis (as described in Section 7.4). In figure 9.10 the results of inversion of single TM and single TE modes are shown for the Profile 1, almost perpendicular to the 2D regional structure. The inversion parameter setting is the one already described for the joint TE and TM inversions of all profiles.

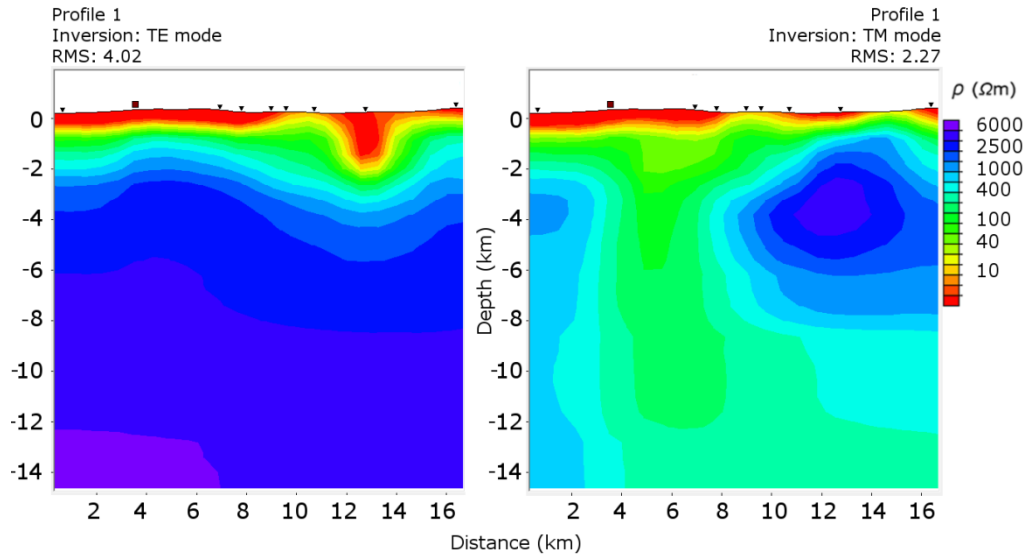


Figure 9.10- 2D inversion of single TE mode (on the left) and single TM mode (on the right) of Profile 1.

It is evident in figure 9.10 that the TM inversion reproduces the low resistivity anomaly C1, which is not imaged by TE inversion results, with much lower RMS than those obtained by the joint TE and TM and single TE mode inversion (figure 9.9 and 9.10).

With regard to the *Travale* sector, i.e. Profile 5-6, some clear features can be pointed out. First of all, a significant difference between the Profile 5 and Profile 6 occur. The Profile 5 is characterized by a local anomaly (C5, figure 9.9) at deep levels (< 3000 m b.g.l.) located in a more general high resistive volume, corresponding to the third layer described for the *Lago Boracifero* sector. The Profile 6 shows a widespread reduction of resistivity at deep levels with average values of 150  $\Omega\text{m}$  (C8). With the exception of few local areas along the profile, the third resistive layer (usually up to 3000-5000  $\Omega\text{m}$ ) seems to be missing. Another important feature of this sector is the Radicondoli Basin, filled with high conductive siliciclastic sediments, that is very well imaged in the two profiles (C6 and C7).

### 9.5.3 Results from inversion constrained with PSO resistivity distribution

Hereafter we present the results of 2D inversion constrained with the PSO models with a focus on the *Lago Boracifero* area that represents the main area of interest. Although the 1D models can be easily obtained by conventional inversion, we implemented and used the Particle Swarm Optimization algorithm. As stated in the previous chapter, the advantage is the exploration of the global space solution and the possibility to compute a-posteriori analysis on the density functions of the solution.

The inversion settings are the same used for the computation of the inversions previously described; the results for all profiles are shown in Appendix C.

In comparison to the inversion from homogeneous halfspaces of figure 9.8, the inversion models constrained with the PSO approach provided the necessary resolution for imaging the complex subsurface structure of the Larderello system. The results are quite consistent in terms of RMS, which are even lower than the corresponding ones obtained by geologically constrained inversions. As an example we show in figure 9.11 the results obtained by joint TE and TM modes inversion along Profile 1 and 3. The final RMSs are 3.85 and 3.81 respectively. The inversion models image low resistivity anomalies (C1 and C3) in the central sector of the profile. In this case the resolution appears even higher than for geologically-constrained inversions, so that the anomalies differentiate into C1a-b and C3a-b.

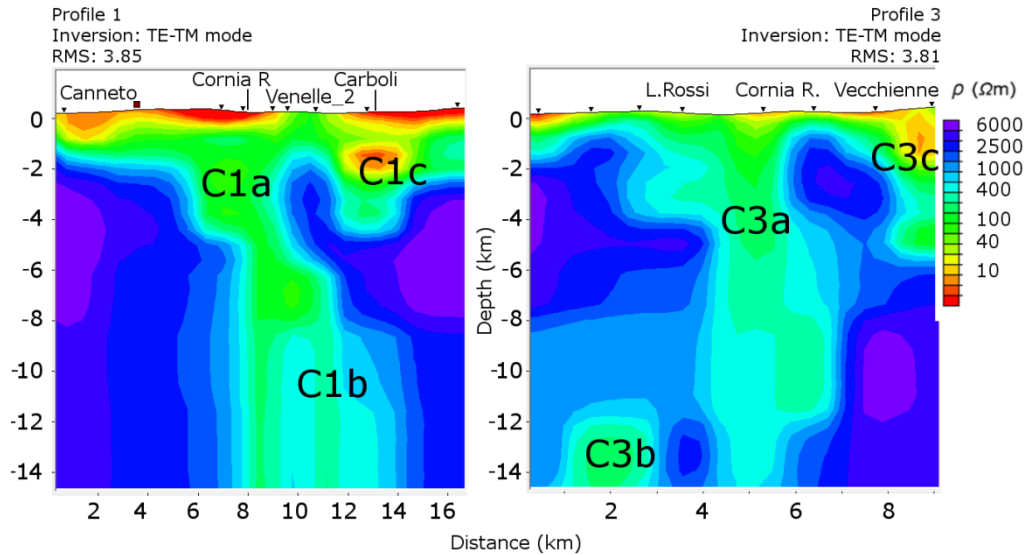


Figure 9.11- Joint Inversion of TE and TM mode along the Profile 1 (on the left) and Profile 3 (on the right) starting with optimized a-priori models.

The main structure still appears sub-vertical with low resistivity in the central part of the Profiles (C1a and C3a), in the proximity of the Cornia River and Lagoni Rossi, with average resistivity of 200  $\Omega\text{m}$ . In addition, we identified two other separate and important low resistivity structures (C1b-C3b) at deeper depth, about 7-8 km for both Profile 1 and Profile 3. C1b and C3b are located below the Venelle-2 well and the T. Massera, with a strong decrease ( $< 200 \Omega\text{m}$ ) of resistivity at 12 km in Profile 3.

We performed a sensitivity test on the inversion model of Profile 1, in two steps, starting from the resulting inversion model in figure 9.11. First, we increased the resistivity of the medium comprised between C1b and C1a (i.e. the narrow conductivity anomaly). Then, we increased the resistivity of C1b and C1a. We computed the forward model and compared the results with the observed data. Since a progressively higher RMS was obtained, we concluded that the low resistivity structures are required to properly fit the data.

Other important anomalies located at the depth of crystalline rocks, up to 4 km b.g.l., are recognized in the right-end side of Profile 1 and Profile 3 in the zones of Carboli wells and the Fattoria Vecchienne (see figure 9.1 for location), respectively C1c and C3c. Important geological structures and hydrothermal

circulation were pointed out from seismic data and wells in correspondence of these anomalies, particularly C1c. However, it should be considered that the C1c anomaly is due to a decrease of apparent resistivity in a frequency band that resulted particularly noisy and its interpretation can be misleading.

## **9.6 Discussion on the geothermal interpretation and the integrated model**

The aim of this work was to improve the knowledge on the deep structures of the *Lago Boracifero* sector (Larderello field) being of interest firstly for its geological complexity and also for the possibility to explore deep-seated unconventional geothermal resources. The results from homogeneous a-priori models appear very smooth and lack the necessary resolution for imaging the subsurface. The adoption of the 3D geological model and geophysical well logs for constraining the 2D inversion allowed the increase in resolution to image the deep structure of the Larderello-Travale field.

In addition to the conventional inversions of MT data, we tested the effectiveness of global optimization algorithms (PSO) in 1D, used also for driving the 2D inversion. We had to admit that the resulting 2D inversion models exceeded our expectations in the sense that we were able to refine the unconstrained inversion and even to improve the reliability of the models with respect to the results constrained with geological information. This conclusion is based not only on the lower RMS values that were achieved, but above all on the integrated analysis with other dataset such as seismic data, as showed in the next subsections. The results here showed indicate the suitability of such data-driven approach to improve the resolution of the 2D inversion, and are considered as benchmark for the interpretation of the field. The approach can be of help for the geophysical prospecting of geothermal greenfield lacking other source of subsoil data.

### **9.6.1 The shallow level of the *Lago Boracifero* sector: cap-rock and reservoir**

In the *Lago Boracifero* sector, the upper units are very conductive due to lithology of the Neoautochthonous and Ligurian Complexes. Their corresponding resistivity

values resulting from inversion was in the range of 3-30  $\Omega\text{m}$ , in perfect agreement with the DLL/IL logs.

The intermediate structural levels (up to 2500 m b.g.l.) coincident mainly with the TWC and most of the Phyllitic Complex are characterized by resistivity values in the range of 40-200  $\Omega\text{m}$  (mostly 100  $\Omega\text{m}$ ). These values are far from the corresponding measured DLL/IL values of the *Travale* area wells. Indeed, the representativeness of resistivity well logs or the effectiveness of the MT methods in Larderello has been debated in the scientific community.

It is possible, in our opinion, that the widespread low resistivity of Phyllites is due to the presence of interbedded layers of interconnected graphite. Along the wells, these layers are recognized by the logs measurement as thin and very conductive layers alternated to extremely resistive ones. Instead, being the magnetotellurics a diffusive method, it provides averaged resistivity values over very large volumes. A high interconnection grade of the graphite would produce a reduction of the averaged-out MT resistivity, and this hypothesis deserves a consideration. As mentioned previously, a recent experimental surface-hole deep ERT (along the Venelle-2), yet unpublished, confirmed a very strong reduction of resistivity values in these metamorphic rocks. The design of the experiments and its preliminary results were presented in Capozzoli et al. (2016) and Santilano et al. (2016b).

On the other hand, in the *Lago Boracifero* area the Micaschist, Gneiss and Intrusive rocks are characterized by high resistivity values in the range of 2500-5000  $\Omega\text{m}$  as expected. Large low resistivity anomalies, with values of about 150  $\Omega\text{m}$ , locally interrupt the resistive metamorphic units. These anomalies appear sub-vertical in the 4 profiles, Profile 1 to Profile 4, and seem related to a structure elongated N30E.

For a detailed interpretation from a geothermal standpoint, we firstly focused on the Profile 1 and Profile 3 constrained with optimized models (PSO). The cap-rocks of the geothermal system (Neoautochthonous and Ligurian Complexes) are well imaged by their high electrical conductivity. The Tuscan Nappe and TWC show a quite homogeneous average low resistivity, as well as the Phyllitic Complexes with some local exception. No clear indication on local anomalies possibly due to hydrothermal circulation can be pointed out in these units due to the homogeneous distribution of the resistivity, with the exception of two

important zones characterized by a reduction of resistivity: *i*) the Carboli area in the Profile 1 as well as the *ii*) Vecchienne area in the Profile 3. This aspect is quite interesting because the Carboli C geothermal well is a highly productive zone of superheated steam with temperature higher than 400 °C at 4000 m b.g.l.

Moving deeper, we recognize the Micaschist, Gneiss and Intrusive complexes, characterized by an abrupt increase of resistivity of one order of magnitude, up to 4000  $\Omega\text{m}$ , with respect to the units above. At intermediate structural level, about 3000-5000m b.g.l., local low resistivity anomalies are clearly imaged below the most important productive areas as for example the Cornia River, Lagoni Rossi (Profile 1-3), Carboli (Profile 1-2), Serrazzano (Profile 4). It is clear that the zones with a high concentration of productive wells, therefore with an intense hydrothermal circulation, are characterized by low resistivity anomalies. We stress that not the entire metamorphic reservoir showed such anomalies; which were clearly identified mainly in the most productive areas.

These observations open the old challenge of interpreting the low resistivity anomalies in Larderello, where hydrothermal circulation occurs at vapour state and in crystalline rocks (resulting with a theoretical high bulk resistivity). This open challenge was discussed in various studies such as Manzella et al. (2010) in the frame of the I-GET project in the *Travale* area (see details in Chapter 7).

Since at depth of reservoir, the occurrence of melt is excluded due to the relative low temperatures (up to 420 °C), the decrease of resistivity in the Micaschist, Gneiss and Intrusive complexes would suggest a strong influence of the hydrothermal circulation. This interpretation can imply two main processes: *i*) the occurrence of a minor contribution of liquid-phase in the vapour dominated reservoir (hypothesis not confirmed by well tests) and/or *ii*) the effect of more or less pervasive hydrothermal alteration.

The hypothesis of a minor contribution of liquid-phase in the reservoir was not proposed here for the first time but some authors suggested this model in literature (e.g. Manzella et al., 2010 and reference therein). The thermodynamic model by Truesdell and White (1973) on the production of superheated vapour in the geothermal system foresees the occurrence of a liquid phase relatively immobilized in small pores, while the vapour is the main phase circulating in fractures and controlling the pressure. Bertani et al. (1999) published the results of

experiments and observations on the Monteverdi sector of the Larderello field, stating that a high amount of adsorbed water inside the pore network of the rocks, in the order of 2 g/kg, might occur. The surface conductivity effect can influence the bulk resistivity. In the *Travale* sector, the geophysical logs of Radicondoli-7bis well showed a decrease of resistivity in granites (<1000  $\Omega\text{m}$ ) hosting an intense high temperature hydrothermal steam circulation. Mineralogical analysis from well samples did not show pervasive alteration in granites (Giolito et al., 2009; Manzella et al., 2010). Since the conductive alteration minerals were sparse and not interconnected, the authors considered this a minor effect, and believed more in the dominant role played by the liquid phase occurring in small pores in the reservoir.

When conductive minerals are involved, they can play an important role in the reduction of the electrical resistivity. The very complex and multi-stage evolution of such processes in Larderello (e.g. Ruggieri and Gianelli, 1999 and references therein) results in a tough challenging problem. The hydrothermal and metasomatic parageneses in different sectors of the field were depicted by various authors. Bertini et al. (1985) defined the most common assemblage in the reservoir of the hottest sectors: K-feldspar, epidote, chlorite, quartz, sulphides, hematite, anhydrite and barite. Cavarretta et al. (1980) described similar assemblages for specific wells. As an example in Serrazzano Sperimentale-1 the main mineral phases of alteration in the basement units are K-feldspar, epidote, chlorite, pyrrhotite, with the occurrence of pyrite, chalcopyrite, galena and quartz.

Regarding the *Lago Boracifero* sector, Boiron et al., 2007 reported the analysis of metasomatic paragenesis on well cores. At depth of 2900 meters in the San Pompeo-2 well (located along Profile 1), abundant graphite was recognized in the Micaschist Complex. This particular factor can strongly influence the resistivity distribution at depth. Indeed, the possible formation of graphite also related to high temperature alteration is a point to be further investigate.

Summarizing, we were able to image a strong reduction of resistivity locally in the Micaschist and Gneiss basement, corresponding to the hottest sectors of the Larderello field, with an active vapour dominated circulation. At this stage, we are not able to evaluate precisely the contribution of a process rather than another, but we must limit to a description of the processes possibly implied in this reduction. The distribution of resistivity we estimated in the reservoir of *Lago Boracifero* sector is probably due to the interplay of such different processes that are related

with the multi-stage hydrothermal circulation and metasomatic processes linked to the emplacement of shallow intrusive bodies. With regard to the Phyllitic Complex the analyses suggest also a role of lithology (graphitic members) for the widespread low resistivity response.

### 9.6.2 Effect of melting phase on resistivity

At mid-crustal level, below 6 km depth, a further reduction of resistivity is recognized in all the MT Profiles in the *Lago Boracifero* area. These anomalies can be ascribed to the partially melted granitic intrusion that act as heat source of the field. Considering this assumption, the heterogeneous distribution of resistivity at this depth can be in part explained as different percentage of melting in the rock volume.

We carried out an analysis by using the SIGMELT software published by Pommier and Le Trong (2011). Firstly, the electrical conductivity of the felsic melt was estimated to be 0.104 S/m accordingly to some specific parameters, e.g. SiO<sub>2</sub>, Na<sub>2</sub>O and water content of the Larderello granites (from Dini et al., 2005).

Based on the numerical modelling scheme by Schmeling (1986b) (see Chapter 3), the estimated bulk resistivity of the two-phase system was computed as function of different melt fraction; using resistivity reference values of ~10 Ωm for melt and 3000 Ωm for the solid matrix, respectively.

In the MT profiles we imaged the supposed igneous intrusions with resistivity values mostly in the range of 50-200 Ωm, which means an approximate residual melt fraction in the range of 4-13 vol.%, with dominant fraction of 5-6% (figure 9.12). The occurrence of completely cooled igneous intrusion, or with a melt fraction lower than 4%, cannot be imaged due to the similar resistivity values of surrounding rocks in the order of 3000 Ωm (Micaschist and Gneiss).

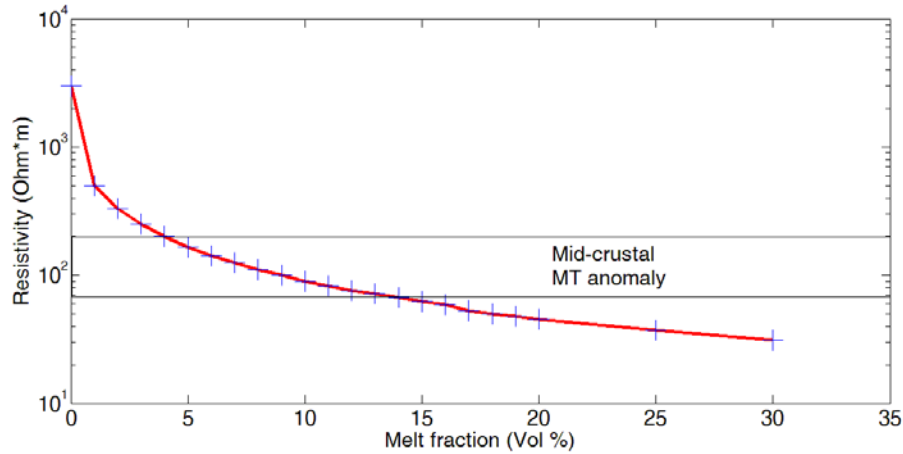


Figure 9.12- Computed electrical resistivity of a partially molten rock as a function of melt fraction following the two phases mixing models by Schmelting (1986b) and implemented in SIGMELT (Pommier and Le Trong, 2011). The conductivity of the melt was estimated as 0.104 S/m with a resistivity of the surrounding rocks fixed to 3000  $\Omega\text{m}$ . The range of resistivity for the mid-crustal anomaly in Larderello is shown.

The presence of a shallow intrusion at 8-10 km depth was inferred also by low seismic velocity anomalies, low density and extremely high heat flow value in the *Lago Boracifero* area, as described in Chapter 2. A more detailed discussion about corresponding depth and location of resistivity and seismic velocity reduction due to the occurrence of magmatic melted intrusions will be provided in the holistic approach of the following paragraphs.

### 9.6.3 Tectonic implication of the resistivity models

Another important aspect that can be pointed out from the MT modelling is the role of faults in controlling the hydrothermal circulation of the Larderello field. This is not trivial considering that even detailed 3D reflection seismic results and decades of exploration did not led to a commonly accepted structural model. Our analysis cannot account for imaging a single fault or a single fracture system at the scale of a well, due to the small number of soundings and above all due to the intrinsic low resolution of the MT methodology.

On the other hand, the results drove us to identify the main geological structures that in our opinion could strongly control the evolution of the geothermal area of *Lago Boracifero*.

We particularly refer to the Cornia Fault that is imaged as a wide sub-vertical low resistivity structure located along the homonymous river. In the proximity of this structure the following elements are recognized: *i*) the depocentre of a Neogene tectonic basin, *ii*) a wide, sub-vertical low resistivity anomaly at the depth of the Micaschists and Gneisses, *iii*) the apex of the mid-crustal resistivity anomaly that we ascribed to igneous intrusion and *iv*) the upwelling of temperature. Other elements related to this area are: *i*) the geometrical apex of the dome-like shape of the K-horizon, *ii*), a seismic anomaly with low P-wave velocity (Batini et al., 1995), and *iii*) the occurrence of many productive areas such as the Val di Cornia or Lagoni Rossi wells.

The MT results led us to interpret this structure as a fault that controlled the magmatic activity in this specific sector and possibly controls the hydrothermal circulation, along a very wide (some kilometres) shear zone oriented N30E. The importance of this fault was initially claimed by Lazzarotto (1967) but in the following years the fault was not taken into particular account in the geothermal exploration analysis. The focus on a detailed structural setting of this shear zone can be speculative, with the actual data, but deserves attention both at geothermal and structural viewpoints. Some authors (see Costantini et al., 2002 for a review) considered this structure a segment of a transfer fault of crustal importance that accommodated the differential extension of the Apennines along antithetic direction. The continuity toward Larderello (NE) of this structure cannot be excluded.

Another important low resistivity structure was identified in correspondence of Carboli wells, where the hydrothermal circulation is enhanced as stated by the occurrence of high productivity. It should be noted that in correspondence of this resistivity structure, a fault was recognized by other authors and reported in a deep geological section (Romagnoli et al., 2010). In this particular sector, however, the MT data quality is too low to produce highly reliable and detailed interpretation, as for the Cornia Fault, and our interpretation is less constrained.

#### **9.6.4 Correlation with seismic models**

In figure 9.13 we summarize one of the main result of this study, i.e. the Cornia Fault imaged by the Profile 1 and its correlation with seismic studies in the area.

The P-wave anomaly, as derived from 3D tomography of local earthquakes (Batini et al., 1995), is showed for values lower than 5000 m/s. The authors related the reduction of P-wave velocity to the occurrence of an intrusive still partial melted body. The CROP18 interpreted Profile (Brogi et al., 2005) is overlapped on the MT Profile 1 since the traces coincide. The correspondence of mid-crustal electrical resistivity anomaly with the low seismic velocity body is striking.

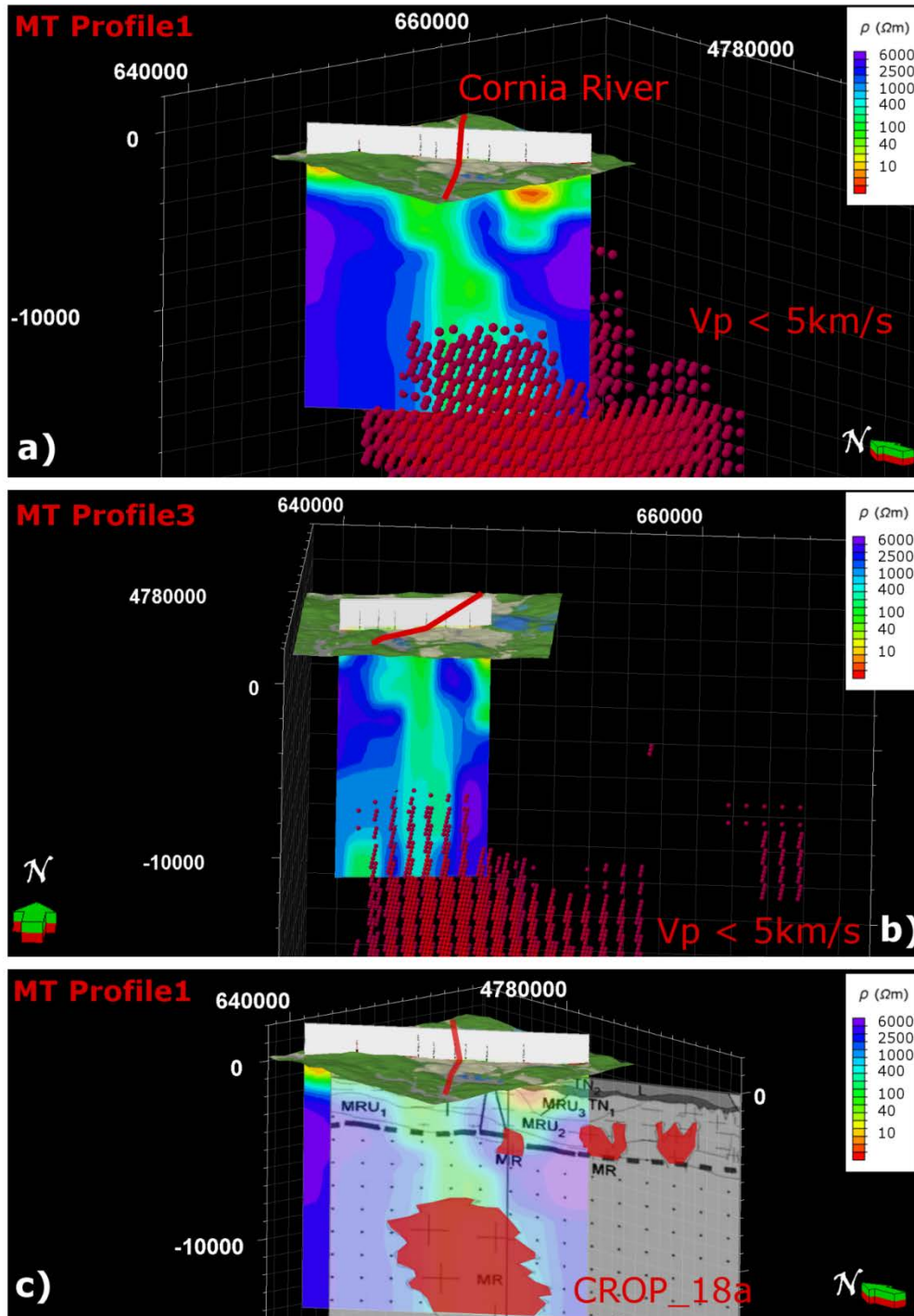


Figure 9.13- MT Profile 1 plotted in 3D and compared with other geophysical data: Comparison between the MT Profile 1 (a) and Profile 3 (b) and the anomaly of seismic low velocity (Batini et al., 1995) here filtered for the values below 5 km/s; b) MT plotted in 3D with the geological map; c) comparison between the Profile1 and the deep seismic profile CROP 18a (Brogi et al., 2005), particularly the intrusive rocks (MR) imaged by the seismic reflection data are highlighted in red.

A control of the sub-vertical structure (i.e. Cornia Fault) in favouring (as regional mechanical discontinuity) the emplacement of intrusive bodies in this area, can be supposed. We would stress that the direct evidences (e.g. well cores of Monteverdi, Carboli wells) and geochemical (e.g. Dini et al., 2005) and geophysical models indicated the occurrences of more intrusive bodies with a polyphased evolution. The occurrence of a low resistivity anomaly interpreted as intrusive and partially melted body does not exclude the occurrence of surrounding cooled magmatic rocks or with a fraction melt lower than 4%, since they cannot be imaged by MT.

The resistivity model in the other MT profiles, particularly in Profile 4 (toward Larderello), show a wider low resistivity anomaly, in terms of spatial extension, at mid-crust depth. This aspect seems in accordance with seismological studies. Particularly interesting is the clear correspondence of the Low Velocity Zone (LVZ) resulting from the inversion of teleseismic travel time residuals (Foley et al., 1992; Batini et al., 1995) and the wide low resistivity anomaly at 7 km depth of the Profile 4. The model parameters of the inversion of teleseismic data are the velocity perturbations with respect to a reference model (see the cited papers for details). In order to visualize the LVZ, which according to the authors, is elongated NE-SW, we filtered the values of seismic velocity perturbation in the range of -4 to -16%, excluding the values in the range of 8 to -4%. In figure 9.14 we show the comparison between the MT Profile 4 (from PSO) and the LVZ after filtering out the zone of minor reduction.

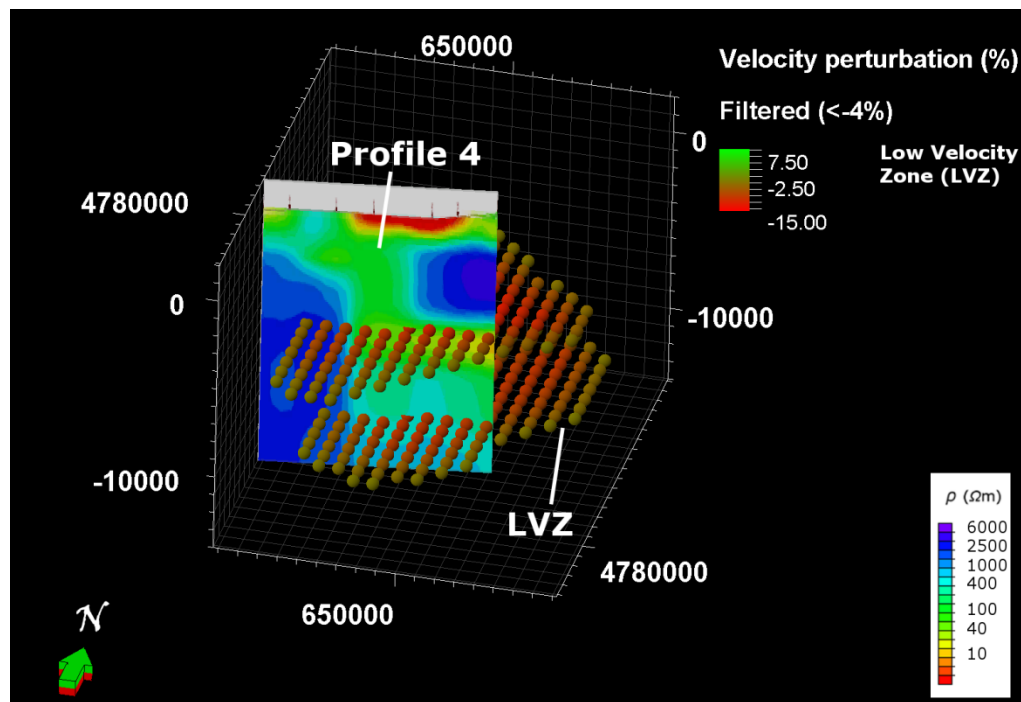


Figure 9.14- Comparison between the MT Profile 4 and the seismic Low Velocity Zone (LVZ) from the inversion of teleseismic travel time (Foley et al., 1992; Batini et al., 1995). The model parameters of the inversion of teleseismic data are the velocity perturbations with respect to a reference model (see the cited papers for details). The points represent the values of seismic velocity perturbation; the values in the range of -4 to -16% are shown.

Finally, it should be noted that the K-horizon was a possible target of our study, but we cannot image any peculiar feature in proximity of this seismic reflector. This could be due to the possible absence of electrical resistivity contrast or the small thickness of the “layer”, whatever is its geological meaning.

#### 9.6.4 Impact on the conceptual model of the *Lago Boracifero* area

The resistivity models we achieved from the inversion of MT data have a great impact on the conceptual model of the *Lago Boracifero* area.

First of all, the Micaschist and Gniess complexes, that were imaged for their highly resistive response, show significant reductions of resistivity, one order of magnitude, in correspondence of the most productive sectors such as *Lago Boracifero* and Lagoni Rossi. Although the information from well tests clearly

indicates the vapour phase of the hydrothermal fluids in the reservoir, the resistivity anomalies imaged in the resistive crystalline reservoir seems to imply a relation with the hydrothermal circulation. The processes we discussed are the hydrothermal alteration, the occurrence of very high conductive minerals (such as graphite) and the possible contribution of a liquid phase in the pores and fractures of the rocks hosting the hydrothermal reservoir.

In addition, the final models highlighted the fundamental role of a large tectonic structure, i.e. the Cornia Fault, antithetic respect to the Northern Apennine. In our opinion, this fault played an important role in the evolution of the field, favouring both the hydrothermal circulation and the emplacement of magma bodies, being possibly deep-rooted in the Crust.

The results can be also intended as a valid support to the petrological model (e.g. Dini et al., 2008) that implied the emplacement of magma along the transfer lineaments of the Northern-Central Apennines. Our theoretical computations on the two-phase mixing model implied a melt fraction of about 5-6% (even higher) for the resistivity anomalies at mid crustal depth.

In figure 9.15 the final conceptual model we built at the end of our study is shown, and corresponds to that of a “young intrusive convective” geothermal play as described in Chapter 2. We support the idea of a composite batholith (Gianelli, 1994) with a polyphased evolution composed of older completely cooled granitic intrusions and local partial melted bodies acting as the actual heat source of the Larderello geothermal field. In figure 9.15, we conceptually used the shape of the intrusion depicted for the Elba Island, which is considered a fossil proxy of the Larderello system (Dini et al., 2008; 2016).

With regard to the possible occurrence of deep-seated supercritical fluids, we could not find any clear evidence of a resistivity change corresponding to the K-horizon (only in some zones of Profile 2 and Profile 4). We cannot exclude that supercritical fluid are present, but their effect is too weak for MT exploration. This could be due to the relatively small thickness of the layers hosting the fluids and/or to the relatively minor change of resistivity with respect to the surrounding units. Hence, the detection of the intrusive and partially melted bodies is the indirect information that MT can provide.

In the *Lago Boracifero* sector we detected a partially melted intrusion at shallow depth confirming the other geophysical and geochemical evidences of shallow intrusion in this area. It should be noted that the mid-crust anomalies are detected also in the northern (toward Larderello) and southern (toward Frassine) zones of the investigated area and seems particularly wide in the northern area (below Profile 4, see figure 9.12 or Appendix C), characterized by a large production of hydrothermal fluids from the deep reservoir. The MT results indicate that it could be worth to investigate also the southern sector immediately close to the *Lago Boracifero* (e.g. Frassine area) which is not very explored, since it is characterized by large deep low resistivity anomalies similar to those of other productive part of the hydrothermal reservoir.

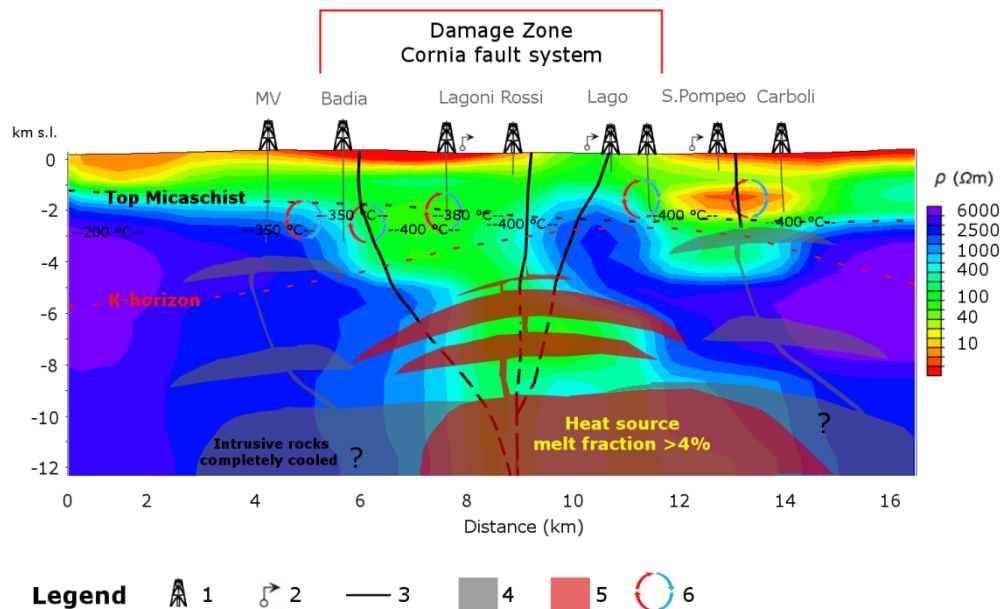


Figure 9.15- Conceptual model of the *Lago Boracifero* sector from the interpretation of the MT Profile1: 1) productive wells in the proximity of the trace profile (max distance 800 m), 2) main geothermal manifestation, 3) main faults, 4) supposed occurrence of completely cooled intrusion that cannot be imaged by resistivity anomaly, 5) granitic intrusion with residual melt fraction higher than 4%, imaged by a wide resistivity anomaly, 6) Active hydrothermal, vapor-dominated circulation and multi-stage hydrothermal alteration.

# Chapter 10

## Concluding remarks

The effort of this research led us to achieve promising results in the context of probabilistic optimization of electromagnetic data and its application to the geothermal exploration.

The integrated study of the Larderello-Travale geothermal field improved the knowledge about the deep structures of the field, with a relevant impact on the definition of the conceptual geothermal model.

### 10.1 On the probabilistic optimization

Let first consider in details that part of this research concerning the probabilistic approach for 1D model parameter estimation. Beside the limits regarding the dimensionality problem of MT, very important information can be retrieved.

In this thesis we discussed the effectiveness of the Particle Swarm Optimization (PSO) algorithm for solving the MT inverse problem. The philosophy is that of (artificial) adaptive behavior, to face the complexity and non-linearity of problems by sampling the global space solution.

We implemented a user-friendly Matlab software “GlobalEM” for the analysis and 1D optimization of magnetotelluric data. The strength and novelty of our implementation lie on the possibility to minimize different objective functions, with or without external constraints, according to the minimum

structure or sharp boundaries approaches. Indeed, we successfully implemented the Occam-like PSO optimization similar to the deterministic approach by Constable et al. (1987).

Firstly, the effectiveness of the algorithm was tested on theoretical MT data from challenging synthetic models, that provided promising results. What we considered the main check on the validity of PSO in MT is the optimization of the COPROD dataset and its comparison with estimated models proposed in literature. The results demonstrated how PSO could be an effective approach in MT data optimization.

The possibility to evaluate the repeatability of the results by running several trials, is particularly helpful. The analysis of the a-posteriori distribution of the results can be of help to understand the reliability of the model as a whole or regarding specific layers (e.g. estimating the reliability of low resistivity layers).

The advantages of the PSO application in MT data processing are also related to the possibility to easily implement customized objective functions accounting for a-priori information of the subsurface. This can be useful in getting more accurate information on the resistivity distribution when additional information from seismic or well logs is available. Furthermore, the direct minimization of the functions, without complex mathematical manipulations, favours the implementation of multi-objective and joint optimization of different geophysical methods. Here, a first attempt of simultaneous optimization of MT and TDEM data, is proposed. Future researches should focus on the data integration by means of joint optimization, related to different forward computations (e.g. MT, TDEM and DC measurements).

This part of the research is intended as a first step for the implementation of PSO in magnetotellurics. Nowadays ongoing research activity is focusing on the implementation of the algorithm for the 2D problem. The higher number of parameters to be optimized makes challenging the computational effort.

## **10.2 On the study of the Larderello-Travale geothermal field**

The results of the magnetotelluric study of the Larderello-Travale field and their interpretation allowed us to contribute on the improvement of the conceptual model of the geothermal system.

The integrated approach greatly improved the knowledge on the deep structures of the system on the basis of the critical review of deep well data, geological and geophysical data and the analysis of new and previously acquired MT data in the Larderello-Travale field.

Important information was retrieved from the PSO optimization of the observed MT data and the theoretical data from synthetic models, simulating the stratigraphy of the field. A wise comparison among this analysis and the geophysical well logs provided very useful information on the features at depth of the geothermal field. Particularly interesting the observed differences of the MT responses and the geophysical well logs related to specific geological unit.

We achieved the resistivity models by 2D MT inversion. We focused on the understanding of the reliability of the a-priori model for the inversion procedure. For this reason we implemented and tested three sets of starting models: *i*) homogeneous (without external constraints), *ii*) geological (from the integrated model) and *iii*) interpolation of 1D PSO models.

As expected, the resulting models constrained with detailed and accurate geological information were more reliable than those unconstrained (i.e. from homogeneous halfspace). We demonstrated how the a-priori information from the analysis of MT data, i.e. by PSO optimization in our case, greatly improved the inversion results even those geologically constrained. This is not a trivial issue for the exploration of geothermal greenfield, lacking of underground data.

The great impact on the definition of the conceptual geothermal model of the Larderello field is the main result of this work, particularly for the deep structures of the Lago Boracifero sector. To be as concise and clear as possible about the relevance of our contribution to the definition of the conceptual model, we propose the following summary:

- In agreement with the previous studies, the cap-rock of the system is correctly imaged as a very low resistivity layer, 3-30  $\Omega\text{m}$ , composed of the Ligurian and Neoautochthonous complexes.
- As observed in previous studies, the metamorphic basement shows locally anomalous low resistivity behavior.

Our contribution in this case is the observation of a whole low resistive response in the Phyllitic Complex, in the range of 40-200  $\Omega\text{m}$  (mostly 100  $\Omega\text{m}$ ). We supposed a dominant contribution of lithology,

in particular the occurrence of thin and extremely low resistive graphitic layers interbedded with high resistive ones. In Micaschist and Gneiss complexes we observed a generally high resistive response, in the range of 2500-5000  $\Omega\text{m}$ , locally interrupted by low resistivity anomalies (about 150  $\Omega\text{m}$ ) that are well correlated with the most productive sectors of the field. Since the hydrothermal fluids are in vapour phase, we discussed the possible interplay of processes acting in the decrease of the resistivity.

- We detected a still partial melted igneous intrusion beneath the Lago Boracifero sector acting as heat source, based on the interpretation of the low resistivity anomalies located at mid-crustal level (> 6 km). This possibility were claimed by previous geophysical studies. Here, we clearly detected the intrusion and estimated a first-order approximation of the melt fraction based on theoretical mixing models computation. In addition, some information on the depth and extension of the heat sources was provided. The comparison of the resistivity models and seismic models (available in literature) shows an impressive match regarding the hypothesis and geometries of the melted igneous intrusions. We support the hypothesis of a complex composite batholite acting as a heat source of the Larderello system.
- We highlighted the fundamental role of a large tectonic structure, i.e. the Cornia Fault, antithetic respect to the Northern Apennine and located along the homonymous river. In our opinion, this fault played an important role in the evolution of the Lago Boracifero sector of the field, favouring both the hydrothermal circulation and the emplacement of magma bodies, being possibly deep-rooted in the Crust. The role of this fault was disregarded in the last decades of exploration of the field. Our analysis drove us to consider the evolution of the most productive sectors of the Larderello field as strictly related to the presence of this large fault.

Future research should be oriented to a better understanding of the different processes in the decrease of the resistivity in the crystalline vapour dominated reservoir. Although we discussed some aspects (e.g. the lithology of the phyllites, the occurrence of very conductive minerals) this issue continue to be an open challenge.

Furthermore, the role of the Cornia fault should be taken into account for the exploration of the areas surrounding the exploited sectors.

We couldn't find any clear evidence of deep-seated hydrothermal fluids at supercritical conditions. It should be noted that this particular conditions at relatively shallow depth can be related to the presence of igneous intrusions. Our imaging of these intrusive bodies represent an essential, although indirect, information for the future deep explorations of the field.

# Appendix A: GlobalEM, the Matlab software for optimization of MT data

## A.1 Introduction

We implemented in Matlab environment the software package “GlobalEM” for the analysis of MT data. The software follows a user-friendly approach in order to compute dimensionality analysis, tensor decomposition and 1D Particle Swarm Optimization (PSO). It should be noted that we implemented also a part for the parameter estimation with “Genetic Algorithms” and deterministic conventional schemes. The package is composed of routines programmed in-house coupled with routines modified from open-source codes available in literature. In this work we only discussed that part of the package related to the PSO; the MT data analysis are also described. The structure is really simple, being composed of few fundamental blocks, with their functions, that are called from the “Main” program (figure A.1):

- *Conversion module*
- *1D Forward module*
- *MT data analysis modules*
- *PSO Optimization module*: from theoretical or measured MT data
- *Print results module*

Each module is implemented with Graphical User Interfaces (GUIs) allowing the users the proper setting of the main parameters. The whole workflow can be accomplished without any modifications of the source scripts. Indeed, we decided to implement also a *Conversion module* in order to convert the MT data stored in standard \*.EDI files in \*.MAT files to be used as input for the “GlobalEM” package. The \*.MAT files contain all the required variables for the *MT data analysis module*. The user can run dimensionality and directionality analyses according to different literature approaches as well as tensor decomposition. The input MT data, to be used for the optimization, can be also computed via numerical simulation and perturbed with a certain noise level in the *1D Forward*

*module*. The *PSO Optimization module* allows the user to obtain optimized resistivity models from theoretical or real measured data. The main setting parameters of the algorithm can be duly inserted by the user throughout specific GUI, such as number of trials, attraction coefficients, Lagrangian, etc. Finally, the results are properly plotted in the *Print results module*. If many  $n$ -trials were chosen, the a-posteriori distribution and statistical parameters can be computed.

## A.2 Input of MT data

The functions we wrote for the analysis and optimization of MT data are able to work only on a specific “structured array” representing the output of the “*Conversion module*”. Obviously, for each MT sounding the conversion is run once and the array is saved in a certain path (to be loaded for starting the optimization procedure. The module is able to convert \*.EDI saved with WinGLink (Geosystem) and Zonge Inc. software. In the initial description of the script, the modifications to be adopted for the conversion of different structures of \*.EDI is provided. The converted \*.MAT structured array contains the main data stored as vectors or matrixes variables, such as frequencies, impedances, apparent resistivity, phase, etc. In this step the average determinant impedances (Berdichevsky and Dmitriev, 1976) are computed, as follow:

$$Z_{det} = \sqrt{(Z_{xx} \times Z_{yy}) - (Z_{xy} \times Z_{yx})} \quad [\text{Eq. A.1}]$$

As previously mentioned the PSO can be adopted on theoretical data, too. In “GlobalEM” it is possible to create a structured array of MT data from numerical simulation by using the *ID forward module*. Obviously, once created the array and saved in a certain path, the optimization can be run by loading the \*.MAT file.

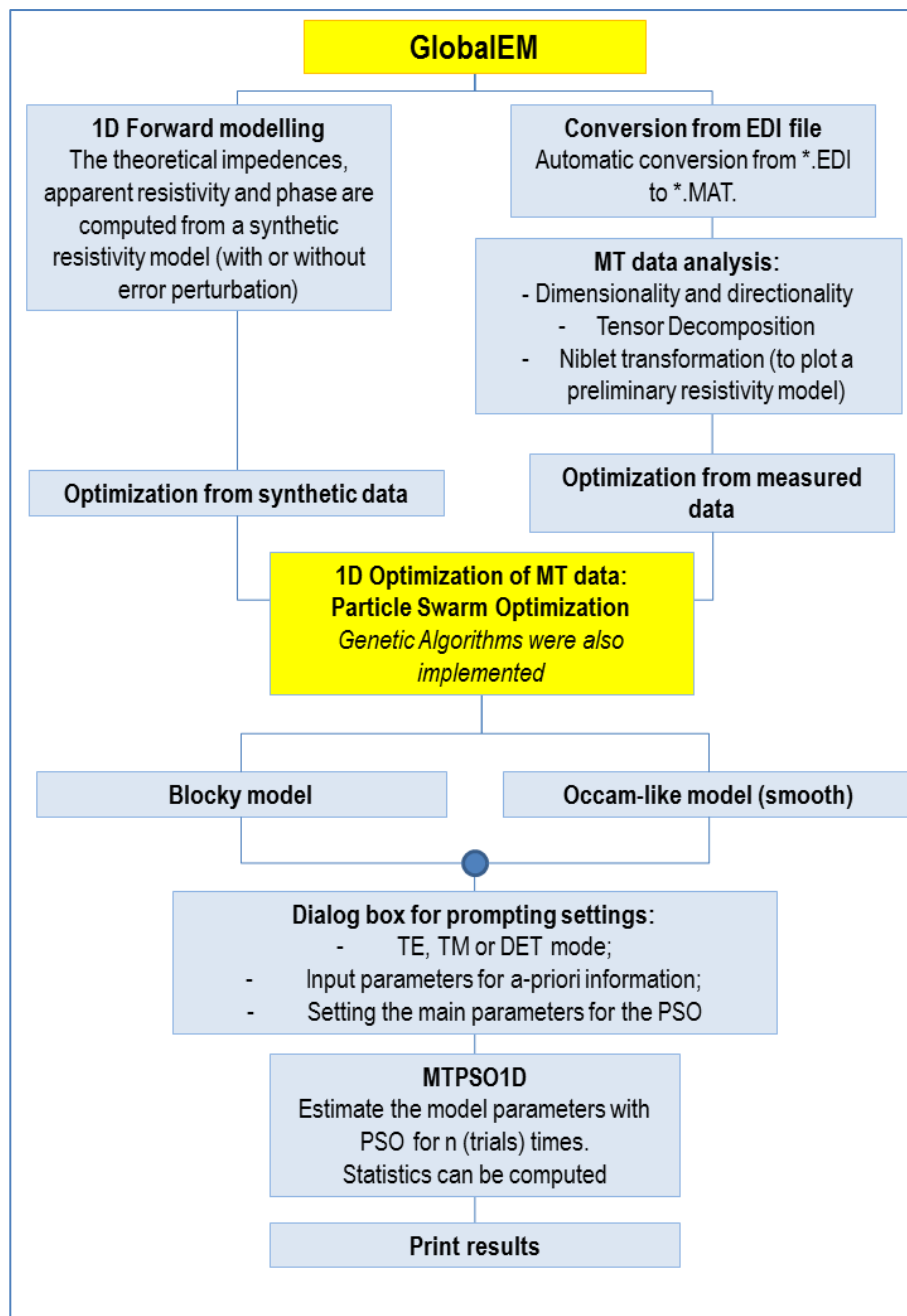


Figure A.1- Structure of the “GlobalEM” software package. Here the PSO workflow is described in detail being the focus of this research, but the Genetic Algorithm was implemented too.

### A.3 MT analysis module

The *MT analysis module* refers to specific functions that we have written in the frame of this research based on literature studies; i.e. no scientific innovation is produced in this module. With regard to the dimensionality and directionality analyses of MT data, we implemented the methodologies named “WAL” and “B-Q” proposed respectively by Weaver et al. (2000) and Marti et al. (2005). The “WAL” approach allows the definition of the MT impedance tensor in terms of seven independent parameters that are invariant under a rotation of the horizontal axes. The dimension of the investigated Earth is computed on the base of five parameters. The user can properly set a threshold value (beneath which the invariants are considered to be zero) in the range of 0.1-0.2. If a 2D structure is recognized, the strike direction is also retrieved. The “B-Q” approach provided for the combined use of different parameters used in Bahr (1991) and Weaver et al. (2000). Finally, the geoelectric dimension for each frequency is shown in a Matlab figure.

If the MT data are affected by distortion problems of the impedance tensor, we implemented the scheme of tensor decomposition proposed by Groom and Bailey (1989). This kind of decomposition is particularly helpful in case of the occurrence of 3D channelling in a regional 2D structure. The output of this tool are the apparent resistivity and phase for the two main components of the tensor after the decomposition. It should be noted that for the study of the Larderello-Travale field we did not use this scheme.

Finally, in order to have a first-order approximation of the distribution of the electrical resistivity with depth, a Niblett transformation (equivalent to the Bostick transformation) is performed as follow (Niblett and Sayn-Wittgenstein, 1960; Jones, 1983):

$$z_n = \sqrt{\frac{\rho_a(T)T}{2\pi\mu_0}} \quad [\text{Eq. A.2}]$$

$$\rho_{zn} = \rho_a(T) \frac{1 + \frac{T}{\rho_a} \frac{d\rho_a}{dT}}{1 - \frac{T}{\rho_a} \frac{d\rho_a}{dT}} \quad [\text{Eq. A.3}]$$

where  $z_n$  is the frequency dependent “penetration depth”,  $\rho_{zn}$  is the resistivity computed at certain  $z_n$  depth. The resulting smooth curve can be of help to get

information useful for the optimization procedure such as the setting boundaries of the search domain in the PSO optimization, etc.

#### A.4 MT forward module

In order to generate the theoretical MT data, by using the *1D forward module*, the user should properly set the main parameters of the synthetic 1D Earth's model. A simple dialog box is implemented to set the values of  $n$  resistivities ( $\Omega\text{m}$ ) and  $n-1$  thicknesses (m) with the  $n$ -th layer considered as halfspace. Furthermore, the frequency band for the computed MT data and the percent of noise can be set in the dialog box.

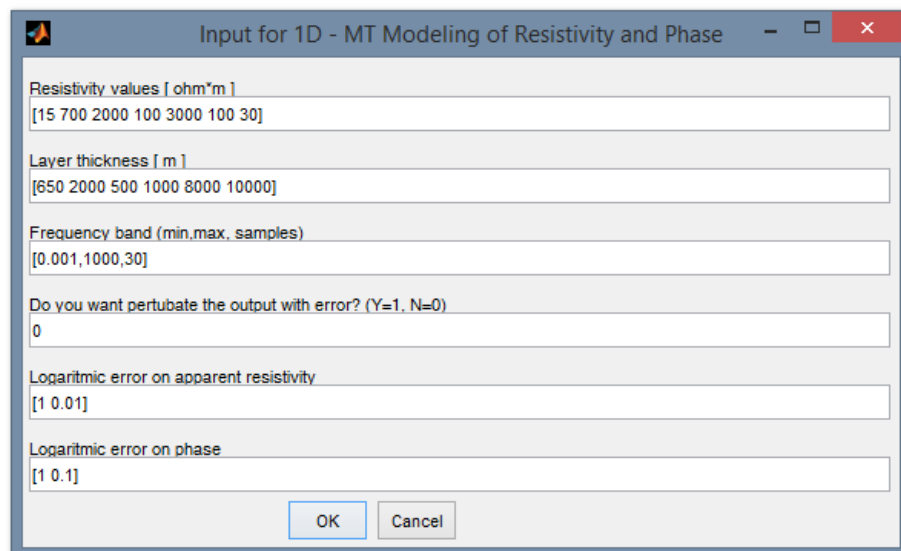


Figure A.2- Simple GUI for computing the MT theoretical data from user-defined synthetic model.

The numerical simulation to solve the forward problem of magnetotelluric data in 1D is really simple and is known in literature since decades (Cagniard, 1953; Wait, 1954; Sims and Bostick, 1969; Niwas et al., 2005). We integrated the *modelMT.m* open-source forward solver available at Digital Earth Lab website (2016) and described in Pethick and Harris (2015). The script is really short and above all is really fast with an elapsed time for one simulation is about 0.06 seconds (computed on a Laptop with Intel Core i7-3537U, 2GHz). The simplicity of the solver is of main importance in a probability optimization procedure

considering that usually the final estimated resistivity model with PSO requires thousands of numerical simulations.

The computation of the MT theoretical response is the result of recursive formulae that solve the Maxwell's equations and relate the impedances of two consecutive layers throughout a reflection coefficient (see Chapter 4 for details). Once the impedances of all the layers (starting from the halfspace) are computed, the apparent resistivities and phases can be retrieved from the impedance of the first layer in function of the frequency. The Matlab code *modelMT.m* was partially modified in order to be used in the Particle Swarm Optimization. Indeed, the code was also used for computing the theoretical data for each particle of the swarm, i.e. an Earth's Model, for each iteration.

### **A.5 Model parameter estimation: the PSO Optimization module**

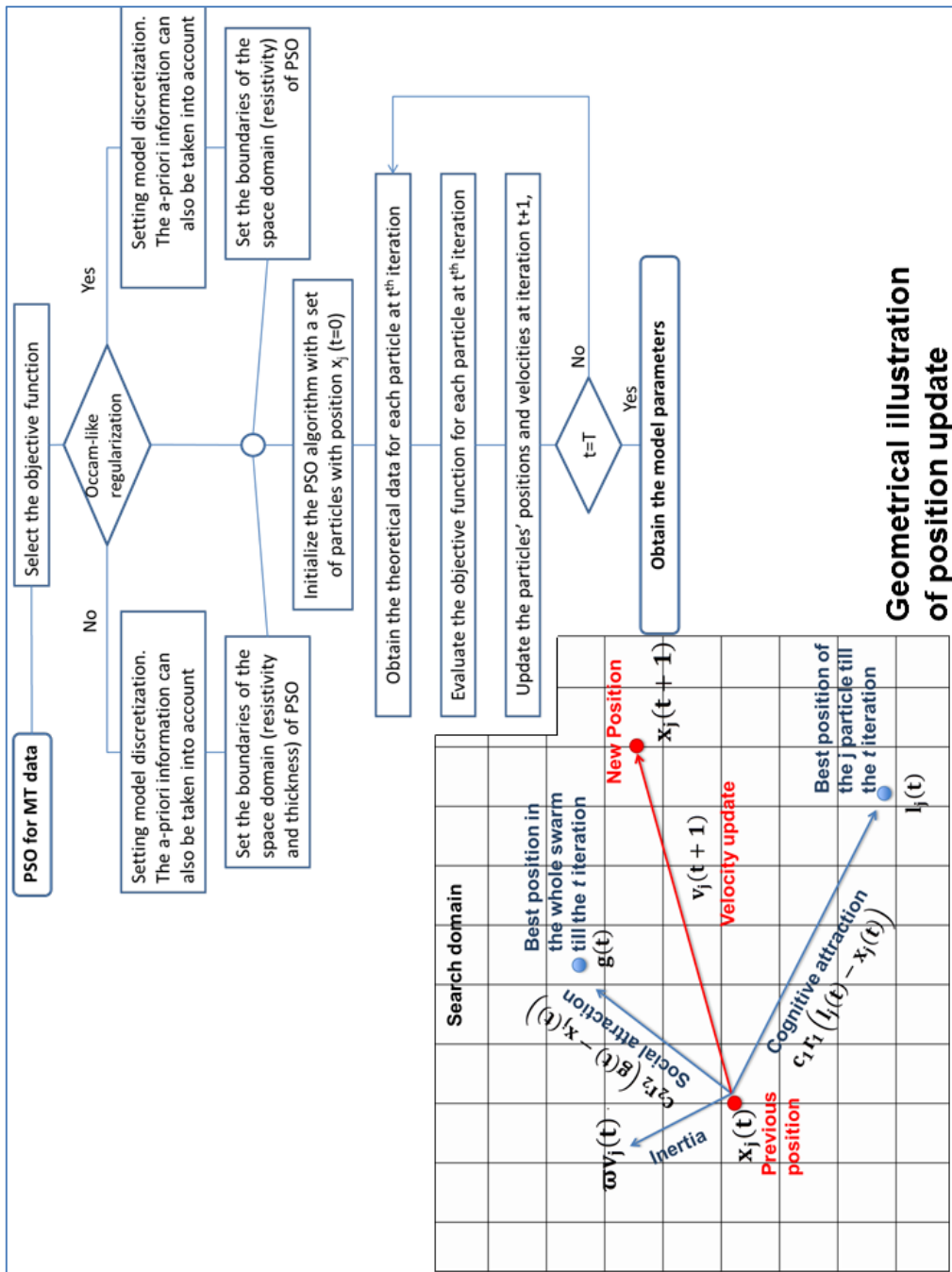
The Particle Swarm Optimization can be adopted for the estimation of an optimized resistivity model from both the theoretical or measured MT data. The philosophy and the mathematics behind the algorithm was yet described in this part of the thesis. Briefly, a swarm of possible Earth's models is initially generated and the objective function is evaluated for each particle. Iteration by iteration the swarm of the Earth's model converge toward an optimized 1D resistivity model on the base of the concept of "Swarm Intelligence". In figure A.3 we summarized graphically the concept of adaptive behaviour of a particle during the optimization, in order to reach the convergence.

With regard to the Matlab implementation of the algorithm we modified the open-source package called "*PSO*" developed by Chen (2009). It is a derivative-free global optimum solver that was implemented by the author using similar syntax as the Genetic Algorithm Matlab Toolbox.

In "*GlobalEM*" the "*PSO*" package is structured as a module and is integrated with the 1D MT forward problem solver and different objective functions according to the kind of optimization the user would accomplish. In the initial stages of the procedure, simple GUIs are called in order to:

- Load the structured array containing the theoretical or measured MT data of the MT sounding;
- Select the MT mode to be optimized; i.e. TE, TM or Determinant average

- Select the kind of optimization: Blocky (few-layered) or Occam-like (smooth).



Geometrical illustration of position update

Figure A.3- Geometrical illustration of the model parameters update for each particle at each iteration. For details on the symbols the reader is referred to the Chapter 5.

Automatically the selected MT curve is extracted from the structured array and the “PSO” module is initialized for the Blocky or Occam-like optimization. The blocky optimization implies the minimization of an objective function of the type described in Eq.5.8, whereas the Occam-like optimization implies the minimization of the function described in Eq.5.9.

With regard to the blocky optimization, the parameters to be estimated are the electrical resistivities and thicknesses of the Earth model with an a-priori fixed number of layers (included the halfspace). Two dialog boxes are used in order to properly set the main conditions of the optimization (figure A.4):

- Search domain: upper and lower limits of resistivity and thicknesses for each layer;
- Coefficients of minimization function:  $a$ ,  $b$ , (weights of the misfit for apparent resistivity and phase) and the Lagrangian multiplier  $\lambda$  (equal to zero for an unconstrained optimization with no a-priori information on model parameters);
- Population size: the number of Earth models (particles of the swarm);
- Generations: iterations for updating the particles velocity;
- Cognitive and Social coefficients; the particle inertia is set 0.9 as default;
- Number of Trials. The optimization can be repeated for the number of trials (in this way a-posteriori distribution of model parameters can be also evaluated).

We stress that in this case the Lagrangian multiplier should be set  $\lambda > 0$  only if a-priori information is available. Indeed  $\lambda$  is used to weight the influence of the misfit between the estimated model parameters and a reference resistivity model.

With regard to the Occam-like optimization, similar GUIs have been implemented in order to set the main conditions of the PSO. Slight changes with respect to the previous dialog boxes are due to the fact that the parameters to be estimated are only the resistivities of a many-layered model with fixed thicknesses. A very important role is played by the model discretization. In “GlobalEM” a routine that allows the computation of the thicknesses (with

logarithmic increase along  $z$ ) is available; the highest and lowest frequency are taken into account for the skin depth concept. In the Occam-like optimization the Lagrangian multiplier should be  $\lambda > 0$  because it refers to the term for minimizing the roughness of the estimated model (see Constable et al., 1987).

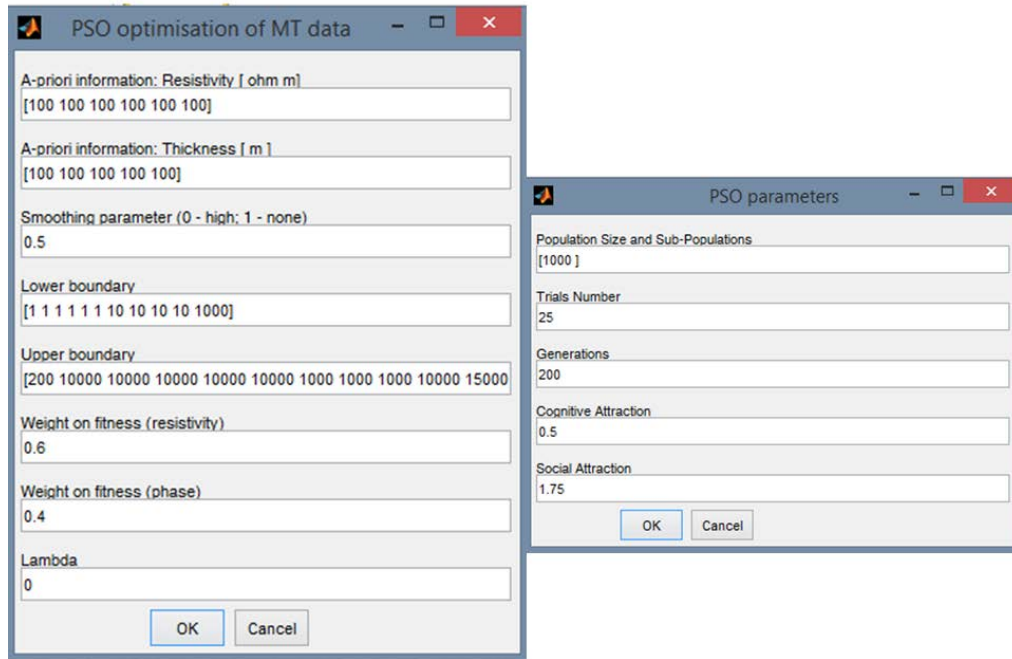


Figure A.4- Simple GUIs (Dialog boxes) for the setting of the main conditions for the Particle Swarm Optimization of “Blocky” model; i.e. the resistivities and thicknesses are the parameter to be estimated.

## A.6 Minimization function: implementation in Matlab

Obviously, the function to be minimized is of main importance. The Matlab function *MT\_vectorized\_objective\_occam.m* was implemented to find the smoothest model as near as possible to the global solution of the problem. *MT\_vectorized\_objective\_occam.m* is called thousands of times (each optimization) by the PSO Optimization module (as well as by the GA Optimization module, here not described). In figure A.5 we reported the command lines of the function. The input variables are: *i*) the solution to be evaluated (vector of resistivity), *ii*) frequencies, *iii-iv*) measured apparent resistivity and phase, *v*) the thicknesses of the model layers, *vi-vii*) the coefficients for weighting

the misfit on apparent resistivity and phase, *viii*) Lagrangian multiplier. The function is structured in few main blocks. Firstly, the theoretical MT data are computed for the solution proposed in the *j*-th particle by solving the forward problem (with “modelMT”). The normalized errors are then computed between the theoretical and measured MT data as well as the roughness of the model. In this latter case a differential operator is applied to the solution vector “*x*”. The Euclidean norms are computed and evaluated according Eq.5.9. A \*.mat file (*pareto*) is also saved to give the possibility of computing the L-curve analysis for the proper selection of the Lagrangian multiplier. For the laterally constrained optimization another term in the objective function is taken into account to penalize higher misfit with a reference model.

```
function fitness =
MT_vectorized_objective_occam(x,s,rho_app,phase,t,a,b,LAMBDA)
%MT_vectorized_objective_occam: Objective function for the global
%optimization of MT data for Occam-like smooth model estimation.
% The function allows the evaluation of each possible solution of the
% swarm (PSO optimization) or generation (GA optimization). The
solutions
% are composed by a vector of resistivity (the thicknesses are a-priori
% fixed), for a number of layers usually higher than 19.
% The minimization function is in the form:
% fitness=(a||ρa_obs-ρa_mod||2 +b||φobs-φmod||2)+ λ ||∂m||2.
% This function is called in the PSO Optimization module and GA
% Optimization module.
% MT_vectorized_objective_occam is written
% by A. Godio and A. Santilano, 2015
% Last update 2016.

% Input variable of MT_vectorized_objective_occam:
% x: solution to be evaluated (vector of resistivity of layers)
% s: frequency (vector)
% rho_app: experimental apparent resistivity (vector)
% phase: experimental phase (vector)
% t: thicknesses of model (vector)
% a, b: coefficients for weighting the misfit on data term (scalar)
% LAMBDA: Lagrangian multiplier (scalar)

%% Computation of the theoretical data of the proposed solution

est = zeros(size(s,1),1); % Pre-allocate app-rho-theor of solution
est_p= zeros(size(s,1),1); % Pre-allocate phase-theor of solution

for i=1:length(s);
    [AppResMod,PhaseMod, Z] = modelMT(x,t,s(i));
    est(i) = AppResMod; % theoretical app. resistivity at s-frequency
    est_p(i) =PhaseMod; % theoretical phase at s-frequency, radians
end
```

```

    est_p=est_p*180/pi;    % theoretical phase at s-frequency, angular
%% Computation of errors

    error_rho=(est-rho_app)./est; % err app_rho_obs/app_rho_theo
    error_phs=(est_p'-phase)./est_p'; % error phs_obs/phs_theo
    roughness=norm(diff(x));      % Approximated model roughness

%% Evaluation of the objective function
    fitness1=a*(norm(error_rho)); % weighted 2-norm of rho_app
    fitness2=b*(norm(error_phs)); % weighted 2-norm of phase
fitness3=LAMBDA*roughness;      % Weighting of roughness with Lagrangian
    fitness=fitness1+fitness2+fitness3; % The objective function
is estimated

%% Saving the single terms of the function for a possible L-curve
analysis
    save pareto fitness1 fitness2 fitness3 LAMBDA
end

```

Figure A.5- Matlab function for evaluating the objective function in the Occam-like optimization. A \*.mat file is also saved to give the possibility of computing the L-curve analysis for the proper selection of the Lagrangian multiplier.

## A1.7 Trials and results

Once the PSO module is initialized, a first generation of models is evaluated according to the described objective functions and at each iteration the models are updated and again evaluated. At iteration  $t=T(\max)$  the algorithm will stop providing the best model toward the swarm has converged. The elapsed time for the whole optimization of a BBMT sounding with an Occam approach, that means usually twice the parameters to estimate respect to the blocky, is approximately 200 seconds (computed on a Laptop with Intel Core i7-3537U, 2GHz) with 150 particles and 150 generations.

If the number of trials is  $> 1$ , the PSO will be again initialized automatically with the same conditions. At the end of the procedure, for each optimized resistivity model ( $n$ -trials models,) the RMS (Root Mean Square) or the normalized NRMS is computed.

The resulting  $n$ -models are stored in a structured array called “*results*” and saved in a \*.MAT file, with the following information (variables):

- `results.resultrf`: layers resistivity for the  $n$ -optimized models (matrix)

- results.resulttf: layers thickness for the  $n$ -optimized models (matrix in blocky and column vector in Occam optimization)
- results.fitness: resulting estimated values of objective function (vector)
- results.NRMS: estimated NRMS values (vector)
- results.RMS: estimated RMS values (vector)
- results.RMS\_app: estimated RMS values for the apparent resistivity (vector)
- results.RMS\_phs: estimated RMS values for the phase (vector)
- results.modappres: resulting theoretical apparent resistivity for each model (matrix)
- results.modphase: resulting theoretical phase for each model (matrix)
- results.rhoobs: measured apparent resistivity of the MT sounding (vector)
- results.phaseobs: measured phase of the MT sounding (vector)
- results.freq: measured frequencies of the MT sounding (vector)
- results.dialog: structured array containing the information related to the PSO settings (e.g. lower and upper boundaries, values of coefficients, etc.)

The structured array contains all the required data for computing the a-posteriori distribution of the estimated parameters. Indeed, a 1-trial optimization, should be able to find a solution near the global minimum. If the solution is stable, a  $n$ -trial optimization should be characterized by a unimodal distribution of the results (resistivity) for each layer. If the solution is not stable, e.g. for high level of noise in the data, the distribution of a  $n$ -trials optimization will show a multi-modal distribution.

### **A1.8 Plotting**

The package is implemented with figures that in real time allow the user to check the validity of the ongoing optimization procedure. The mean and best score of the objective function is continuously shown as well as the behaviour of the swam particles in the search domain. A preliminary figure of the resistivity models ( $\rho$  vs  $z$ ) is also shown.

We also implemented the *Print results module* for allowing the user to better visualize and analyse the results. In this module a preliminary statistical analysis is carried out. For the  $n$ -models Occam optimization, the median resistivity values

for each layer is computed and a resistivity model is built. The theoretical MT data from this “statistical” model is also computed. Simple GUIs help the user to accomplish the following actions:

- loading the *results.mat* file of the specific MT sounding
- highlighting a specific n-model or the model with the minimum RMS value
- choosing (if required) the synthetic resistivity model or a reference model

Once compiled the required actions, a complex figure is built composed of three main subplots. In the left panel the MT curves of apparent resistivity and phase are shown for the measured data and for the theoretical data from the highlighted model and from the “statistical model”. In the central panel, all the n-models of the optimizations are shown a plot  $\rho$  vs  $z$ . In this panel, in blue is shown the highlighted model as well as the statistical model in green and the synthetic model (if required) in black. In the right panel the values of resistivity and thickness of the highlighted model are shown.

## Appendix B: EM soundings

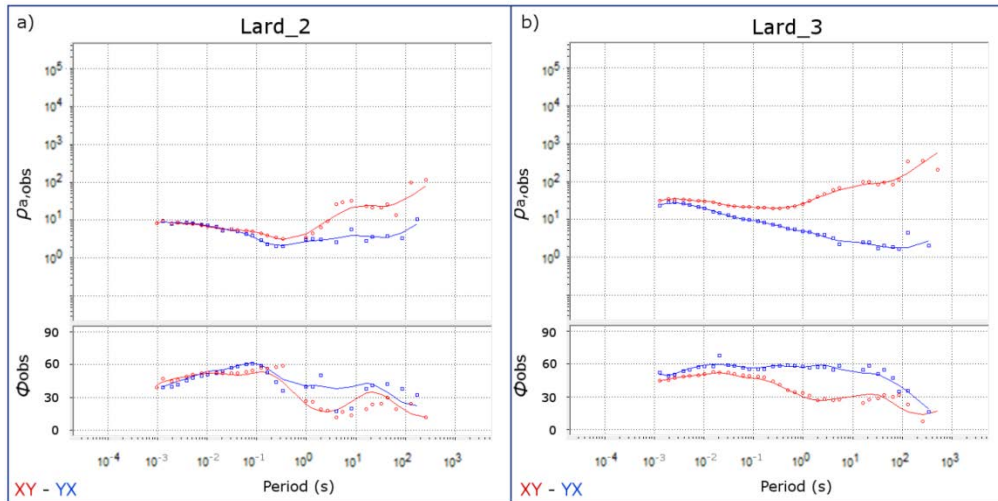


Figure B.1- MT curves, acquired in the survey larderello\_2016, are showed after La Torraca decomposition, editing and smoothing of the curves and static shift correction (see text for details): a) Lard\_2 Site, b) Lard\_3 site.

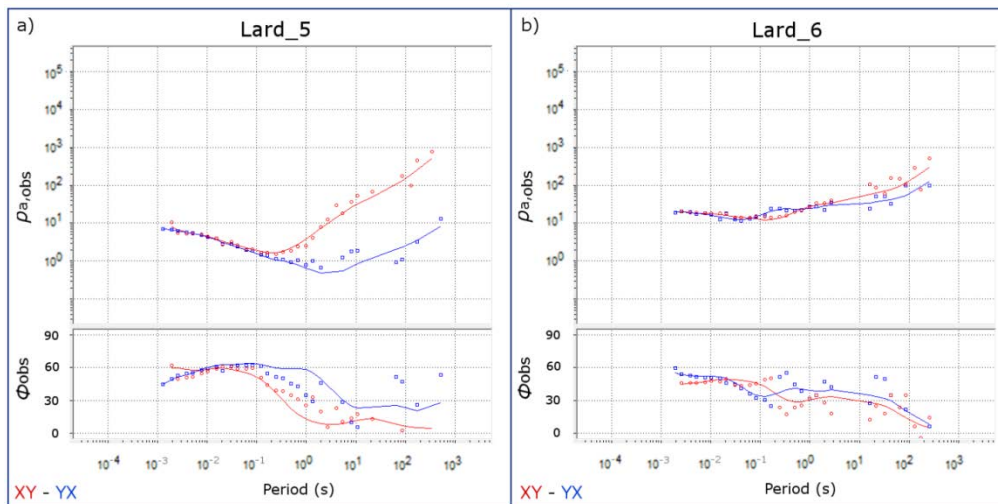


Figure B.2- MT curves, acquired in the survey larderello\_2016, are showed after La Torraca decomposition, editing and smoothing of the curves and static shift correction (see text for details): a) Lard\_5 Site, b) Lard\_6 site.

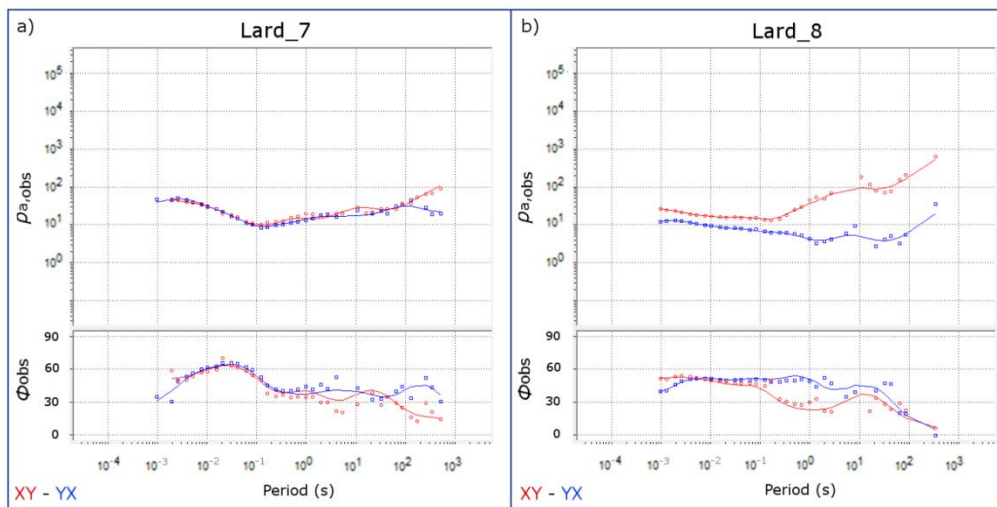


Figure B.3- MT curves, acquired in the survey larderello\_2016, are showed after La Torraca decomposition, editing and smoothing of the curves and static shift correction (see text for details): a) Lard\_7 Site, b) Lard\_8 site.

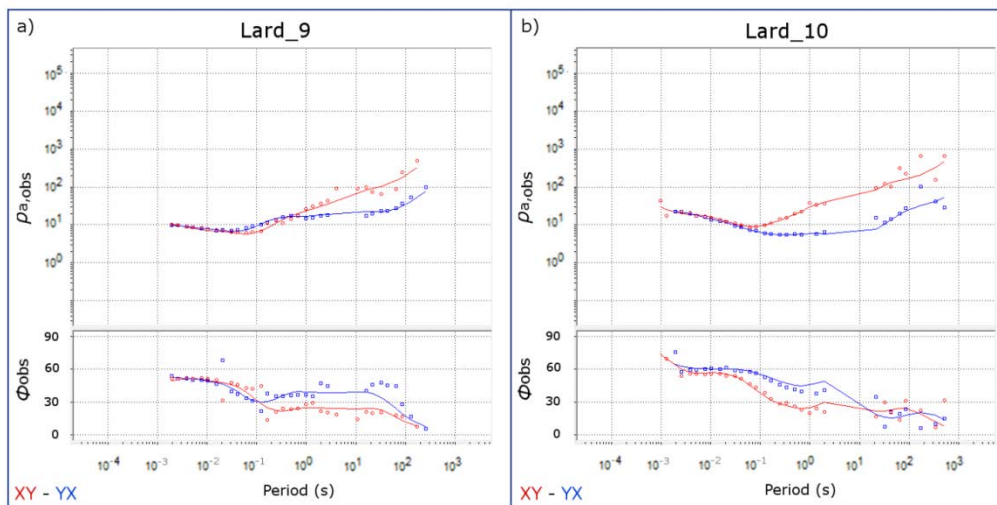


Figure B.4- MT curves, acquired in the survey larderello\_2016, are showed after La Torraca decomposition, editing and smoothing of the curves and static shift correction (see text for details): a) Lard\_9 Site, b) Lard\_10 site.

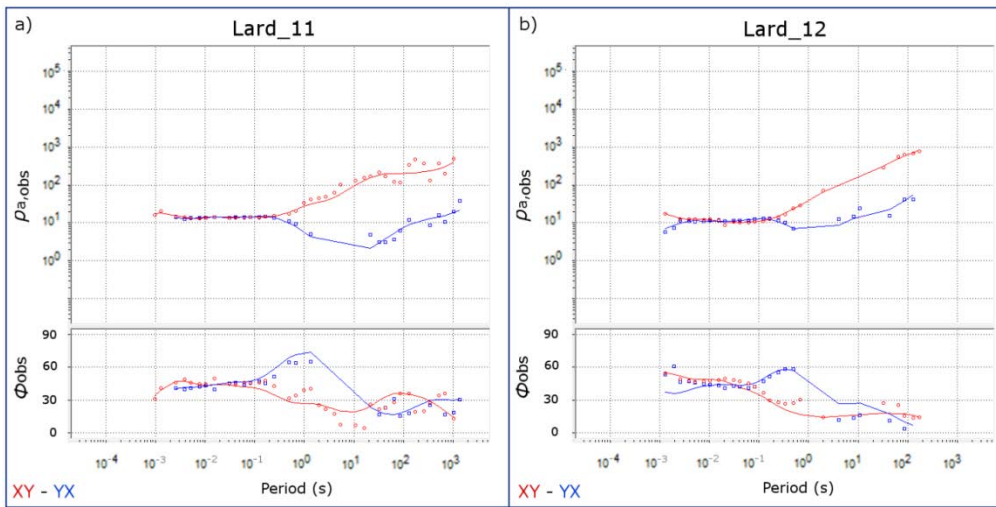


Figure B.5- MT curves, acquired in the survey larderello\_2016, are showed after La Torraca decomposition, editing and smoothing of the curves and static shift correction (see text for details): a) Lard\_11 Site, b) Lard\_12 site.

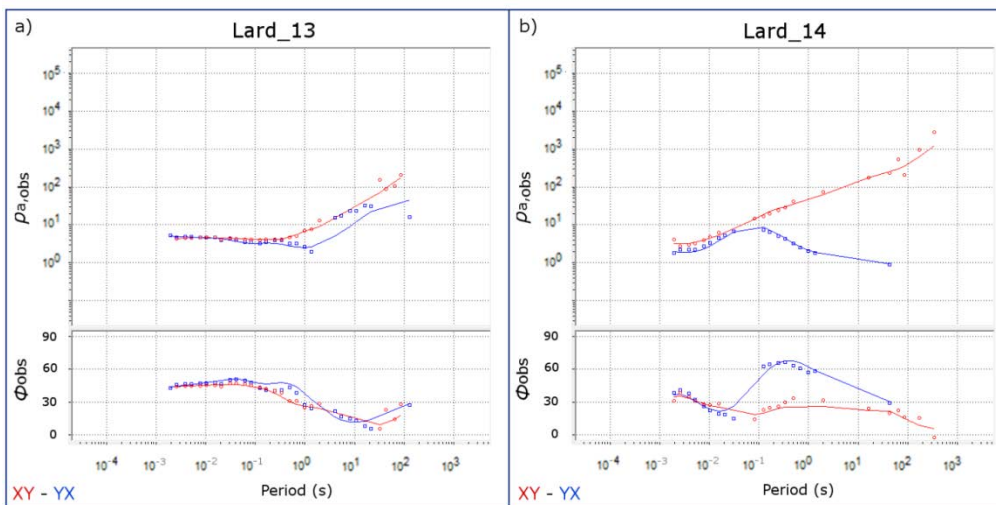


Figure B.6- MT curves, acquired in the survey larderello\_2016, are showed after La Torraca decomposition, editing and smoothing of the curves and static shift correction (see text for details): a) Lard\_13 Site, b) Lard\_14 site.

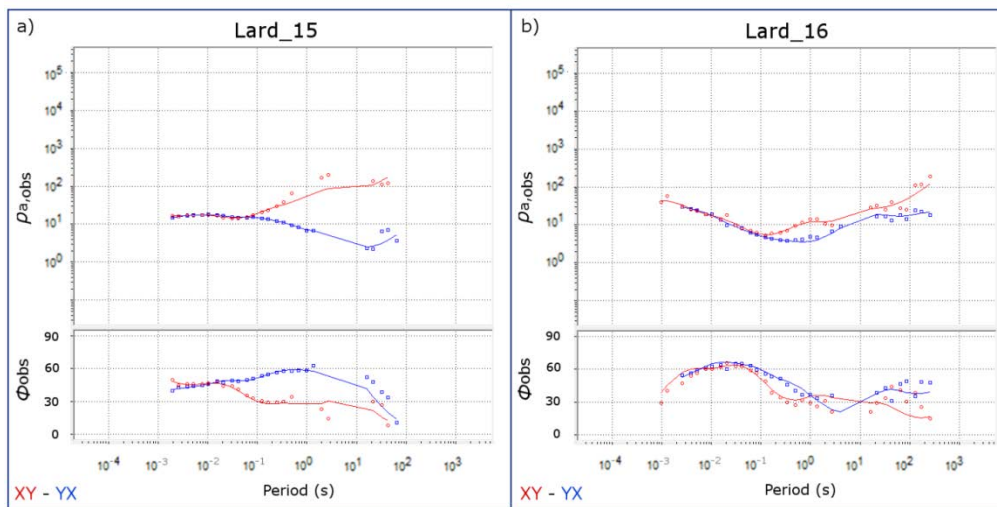


Figure B.7- MT curves, acquired in the survey larderello\_2016, are showed after La Torraca decomposition, editing and smoothing of the curves and static shift correction (see text for details): a) Lard\_15 Site, b) Lard\_16 site.

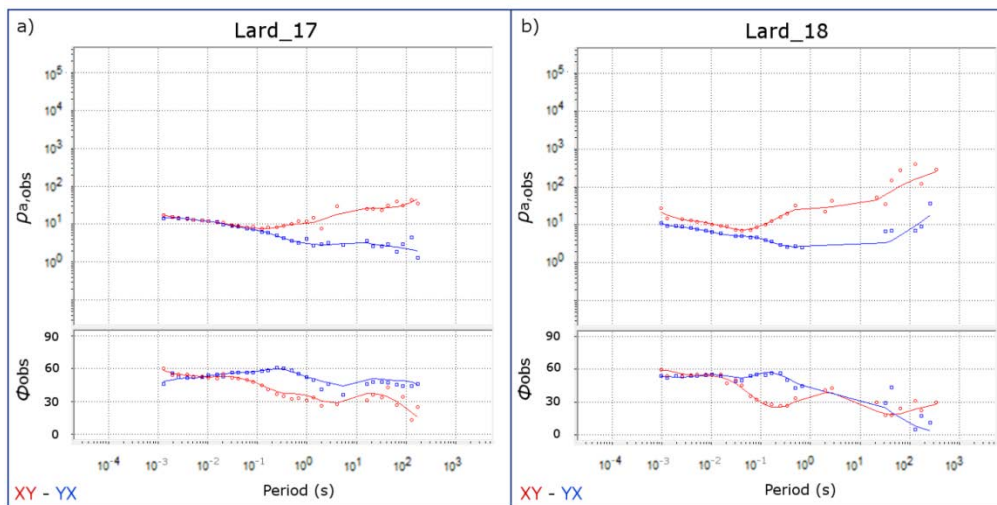


Figure B.8- MT curves, acquired in the survey larderello\_2016, are showed after La Torraca decomposition, editing and smoothing of the curves and static shift correction (see text for details): a) Lard\_17 Site, b) Lard\_18 site.

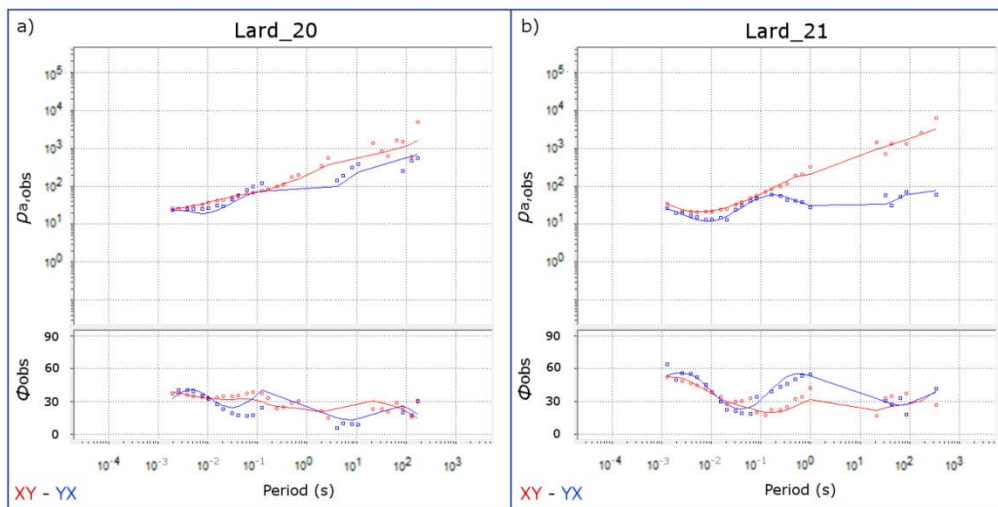


Figure B.9- MT curves, acquired in the survey larderello\_2016, are showed after La Torraca decomposition, editing and smoothing of the curves and static shift correction (see text for details): a) Lard\_20 Site, b) Lard\_21 site.

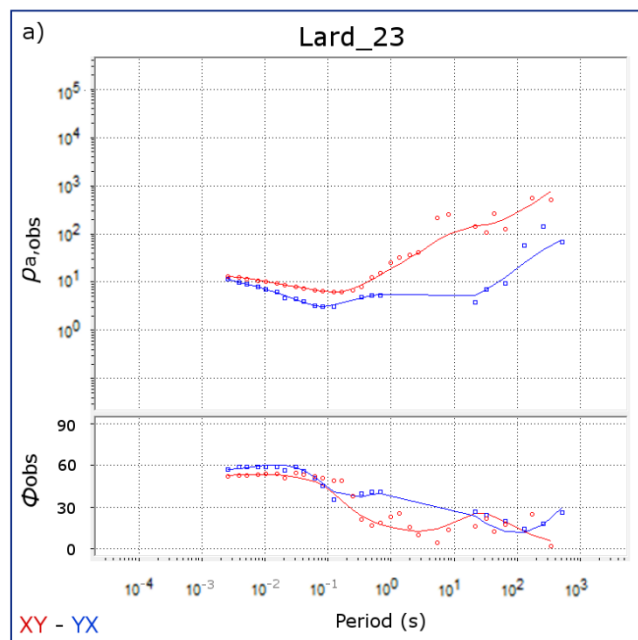


Figure B.10- MT curve, acquired in the survey larderello\_2016, are showed after La Torraca decomposition, editing and smoothing of the curves and static shift correction (see text for details): a) Lard\_23.

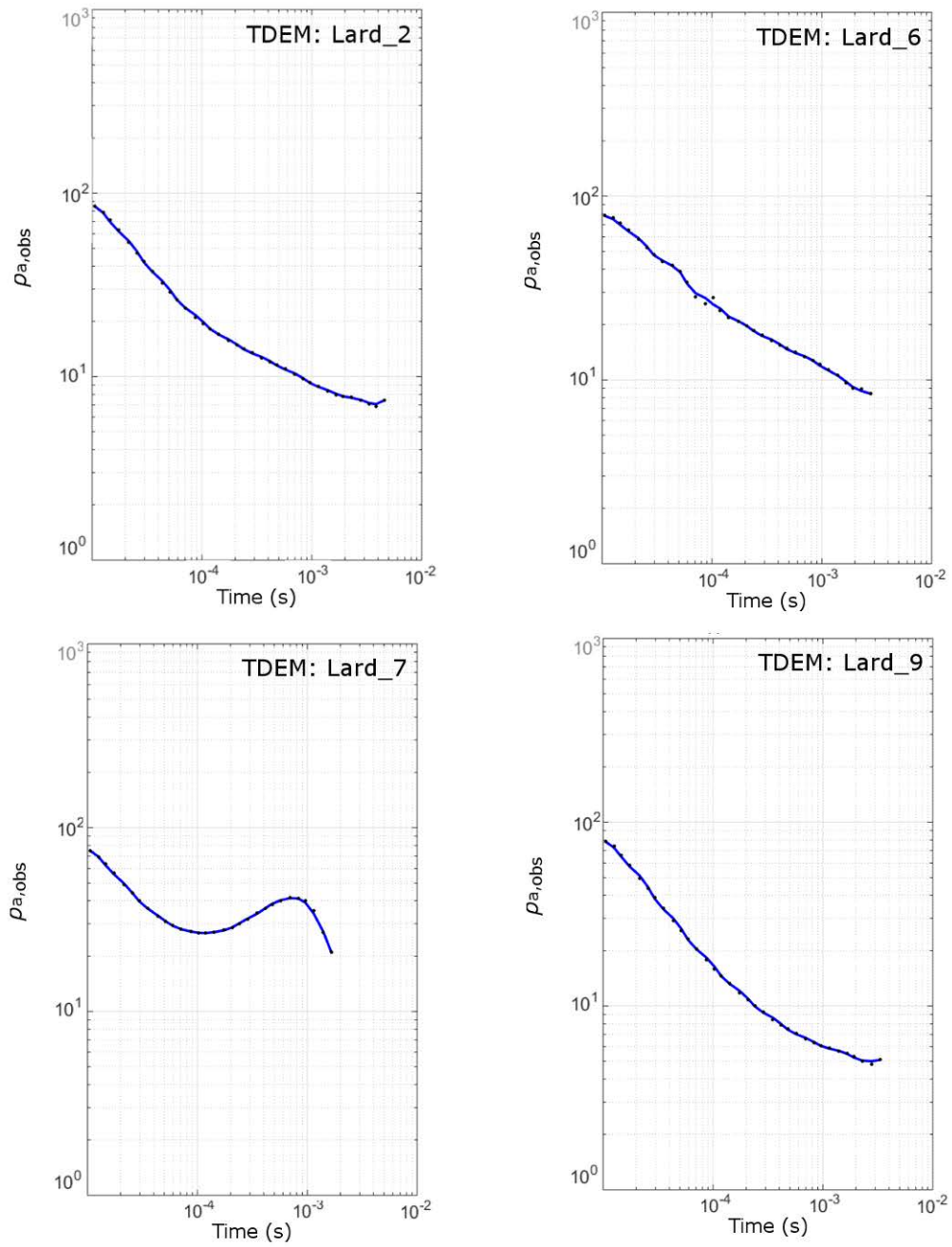


Figure B.11- TDEM data: Lard\_2, Lard\_6, Lard\_7, Lard\_9.

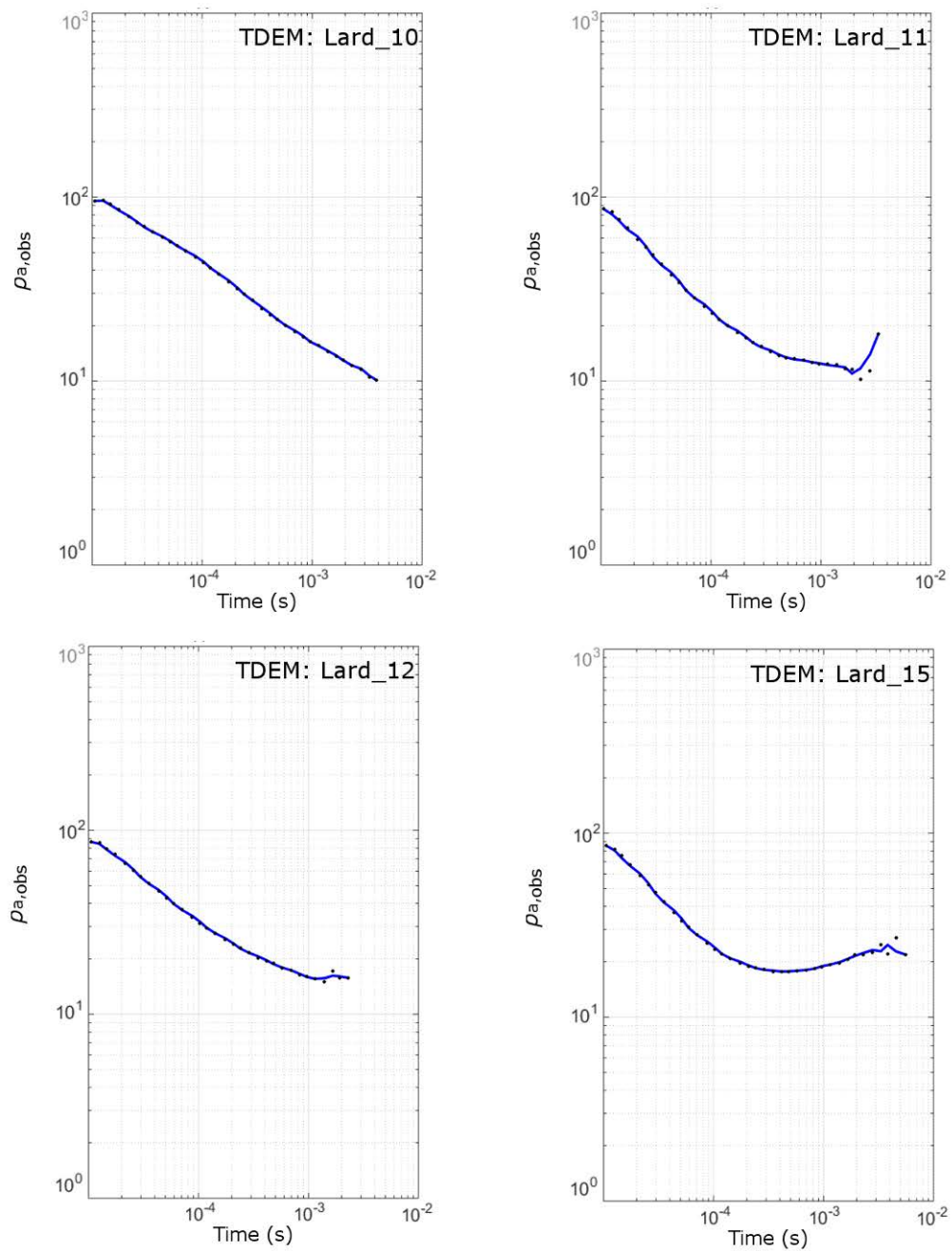


Figure B.12- TDEM data: Lard\_10, Lard\_11, Lard\_12, Lard\_15.

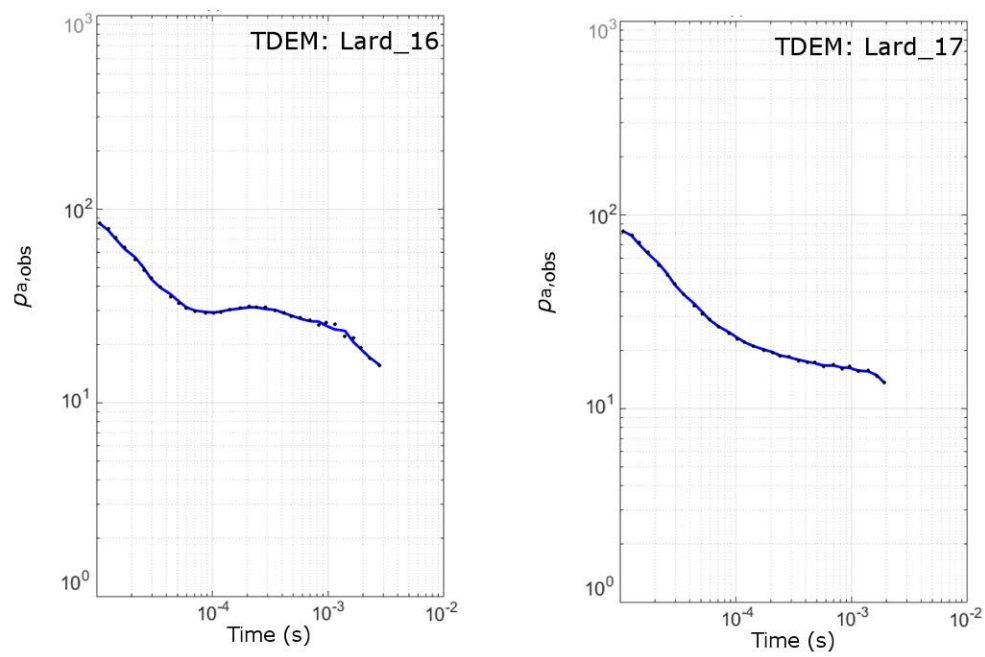


Figure B.13- TDEM data: Lard\_16, Lard\_17.

# Appendix C: MT modelling

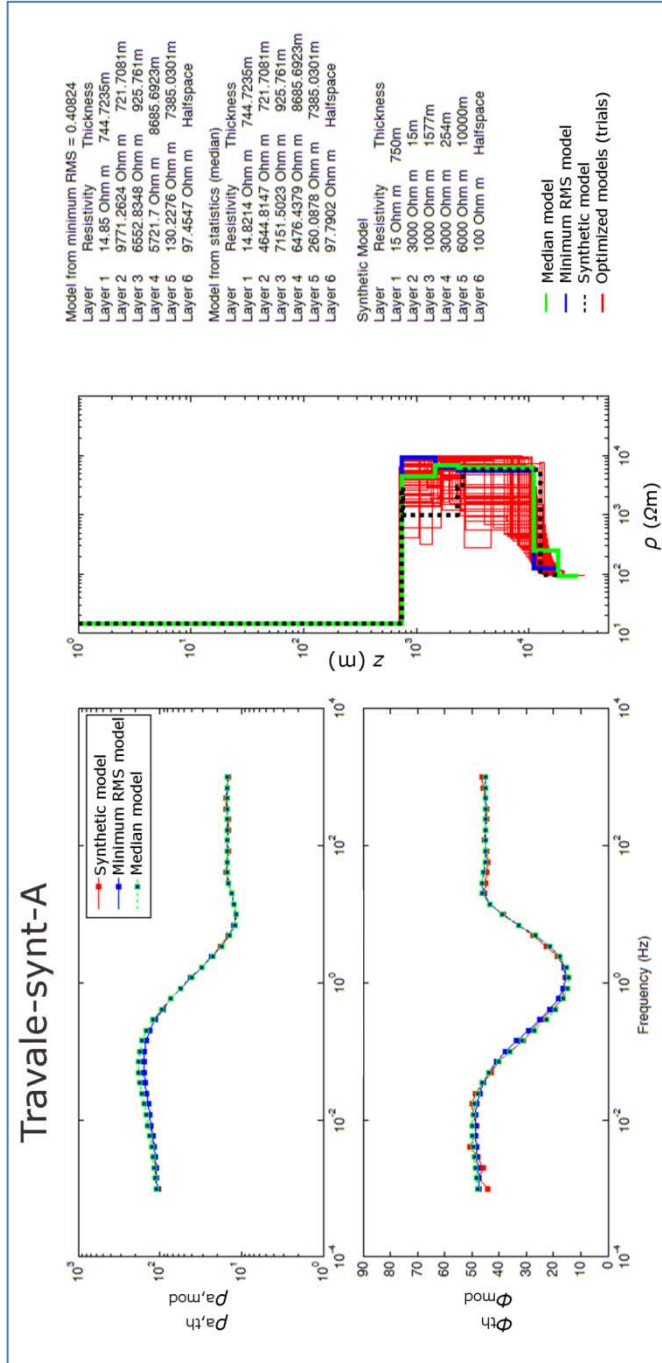


Figure C.1- Results from optimization of theoretical data from the *Travale-synt-A* model. On the left, the theoretical and modelled  $\rho_a$  and  $\Phi$  are shown. In the center, the 100 models are shown. In blue the final model with the minimum RMS is highlighted. In green the model from the statistics is shown. On the right, the estimated parameters are listed for the final model and for the model from statistic. The parameters of the synthetic model are shown, too.

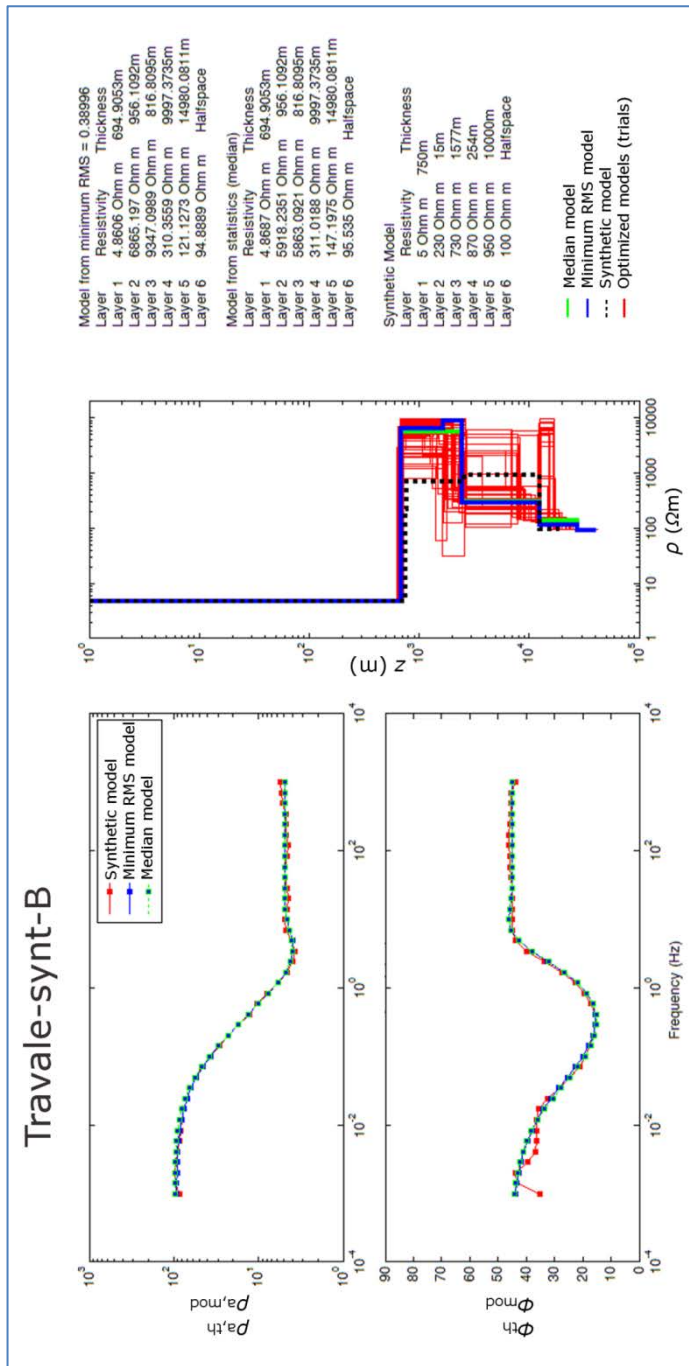


Figure C.2- Results from optimization of theoretical data from the *Travale-synt-B* model. On the left, the theoretical and modelled  $\rho_a$  and  $\Phi$  are shown. In the center, the 100 models are shown. In blue the final model with the minimum RMS is highlighted. In green the model from the statistics is shown. On the right, the estimated parameters are listed for the final model and for the model from statistic. The parameters of the synthetic model are shown, too.

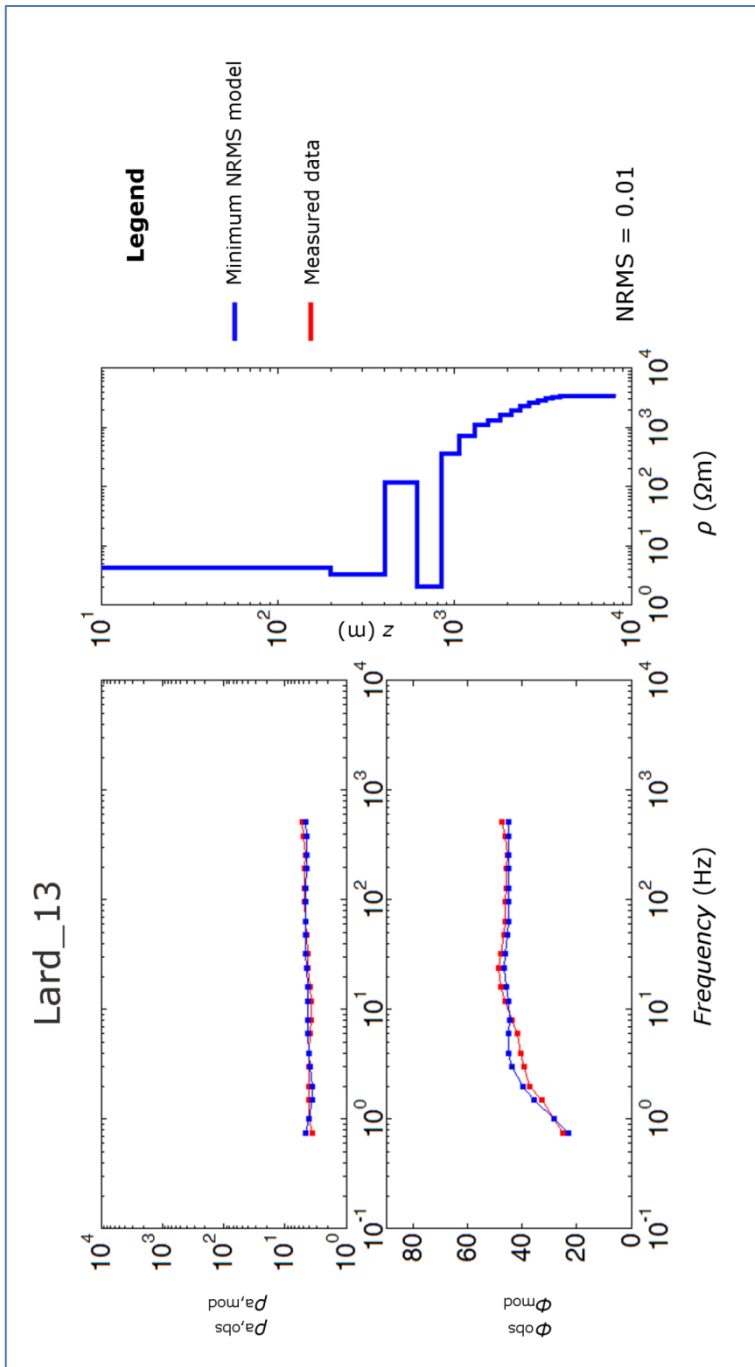


Figure C.3- Results from optimization of measured data in the *Lago Boracifero* area: Lard\_13 site. On the left, the theoretical and modelled  $\rho_a$  and  $\Phi$  are shown. On the right, the model with minimum NRMS, among 25 models is shown.

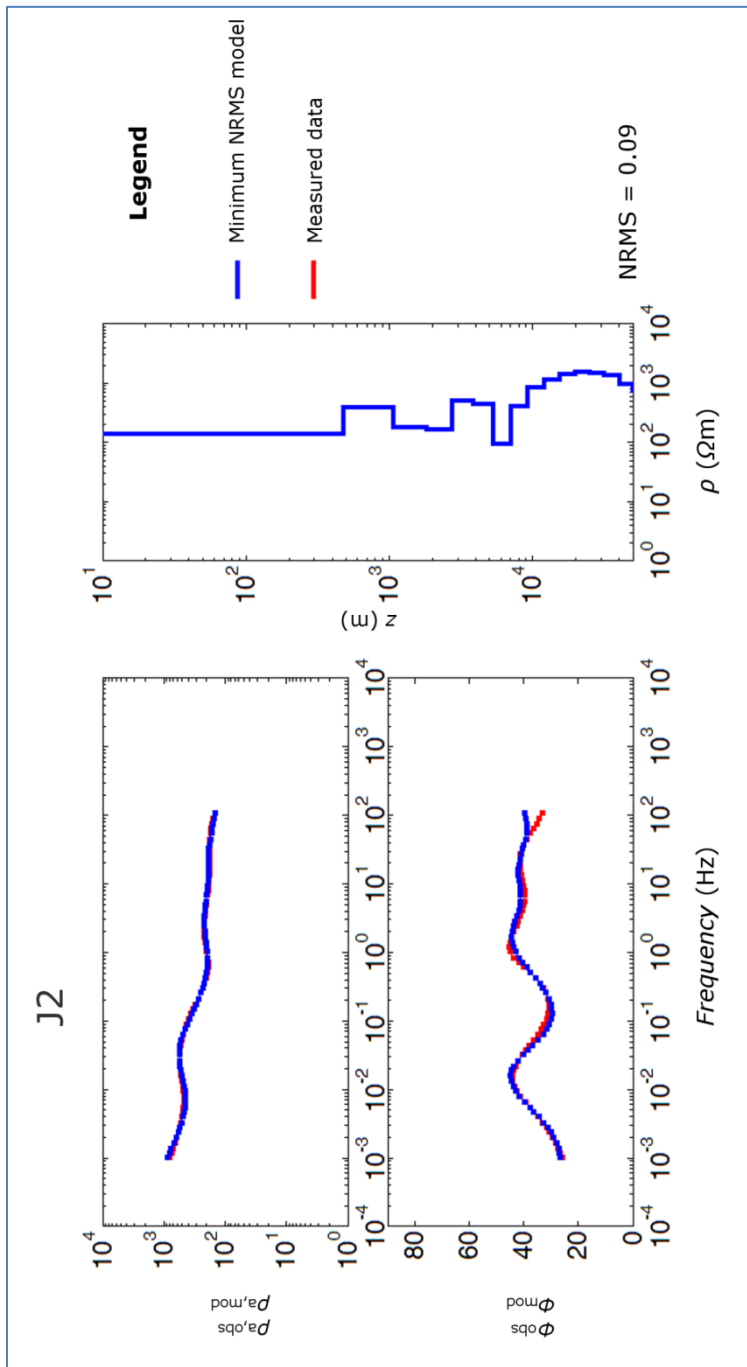


Figure C.4- Results from optimization of measured data in the Travale area: J2 site. On the left, the theoretical and modelled  $\rho_a$  and  $\Phi$  are shown. On the right, the model with minimum NRMS, among 25 models is shown.

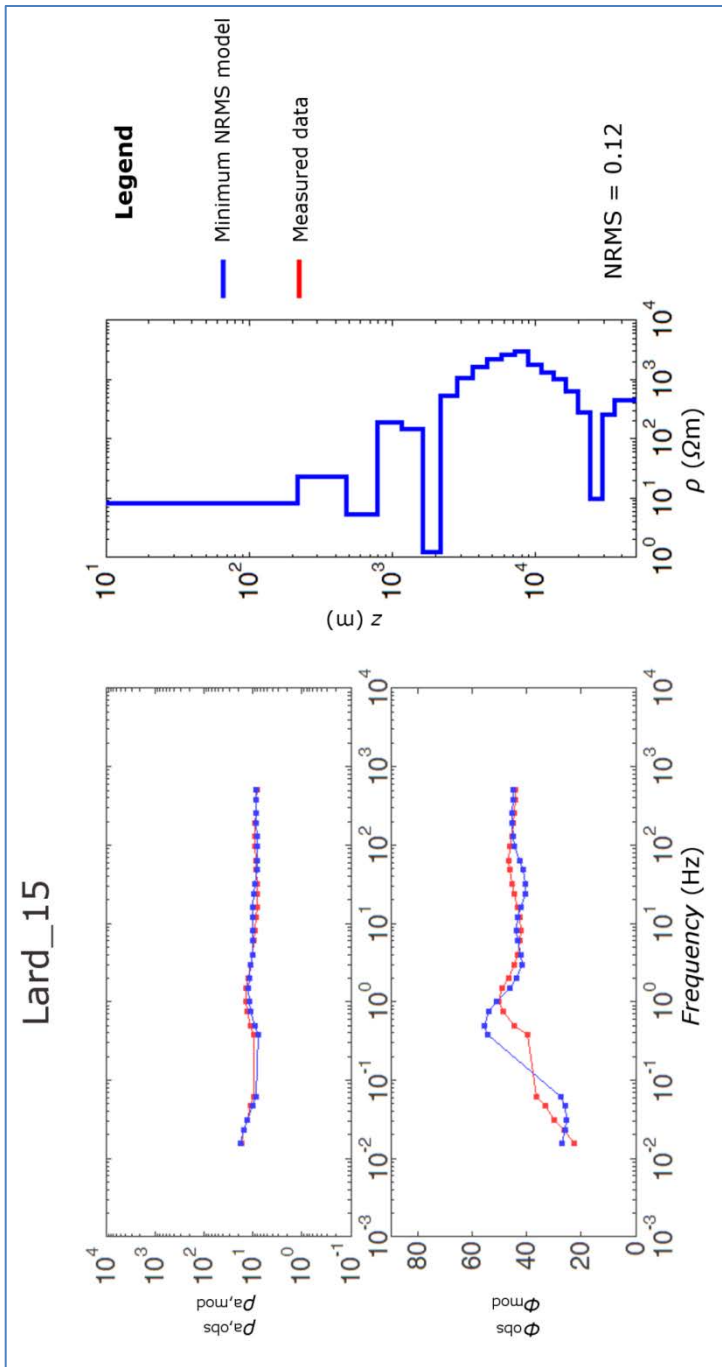


Figure C.5-Example of bad result of optimization procedure on noisy real data. Results from optimization of measured data in the *Lago Boracifero* area: Lard\_15 site. On the left, the theoretical and modelled  $\rho_a$  and  $\Phi$  are shown. On the right, the model with minimum NRMS, among 25 models is shown.

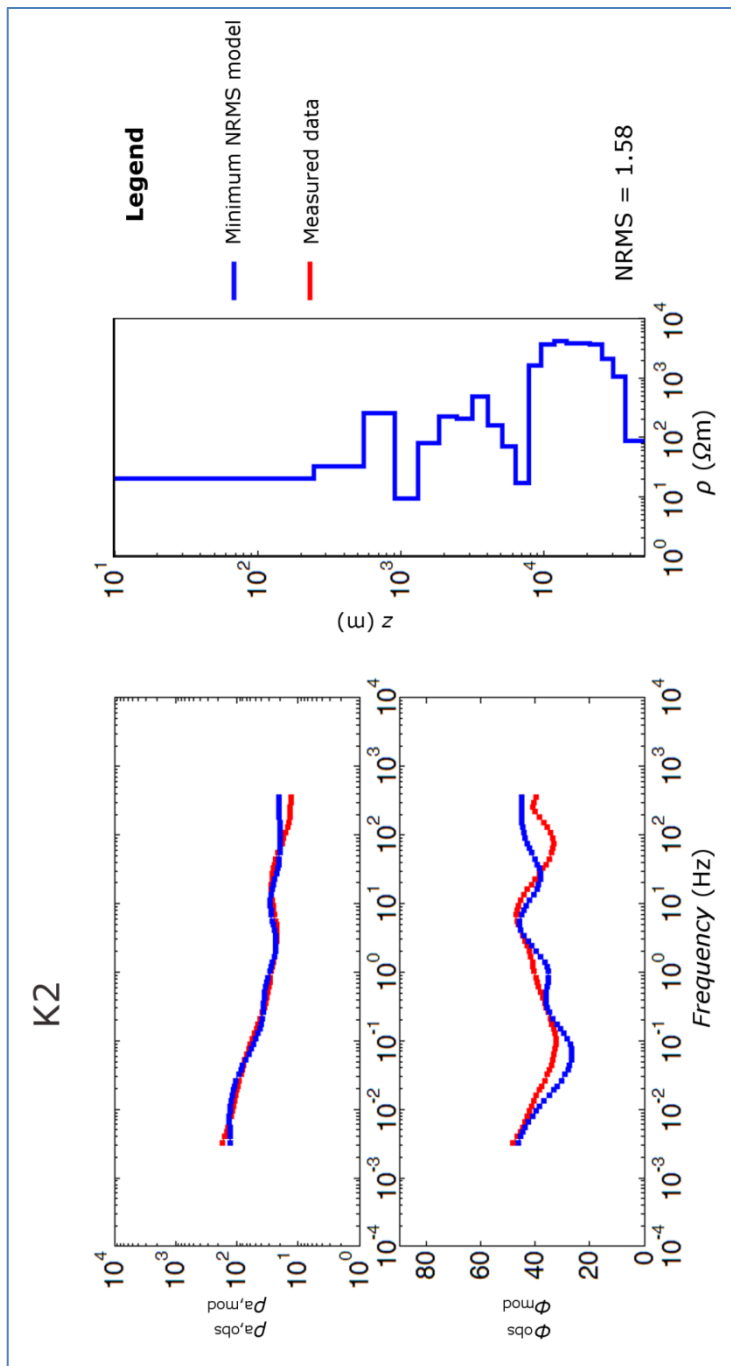


Figure C.6- Example of bad result of optimization procedure on noisy real data Results from optimization of measured data in the *Travale* area: k2 site. On the left, the theoretical and modelled  $\rho_a$  and  $\Phi$  are shown. On the right, the model with minimum NRMS, among 25 models is shown.

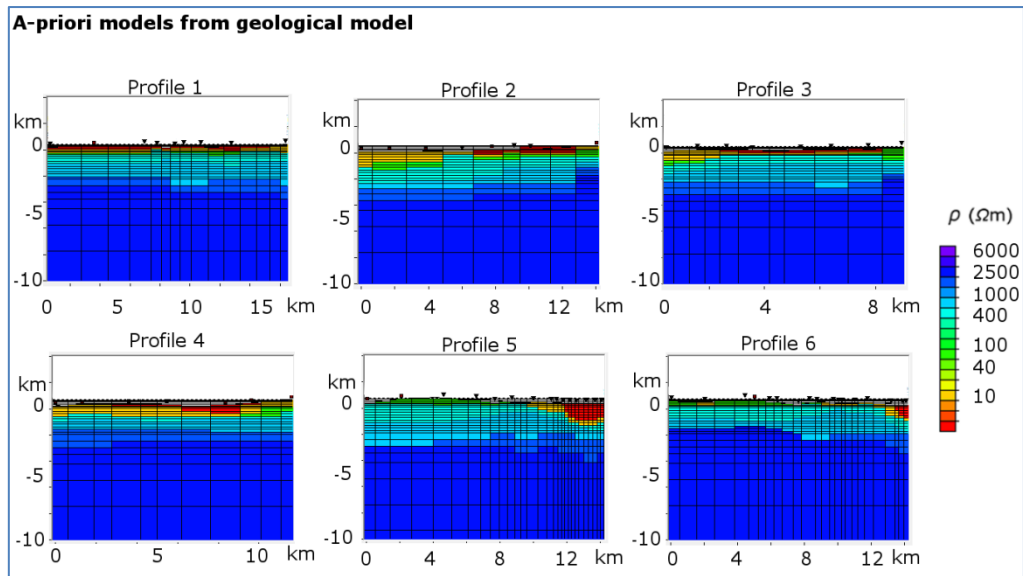


Figure C.7- Resistivity models extracted from the 3D geological model as 2D slice. These models were used as starting models for the 2D inversion.

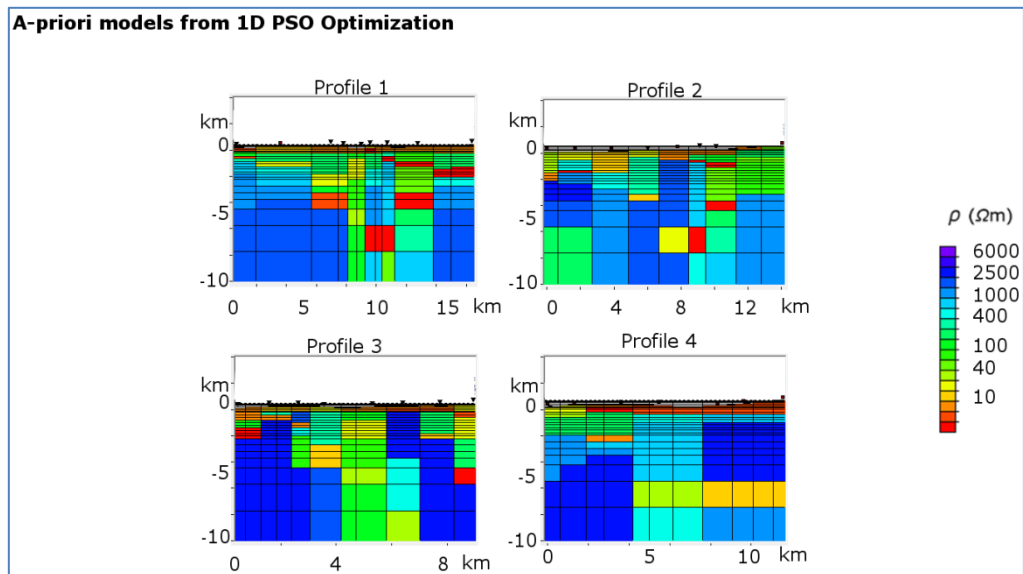


Figure C.8- Resistivity models obtained from the interpolation of 1D models computed with Particle Swarm Optimization. These models were used as starting models for the 2D inversion. The focus is on the *Lago Boracifero* and the Profile 1 to 4 are shown.

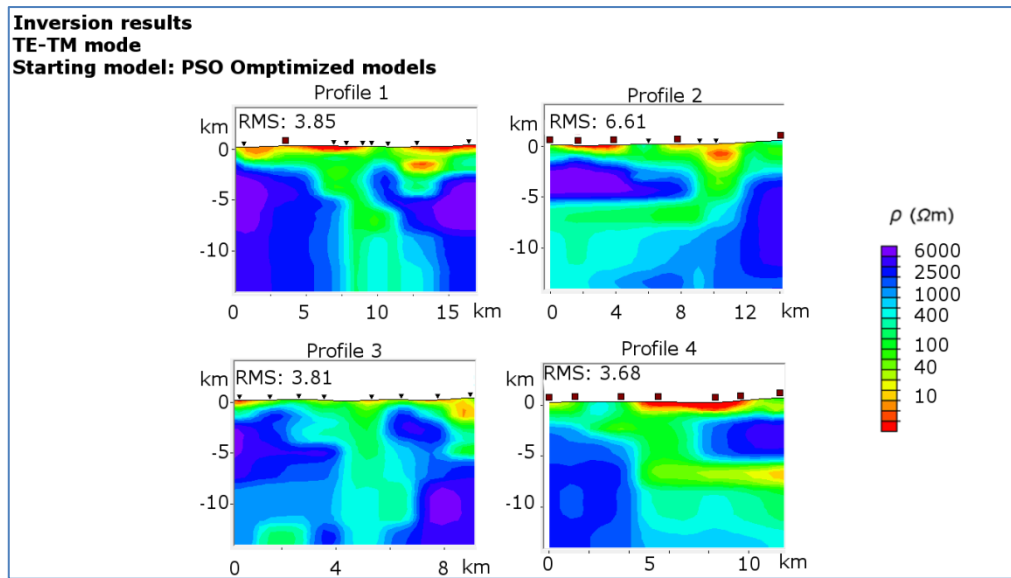


Figure C.9- Resulting models of 2D inversion for the Profile 1 to Profile 4 MT profiles. Here we tested the a-priori models from the interpolation of 1D PSO models. The TE and TM modes were jointly inverted.

## References

Accaino, F., Nicolich, R., Tinivella, U. (2006). Highlighting the crustal structure of southern Tuscany by the reprocessing of the CROP03 NVR profile. *Bollettino di Geofisica Teorica ed Applicata*, 47 (3), 425-445.

Acocella, V. and Funiciello, R. (2006). Transverse systems along the extensional Tyrrhenian margin of central Italy and their influence on volcanism. *Tectonics*, 25, 1-24, doi:10.1029/2005TC001845.

Allegrini, G., Luccioli, F., Trivella, A. (1992). Industrial uses of geothermal fluids at Larderello. *Geothermics*, 21, 5-6. doi:10.1016/0375-6505(92)90015-2.

Allen, P.A and Allen, J.R. (2005). The Petroleum Play, in: *Basin Analysis-Principles and Applications*, Allen, P.A., and Allen, J.R., Blackwell Science Ltd., 405-494.

Archie, G.E. (1942). The electrical resistivity log as an aid in determining some reservoir characteristics. *Trans. AIME* 146, 54–67.

Arias, A., Dini, I., Casini, M., Fiordelisi, A., Perticone, I., Dell’Aiuto, P. (2010). Geoscientific feature update of the Larderello–Travale geothermal system (Italy), for a regional numerical modelling. In: *Proceedings World Geothermal Congress, 2010, Bali, Indonesia*, p. 11.

Armadillo, E., Bozzo, E., Cerv, V., De Santis, A., Di Mauro, D., Gambetta, M., Meloni, A., Pek, J., Speranza, F. (2001). Geomagnetic depth sounding in the Northern Apennines (Italy). *Earth Planets Space*, 53, 385–396.

Arnason, K. (2015). The Static Shift problem in MT soundings. *Proceeding of World Geothermal Congress, 2015, Melbourne, Australia 2015*.

Aster, R., Borchers, B., Thurber, C.H. (2013). *Parameter Estimation And Inverse Problems*. Elsevier, USA, 360 pp.

- Auken, E. and Christiansen, A. (2004). Layered and laterally constrained 2D inversion of resistivity data. *Geophysics*, 69, pp 752–761.
- Bahr, K. (1991). Geological noise in magnetotelluric data: a classification of distortion types, *Phys. Earth planet. Inter.*, 66, 24–38.
- Baldi, P., Bellani, S., Ceccarelli, A., Fiordelisi, A., Squarci, P., and Taffi, L. (1994). Correlazioni tra le anomalie termiche ed altri elementi geofisici e strutturali della Toscana meridionale, *Studi Geologici Camerti, Volume Speciale 1994-1*, 139-149.
- Barbier E, Bellani S, Musmeci F. (2000). The Italian Geothermal Database. *Proceeding of World Geothermal Congress 2000, Kyushu - Tohoku, Japan, 3991 – 3995*.
- Barelli, A., Ceccarelli, A., Dini, I., Fiordelisi, A., Giorgi, N., Lovari, F., Romagnoli, P. (2010). A Review of the Mt. Amiata Geothermal System (Italy), in: *Proceedings of the World Geothermal Congress, Bali, Indonesia, 2010*.
- Barrocu, G. and Ranieri, G. (2000). TDEM: A useful tool for identifying and monitoring the fresh salt water interface. In: Sadurski, A. (ed.), *Hydrogeology of the Coastal Aquifers. Proceedings of the 16th Salt Water intrusion meeting. Poland*.
- Barsukov, P.O., Fainberg E.B., Khabensky, E.O. (2015). Shallow investigation by TEM-FAST Technique: Methodology and Examples. In Spichak V.V., *Electromagnetic sounding of the Earth's Interior. Elsevier*.
- Batini, F., Bertini, G., Gianelli, G., Pandeli, E., Puxeddu, M. (1983). Deep structure of the Larderello field: contribution from recent geophysical and geological data. *Mem. Soc. Geol. It.*, 25, 219-235.
- Batini, F., Console, R., Luongo, G. (1985). Seismological study of Larderello-Travale geothermal area. *Geothermics*, 14, 255-272.
- Batini, F., Fiordelisi, A., Graziano, F., Toksöz, M.N. (1995). Earthquake Tomography in the Larderello Geothermal Area, in: *Proceedings of the World Geothermal Congress, 1995-2*, 817-820.

Batini, F., Brogi A., Lazzarotto, A., Liotta, D., Pandeli, E. (2003). Geological features of Larderello-Travale and Mt. Amiata geothermal areas (southern Tuscany, Italy). *Episodes*, 26 (3), 239-244.

Beamish, D., Travassos, J.M. (1992). The use of the D+ solution in magnetotelluric interpretation. *J. Appl. Geophys.*, 29, 1-19.

Bellani, S., Brogi, A., Lazzarotto, A., Liotta, D., Ranalli, G. (2004). Heat flow, deep temperatures and extensional structures in the Larderello Geothermal Field (Italy): constraints on geothermal fluid flow. *J Volcan Geotherm Res* 132:15–29.

Berdichevsky, M.N. and Dmitriev, V.I. (1976). Basic principles of interpretation of magnetotelluric sounding curves. In: A. Adam, *Geoelectric and geothermal studies*. KAGP Budapest, 165-221.

Berdichevsky, M.N. and Dmitriev, I.V. (2002). Magnetotellurics in the context of the theory of ill-posed problems. *Society of Exploration Geophysicists, USA*, 214 pp.

Berdichevsky, M.N. and Dmitriev, I.V. (2008). *Models and Methods of Magnetotellurics*. Berlin: Springer.

Bernabini, M., Bertini, G., Cameli, G.M., Dini, I., Orlando, L. (1995). Gravity Interpretation of Mt. Amiata Geothermal Area (Central Italy), in: *Proceedings of the World Geothermal Congress, 1995-2*, 817-820.

Bertani, R. (2015). Geothermal Power Generation in the World 2010-2014 Update Report. In *Proceedings of World Geothermal Congress 2015, Melbourne, Australia*.

Bertani, R., Bertini G., Cappetti, G., Fiordelisi, A., Marocco, B.M. (2005) An update of the Larderello-Travale/Radicondoli deep geothermal system. *Proceedings World Geothermal Congress, 2005, Antalya, Turkey*.

Bertani, R., Parisi, L., Perini, R., Tarquini, B. (1999). High-temperature measurements of water adsorption in geothermal rocks. *Geothermics*, 28, 277-294

Bertini, G., Gianelli, G., Pandeli, E., Puxeddu, M. (1985). Distribution of hydrothermal minerals in Larderello-Travale and Mt. Amiata geothermal fields (Italy). *Geothermal Research Council Transaction, Vol. 9 part I*.

Bertini, G., Casini, M., Gianelli, G., Pandeli E. (2006). Geological structure of a long-living geothermal system, Larderello, Italy. *Terra Nova*, 18, 163-169.

Boccaletti, M., Gianelli, G., Sani, F. (1997). Tectonic regime, granite emplacement and crustal structure in the inner zone of the Northern Apennines (Tuscany, Italy): A new hypothesis. *Tectonophysics*, 270, 127-143, doi: 10.1016/S0040-1951(96)00177-1.

Boccaletti, M., Corti, G., Martelli, L. (2011). Recent and active tectonics of the external zone of the Northern Apennines (Italy). *Int. J. Earth. Sci.*, 100, 1331-1348, doi:10.1007/s00531-010-0545-y.

Bonini, M. and Sani, F. (2002). Extension and compression in the Northern Apennines (Italy) hinterland: Evidence from the late Miocene-Pliocene Siena-Radicofani Basin and relations with basement structures. *Tectonics*, 21, 1-33, doi: 10.1029/2001TC900024.

Bonini, M., Boccaletti, M., Moratti, G. and Sani, F. (2001). Neogene crustal shortening and basin evolution in Tuscany (Northern Apennines). *Ofioliti*, 26, 275-286.

Bostick F.X. (1977). A simple almost exact method of MT analysis. Workshop on Electrical Methods in Geothermal Exploration. US Geological Survey, Contract no. 14080001-8-359.

Boyle, K. and Zoback, M. (2013). Stress and fracture orientation in the northwest Geysers geothermal field, in: *Proceedings of Thirty-Eighth Workshop on Geothermal Reservoir Engineering*, Stanford University, Stanford, California, 2013.

Brace, W.F., Orange, A.S., Madden, T.R. (1965). The effect of pressure on the electrical resistivity of water-saturated crystalline rocks. *J. Geophysical Research*, 70 (22), 5669-5678.

Brace, W.F., and Orange, (1968). Further studies of the effects of pressure on electrical resistivity of rocks. *J. Geophysical Research*, 73 (16), 5407-5420.

Brogi, A. (2006). Neogene extension in the Northern Apennines (Italy): insights from the southern part of the Mt. Amiata geothermal area. *Geodin. Acta*, 19/1, 1-9, doi:10.3166/ga.19.33-50.

Brogi, A. and Fabbrini, L. (2009). Extensional and strike-slip tectonics across the Monte Amiata–Monte Cetona transect (Northern Apennines, Italy) and seismotectonic implications. *Tectonophysics*, 476, 195–209, doi:10.1016/j.tecto.2009.02.020.

Brogi, A. and Cerboneschi, A., (2007). Upper crust “boudinage” during post-collisional Miocene extension in Tuscany: Insights from the southern part of the Larderello geothermal area (Northern Apennines, Italy). *Geodinamica Acta*, 20 (5), 327-351.

Brogi, A., Lazzarotto, A., Liotta, D., Ranalli, G. (2003). Extensional shear zones as imaged by reflection seismic lines: the Larderello geothermal field (Central Italy). *Tectonophysics*, 363, 127-139.

Brogi, A., Lazzarotto A., Liotta, D., Ranalli, G., CROP18 Working Group (2005). Crustal structures in the geothermal areas of southern Tuscany (Italy): Insights from the CROP 18 deep seismic reflection lines. *Journal of Volcanology and Geothermal Research*, 148, 60– 80.

Burgassi P.D. (1987). Historical Outline of Geothermal Technology in the Larderello Region to the Middle of the 20th Century. *Geothermal Resources Council Bulletin*, March.

Cagniard, L. (1953). Basic theory of the magnetotelluric method of geophysical prospecting. *Geophysics*, 18, 605–635.

Caldwell, G., Pearson, C., Zayadi, H. (1986). Resistivity of rocks in geothermal systems: a laboratory study. In *Proceedings 8th NZ Geothermal Workshop*, 227-231.

Calore, C., Celati, R., Gianelli, G., Norton, D., Squarci, P. (1981). Studi sull'origine del sistema geotermico di Larderello. *Atti II Seminario Informativo del Sottoprogetto Energia Geotermica, Progetto Finalizzato Energetica*, Roma 16-19 giugno 1981, PEG Editrice, 218-225.

Cameli, G.M., Batini, F., Dini, I., Lee, J.M., Gibson R.L., Toksoz M.N. (1995). Seismic delineation of a geothermal reservoir in the Monteverdi area from VSP data, in: *Proceedings of World Geothermal Congress*, Florence, Italy, 821-826.

- Cameli, G.M., Dini, I., Liotta D. (1993). Upper crustal structure of the Larderello geothermal field as a feature of post-collisional extensional tectonics (Southern Tuscany, Italy). *Tectonophysics*, 224, 413-423.
- Cameli, G.M., Dini, I., Liotta D. (1998). Brittle/Ductile boundary from seismic reflection lines of southern Tuscany (Northern Apennines, Italy). *Memorie Società Geologica Italiana*, 52, 152-162.
- Capozzoli, L., De Martino, G., Giampaolo, V., Godio, A., Manzella, A., Perciante, F., Rizzo, E., Santilano, A. (2016). Deep electrical resistivity model of the Larderello geothermal field (Italy): preliminary results of the FP7 IMAGE experiment. Abstract, GNGTS 2016, Lecce.
- Caranova, R., Buonasorte, G., Fiordelisi, A., Barreto, M. (2015). Gesto Italia Activities in the Exploration of Italian Geothermal Resources Preliminary Results. In *Proceedings of World Geothermal Congress 2015, Melbourne, Australia*.
- Carmignani, L., Decandia, F.A., Fantozzi, P.L., Lazzarotto, A., Liotta, D., Meccheri, M. (1994). Tertiary extensional tectonics in Tuscany (Northern Apennines, Italy). *Tectonophysics*, 238, 295-315.
- Casini, M., Ciuffi, S., Fiordelisi, A., Mazzotti, A. (2010a). 3D Seismic Surveys and Deep Target Detection in the Larderello-Travale Geothermal Field (Italy). *Proceedings of World Geothermal Congress 2010, Bali, Indonesia*, 25-30 April 2010.
- Casini, M., Ciuffi, S., Fiordelisi, A., Mazzotti, A., Stucchi, E. (2010b). Results of a 3D Seismic Survey at Travale geothermal field (Italy). *Geothermics*, 39, 4-12.
- Cathless, L.M. and Erendi, A.H.J. (1997). How long can a hydrothermal system be sustained by a single event? *Econ. Geol.*, 77, 1071-1084.
- Cavarretta, G., Gianelli, G., Puxeddu, M. (1980). Hydrothermal metamorphism in the Larderello geothermal field. *Geothermics*, 9, 297-314.
- Celati, R., Cappetti, G., Calore, C., Grassi, S., D'Amore F. (1991). Water recharge in Larderello geothermal field. *Geothermics*, 20 (3), 119-133.
- Chave, A.D. and Jones, A.G. (2012). *The Magnetotelluric Method, Theory and Practice*. Cambridge University Press. 604 pp.

Chave, A.D. and Weidelt, P. (2012). The theoretical basis for electromagnetic induction. In: Chave, A.D. and Jones, A.G. 2012. *The Magnetotelluric Method, Theory and Practice*. Cambridge University Press. 19-49.

Chen, S. (2009). *Constrained Particle Swarm Optimization*. Matlab software package available in the “file exchange” environment of MathWorks and distributed under BSD license. Available at <http://www.mathworks.com/matlabcentral/fileexchange/25986>.

Christiansen, A.V., Auken, E., Soerensen K.I. (2009). The transient electromagnetic method – Airborne TEM. In: *Groundwater Geophysics – A Tool for Hydrogeology* (ed. R. Kirsch) 209-225, Springer.

Ciardi M. and Cataldi R. (2005). *Il Calore della Terra, Contributo alla Storia della Geotermia in Italia*. Edizioni ETS, Pisa. 344 pp.

Constable, S.C., Parker, R.I., Constable, G.C. (1987). Occam’s inversion: A practical algorithm for generating smooth models from electromagnetic sounding data. *Geophysics*, 52 (3), 289-300.

Coppo, N., Darnet, M., Harcouët-Menou, V., Wawrzyniak, P., Manzella, A., Breteau, F., Romano, G., Lagrou, D., Girard J.F. (2016). Characterization of deep geothermal energy resources in low enthalpy sedimentary basins in Belgium using ElectroMagnetic methods –CSEM and MT results. *Proceedings of European Geothermal Congress 2016, Strasbourg*.

Costantini, A., Lazzarotto, A., Liotta, D., Mazzanti, R., Mazzei, R., Salvatorini, G.F. (2002). Note illustrative della carta geologica d’Italia alla scala 1:50.000, foglio 306 Massa Marittima. ISPRA Progetto CARG.

D’Amore, F. and Truesdell, A.H. (1979). Models for steam chemistry at Larderello and The Geysers. *Proc. 5th Workshop on Geothermal Reservoir Engineering*, 283-297, Stanford.

Dalrymple, G.B., Grove, M., Lovera, O.M., Harrison, T.M., Hulen, J.B., Lanphere, M.A. (1999). Age and thermal history of the Geysers plutonic complex (felsite unit), Geysers geothermal field, California: a  $^{40}\text{Ar}/^{39}\text{Ar}$  and U–Pb study. *Earth Planet. Sci. Lett.*, 173, 285-298.

- Decandia, F.A., Lazzarotto, A., Liotta, D. (1993). La “serie ridotta” nel quadro della evoluzione geologica della Toscana Meridionale. *Mem. Soc. Geol. It.*, 49, 181-191.
- Degroot-Hedlin, C. (1991). Removal of static shift in two dimensions by regularized inversion. *Geophysics*, 56, 2102-2106.
- Degroot-Hedlin C. and Constable S. (1990). Occam’s inversion to generate smooth, two-dimensional models from magnetotelluric data. *Geophysics* 55 (12):1613–1624.
- Di Maio R., Mauriello P., Patella D., Petrillo Z., Piscitelli S., Siniscalchi A. (1998). Electric and electromagnetic outline of the Mount Somma-Vesuvius structural setting. *Journal of Volcanology and Geothermal Research*, 82, 219-238.
- Di Stefano, R., Bianchi, I., Ciaccio, M.G., Carrara, G., Kissling, E. (2011). Three-dimensional Moho topography in Italy: New constraints from receiver functions and controlled source seismology. *G3*, 12 (9)
- Dickson, M.H. and Fanelli, M. (2004). What is Geothermal Energy? IGA International Geothermal association website (last accessed 06/2015). [http://www.geothermal-energy.org/what\\_is\\_geothermal\\_energy.html](http://www.geothermal-energy.org/what_is_geothermal_energy.html).
- Digital Earth Lab (2016). [www.digitalearthlab.com/download/1d-magnetotelluric-forward-modelling-matlab-2](http://www.digitalearthlab.com/download/1d-magnetotelluric-forward-modelling-matlab-2). Last accessed December 2016.
- Dini, A., Gianelli, G., Puxeddu, M., Ruggieri, G. (2005). Origin and evolution of Pliocene–Pleistocene granites from the Larderello geothermal field (Tuscan Magmatic Province, Italy), *Lithos*, 81, 1-31, doi:10.1016/j.lithos.2004.09.002.
- Dini, A., Westerman, D.S., Innocenti, F., Rocchi, S. (2008). Magma emplacement in a transfer zone: The Miocene mafic Orano dyke swarm of Elba Island, Tuscany, Italy. *Geological Society, London, Special Publications* 2008; v. 302; p. 131-148.
- Dini, A., Brogi, A., Liotta, D., Rimondi, V., Ruggieri, G., Zucchi, M. (2016). The eastern Elba Island magmatic-hydrothermal complex: a proxy for the supercritical roots of Larderello geothermal system (Italy). *Goldschmidt Conference 2016, Yokohama, Japan*.

- Donnelly-Nolan, J.M., Burns, M.G., Goff, F. E., Peters, E.K., Thompson, J.M. (1993). The Geysers-Clear Lake area, California: thermal waters, mineralization, volcanism, and geothermal potential. *Econ. Geol.*, 88, 301-316, doi:10.2113/gsecongeo.88.2.301.
- Dosso, S.E. and Oldenburg, D.W. (1991). Magnetotelluric appraisal using simulated annealing. *Geophys. J. Int.*, 106, 379-385.
- Duba, A., Roberts, J., Bonner, B. (1997). Electrical properties of geothermal reservoir rocks as indicators of porosity distribution. Twenty-Second Workshop on Geothermal Reservoir Engineering Stanford University, Stanford, California, SGP-TR-155
- Duchi, V., Minissale, A., Rossi, R. (1986). Chemistry of thermal springs in the Larderello-Travale geothermal region, southern Tuscany, Italy, *Appl. Geochem.*, 1, 659-667.
- Duprat, A., and Cole, F. 1985. Magnetotelluric soundings in the Travale area, Tuscany. *Geothermics*, 14, 689–696.
- Ebbesen S., Kiwitz, P., Guzzella, L. (2012). A Generic Particle Swarm Optimization Matlab Function: American Control Conference Fairmont Queen Elizabeth, Montréal, Canada.
- Egbert, G.D. and Booker, J.R. (1986). Robust estimation of geomagnetic transfer functions. *Geophysical J. R. Astr. Soc.*, 87, 173–194.
- Engelbrecht, A.P. (2007). *Computational Intelligence, An introduction*. John Wiley & Sons, Chichester, England.
- Erkan, K., Blackwell D.D., Leidig M.M. (2005). Crustal thermal regime at The Geysers/Clear Lake Area, California, in: *Proceedings World Geothermal Congress, Antalya, Turkey, 2005*.
- Evans, R.I. (2012) Earth's electromagnetic environment, Conductivity of Earth materials. In: Chave A.D., Jones A.G., *The Magnetotelluric method, theory and practice*. Cambridge University Press.
- Everett, M.E. and Schultz, A. (1993). Two-Dimensional Nonlinear Magnetotelluric Inversion Using a Genetic Algorithm. *J. Geomag Geoelectr.*, 45, 1013-1026.

Farquharson, C.G. and Miensopust, M.P. (2011). Three-dimensional finite-element modelling of magnetotelluric data with a divergence correction. *Journal of Applied Geophysics*, 75(4), 699-710.

Farquharson, C.G. and Oldenburg, D.W. (2004). A comparison of automatic techniques for estimating the regularization parameter in non-linear inverse problems. *Geophys. J. Int.*, 156, 411-425 doi: 10.1111/j.1365-246X.2004.02190.x.

Fernández-Martínez, J. L., García-Gonzalo, E., Álvarez, J. P. F., Kuzma, H. A. and Menéndez-Pérez, C.O (2010a). PSO: A Powerful Algorithm to Solve Geophysical Inverse Problems. Application to a 1D-DC Resistivity Case. *Journal of Applied Geophysics*, 71, 13-25.

Fernández-Martínez, J. L., García-Gonzalo, E., Naudet, V. (2010b). Particle swarm optimization applied to solving and appraising the streaming-potential inverse problem. *Geophysics*, 75 (4), 3-15. Doi: 10.1190/1.3460842.

Finetti I.R., Boccaletti, M., Bonini, M., Del Bena, A., Geletti, R., Pipan, M., Sani, F. (2001). Crustal section based on CROP seismic data across the North Tyrrhenian–Northern Apennines–Adriatic Sea. *Tectonophysics*, 343, 135– 163.

Finetti, I.R. (2006). Basic regional crustal setting and superimposed local pluton-intrusion-related tectonics in the Larderello-M. Amiata geothermal province, from integrated CROP seismic data. *Boll. Soc. Geol. It.*, 125.

Fiordelisi, A., Mackie, R., Manzella, A. Zaja, A. (1998). Electrical features of deep structures in Southern Tuscany (Italy). *Annals of Geophysics*, 41(3), 333-341.

Flóvenz, Ó.G., Georgsson, L.S., Árnason, K. (1985). Resistivity structure of the upper crust in Iceland. *Geophysical Research letters*, 90 (B12), 10123-10150.

Flóvenz, Ó.G., Spangenberg, E., Kulenkampff, J., Árnason, K., Karlsdóttir, R., Huenges E., (2005). The role of electrical conduction in geothermal exploration. *Proceedings World Geothermal Congress 2005, Antalya, Turkey* 9 pp.

Foley, J.E., Toksoz, M.N., Batini, F. (1992). Inversion of teleseismic travelttime residuals for velocity structure in the Larderello geothermal system, Italy. *Geophys. Res. Letters*, 19, 5-8.

Fron dini, F., Caliro, S., Cardellini, C., Chiodini, G., Morgantini, N. (2009). Carbon dioxide degassing and thermal energy release in the Monte Amiata volcanic-geothermal area (Italy). *Applied Geochemistry*, 24, 860-875.

Galgaro, A., Di Sipio, E., Teza, G., Destro, E., De Carli, M., Chiesa, S., Zarrella, A., Emmi, G., Manzella, A., (2015). Empirical modeling of maps of geo-exchange potential for shallow geothermal energy at regional scale. *Geothermics*, 57, 173-184.

Gamble, T. D., Goubau, W. M., Clarke J. (1979). Magnetotellurics with a remote reference. *Geophysics*, 44, 53–68.

Garcia, X. and Jones, A.G. (2002). Atmospheric sources for audio-magnetotelluric (AMT) sounding. *Geophysics*, 67, 448–458.

Garcia, J., Walters, M., Beall, J., Hartline, C., Pingol, A., Pistone, S., Wright, M. (2012). Overview of The Northwest Geysers EGS Demonstration Project, in: *Proceedings of Thirty-Seventh Workshop on Geothermal Reservoir Engineering*, Stanford, California.

Geothopica web site. Italian Geothermal Database. <http://geothopica.igg.cnr.it/> Last accessed September 2016.

Gherardi, F., Panichi, C., Gonfiantini, R., Magro, G., Scandiffio, G. (2005). Isotope systematics of C-bearing gas compounds in the geothermal fluids of Larderello, Italy. *Geothermics*, 34, 442–470.

Gianelli, G. (1994). Nature of deep seated geothermal resources in Italy. *Proceedings of Workshop "Deep-seated and Magma Ambient Geothermal Systems 1994"*, Japan, pp. 27 - 36.

Gianelli, G. (2008). A comparative analysis of the geothermal fields of Larderello and Mt Amiata, Italy, in: *Geothermal energy research trends*, Ueckermann, H.I.. Nova Science Publishers, 59-85.

Gianelli, G. and Bertini, G. (1993). Natural hydraulic fracturing in the Larderello geothermal field: evidence from well MV5A. *Boll. Soc. Geol. It.*, 112, 507-512.

Gianelli, G. and Puxeddu, M. (1994). Geological comparison between Larderello and The Geysers geothermal fields. *Mem. Soc. Geol. It.*, 48, 715-717.

- Gianelli, G., and Ruggieri, G. (2002). Evidence of a contact metamorphic aureole with high-temperature metasomatism in the deepest part of the active geothermal field of Larderello, Italy. *Geothermics*, 31, 443-474.
- Gianelli, G., Manzella, A., Puxeddu, M. (1997). Crustal models of the geothermal areas of southern Tuscany (Italy), *Tectonophysics*, 281, 221-239.
- Gianelli G., Puxeddu M., Squarci P. (1978). Structural setting of the Larderello-Travale geothermal region. *Mem.Soc. Geol. It.*, 19, 469-476.
- Giolito, C., Ruggieri, G., Manzella, A. (2009). The relationship between resistivity and mineralogy at Travale, Italy. *GRC Transaction*, vol 33, 2009.
- Glover, P.W.J., Hole, M.J., Pous, J. (2000). A modified Archie's law for two conducting phases. *Earth and Planetary Science Letters*, 180,369–383.
- Glover, P.W.J. (2010). A generalized Archie's law for n phases. *Geophysics*, 75 (6), E247--E265.
- Godio, A. (2016). Multi Population Genetic Algorithm to estimate snow properties from GPR data. *Journal of Applied Geophysics*, 131, 133–144. DOI: 10.1016/j.jappgeo.2016.05.015.
- Grandis, H., Menvielle, M., Roussignol, M. (1999). Bayesian inversion with Markov chains—I. The magnetotelluric one-dimensional case. *Geophys. J. Int.*, 138, 757–768
- Groom, R.W. and Bailey, R.C. (1989). Decomposition of magnetotelluric impedance tensor in the presence of local three-dimensional galvanic distortion. *Journal of Geophysical Research*, 94 (B2), 1913-1925.
- Hashin, Z. and Shtrikman, S. (1962). On some variational principles in anisotropic and non homogeneous elasticity. *Journal of the Mechanics and Physics of Solids*, 10, 335-342.
- Hersir, G.P. and Árnason, K. (2010). Resistivity of rocks. Short Course V on exploration for geothermal resources. United Nations University. 1-8 pp.
- Holland, J. H. (1975). *Adaptation in Natural and Artificial Systems*, University of Michigan Press.

Hulen, J.B. and Nielson, L.D. (1993). Interim Report on Geology of The Geysers Felsite, Northwestern California. *Geoth. Res. T.*, 17, 249-258.

Hulen, J.B. and Nielson, L.D. (1996). The Geysers felsite. *Geoth. Res. T.*, 20, 295-306.

Hulen, J.B. and Norton, D.L. (2000). Wrench-fault tectonics and emplacement of The Geysers Felsite. *Geoth. Res. T.*, 24, 289-298.

Hutton, V.R.S. (1985). Magnetic, telluric and magnetotelluric measurements at the Travale test site, Tuscany, Italy, 1980–1983: An overview. *Geothermics*, 14, 637–644

IGA: Workshop (2013). Developing Best Practice for Geothermal Exploration and Resource / Reserve Classification, 14 November 2013, Essen, Germany, website, [http://www.geothermal-energy.org/reserves\\_and\\_resources/workshop\\_essen.html](http://www.geothermal-energy.org/reserves_and_resources/workshop_essen.html), last accessed 06/2014.

IGA, IFC (2014). Best practices guide for geothermal exploration. IGA Service GmbH.

Image web site. <http://www.image-fp7.eu/Pages/default.aspx> (last accessed 06/2015).

Ingeman-Nielsen T, Baumgartner F. (2006). CR1Dmod: a MATLAB program to model 1D complex resistivity effects in electrical and electromagnetic survey. *Comput. Geosci.*, 32:1411–1419.

ISPRA. Carta Geologica d'Italia alla scala 1:50.000 (Geological map of Italy at scale 1:50.000). <http://www.isprambiente.gov.it/it> Last accessed April 2015

Jödicke, H., Jording, A., Ferrari, L., Arzate, J., Mezger, K., Rüpke, L. (2006). Fluid release from the subducted Cocos plate and partial melting of the crust deduced from magnetotelluric studies in southern Mexico: Implications for the generation of volcanism and subduction dynamics. *Journal of Geophysical Research: Solid Earth*, 111 (B8), 1-22.

Jolivet, L., Faccenna, C., Goffé, B., Mattei, M., Rossetti, F., Brunet, C., Storti, F., Funicello, R., Cadet, J.P., d'Agostino, N., Parra, T. (1998). Midcrustal shear zones in postorogenic extension: Example from the northern Tyrrhenian Sea. *J. Geophys. Res.*, 103, 12-123 – 12-160.

- Jones, A.G. (1983). On the Equivalence of the "Niblett" and "Bostick" Transformations in the Magnetotelluric Method. *Journal of Geophysics*, 53, 72-73.
- Jones, A.G. (1988). Static shift of magnetotelluric data and its removal in a sedimentary basin environment. *Geophysics*, 53 (7), 967-978.
- Jones, A.G. (1992). Electrical conductivity of the continental lower crust. In: Arculus, R.J., and Kay, R.W., *Continental Lower Crust*, Elsevier.
- Jones, A.G. (2012). Distortion of magnetotelluric data: its identification and removal. In: Chave, A.D. and Jones, A.G. 2012. *The Magnetotelluric Method, Theory and Practice*. Cambridge University Press. 219-302 pp.
- Jones, A.G., Chave, A.D., Egbert, G., Auld, D. Bahr, K. (1989). A Comparison of techniques for magnetotelluric response function estimation. *Journal of Geophysical Research (Solid Earth)*, 94(10), pages 14201 – 14213.
- Jones, A.G. and Hutton, R. (1979a). A multi-station magnetotelluric study in Southern Scotland, I. Fieldwork, data analysis and results, *Geophys. J. R. Astron. Soc.*, 56, 329-349.
- Jones, A.G. and Hutton, R. (1979b). A multi-station magnetotelluric study in Southern Scotland, II. Monte-Carlo inversion of the data and its geophysical and tectonic implications, *Geophys. J. R. Astron. Soc.*, 56, 351-368.
- Karato, S. and Wang, D. (2013). Electrical conductivity of minerals and rocks. In: Karato, S. *Physics and Chemistry of the Deep Earth*. Wiley-Blackwell, New York.
- Kato, Y., and Kikuchi, T. (1950a). On the phase difference of earth current induced by the changes of the earth's magnetic field, part 1. *Sci. Rep. Tohoku Univ.*, 5th Ser., 2, 139–141.
- Kato, Y. and Kikuchi, T. (1950b). On the phase difference of earth current induced by the changes of the earth's magnetic field, part 2. *Sci. Rep. Tohoku Univ.*, 5th Ser., 2, 142–145.
- Kauahikaua, J. (1981). Interpretation of time-domain electromagnetic soundings in the East Rift geothermal area of Kilauea volcano, Hawaii. US Geological Survey Open-file. Rep. 81-979.

- Kennedy, J. and Eberhart R. (1995). Particle Swarm Optimization. Proc. IEEE international Conference on Neural Networks, IV, 1942-1948.
- Kirkpatrick, S., Gelatt, C.D., Jr., Vecchi, M.P. (1983). Optimization by simulated annealing, *Science*, 220, 671 -680.
- Korja, T. (2007). How is the European Lithosphere Imaged by Magnetotellurics? *Suv. Geophys.*, 28, 239-272.
- Kummerow, J. and Raab, S. (2015). Temperature Dependence of Electrical Resistivity. Part I: Experimental Investigations of Hydrothermal Fluids. *Energy Procedia*, 76, 240-246.
- La Torraca, G.A., Madden, T.R. Korringa, J. (1986). An analysis of the magnetotelluric impedance for three dimensional conductivity structures. *Geophysics*, 51, 1819-1829.
- Larsen, J.C., Mackie, R.L., Fiordelisi, A., Manzella, A., Rieven S. (1995). Robust processing for removing train signals from magnetotelluric data in central Italy. In *Proceedings of World Geothermal Congress 1995, Florence, Italy*.
- Larsen, J.C., Mackie, R.L., Manzella, A., Fiordelisi, A., Rieven, S. (1996). Robust smooth magnetotelluric transfer functions. *Geophysical Journal International*, 124, 801-819.
- Lazzarotto, A. (1967). Geologia della zona compresa fra l'alta valle del Fiume Cornia ed il Torrente Pavone (Prov. Di Pisa e Grosseto). *Mem. Soc. Geol. It.*, 6, 151-197.
- Ledo, J. (2005). 2-D versus 3-D magnetotelluric data interpretation. *Surv. Geophys.*, 26 (5), 511-543. doi:10.1007/s10712-005-1757-8.
- Lindgren, W. (1933). *Mineral deposits*. 4th edition. McGraw-Hill Book Company. 930 pp.
- Liotta D. (1991). The Arbia-Val Marecchia Line, Northern Apennines. *Eclogae Geol. Helv.*, 84 (2), 413-430.
- Liotta, D. and Ranalli, G. (1999). Correlation between seismic reflectivity and rheology in extended lithosphere: southern Tuscany, Inner Northern Apennines, Italy. *Tectonophysics*, 315, 109–122.

- Loucks, R.G., Richmann, D.L. Millken, K.L. (1981). Factors controlling reservoir quality in Tertiary Sandstones and their significance to georpressured geothermal production. Bureau of Economic Geology. Report of investigation n.111.
- Mackie, R. L., Bennett, B. R., and Madden, T. R. (1988). Long-period magnetotelluric measurements near the central California coast: A land-locked view of the conductivity structure under the Pacific Ocean. *Geophys. J.*, 95, 181–194.
- Mackie, R.L., Madden, T.R., Wannamaker, P.E. (1993). Three-dimensional magnetotelluric modeling using difference equations, Theory and comparisons to integral equation solutions, *Geophysics*, 58, 215-226.
- Madden, T.R. (1972). Transmission systems and network analogies to geophysical forward and inverse problems. MIT Technical Report, 72-3.
- Magro, G., Ruggieri, G., Gianelli, G., Bellani, S., Scandiffio, G. (2003). Helium isotopes in paleofluids and presentday fluids in the Larderello geothermal field: constraints on the heat source. *J Geophys Res* 108:1–12.
- Manzella, A. (2004). Resistivity and heterogeneity of Earth crust in an active tectonic region, Southern Tuscany (Italy). *Annals of Geophysics*, 47(1), 107-118.
- Manzella, A., Ruggieri, G., Gianelli, G., Puxeddu, M. (1998). Plutonic-Geothermal systems of southern Tuscany: a review of the crustal models. *Mem. Soc. Geol. It.*, 52, 283-294.
- Manzella, A., Santilano, A., Romano, G. (2016). Magnetotelluric exploration in Balmatt (Belgium): results from MT data processing. Report of CNR-IGG.
- Manzella, A., Spichak, V., Pushkarev, P., Sileva, D., Oskooi, B., Ruggieri, G., Sizov, Y. (2006). Deep fluid circulation in the Travale geothermal area and its relation with tectonic structure investigated by a magnetotelluric survey. In *Proceedings, Thirty-First Workshop on Geothermal Reservoir Engineering* Stanford University, Stanford, California.
- Manzella, A., Ungarelli C., Ruggieri G., Giolito C., Fiordelisi A. (2010). Electrical resistivity at the Travale geothermal field (Italy). *Proceedings of World Geothermal Congress, 2010, Bali (Indonesia)*.

- Manzella, A., Volpi, G., Zaja, A., Meju, M. (2004). Combined TEM-MT investigation of shallow-depth resistivity structure of Mt Somma-Vesuvius. *Journal of Volcanology and Geothermal Research*, 131, 19-32, doi:10.1016/S0377-0273(03)00313-5.
- Marroni, M. and Pandolfi, L. (2007). The architecture of the Jurassic Ligure-Piemontese oceanic basin: Tentative reconstruction along the Northern Apennine–Alpine Corsica transect. *International Journal of Earth Science*, v. 96, p. 1059–1078.
- Marti, A., Queralt, P., Jones, A.G., Ledo, J. (2005). Improving Bahr’s invariant parameters using the WAL approach. *Geophys. J. Int.*, 163, 38–41.
- Marti, A., Queralt, P., Ledo, J. (2009). WALDIM: A code for the dimensionality analysis of magnetotelluric data using the rotational invariants of the magnetotelluric tensor. *Computers & Geosciences*, 35, 2295–2303.
- Maxwell, J.C. (1861). On physical lines of force. Part\_1. The theory of molecular vortices applied to magnetic phenomena. *Phil. Mag.* 21, 161–175.
- Maxwell, J.C. (1865). A dynamical theory of the electromagnetic field. *Phil. Trans. R. Soc.* 155, 459–512.
- Meju, M.A. (1996). Joint inversion of TEM and distorted MT soundings: Some effective practical considerations. *Geophysics*, 61, 56–65.
- Meju M.A. (1998) A simple method of transient electromagnetic data analysis. *Geophysics*, 63:405–410.
- Meju, M.A. (2002). Geoelectromagnetic exploration for natural resources: models, case studies and challenges. *Surveys in Geophysics*, 23, 133-205.
- Menghini, A., Pagano, G., Floris, S. (2002). TDEM Prospection in the ‘Terme di Traiano’ geothermal field, Civitavecchia, Rome, Italy. 64th EAGE Conference & Exhibition, Florence, Italy.
- Menghini, A., Pagano, G., Floris, S., Bernini, E., Pelorosso, M. (2010). TDEM method for hydrothermal water detection. *First Break*, 28, 93-101.
- Menke, W. (2012). *Geophysical Data Analysis: Discrete Inverse Theory*. MATLAB Edition. Elsevier, USA. 276.pp

Metropolis, N. and Ulam, S. (1949). The Monte Carlo method. *J. Acous. Soc. Am.* 44, 335–341.

Miensopust, M.P. (2010). Multidimensional magnetotellurics. A 2D case study and a 3D approach to simultaneously invert for resistivity structure and distortion parameters. PhD thesis, Faculty of Science, National University of Ireland, Galway.

Minambiente. Il Geoportale Nazionale. Last accessed April 2016 <http://www.pcn.minambiente.it/GN/>.

Minissale, A. (1991). The Larderello geothermal field: a review. *Earth-Science Reviews*, 31 133-151.

Minissale, A. (1997). The Larderello geothermal field: a review. *Earth-Science Rev* Minissale, A., Magro, G., Vaselli, O., Verrucchi, C., and Perticone, I.: Geochemistry of water and gas discharges from the Mt. Amiata silicic complex and surrounding areas (central Italy), *J. Volcanol. Geoth. Res.*, 79, 223-251.

Moeck, I.S. (2014). Catalog of geothermal play types based on geologic controls. *Renew. Sust. Energ. Rev.*, 37, 867-882, doi:10.1016/j.rser.2014.05.032.

Mohana, S.J., Saroja, M., Venkatachalam, M. (2014). Comparative Analysis of Swarm Intelligence Optimization Techniques for Cloud Scheduling. *International Journal of Innovative Science, Engineering & Technology*, 1 (10), 15-19.

Mongelli, F., Palumbo, F., Puxeddu, M., Villa, I.M. Zito, G. (1998). Interpretation of the geothermal anomaly of Larderello. *Italy. Mem. Soc. Geol. It.*, 52, 305-318.

Montone P., Mariucci, M.T., and Pierdominici, S.: The Italian present-day stress map, *Geophys. J. Int.*, 189, 705–716, doi: 10.1111/j.1365-246X.2012.05391.x, 2012.

Mosnier, J. and Planson, F. (1985). Differential magnetic soundings in the Travale geothermal area. *Geothermics*, 14, 5/6, 749-754.

MTnet website. <http://www.complete-mt-solutions.com/mtnet/main/> Last accessed (December 2016).

- Muffler, L.J.P. (1997). Assessment of geothermal resources of the United States – 1978. USGS, Circular 790, pp. 163.
- Muñoz, G. (2014). Exploring for Geothermal Resources with Electromagnetic Methods. *Surveys in Geophysics*, 35, 101-122. DOI 10.1007/s10712-013-9236-0.
- Nabighian, M.N. (1979). Quasi-static Transient Response of a Conducting Half-Space, an Approximate Representation. *Geophysics*, 44 (10), pp. 1700-1705.
- Niblett, E.R., Sayn-Wittgenstein (1960). Variation of electrical conductivity with depth by the magnetotelluric method. *Geophys.*, 25, 998-1008.
- Nielson, D. and Moore, J.N. (2000). The Deeper Parts of The Geysers Thermal System-Implications for Heat Recovery. *Geoth. Res. T.*, 24, 299-302.
- Nirta, G., Pandeli, E., Principi G., Bertini, G., Cipriani, N. (2005). The Ligurian Units of Southern Tuscany. *Boll. Soc. Geol. It.*, Vol. Spec. 3, 29-54.
- Niwas, S., Gupta, P. K., Gaur, V. K. (2005). Normalized impedance function and the straightforward inversion scheme for magnetotelluric data. *J. Earth Syst. Sci.*, 114, 5, 523-531.
- Norton, D. and Knight, J. (1977). Transport phenomena in hydrothermal systems: cooling plutons. *Am. J. Sci.*, 277, 937-981.
- Oettinger, G., Haak, V., Larsen, J.C. (2001). Noise reduction in magnetotelluric time-series with a new signal–noise separation method and its application to a field experiment in the Saxonian Granulite Massif. *Geophys. J. Int.*, 146, 659-669.
- Olhoeft, G.R. (1981a). Electrical properties of rocks. In: *Physical Properties of Rocks and Minerals*, Touloukian, Y.S., Judd, W.R. Roy, R.F. (Eds.) McGraw-Hill, New York.
- Olhoeft, G.R. (1981b). Electrical properties of granite with implication for the lower crust. *Geophysical Research letters*, 86 (B2), 931-936.
- Oppenheimer, D.H. (1986). Extensional tectonics at The Geysers geothermal area. *J. Geophys. Res.*, 91, 11,463-11,476.

- Palacky, G. J. (1987). Resistivity characteristics of geologic targets. In: M. N. Nabighian (ed), *Electromagnetic Methods in Applied Geophysics*, volume 1 - Theory, Society of Exploration Geophysicists.
- Pandeli, E., Bertini G., Castellucci, P. (1991). The tectonic wedge complex of the Larderello area (Southern Tuscany, Italy). *Boll. Soc. Geol. It.*, 110, 621-629.
- Pandeli, E., Bertini, G., Castellucci, P., Morelli, M., Monechi, S. (2005). The Ligurian, Subligurian and Tuscan Units of the Monte Amiata geothermal region (Southeastern Tuscany): new stratigraphic and tectonic data. *Boll. Soc. Geol. It., Spec 3*, 55–71.
- Pandeli, E., Puxeddu, M., Gianelli, G., Bertini, G., Castellucci, P. (1988). Paleozoic sequences crossed by deep drillings in the Monte Amiata geothermal region (Italy). *Boll. Soc. Geol. It.*, 107, 593-606.
- Panichi, C., Celati, R., Noto, P., Squarci, P., Taffi, L., Tongiorgi, E. (1974). Oxygen and hydrogen isotope studies of the Larderello (Italy) geothermal system, In: *Isotope techniques in groundwater hydrology vol.II*. Vienna Internat. Atomic Energy Agency, 3-28.
- Pellerin, L., Hohmann, G.W. (1990). Transient electromagnetic inversion: A remedy for magnetotelluric static shifts. *Geophysics*, 55, 1242-1250.
- Pérez-Flores, M.A. and Schultz, A. (2002). Application of 2-D inversion with genetic algorithms to magnetotelluric data from geothermal areas. *Earth, planets and space*, 54 (5), 607-616.
- Pethick, A. and Harris, B. (2015). 1D Magnetotelluric forward modelling Web App. ASEG-PESA 2015, Perth Australia. 1-4.
- Piatti, C., Boiero, D., Godio, A., Socco, L.V. (2010). Improved Monte Carlo 1D-Inversion of vertical electrical sounding and time-domain electromagnetic data. *Near Surface Geophysics*, 8, 117-133.
- Pirajno, F. (2009). *Hydrothermal Processes and Mineral Systems*. Springer, 1250 pp.
- Pommier, A. and Le-Trong, E. (2011). "SIGMELTS: A web portal for electrical conductivity calculations in geosciences". *Computers and Geosciences*, vol. 37, 1450-1459.

- Pommier, A., Tarits, P., Hautot, S., Pichavant, M., Scaillet, B., Gaillard, F. (2010). A new petrological and geophysical investigation of the present-day plumbing system of Mount Vesuvius. *Geochemistry Geophysics Geosystems*, 11 (7), 1-23.
- Ranieri, G. (2000). Tem-fast: a useful tool for hydro-geologists and environmental engineers. *Annals of Geophysics*, 43 (6), 1147-1158.
- Revil, A. and Glover, P.W.J. (1998). Nature of surface electrical conductivity sandstones, and clays. *Geophysical Research letters*, 25 (5), 691-694.
- Rikitake, T. (1951). Changes in earth current and their relation to the electrical state of the earth's crust. *Bull. Earthq. Res. Inst., Univ. Tokyo*, 29, 271-276.
- Roberts, J.J. (2002). Electrical properties of microporous rock as a function of saturation and temperature. *American Institute of Physics*, 91 (3), 1687-1694.
- Rodi, W. and Mackie, R.L., (2001). Nonlinear conjugate gradients algorithm for 2-D magnetotelluric inversion. *Geophysics*, 66, 174-187.
- Romagnoli, P., Arias, A., Barelli, A., Cei, M. and Casini, M. (2010). An updated numerical model of the Larderello-Travale geothermal system, Italy. *Geothermics*, 39, 292-313.
- Ruggieri, G. and Gianelli, G. (1999). Multi-stage fluid circulation in a hydraulic fracture breccia of the Larderello geothermal field (Italy). *Journal of Volcanology and Geothermal Research*, 90, 241-261.
- Ruggieri G., Giolito C., Gianelli G., Manzella A., Boiron M.C. (2004). Application of fluid inclusions to the study of Bagnore geothermal field (Tuscany, Italy). *Geothermics*, 33, 675-692.
- Sambridge, M. and Mosegaard, K. (2002). Monte Carlo methods in geophysical inverse problems. *Reviews of Geophysics*, 40, 3 September 2002.
- Santilano, A., Manzella, A., Gianelli, G., Donato, A., Gola, G., Nardini, I., Trumpy, E., Botteghi, S. (2015a). Convective, Intrusive Geothermal Plays: what about tectonics? *Geothermal Energy Science*, 3, 51-59. doi:10.5194/gtes-3-51-2015.

Santilano, A., Godio, A., Manzella, A., Menghini, A., Rizzo, E., Romano, G., Viezzoli, A., 2015b: Electromagnetic and DC methods for geothermal exploration in Italy – case studies and future developments. *First Break*, 33 (8), 81-86 August 2015.

Santilano, A., Godio A., Manzella A., Dini I. (2015c). Electrical Resistivity Structures and their Relation to Geological Features at the Larderello Geothermal Field (Italy). *Proceeding of Near Surface Geoscience 2015*, 1-5. doi: 10.3997/2214-4609.201413727.

Santilano A., Donato A., Galgaro A., Montanari D., Menghini A., Viezzoli A., Di Sipio E., Destro E., Manzella, A. (2016a). An integrated 3D approach to assess the geothermal heat-exchange potential: the case study of western Sicily (southern Italy). *Renewable Energy*, 97, 611-624.

Santilano, A., Manzella, A., Rizzo, E., Giampaolo, V., Capozzoli, L., Godio, A. (2016b). Imaging the deep structures of the Larderello geothermal field (Italy) by electrical resistivity measurements: the IMAGE experiment. *Proceeding, European Geothermal Congress 2016, Strasbourg (France)*, 1-5 pp.

Schmeling, H. (1986a). A simple statistical model on the degree of interconnection in partially molten rocks. *J. Geophys*, 59, 142-145.

Schmeling, H. (1986b). Numerical models on the influence of partial melt on elastic, anelastic and electric properties of rocks. Part II: electrical conductivity. *Physics of the Earth and Planetary Interiors*, 43, 123–136.

Schmucker, U. (1973). Regional induction studies: a review of methods and results. *Phys. Earth Planet. Inter.*, 7: 365–378.

Sen, M.K., Stoffa, P.L. (1995). *Global Optimization Methods in Geophysical Inversion*. Elsevier Science.

Sen, M.K. and Stoffa, P.L. (2013). *Global Optimization Methods in Geophysical Inversion*. Elsevier, USA.

Shaw, R. and Srivastava, S. (2007). Particle swarm optimization: A new tool to invert Geophysical data. *Geophysics*, 72, F75-F83.

Shi, Y. and Eberhart, R. (1998). A Modified Particle Swarm Optimizer. *Evolutionary Computation Proceedings, 1998. IEEE World Congress on Computational Intelligence*, May 1998, Anchorage, AK.

Sibson, R.H. (1996). Structural permeability of fluid-driven fault-fracture meshes. *J. Struct. Geol.*, 18, 1031-1042.

Siemon B., Christiansen A.V. Auken E. (2009). A review of helicopter-borne electromagnetic methods for groundwater exploration. *Near Surface Geophysics*, 7, 629-646.

Simpson, F. and Bahr, K. (2005). *Practical Magnetotellurics*. Cambridge University Press.

Sims, W. E. and Bostick, F. X. (1969). *Methods of magnetotelluric analysis*. Univ. of Texas Elec. Geophys. Res. Lab. Tech. Rpt.58

Siripunvaraporn, W. (2012). Three-Dimensional Magnetotelluric Inversion: An Introductory Guide for Developers and Users. *Surv. Geophys.* 33:5–27, DOI 10.1007/s10712-011-9122-6

Smith, J. T. (1995). Understanding telluric distortion matrices. *Geophysical Journal International*, 122(1), 219–226.

Smith, J.T. and Booker J.R. (1988). Magnetotelluric inversion for minimum structure. *Geophysics*, 53 (12), 1565-1576.

Spichak V.V. and Manzella, A. (2009). Electromagnetic sounding of geothermal zones. *Journal of Applied Geophysics*, 68, 459-478. doi:10.1016/j.jappgeo.2008.05.007.

Spichak, V.V. and Popova, I.V. (2000). Artificial neural network inversion of MT data in terms of 3D earth macro-parameters. *Geophysical Journal International*, 42, 15-26.

Spichak, V.V. and Zakharova, O.K. (2014). Gaseous vs aqueous fluids: Travale (Italy) case study using EM geothermometry. *Proceeding of 39th Workshop on Geothermal Reservoir Engineering*, Stanford University, USA.

- Spichak, V.V. and Zakharova, O.K. (2015a). Constructing the Deep Temperature Section of the Travale Geothermal Area in Italy, with the Use of an Electromagnetic Geothermometer. *Physics of the Solid Earth*, 51(1), 87–94.
- Spichak, V.V. and Zakharova, O.K. (2015b). *Electromagnetic Geothermometry*. Elsevier, 183 pp.
- Spies, B.R. and Frischknecht, F.C. (1991). Electromagnetic Sounding. In: Nabighian, M.N. (Ed) *Electromagnetic methods in applied geophysics*, Vol. 2 – Application, part A. SEG, 285-386.
- Stanley, W.D. and Rodriguez, B.D. (1995). A Revised Tectonic Model for The Geysers- Clear Lake Geothermal Region, California, in: *Proceedings of the World Geothermal Congress, Florence Italy*, 1193-1198.
- Sternberg, B.K., Washburne, J.C., Pellerin, L. (1988). Correction for the static shift in magnetotellurics using transient electromagnetic soundings. *Geophysics*, 53 (11), 1459-1468. doi: 10.1190/1.1442426
- Schwartz, G., Haak, V., Rath, V. (1985). Electrical conductivity studies in the Travale geothermal field, Italy *Geothermics*, 14, 653–662
- Swift, C. M. (1967). A magnetotelluric investigation of an electrical conductivity anomaly in the southwestern United States. *Geology and geophysics*. Ph.D. thesis, Massachusetts Institute of Technology, Cambridge, MA.
- Szarka, L. (1988). Geophysical aspects of man-made electromagnetic noise in the Earth-A review. *Surveys in Geophysics*, 9, 287-318.
- Tarantola, A. (2005). *Inverse Problem Theory and Methods for Model Parameter Estimation*. Society for Industrial and Applied Mathematics. Philadelphia. 342 pp.
- Targioni Tozzetti, G. (1769). *Relazioni d'alcuni viaggi fatti in diverse parti della Toscana per osservare le produzioni naturali, e gli antichi monumenti di essa*, III. Stamperia Granducale, 473 pp.
- Telford, W.M., Geldart L.P., Sheriff R.E. (1990). *Applied Geophysics* 2nd edition. Cambridge University Press.

- Tikhonov, A.N. (1950). On determination of electric characteristics of deep layers of the earth's crust. *Dokl. Acad. Nauk SSSR*, 151, 295–297.
- Tikhonov, A. N., and Arsenin, V. Y. (1977). *Solutions of ill-posed problems*. V. H. Winston and Sons.
- Truesdell, A.H. and White, D.E. (1973). Production of superheated steam from vapor-dominated geothermal reservoirs. *Geothermics*, 2, 154-173.
- Trumpy, E. and Manzella, A. (2017). Geothopica and the interactive analysis and visualization of the updated Italian National Geothermal Database. *International Journal of Applied Earth Observation and Geoinformation*, 54:28-37. DOI: 10.1016/j.jag.2016.09.004.
- Tuscan Region web site (2015) Continuum Geologico at scale 1:10000. Last accessed April 2015. <http://www.regione.toscana.it/-/banche-dati-cartografiageologica#Carta%20Geologica%20Regionale%201:10.000>.
- Ussher, G., Harvey, C., Johnstone, R., Anderson, E. (2000). Understanding the resistivities observed in geothermal systems. *Proc. World Geothermal Congress, Kyushu-Tohoku, Japan*, pp. 1915–1920.
- Vigor web site. <http://www.vigor-geotermia.it/> (last accessed 06/2015).
- Viljanen, A. (2012). Description of the magnetospheric/ionospheric sources. In: Chave, A.D. and Jones, A.G. 2012. *The Magnetotelluric Method, Theory and Practice*. Cambridge University Press. 96-121.
- Volpi, G., Manzella, A., Fiordelisi, A. (2003). Investigation of geothermal structures by magnetotellurics (MT): an example from the Mt. Amiata area, Italy. *Geothermics* 32, 131–145.
- Waff, H.S. (1974). Theoretical considerations of electrical conductivity in a partially molten mantle and implications for geothermometry. *Journal of Geophysical Research*, 79 (26), 4003—4010.
- Wait, J.R. (1954). On the relation between telluric currents and the earth's magnetic field. *Geophysics*, 19, 281-289.
- Walters, M. and Combs, J. (1989). Heat Flow Regime in The Geysers-Clear Lake Area of Northern California, U.S.A.. *Geoth. Res. T.*, 13, 491-502.

Wannamaker, P.E., Hasterok, D.P., Johnston, J.M., Stodt, J.A., Hall, D.B., Sodergren, T.L., Pellerin, L., Maris, V., Doerner, W.M., Groenewold, K.A., Unsworth, M.J. (2008). Lithospheric dismemberment and magmatic processes of the Great Basin–Colorado Plateau transition, Utah, implied from magnetotellurics, *Geochem. Geophys. Geosyst.*, 9, Q05019, doi:10.1029/2007GC001886.

Ward, S.H. and Hohmann, G.W. (1988). Electromagnetic theory for geophysical applications. In: Nabighian, M.N. (Ed) *Electromagnetic Methods in Applied Geophysics*, vol.1, 131-311, SEG publication.

Waxman, M.H. and Smith, J.M. (1968). Electrical conductivities in oil-bearing shaley sands. *Soc. Pet. Eng. J.* 102–122 SPE Paper 1863-A at SPE Ann. Fall Meeting, Houston.

Weaver, J.T., Agarwal, A.K., Lilley, F.E.M. (2000). Characterization of the magnetotelluric tensor in terms of its invariants. *Geophys. J. Int.*, 141, 321-336.

Weidelt, P. (1972). The inverse problem of geomagnetic induction. *Z. Geophys.* 38: 257–289.

Weiss, C. (2012). The two- and three-dimensional forward problems. In: Chave, A.D. and Jones, A.G. *The Magnetotelluric Method, Theory and Practice*. Cambridge University Press. 219-302 pp.

Wright, P.M., Ward, S.H., Ross, H.P. West, R.C. (1985). State-of-the-art geophysical exploration for geothermal resources. *Geophysics*, 50, 2666-2699.

Yin, C. (2003). Inherent nonuniqueness in magnetotelluric inversion for 1D anisotropic models. *Geophysics*, 68, 138- 146.

Yuan, S., Wang, S., Tian, N. (2009). Swarm intelligence optimization and its application in geophysical data inversion. *Applied Geophysics*, 6, 166–174.

Zhdanov, M.S. (2009). *Geophysical Electromagnetic Theory and Methods*. Amsterdam, Elsevier, 848 pp.

Zhdanov, M.S. and Keller, G.V. (1994). *The geoelectrical methods in geophysical exploration*. Amsterdam, Elsevier, 873 pp.

Zonge (2016). The AMT Method: Audio-frequency MagnetoTelluric Surveys. Available at [http://zonge.com/wp-content/uploads/2016/06/AMT\\_Method\\_20160512.pdf](http://zonge.com/wp-content/uploads/2016/06/AMT_Method_20160512.pdf).